

**IDENTIFICATION OF PATHWAYS THAT DETERMINE
TUMOR SURVIVAL AND RADIO-RESISTANCE UPON
PLAKOPHILIN3 LOSS**

By

SRIKANTA BASU

[LIFE09200904002]

TATA MEMORIAL CENTRE

MUMBAI

A thesis submitted to

the Board of Studies in Life Sciences

in partial fulfillment of the requirements

for the Degree of

DOCTOR OF PHILOSOPHY

of

HOMI BHABHA NATIONAL INSTITUTE

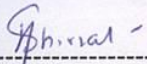
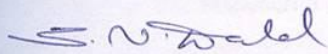
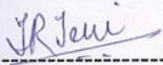
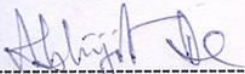


January, 2016

Homi Bhabha National Institute

Recommendations of the Viva Voce Board

As members of the Viva Voce Board, we recommend that the dissertation prepared by Mr. Srikanta Basu titled 'Identification of pathways that determine tumor survival and radio-resistance upon plakophilin3 loss' be accepted as fulfilling the requirements for the Degree of Doctor of Philosophy.

 ----- Chairperson: Dr. Neelam Shirsat	21/1/2016 ----- Date:
 ----- Convener: Dr. Sorab N. Dalal	21/1/2016 ----- Date: 21/1/16
 ----- Member 1: Dr. Tanuja Teni	----- Date:
 ----- Member 2: Dr. Abhijit De	21/1/2016 ----- Date:
 ----- External Examiner: Prof. Paturu Kondaiah	21/1/2016 ----- Date:

The final approval and acceptance of this dissertation is contingent upon the candidate's submission of the final copies of the dissertation to HBNI.

I hereby certify that I have read this dissertation prepared under my direction and recommend that it may be accepted as fulfilling the dissertation requirement.

Date: 21/1/2016

Place: Kharghar, Navi Mumbai.



Guide: Dr. Sorab N. Dalal.

Statement by Author

This dissertation has been submitted in partial fulfilment of requirements for an advanced degree at Homi Bhabha National Institute (HBNI) and is deposited in the library to be made available to borrowers under rules of the HBNI.

Brief quotations from this dissertation are allowable without special permission, provided that accurate acknowledgement of source is made. Requests for permission for extended quotation from or reproduction of this manuscript in whole or in part may be granted by the competent authority of HBNI when in his or her judgment the proposed use of the material is in the interests of scholarship. In all other instances, however, permission must be obtained from the author.

Srikanta Basu

Navi Mumbai

Date:

Declaration

I, hereby declare that the investigation presented in the thesis has been carried out by me. The work is original and has not been submitted earlier as a whole or in part for a degree / diploma at this or any other Institution / University.

Srikanta Basu

Navi Mumbai

Date:

List of Publication Arising From Thesis

Research articles:

- **MMP7 is required to mediate cell invasion and tumor formation upon plakophilin3 loss.** Srikanta Basu, Rahul Thorat and Sorab N. Dalal, PLOS One., DOI: 10.1371/journal.pone.0123979.
- **LCN2 is required to mediate cell invasion, anchorage independent growth, and tumor formation upon plakophilin3 loss.** Srikanta Basu, Aakanksha Sawant, Anushree Sawant, Carol Braggs, Rabiya Sheikh, Simone Vaz, Rahul Thorat and Sorab N. Dalal (manuscript in preparation).

Other Publications:

- **14-3-3 γ -Mediated transport of plakoglobin to the cell border is required for the initiation of desmosome assembly in vitro and in vivo.** Sehgal L, Mukhopadhyay A, Rajan A, Khapare N, Sawant M, Vishal SS, Bhatt K, Ambatipudi S, Antao N, Alam H, Gurjar M, **Basu S**, Mathur R, Borde L, Hosing AS, Vaidya MM, Thorat R, Samaniego F, Kolthur-Seetharam U, Dalal SN, J Cell Sci. 2014 May 15;127(Pt 10):2174-88.
- **14-3-3 γ Inhibits Centrosome Amplification and Tumor Formation.** Amitabha Mukhopadhyay, Lalit Sehgal, Arunabha Bose, Anushree Gulvady, Parijat Senapati, Rahul Thorat, **Srikanta Basu**, Khyati Bhatt, Amol S. Hosing, Renu Balyan, Lalit Borde, Tapas K. Kundu⁴ and Sorab N. Dalal (**Manuscript communicated to Scientific Reports**).

Conferences attended:

Oral Presentations:

- Oral presentation titled “**Identification of pathways regulating tumor formation upon plakophilin3 loss**” at the 10th National Research Scholars Meet (NRSM) conference, ACTREC, Navi Mumbai, 2014.
- Oral presentation on the topic “Identifying mechanisms regulating tumor progression upon plakophilin3 loss” at the 33rd Annual Convention of Indian Association for Cancer Research (IACR), 2014 held at Kollam, Kerala.

Poster Presentations:

- Poster presentation titled “**Identification of pathways regulating tumor formation upon plakophilin3 loss**” at Carcinogenesis 2015 Conference, held at ACTREC, Navi Mumbai, 2015.
- Presented poster titled “**Identification of pathways regulating radio-resistance upon plakophilin3 loss**” at the 2nd Global Cancer Genomics Consortium (GCGC), ACTREC, Navi Mumbai, 2012.
- Presented poster titled “**Identification of pathways regulating tumor formation and radio-resistance upon plakophilin3 loss**” at XXVI All India Cell Biology Conference (AICBC), BARC, MUMBAI, 2012.
- Presented poster titled “**Identification of pathways regulating tumor formation and radio-resistance upon plakophilin3 loss**” at 1st Global Cancer Genomics Consortium (GCGC), ACTREC, NAVI MUMBAI, 2011.

ACKNOWLEDGEMENTS

I had joined ACTREC on the 17th of August, 2009 and was lucky to be selected in Sorab's lab (the lab I so dearly wanted to work in). I always had a huge interest in cancer cell biology but no work experience at all in this field. I would like to thank my guide, Sorab, for giving me the opportunity to pursue my interest in the course of my PhD work. It was in Sorab's lab where I saw human cancer cells for the first time and was really thrilled to see the moving and dividing cancer cells. Sorab has been the best scientific guide I could ever have. He taught me the importance of critical thinking, reasoning and experimentation to solve biological questions and instructed me not to treat every research article or review as a bible. He was not just a scientific guide to me; he was also my English teacher. He would say "Stop using English as a blunt instrument". I am grateful to him for helping me develop my scientific English writing and oral presentation skills. Sorab's role has been pivotal in the course of my development as a research scientist.

I would like to thank Dr. Shubhada Chiplunkar (Director, ACTREC), Dr. Rajiv Sarin (ex-Director, ACTREC) and Dr. Surekha Zingde (ex-Dy. Director, ACTREC) for providing me with an excellent research atmosphere and infrastructure at ACTREC. I thank Dr. Neelam Shirsat (my present DC Chairperson), Rita Mulherkar (my Ex-DC Chairperson), Dr. Tanuja Teni and Dr. Abhijit De (my present DC members) for giving their valuable suggestions and technical inputs during my PhD work.

I would like to sincerely acknowledge the Council of Scientific and Industrial Research (CSIR, Government of India) for providing me financial support (CSIR fellowships) and the Department of Science and Technology (DST) for funding my research project.

I am thankful to all members of the Common Instrumentation facility, the Animal house facility, the Microscopy facility, the Library facility and the Administrative Department of ACTREC for all the help they had provided in the course of my PhD work. I would specially thank Dr. Rahul Thorat for his help in performing the animal experiments related to my thesis.

Next, I would like to thank my lab-mates: Amitabho, Lalit, Rashmi, Sonali, Abha, Sarika, Akash, Mugdha, Neelima, Pawar, Rahul, Kumar, Mansa, Khreivono, Prajakta, Vishal and Arun, Anushree (Sawant), Rabiya, Aakanksha, Aparajitha, Carol, Asma and Simone, Apurva, Ria, Keerthana, Trupti, Roseline, Noelle, Anandi, Nikita, Khyati, Anushree (Gulvady), Kruthi, Neha, Paloma, Dipika, Shraddha and Jazeel. They have all contributed to make Sorab's laboratory a very lively place to work and live. I would thank everyone for being receptors to my poor jokes (PJs). Those were the best stress busters for me and I wish you all must have enjoyed them. I would especially like to thank Sonali, Abha and Sarika for understanding me and helping me out in some tough times of my life.

I thank my family which includes my father, my mother, my beautiful wife (Snehal), my brother, my sister and my nephew. My family has always been like pillars supporting my life. I thank ACTREC for giving me the opportunity to meet Snehal, my batch-mate and now my life partner. She has lived with me in all my joys and sorrows and I will always cherish her company. I also had a great time with my seniors in ACTREC,: Ajit, Padma, Ratika, Monica, Tabish, Cheryl, Dimpu, Asha, Manohar, A Srikant, Hemant, Satyajeet, Manoj, Akhil, Atul, Amit (x3), Poulomi, Deepika, Samrat, Amol, B Srikant and Sameer. They have been a constant source of knowledge and encouragement for my PhD research work. I would like to thank all my friends: Priyanka, Rupa, Madhura, Pooja, Sushmita, Kedar, Tanmoy, Shafqat, Abira, Manish, Amir, Asmita, Rubina, Swati, Vahbiz, Bhanu, Aparna, Ram, Rajan, Richa, Crishmita, Indrajeet, Ekjot,

Bhushan, Smrita, Sayali, Ankit, Bhavik, Mukul, Jacinth, Gauri, Kaushal, Avinash, Mahalaksmi, Prateek, Shalini, Ajay and Gopal for making my life in ACTREC so happy and worth remembering for a lifetime. I have had a wonderful time with all of you and I will miss you all.

My journey to attain a PhD degree has continued for about six years and its coming to an end now. A journey filled with good and bad times (cues). The responses to these cues were governed by multiple signaling pathways (knowledge, ideologies, physical, financial and psychological conditions) leading to the dynamic transcription of the genes encoding the five proteins (emotions) expressed by every human being: Joy, Sorrow, Disgust, Anger and Fear (Reference: Inside out (a movie released in 2015)). Post-transcriptional and post-translational modifications (help and support of my friends and family) regulated the effective or functional levels of these emotions and the net intensity of these emotions determined my phenotype. Cell signaling has always shaped the course of my life and also my PhD work. As you (the person reading this thesis) would turn the pages, you would learn more about my research work which deals with the various cell signaling pathways activated upon the loss of a protein called plakophilin3. Last but not least, I would like to thank you for reading this thesis.

Dedicated to My Family and Friends.....

INDEX	
NAME OF TOPIC	PAGE NUMBER
SYNOPSIS	13
LIST OF TABLES	28
LIST OF FIGURES	29
1: INTRODUCTION	34
1.1. Epithelial cell adhesion junctions	35
1.2. The Desmosome	38
1.2.1. Ultra-structure and molecular architecture of the desmosome	38
1.2.2. Desmosomal cadherins	40
1.2.3. Plakin family of proteins	49
1.2.3.1. Desmoplakin (DP)	50
1.2.4. The Armadillo repeat proteins	56
1.2.4.1. Plakoglobin (PG)	57
1.2.4.2. Plakophilins (PKPs):	62
1.2.4.2.1. <u>PKP1</u>	63
1.2.4.2.1. <u>PKP2</u>	67
1.2.4.2.1. <u>PKP3</u>	69
1.3. Radio-resistance of cancer cells	77
1.3.1. Intrinsic radio-resistance	77
1.3.2. Radiation induced radio-resistance	85
1.4. PKP3 loss and radio-resistance	90
2. AIMS AND OBJECTIVES	92
3. MATERIALS AND METHODS	94
3.1. Plasmids and constructs.	95
3.2. Cloning of oligonucleotides encoding shRNAs into pLKO.1 EGFP-f-puro vector	97
3.3. Cell lines, Transfections and Inhibitors.	99

3.4. Microarray analysis	102
3.5. Semi-quantitative reverse transcriptase coupled PCR reaction (sqRT-PCR) and real time PCR or quantitative RT-PCR (qRT-PCR) reactions.	103
3.6. Antibodies and Western blot analysis.	110
3.7. Immuno-flourescence assays	113
3.8. Immuno-precipitation assays	114
3.9. Scratch wound healing assays	115
3.10. Matrigel invasion assays.	116
3.11. Soft agar colony formation assays	117
3.12. Growth Curves	118
3.13. Luciferase reporter assays	118
3.14. Nuclear cytoplasm fractionation	120
3.15. Tumor formation in nude mice	120
3.16. Ethics statement	122
3.17. Clonogenic survival assays	122
3.17. Reagents for different experiments	124
4. RESULTS	132
4.1. PKP3 loss leads to alterations in transcriptome of multiple cell types.	133
4.2. PKP3 loss in FBM cells lead to cell type specific alterations of ΔNp63 target genes.	141
4.3. PKP3 loss leads to up-regulation of Lipocalin2 (LCN2) and Matrix metalloprotease7 (MMP7) in three different cell lines.	147
4.4. LCN2 is required for neoplastic transformation upon PKP3 loss.	151
4.5. LCN2 up-regulation upon PKP3 loss is regulated by p38MAPK	159
4.6. ELK1 is required for the increase in LCN2 expression observed upon PKP3 loss.	172
4.7. p38β MAPK and ELK1 independently regulates increase in LCN2 expression upon PKP3 loss	177
4.8. PKP3 binds to p38β MAPK.	179
4.9. MMP7 is necessary for neoplastic transformation upon PKP3 loss.	183

4.10. MMP7 up-regulation upon PKP3 loss is regulated by PRL-3 activity	193
4.11. PKP3 loss in HaCaT cells lead to activation of the EGFR/ERK1/2 signaling pathway.	197
4.12. PKP3 loss leads to increased radio-resistance in HaCaT, HCT116 and FBM cells.	201
4.13. LCN2 is required for increased radio-resistance in HCT116 cells, upon PKP3 loss.	204
5. DISCUSSION	208
5.1. LCN2 is necessary for neoplastic progression upon PKP3 loss	209
5.2. p38β MAPK is required to increase LCN2 expression upon PKP3 loss in HCT116 cells while the EGFR/MEK/ERK pathway may increase LCN2 expression in HaCaT cells.	211
5.3. PKP3 binds to p38β MAPK and may inhibit activation of p38β MAPK.	212
5.4. ELK1 is required for the increase in LCN2 expression observed upon PKP3 loss.	214
5.5. MMP7 mediates cell invasion and tumor formation upon PKP3 loss	215
5.6. MMP7 over-expression upon PKP3 loss is regulated by PRL-3	217
5.7. PKP3 loss in HaCaT and FBM cells lead to increase in expression of inflammatory associated genes.	218
5.8. PKP3 knockdown leads to differential alterations in transcriptome of three different cell types	221
5.9. LCN2, but not MMP7, is required to increase radio-resistance of HCT116 cells upon PKP3 loss.	222
5.10. Conclusion	222
6. BIBLIOGRAPHY	226
7. Annexure I: List of genes altered upon PKP3 loss in FBM cells.	286
8. Annexure II: List of genes altered upon PKP3 loss in HCT116 cells.	291

SYNOPSIS

of Ph.D. Thesis

**Homi Bhabha National Institute****Ph. D. PROGRAMME****SYNOPSIS OF PHD THESIS**

- | | |
|--|--|
| 1. Name of the Student: | Srikanta Basu |
| 2. Name of the Constituent Institution: | Tata Memorial Centre, Advanced Centre for
Treatment Research and Education in Cancer |
| 3. Enrolment No. : | LIFE09200904002 |
| 4. Title of the Thesis: | Identification of pathways that determine tumor
survival and radio-resistance upon plakophilin3 loss. |
| 5. Board of study: | Life Science |

SYNOPSIS

Introduction. Desmosomes are adherens like junctions that anchor intermediate filaments at membrane associated plaques in adjoining cells and thus allow the formation of an intercellular network that promotes tissue organization and rigidity. The desmosome is composed of proteins belonging to three different protein families: the desmosomal cadherins (the desmogleins and desmocollins), the plakin family proteins (desmoplakin) and the proteins containing armadillo (ARM) repeats (plakoglobin and plakophilins) [1, 2]. Plakophilin3 (PKP3) is the most widely expressed isoform in the plakophilin family and is ubiquitously present in all the layers of the stratified epithelia and simple epithelia except in hepatocytes [3]. PKP3 binds to a broad repertoire of proteins such as the desmosomal cadherins: desmoglein 1-3, desmocollins 1 and 3, plakoglobin, desmoplakin and keratin18 [4]. PKP3 plays a crucial role in the maintenance of the desmosomal structure and function by mediating recruitment of other desmosomal components to the cell border [5].

PKP3 expression is decreased in high grade poorly differentiated oropharyngeal cancer [6], colon cancer [7], gastric cancer [8] and bladder cancers [9]. Previous results from our laboratory demonstrated that PKP3 loss led to a decrease in desmosome size, a decrease in cell-cell adhesion, increased cell migration, increased anchorage independent growth, accelerated tumor formation in nude mice and increased metastasis to lung [10], partly due to an increase in the stability of keratin8 [11]. The increased stability of keratin8 was due to an increase in the levels of Phosphatase of Regenerating Liver -3 (PRL-3) [11, 12]. PRL-3 levels are increased in colorectal cancers [13] and PRL-3 expression leads to metastasis in tumors derived from the colon [14].

In addition to regulating cell-cell adhesion, PKP3 has been postulated to have functions in regulating the transcription and translation of gene products. It has been postulated that PKP3, like the other plakophilin family members, may play a role in integrating extracellular signaling with signals occurring inside the cells [15-19]. PKP3 has also been detected in stress granules in complex with RNA binding like FXR1, eIF4E, poly-A binding protein and Ras-GAP SH3 binding protein [20, 21]. Thus PKP3 loss may lead to alterations in transcription or translation of genes and this might have a role to play in the inhibition of transformation and metastasis by PKP3.

Objectives. 1. To determine the alterations in the transcriptome of cells lacking PKP3 and their relevance to neoplastic progression.

2. To determine if PKP3 loss leads to radio-resistance and to identify the mechanism underlying this radio-resistance phenotype.

Results. 1. **To determine the alterations in the transcriptome of cells lacking PKP3 and their relevance to neoplastic progression.** To identify mechanisms downstream of PKP3 loss leading to tumor progression and metastasis, a gene expression analysis was performed to compare the transcriptome of FBM and HCT116 derived vector control clone (vec) and a PKP3 knockdown clone (shPKP3-2) using the Agilent 8x60K microarray format. Microarray data analysis was done using the Bio-interpreter software (Genotypic, India). Gene expression changes between FBM, HCT116 and HaCaT derived vector control and PKP3 knockdown clones were validated using real time PCR. The microarray data for FBM and HCT116 has been uploaded to the NCBI GEO database (Accession nos. GSE61512 and GSE64580). Real time PCR assays demonstrated that an inflammation associated signature was observed to be increased in HaCaT and FBM derived PKP3 knockdown clones but not in the HCT116 derived

PKP3 knockdown clones. These results suggested that PKP3 loss leads to varying alterations in the transcriptome in the three cell types studied and that PKP3 loss leads to the generation of an inflammation associated signature in stratified epithelia derived cell lines, which is consistent with the observation that inflammation is observed in the epidermis of mice lacking PKP3 [22].

Matrix-metalloprotease 7 (MMP7) and Lipocalin2 (LCN2) expression were up-regulated in all the three cell lines tested. LCN2 is an iron binding protein and regulates iron homeostasis in cells and is often over-expressed in many types of cancers [23]. LCN2 up-regulation has been found in patients suffering from colorectal carcinoma in multiple clinical studies and is an indicator of colon cancer progression from adenoma to carcinoma [24, 25]. MMP7 (also known as matrilysin) is up-regulated in many cancers like colon cancer [26], gastric cancer [27], oral cancer [28] and bladder cancer [29]. To test if LCN2 or MMP7 is functionally important in regulating tumor formation upon PKP3 loss, HCT116 derived PKP3 knockdown clone (shpkp3-2) was transfected with plasmid encoding shRNA against LCN2 or MMP7. Four LCN2 double knockdown clones and two MMP7 double knockdown clones were generated. Compared to the vector control, the LCN2 double knockdown clones had decreased cell migration, cell invasion, anchorage independent growth and a decreased ability to form tumors in nude mice. The MMP7 double knockdown clones showed decreased cell migration, cell invasion, increase in anchorage independent growth and a decreased ability to form tumors in nude mice. Thus, increase in the expression of both MMP7 and LCN2 was found to be essential for the neoplastic progression observed upon PKP3 loss.

Previous reports suggested that LCN2 transcription can be increased upon activation of the p38MAPK/AP1 pathway [30, 31]. To determine if PKP3 loss leads to an increase in the activation of p38 MAPK, a Western blot analysis in HCT116 derived PKP3 knockdown clones

was performed. These experiments demonstrated that PKP3 loss results in increased p38MAPK activation and increased nuclear localization of p38MAPK. Inhibition of the activity of p38 α and β decreased LCN2 expression, suggesting that activation of either p38 α or p38 β was required for LCN2 transcription upon PKP3 loss. A real time PCR analysis demonstrated that p38 β knockdown decreased LCN2 expression, while p38 α knockdown increased LCN2 expression.

As p38MAPK is known to phosphorylate and activate transcription factors like ATF2 [32], MSK1[32] and ELK1[33], , alterations in phosphorylation status and total protein levels of these transcription factors were analyzed by Western blotting. Phosphorylated ELK1 and total ELK1 protein levels were found to be up-regulated upon PKP3 loss. To analyze if ELK1 regulates LCN2 over-expression upon PKP3 loss, ELK1 was knocked down in a HCT116 derived PKP3 knockdown clone generating ELK1 double knockdown clones. Real time PCR assays demonstrated that LCN2 levels were decreased in these double knockdown clones. Luciferase reporter assays demonstrated that ELK1 was required for increased LCN2 promoter activity in the PKP3 knockdown clones. As the knockdown of both p38 β and ELK1 resulted in a decrease in LCN2 transcription and p38MAPK is known to phosphorylate and activate ELK1 [33], it was hypothesized that probably p38 β activates ELK1 and this in turn regulates LCN2 up-regulation. Real time PCR and Western blotting demonstrated that ELK1 levels were decreased upon p38 β down-regulation both at mRNA and protein levels while p38 β expression was un-altered in the ELK1double knockdown clones. Thus the p38 β /ELK1 pathway was demonstrated to be important in regulating LCN2 over-expression upon PKP3 loss.

A recent report demonstrated that MMP7 expression in the colon cancer derived cell line, DLD1 is increased upon an increase in PRL-3 levels via the PI3K/AKT and ERK signaling pathway [34]. Inhibition of PRL-3 activity in the HCT116 derived vector control and PKP3 knockdown

clones caused a concentration dependent decrease in MMP7 mRNA levels and protein levels. To determine if PRL3 inhibition was specific to MMP7, expression of LCN2 was analyzed upon PRL3 inhibition. LCN2 expression was not decreased upon PRL3 inhibition. Thus, it was demonstrated that PRL-3 up-regulates MMP7 expression upon PKP3 loss.

2. To determine if PKP3 loss leads to radio-resistance and to identify the mechanism underlying this radio-resistance phenotype.

To determine whether PKP3 loss leads to increase in radio-resistance, clonogenic survival assays were performed [35] to quantify the effect of γ irradiation on HaCaT, HCT116 and FBM derived PKP3 knockdown clones as compared to their respective vector control clones. The results obtained from this experiment demonstrated that loss of PKP3 leads to the phenotype of increased radio-resistance in all the three cell lines under study. To determine whether radio-resistance upon PKP3 loss is intrinsic or radiation induced [36, 37], a gene expression analysis was performed to compare the transcriptome of FBM derived vector control clone (vec) and a PKP3 knockdown clone (shPKP3-2) harvested un-irradiated or irradiated (4grays γ -irradiation). Microarray was performed using the Agilent 8x60K format and data analysis was done using the Bio-interpreter software (Genotypic, India). This analysis demonstrated that there were very few radiation induced differences in mRNA between the vector control and PKP3 knockdown clones which could lead to radio-resistance. So, it was hypothesized that the phenotype of radio-resistance shown by PKP3 knockdown clones was an intrinsic radio-resistance phenotype.

To analyze if LCN2 or MMP7 up-regulation regulates the observed radio-resistance phenotype, clonogenic survival assay was performed for shpkp3-2 derived LCN2 double knockdown clones, shpkp3-2 derived MMP7 double knockdown clones and the shpkp3-2 derived vector control clone. ANOVA analysis and the survival curves obtained from this experiment demonstrated that

LCN2 knockdown can reverse the phenotype of radio-resistance observed upon PKP3 loss but MMP7 was not involved in regulating radio-resistance.

4. Conclusions and Future directions. PKP3 loss leads to both cell type dependent and cell type independent alterations in gene expression. PKP3 loss leads to activation of the p38 β /ELK1 pathway which leads to LCN2 up-regulation. PKP3 loss also increases PRL-3 protein levels which in turn up-regulates MMP7 expression. Up-regulation of LCN2 and MMP7 contributes to the increased neoplastic progression observed in HCT116 derived PKP3 knockdown clones. LCN2 up-regulation but not MMP7 up-regulation confers the property of radio-resistance to the PKP3 knockdown clones.

5. References

1. Desai BV, Harmon RM, Green KJ. Desmosomes at a glance. *J Cell Sci.* 2009;122(Pt 24):4401-7.
2. Garrod DR, Merritt AJ, Nie Z. Desmosomal adhesion: structural basis, molecular mechanism and regulation (Review). *Molecular membrane biology.* 2002;19(2):81-94.
3. Schmidt A, Langbein L, Pratzel S, Rode M, Rackwitz HR, Franke WW. Plakophilin 3--a novel cell-type-specific desmosomal plaque protein. *Differentiation; research in biological diversity.* 1999;64(5):291-306.
4. Bonne S, Gilbert B, Hatzfeld M, Chen X, Green KJ, van Roy F. Defining desmosomal plakophilin-3 interactions. *J Cell Biol.* 2003;161(2):403-16.
5. Gosavi P, Kundu ST, Khapare N, Sehgal L, Karkhanis MS, Dalal SN. E-cadherin and plakoglobin recruit plakophilin3 to the cell border to initiate desmosome assembly. *Cell Mol Life Sci.* 2011;68(8):1439-54.

6. Papagerakis S, Shabana AH, Depondt J, Gehanno P, Forest N. Immunohistochemical localization of plakophilins (PKP1, PKP2, PKP3, and p0071) in primary oropharyngeal tumors: correlation with clinical parameters. *Human pathology*. 2003;34(6):565-72.
7. Aigner K, Descovich L, Mikula M, Sultan A, Dampier B, Bonne S, et al. The transcription factor ZEB1 (deltaEF1) represses Plakophilin 3 during human cancer progression. *FEBS letters*. 2007;581(8):1617-24.
8. Demirag GG, Sullu Y, Gurgenyatagi D, Okumus NO, Yucel I. Expression of plakophilins (PKP1, PKP2, and PKP3) in gastric cancers. *Diagn Pathol*. 2011;6:1.
9. Takahashi H, Nakatsuji H, Takahashi M, Avirmed S, Fukawa T, Takemura M, et al. Up-regulation of plakophilin-2 and Down-regulation of plakophilin-3 are correlated with invasiveness in bladder cancer. *Urology*. 2012;79(1):240 e1-8.
10. Kundu ST, Gosavi P, Khapare N, Patel R, Hosing AS, Maru GB, et al. Plakophilin3 downregulation leads to a decrease in cell adhesion and promotes metastasis. *International journal of cancer*. 2008;123(10):2303-14.
11. Khapare N, Kundu ST, Sehgal L, Sawant M, Priya R, Gosavi P, et al. Plakophilin3 Loss Leads to an Increase in PRL3 Levels Promoting K8 Dephosphorylation, Which Is Required for Transformation and Metastasis. *PLoS One*. 2012;7(6):e38561.
12. Mizuuchi E, Semba S, Kodama Y, Yokozaki H. Down-modulation of keratin 8 phosphorylation levels by PRL-3 contributes to colorectal carcinoma progression. *International journal of cancer*. 2009;124(8):1802-10.
13. Rouleau C, Roy A, St Martin T, Dufault MR, Boutin P, Liu D, et al. Protein tyrosine phosphatase PRL-3 in malignant cells and endothelial cells: expression and function. *Molecular cancer therapeutics*. 2006;5(2):219-29.

14. Saha S, Bardelli A, Buckhaults P, Velculescu VE, Rago C, St Croix B, et al. A phosphatase associated with metastasis of colorectal cancer. *Science*. 2001;294(5545):1343-6.
15. Chen X, Bonne S, Hatzfeld M, van Roy F, Green KJ. Protein binding and functional characterization of plakophilin 2. Evidence for its diverse roles in desmosomes and beta -catenin signaling. *The Journal of biological chemistry*. 2002;277(12):10512-22.
16. Hatzfeld M. Plakophilins: Multifunctional proteins or just regulators of desmosomal adhesion? *Biochim Biophys Acta*. 2007;1773(1):69-77.
17. Wolf A, Keil R, Gotzl O, Mun A, Schwarze K, Lederer M, et al. The armadillo protein p0071 regulates Rho signalling during cytokinesis. *Nat Cell Biol*. 2006;8(12):1432-40.
18. Hatzfeld M. A nuclear function for plakophilin-1 in the DNA damage response? *J Invest Dermatol*. 2010;130(11):2538-40.
19. Wolf A, Krause-Gruszczynska M, Birkenmeier O, Ostareck-Lederer A, Huttelmaier S, Hatzfeld M. Plakophilin 1 stimulates translation by promoting eIF4A1 activity. *J Cell Biol*. 2010;188(4):463-71.
20. Hofmann I, Casella M, Schnolzer M, Schlechter T, Spring H, Franke WW. Identification of the junctional plaque protein plakophilin 3 in cytoplasmic particles containing RNA-binding proteins and the recruitment of plakophilins 1 and 3 to stress granules. *Molecular biology of the cell*. 2006;17(3):1388-98.
21. Fischer-Keso R, Breuninger S, Hofmann S, Henn M, Rohrig T, Strobel P, et al. Plakophilins 1 and 3 bind to FXR1 and thereby influence the mRNA stability of desmosomal proteins. *Molecular and cellular biology*. 2014.

22. Sklyarova T, Bonne S, D'Hooge P, Denecker G, Goossens S, De Rycke R, et al. Plakophilin-3-deficient mice develop hair coat abnormalities and are prone to cutaneous inflammation. *J Invest Dermatol.* 2008;128(6):1375-85.
23. Bolignano D, Donato V, Lacquaniti A, Fazio MR, Bono C, Coppolino G, et al. Neutrophil gelatinase-associated lipocalin (NGAL) in human neoplasias: a new protein enters the scene. *Cancer Lett.* 2010;288(1):10-6.
24. Nielsen BS, Borregaard N, Bundgaard JR, Timshel S, Sehested M, Kjeldsen L. Induction of NGAL synthesis in epithelial cells of human colorectal neoplasia and inflammatory bowel diseases. *Gut.* 1996;38(3):414-20.
25. Sun Y, Yokoi K, Li H, Gao J, Hu L, Liu B, et al. NGAL expression is elevated in both colorectal adenoma-carcinoma sequence and cancer progression and enhances tumorigenesis in xenograft mouse models. *Clin Cancer Res.* 2011;17(13):4331-40.
26. Adachi Y, Yamamoto H, Itoh F, Hinoda Y, Okada Y, Imai K. Contribution of matrilysin (MMP-7) to the metastatic pathway of human colorectal cancers. *Gut.* 1999;45(2):252-8.
27. Wroblewski LE, Noble PJ, Pagliocca A, Pritchard DM, Hart CA, Campbell F, et al. Stimulation of MMP-7 (matrilysin) by *Helicobacter pylori* in human gastric epithelial cells: role in epithelial cell migration. *J Cell Sci.* 2003;116(Pt 14):3017-26.
28. Vairaktaris E, Serefoglou Z, Yapijakis C, Vylliotis A, Nkenke E, Derka S, et al. High gene expression of matrix metalloproteinase-7 is associated with early stages of oral cancer. *Anticancer Res.* 2007;27(4B):2493-8.
29. Szarvas T, Becker M, vom Dorp F, Gethmann C, Totsch M, Bankfalvi A, et al. Matrix metalloproteinase-7 as a marker of metastasis and predictor of poor survival in bladder cancer. *Cancer science.* 2010;101(5):1300-8.

30. Wang LH, Chang GQ, Zhang HJ, Wang J, Lin YN, Jin WN, et al. Neutrophil gelatinase-associated lipocalin regulates intracellular accumulation of Rh123 in cancer cells. *Genes Cells*. 2012;17(3):205-17.
31. Yoo do Y, Ko SH, Jung J, Kim YJ, Kim JS, Kim JM. *Bacteroides fragilis* enterotoxin upregulates lipocalin-2 expression in intestinal epithelial cells. *Lab Invest*. 2013;93(4):384-96.
32. de Nadal E, Ammerer G, Posas F. Controlling gene expression in response to stress. *Nature reviews Genetics*. 2011;12(12):833-45.
33. Patel M, Predescu D, Tandon R, Bardita C, Pogoriler J, Borhade S, et al. A novel p38 mitogen-activated protein kinase/Elk-1 transcription factor-dependent molecular mechanism underlying abnormal endothelial cell proliferation in plexogenic pulmonary arterial hypertension. *The Journal of biological chemistry*. 2013;288(36):25701-16.
34. Lee SK, Han YM, Yun J, Lee CW, Shin DS, Ha YR, et al. Phosphatase of regenerating liver-3 promotes migration and invasion by upregulating matrix metalloproteinases-7 in human colorectal cancer cells. *International journal of cancer*. 2012;131(3):E190-203.
35. Franken NA, Rodermond HM, Stap J, Haveman J, van Bree C. Clonogenic assay of cells in vitro. *Nat Protoc*. 2006;1(5):2315-9.
36. Huber SM, Butz L, Stegen B, Klumpp D, Braun N, Ruth P, et al. Ionizing radiation, ion transports, and radioresistance of cancer cells. *Frontiers in physiology*. 2013;4:212.
37. Valerie K, Yacoub A, Hagan MP, Curiel DT, Fisher PB, Grant S, et al. Radiation-induced cell signaling: inside-out and outside-in. *Molecular cancer therapeutics*. 2007;6(3):789-801.

Publications in Refereed Journal:a. Published

MMP7 is required to mediate cell invasion and tumor formation upon plakophilin3 loss.

Srikanta Basu, Rahul Thorat and Sorab N. Dalal, PLOS One., DOI: 10.1371/journal.pone.0123979.

b. Other Publications:

i. 14-3-3 γ -Mediated transport of plakoglobin to the cell border is required for the initiation of desmosome assembly in vitro and in vivo. Sehgal L, Mukhopadhyay A, Rajan A, Khapare N, Sawant M, Vishal SS, Bhatt K, Ambatipudi S, Antao N, Alam H, Gurjar M, **Basu S**, Mathur R, Borde L, Hosing AS, Vaidya MM, Thorat R, Samaniego F, Kolthur-Seetharam U, Dalal SN, J Cell Sci. 2014 May 15;127(Pt 10):2174-88.

ii. 14-3-3 γ Inhibits Centrosome Amplification and Tumor Formation. Amitabha Mukhopadhyay, Lalit Sehgal, Arunabha Bose, Anushree Gulvady, Parijat Senapati, Rahul Thorat, **Srikanta Basu**, Khyati Bhatt, Amol S. Hosing, Renu Balyan, Lalit Borde, Tapas K. Kundu⁴ and Sorab N. Dalal (**Manuscript communicated to Scientific Reports**).

Conferences attended:**Oral Presentations:**

- Oral presentation titled “**Identification of pathways regulating tumor formation upon plakophilin3 loss**” at the 10th National Research Scholars Meet (NRSM) conference, ACTREC, Navi Mumbai, 2014.

- Oral presentation on the topic “Identifying mechanisms regulating tumor progression upon plakophilin3 loss” at the 33rd Annual Convention of Indian Association for Cancer Research (IACR), 2014 held at Kollam, Kerala.

Poster Presentations:

- Poster presentation titled “**Identification of pathways regulating tumor formation upon plakophilin3 loss**” at Carcinogenesis 2015 Conference, held at ACTREC, Navi Mumbai, 2015.

- Presented poster titled “**Identification of pathways regulating radio-resistance upon plakophilin3 loss**” at the 2nd Global Cancer Genomics Consortium (GCGC), ACTREC, Navi Mumbai, 2012.

- Presented poster titled “**Identification of pathways regulating tumor formation and radio-resistance upon plakophilin3 loss**” at XXVI All India Cell Biology Conference (AICBC), BARC, MUMBAI, 2012.

- Presented poster titled “Identification of pathways regulating tumor formation and radio-resistance upon plakophilin3 loss” at 1st Global Cancer Genomics Consortium (GCGC), ACTREC, NAVI MUMBAI, 2011.

Shikanta Bam

Signature of Student:

Date: 8/4/15

Doctoral Committee:

Sr. No.	Name	Designation	Signature	Date
1	Dr. Neelam V. Shirsat	Chairman	<i>Shirsat</i>	8/4/15
2	Dr. Sorab N. Dalal	Guide & Convener	<i>S. N. Dalal</i>	8/4/15
3	Dr. Tanuja Teni	Member	<i>T. Teni</i>	8/4/15
4	Dr. Abhijit De	Member	<i>Abhijit De</i>	8/4/15

Forwarded through:

S. V. Chiplunkar

Dr. S.V. Chiplunkar,
Director,
ACTREC-TMC.

Dr. S. V. Chiplunkar
Director
Advanced Centre for Treatment, Research &
Education in Cancer (ACTREC)
Tata Memorial Centre
Kharghar, Navi Mumbai 410210.

K. S. Sharma

Dr. K. S. Sharma,
Director Academics,
TMC.

PROF. K. S. SHARMA
DIRECTOR (ACADEMICS)
TATA MEMORIAL CENTRE,
PAREL, MUMBAI

LIST OF TABLES

Table number	Title of Table	Page number
1.1	Phenotypes of mice having knockout of individual desmosomal cadherin genes.	44
1.2	Diseases associated with desmosomal cadherins.	48
1.3	Cancers associated with alterations in desmosomal cadherins.	49
1.4	Phenotypes of mice having knockout of DP	54
1.5	Diseases associated with DP.	54
1.6	Cancers caused by alterations in DP.	55
1.7	Phenotypes of mice having knockout of individual armadillo repeat protein encoding genes.	61
1.8	Diseases associated with desmosomal proteins.	62
1.9	Cancers caused by alterations in armadillo repeat proteins.	63
1.10	Some cancers can be cured with only radiation if detected early while others require combination of other modalities.	79
3.1	List of oligonucleotides used for generating shRNA constructs in pLKO.1 EGFP-f puro vector	95-96
3.2	List of oligonucleotides used for generating LCN2 overlapping promoter fragements.	97
3.3	Reaction mix for ligation of oligonucleotides to the pLKO.1 EGFP-f-puro vector backbone.	98
3.4	Calcium phosphate transfection mix.	100
3.5	Lipofectamine LTX transfection mix.	101
3.6	List of oligonucleotides used for sqRT-PCRs and qRT-PCRs.	105-106
3.7	Reaction mix and PCR conditions for sqRT-PCR.	107
3.8	Reaction mix of SYBR green and primers used for qRT-PCR.	107-108
4.1	Δ Np63 α target genes were up-regulated upon PKP3 loss in FBM cells.	142

LIST OF FIGURES

Figure number	Figure title	Page number
1.1	Epithelial cell to cell and cell to ECM junctions.	36
1.2	Desmosome ultra structure and molecular composition.	39
1.3	Structural domains, isoforms and splice variants of desmosomal cadherins.	41
1.4	Differential expression of desmosomal cadherins in skin epidermis.	44
1.5	The desmoglein compensation hypothesis.	47
1.6	Alternative splice variants of DP and their domain structure.	50
1.7	The spectrin repeats in plakin domain of DP.	51
1.8	Expression of DP in the different layers of the stratified epithelium.	53
1.9	Secondary structure of a typical armadillo protein, β catenin.	58
1.10	Structural domains of PG.	58
1.11	Expression of PG in the different layers of the stratified epithelium.	60
1.12	Structural domains of PKPs and alternative splice variants of PKP1 and PKP2.	65
1.13	Expression of PKP isoforms in the different layers of the stratified epithelium.	66
1.14	Alternative splice variants of PKP3.	70
1.15	The cell cycle, the cell cycle checkpoints and the contribution of the HR and NHEJ pathways in the cell cycle.	80
1.16	The double stranded DNA repair pathways: NHEJ and HR.	81
1.17	Radiation induced radio-resistance.	86
1.18	Radiation induced resistance is caused by CSC enrichment.	87
1.19	Schematic representation of the bystander effect.	90
3.1	Thermal cycling conditions for a typical qRT-PCR.	109
3.2	Principle of SYBR green based qRT-PCR.	110

4.1	Functional classification of the genes up-regulated upon PKP3 loss in FBM cells.	134
4.2	Functional classification of the genes down-regulated upon PKP3 loss in FBM cells.	135
4.3	Functional classification of the genes up-regulated upon PKP3 loss in HCT116 cells.	136
4.4	Functional classification of the genes down-regulated upon PKP3 loss in HCT116 cells.	137
4.5	Validation of the HaCaT, HCT116 and FBM derived PKP3 knockdown clones.	138
4.6	PKP3 loss in HaCaT and FBM cells leads to up-regulation of inflammation associated genes	140
4.7	Cell type specific alterations in FBM derived PKP3 knockdown clones.	141
4.8	P cadherin RNA expression levels and protein expression levels are higher in FBM derived PKP3 knockdown clones	142
4.9	Schematic representation of p63 isoforms encoded by the <i>TP73L</i> gene by alternate promoter usage and alternate splicing.	143
4.10	Cell type specific alterations of Δ Np63 in FBM derived PKP3 knockdown clones.	144
4.11	PKP3 loss does not alter Δ Np63 expression in HaCaT cells, while in HCT116, Δ Np63 is not expressed.	145
4.12	Cloning of Δ Np63 shRNA in pLKO.1 EGFP-f-puro vector and analysing EGFP-f expression.	146
4.13	PKP3 loss leads to up-regulation of LCN2 in multiple cell types.	148
4.14	PKP3 loss leads to up-regulation of MMP7 in multiple cell types.	149
4.15	Cloning of 2 different LCN2 shRNAs (A and B) in pLKO.1 EGFP-f-puro vector and generation of stable double knockdown clones of LCN2 derived from the HCT116 based PKP3 knockdown clone	151

	shpkp3-2.	
4.16	Validation of LCN2+PKP3 double knockdown clones by qRT-PCR and Western blotting (of acetone precipitated cell supernatant).	152
4.17	PKP3 loss in HaCaT cells lead to increased protein expression of the secreted protein LCN2.	154
4.18	LCN2 loss leads to a decrease in migration.	155
4.19	LCN2 loss leads to a decrease in cell invasion.	156
4.20	LCN2 loss leads to a decrease in anchorage independent growth.	157
4.21	Tumor formation is inhibited in the PKP3 knockdown cells upon LCN2 knockdown.	158
4.22	LCN2 promoter activity is higher in PKP3 knockdown clones.	160
4.23	Phosphorylation of p38MAPK increases while ERK phosphorylation is not altered in HCT116 derived PKP3 knockdown clones.	162
4.24	Nuclear localization of p38MAPK increases upon PKP3 knockdown in HCT116 cells.	163
4.25	Localization of p38MAPK in the nucleus increases upon PKP3 loss: Nuclear cytoplasmic fractionation	164
4.26	PKP3 loss in HCT116 cells doesnot alter expression of any of the p38MAPK isoforms	165
4.27	Inhibition of the activity of p38α/β results in a decrease in LCN2 but not MMP7 expression in PKP3 knockdown cells.	166
4.28	Validation of p38α+PKP3 double knockdown clones and p38β+PKP3 double knockdown clones by Western blotting.	167
4.29	Validation of p38α+PKP3 double knockdown clones and p38β+PKP3 double knockdown clones by qRT-PCR.	168
4.30	p38β knockdown in HCT116 derived PKP3 knockdown clones decreases LCN2 expression but p38α knockdown highly inceases LCN2 expression.	169
4.31	The p38MAPK signaling pathway.	170

4.32	No alteration in activation of ATF2 and MSK1 upon PKP3 loss.	171
4.33	ELK1 expression and activation increases upon PKP3 loss in HCT116 cells.	171
4.34	ELK1 is a member of the ETS family of transcription factors.	172
4.35	ELK1 and ETS1 binding sites are present in the LCN2 promoter region of interest (ROI).	173
4.36	Validation of ELK1+PKP3 double knockdown clones by qRT-PCR and Western blotting.	174
4.37	ELK1 regulates LCN2 expression upon PKP3 loss in HCT116 cells.	175
4.38	LCN2 promoter activity is decreased upon ELK1 knockdown in PKP3 knockdown cells.	176
4.39	Activation of p38β MAPK and ELK1 upon PKP3 loss is independent of each other.	178
4.40	PKP3 may inhibit auto-phosphorylation of p38β MAPK by binding its C terminus.	180
4.41	Schematic representation of the wild type (WT) and C terminal truncated mutants of p38β MAPK	180
4.42	PKP3 binds to p38β but not via the C terminus of p38β MAPK	181
4.43	PKP3 interacts with both p38β and p38α MAPK	182
4.44	Cloning of MMP7 shRNA in pLKO.1-EGFP-f-puro vector and generation of stable double knockdown clones of MMP7 derived from the HCT116 based PKP3 knockdown clone shpkp3-2.	184
4.45	Validation of MMP7+PKP3 double knockdown clones by qRT-PCR and Western blotting (of acetone precipitated cell supernatant).	185
4.46	MMP7 loss leads to a decrease in cell migration.	186
4.47	MMP7 loss leads to a decrease in cell invasion.	187
4.48	MMP7 loss leads to a decrease in cell growth to higher density	188
4.49	MMP7 loss leads to an increase in anchorage independent growth.	189
4.50	MMP7 loss leads to a huge increase in LCN2 levels but LCN2 loss	190

	does not alter MMP7 levels.	
4.51	MMP7 loss leads to a huge increase in LCN2 levels even at the protein level.	191
4.52	Tumor formation is inhibited in the PKP3 knockdown cells upon MMP7 knockdown	192
4.53	MMP7 but not LCN2 expression decreases upon inhibition of PRL-3 activity.	194
4.54	MMP7 protein expression decreases upon PRL-3 inhibition only in HCT116 cells but not in HaCaT cells.	195
4.55	PRL-3 protein levels do not change upon inhibition of PRL-3 activity.	196
4.56	The ERK1/2 pathway and PKCα/β pathways are activated upon PKP3 loss in HaCaT cells unlike HCT116 cells.	199
4.57	The EGFR/MEK/ERK pathway is activated upon PKP3 loss in HaCaT cells which may lead to activation of the downstream targets ERK1/2 and ELK1.	200
4.58	PKP3 loss causes radio-resistance in HaCaT cell line.	201
4.59	PKP3 loss causes radio-resistance in HCT116 cell line.	202
4.60	PKP3 loss causes radio-resistance in FBM cell line.	203
4.61	The shpkp3-2 derived LCN2 knockdown clones were more radio-sensitive than the vector control clones.	205
4.62	The shpkp3-2 derived MMP7 knockdown clones were more radio-sensitive than the vector control clones.	206
5.1	Detection of D domain motifs in PKP3 amino acid sequence by Motif Scan software	213
5.2	Mechanisms leading to increased tumor formation, metastasis and radioresistance upon PKP3 loss in HCT116 cells	223
5.3	Possible mechanisms leading to increased tumor formation, metastasis and radioresistance upon PKP3 loss in HaCaT cells.	224

1. INTRODUCTION

1.1. Epithelial cell adhesion junctions

The epithelium is a tissue that forms a lining over both the inner and outer surfaces of the body including the skin, intestine, airway passages and glands. The epithelium is made up of epithelial cells which are tightly adhered to each other and to the basement membrane in a definite orientation to form epithelial sheets. Orientation refers to formation of apical-basolateral polarity, a characteristic of epithelial cells [1]. Apical-basolateral polarity of simple epithelial cells is characterized by presence of the basal surface where cell membrane receptors contact the extracellular matrix (ECM); a lateral surface defined by cell receptors being in contact with other cells; and an apical surface facing the hollow lumen (Figure 1.1) [1]. Apical basolateral polarity is only found in the basal progenitor cells, present at the basal layer of a stratified epidermis. An essential requirement for maintaining epithelial polarity is the differentiation of protein and lipid composition of each surface (reviewed in [2]). Epithelial apical basolateral polarity is essential for maintaining tissue homeostasis (reviewed in [3, 4]), epidermal morphogenesis (reviewed in [5]) and tissue functions like maintaining homeostasis between commensal bacteria and immune cells of the gastro-intestinal tract (reviewed in [6]), regulating barrier function and maintaining symmetric and asymmetric cell division in the different compartments of the skin epidermis (reviewed in [7, 8]). Loss of epithelial cell polarity leads to increased neoplastic progression and metastasis (reviewed in [9-11]).

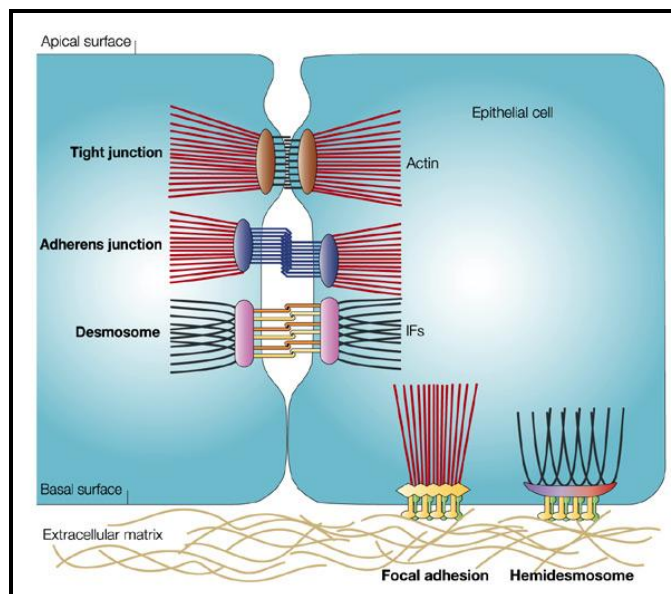


Figure 1.1. Epithelial cell to cell and cell to ECM junctions. Cell to cell adhesion is maintained by the tight junctions, adherens junctions and the desmosomes present at the lateral surface of the plasma membrane of the adjacent epithelial cells, while cell to ECM adhesion is maintained by the focal adhesions and hemidesmosomes present at the basal surface of the plasma membrane [12]

Establishment of the epithelial polarity requires the formation of the apical junctional complexes at the lateral surface of the cells (reviewed in [13-15]). The apical junctional complex consists of the tight junctions and the adherens junction. Tight junctions (or zona occludens) play a very important role in maintaining epithelial polarity by restricting apical/basolateral intramembrane diffusion of lipids and by preventing paracellular diffusion of water and solutes [16]. The transmembrane proteins in the tight junctions are claudins and occludins which link the tight junctions to the actin cytoskeleton via Zonula occludens1 (ZO1) and ZO2 proteins. Decreased expression of the tight junction proteins ZO-1 [17] and occludin [18] are known to cause breast cancer.

Adherens junctions are calcium dependent adhesion junctions that anchor actin filaments and form a strong intracellular actin cytoskeleton. They are made of transmembrane classical cadherins E cadherin, P cadherin and N cadherin. These cadherins bind to actin filaments intracellularly via the catenin and vinculin family proteins. The adherens junction protein E cadherin has been demonstrated to be very important in maintaining epithelial polarity ([19] and reviewed in [20]) and homeostasis (reviewed in [21]). E cadherin expression has been shown to be decreased in colorectal [22] cancer, gastric cancer, non small cell like lung carcinoma [23] and breast cancer [24]. Loss of E cadherin has been shown to disrupt cell polarity and cause increased metastasis [25]. It was demonstrated that expression of multiple transcription factors are induced upon E cadherin loss. One of these transcription factors, Twist is required for E cadherin loss mediated metastasis [25]. Thus, loss of cell to cell adhesion in between epithelial cells can lead to loss of cell polarity and also increased neoplastic progression and metastasis.

Epithelial cell polarity is also maintained by the attachment of cells to the ECM via the focal adhesions and hemidesmosomes present at the basal side of the plasma membrane (reviewed in [26]). The focal adhesions are formed by transmembrane integrins and linked to actin filaments by adaptor proteins talin, filamin and vinculin (reviewed in [27]). Hemidesmosomes are formed by $\alpha 6 \beta 4$ integrins and bullous pemphigoid antigen-2 (BPAG2) and are linked to intermediate filaments through plectin and the epithelial form of bullous pemphigoid antigen-1 (BPAG1e) (reviewed in [27]). The cell to ECM adhesion is important not just to maintain epithelial cell polarity but has been demonstrated to regulate epidermal morphogenesis (reviewed in [28, 29]) and cell motility (reviewed in [30, 31]). Thus, loss of cell to ECM adhesions also leads to increased neoplastic progression and metastasis (reviewed in [26, 32]).

1.2. The Desmosome

Desmosomes are specialized cell-cell adhesion junctions that are present abundantly in cells, which constantly encounter mechanical stress such as epithelial cells and myocardial cells ([33] reviewed in [34, 35]). They are also found in purkinje cells, meningeal cells and the follicular dendritic cells of the lymph nodes and thymus [36-38]. Desmosomes are calcium dependant junctions, thus, cell-cell adhesion is based on the presence of extra-cellular calcium [39-41]. In confluent cultures of epithelial cells and in tissues such as the epidermis, desmosomes become “hyper-adhesive” and acquire calcium independence and do not require calcium for cell-cell adhesion [41-43]. Desmosomes anchor intermediate filaments in adjacent cells of the epithelium and allow the formation of an inter-cellular intermediate filament network, which helps maintain epithelial tissue integrity and helps epithelial cells withstand mechanical stress [44-46]. Desmosomes have been demonstrated to regulate epithelial polarity (reviewed in [47, 48]), epidermal morphogenesis and cell positioning [20]. It was demonstrated that desmosomes can regulate alveolar morphogenesis by the luminal epithelial cells and cell positioning of the luminal and myo-epithelial cells of the breast [20].

1.2.1. Ultra-structure and molecular architecture of the desmosome.

The desmosome is made up of proteins belonging to four major protein families: the desmosomal cadherins, armadillo repeat (ARM) containing proteins and the plakin family of proteins (Figure 1.1) [49, 50]. Under the electron microscope, desmosomes appear as a pair of electron dense plaques that are bilaterally symmetrical to each other and present at the cell-cell border of adjoining epithelial cells (Figure 1.2). The plasma membranes of adjacent cells are separated by an intercellular space of approximately 30 to 35 nm. In mature desmosomes, this space is bisected by an electron dense midline (DM). The DM represents the site of interaction between

the desmosomal cadherins, the desmogleins (Dsg) and desmocollins (Dsc). The Dsgs and Dscs engage in calcium dependent homophilic and heterophilic adhesive interactions.

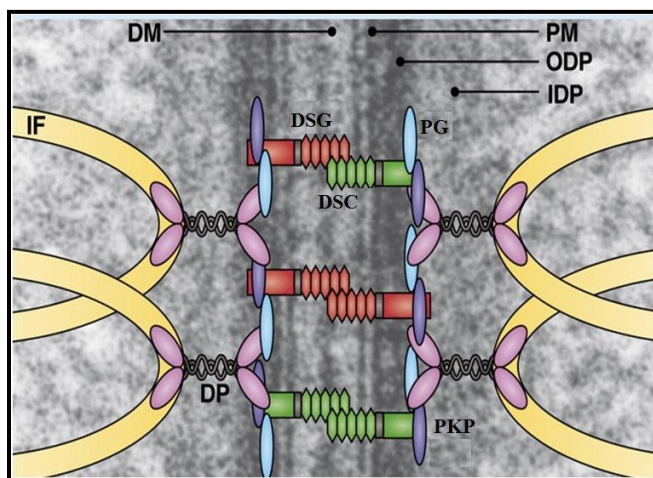


Figure 1.2. Desmosome ultra structure and molecular composition. The figure depicts a cartoon representing the molecular architecture of the desmosome superimposed on an electron micrograph of the desmosome. Abbreviations: DM= dense midline, PM= plasma membrane, ODP= outer dense plaque, IDP= inner dense plaque, DSG=desmoglein, DSC=desmocollin, PG=plakoglobin, PKP=plakophilin, DP=desmoplakin (adapted from [51]).

The intracellular side of the plasma membrane consists of two large discoid or oval shaped electron dense plaques called outer dense plaque (ODP) (closer to the plasma membrane) and inner dense plaque (IDP) (further away from the plasma membrane than ODP). Both ODP and IDP are approximately 15 to 20 nm thick and the distance between these two plaques are approximately 8 nm thick. The ODP represents the site where the intracellular domains of DSGs and DSCs interact with armadillo repeat family proteins plakoglobin (Pg) and plakophilin (Pkp) and the plakin family protein desmoplakin (DP). The IDP is at about 50 to 70 nm away from the plasma membrane. At the IDP, DP interacts with intermediate filament (IF) proteins like keratin

and vimentin, thus linking the desmosome with intermediate filaments [51]. The intermediate filaments loop at the inner face of the IDP in the form of an electron dense wide arc and seem to spread out in the cytoplasm ([49, 52-55] and reviewed in [56]).

1.2.2. Desmosomal cadherins:

The cadherin protein family consists of glycosylated transmembrane proteins [57, 58]. Cadherins are broadly classified into six subfamilies namely classical cadherins (type I cadherins), atypical cadherins (type II cadherins), desmogleins (DSGs), desmocollins (DSCs), protocadherins and flamingo cadherins (reviewed in [59]). DSGs and DSCs are the cadherins present in the desmosome and are therefore called desmosomal cadherins (reviewed in [59, 60]). In humans there are four DSG genes (DSG1-4) [61-65] and three DSC genes (DSC1-3) and all DSC gene products undergo alternate splicing to form two splice variants. The longer form is designated as “a” and the shorter form “b” (Figure 1.4) [63, 66-68]. Unlike the “a” form, the “b” form lacks binding site for Pg and Pkps, but can still localize to functional desmosomes [69].

Desmosomal cadherins are structurally very similar to classical cadherins (Figure 1.3). The N terminus of DSGs and DSCs are made of five highly conserved extracellular cadherin (EC) like domains named EC 1-5. The fifth EC domain which is closest to the plasma membrane is also called the extracellular anchor (EA) domain. The EC and EA domains are connected by flexible linker peptides which serve as binding sites for calcium ions. Each binding site can hold three calcium ions. The EC domains are important for the homophilic and heterophilic interactions between cadherins. This interaction between cadherins of adjacent cells leads to formation of the dense midline in a desmosome. Multiple EC domain repeats are followed by a short transmembrane motif (TM) which spans the membrane only once. The cytoplasmic side of DSGs

and DSCs are made up of intracellular anchor (IA) domain and an intracellular catenin binding site (ICS). The intercellular proline rich linker (IPL), a variable number of repeat unit domains (RUDs) and a desmoglein terminal domain (DTD) are present exclusively in DSGs.

The intracellular domains of the desmosomal cadherins associate with the armadillo repeat containing proteins and the plakin family proteins ([70] and reviewed in [59, 71]). The desmosomal cadherins have cell type and tissue type specific expression patterns. DSG2 and DSC2 are expressed in most human tissues, while, DSG1, DSG3, DSC1 and DSC3 are only expressed in the stratified epithelium. DSG4 is expressed only in the highly differentiated epithelial cells and in the hair shaft cortex, the lower hair cuticle, and the upper inner root sheath (IRS) cuticle [72-76].

The expression of desmosomal cadherins is stringently regulated during the formation of the epidermis. At approximately 5 to 8 weeks after embryonic gene activation, the developing epidermis exists as a two layered structure, one layer made up of peridermal cells and the other made up of basal cells. The peridermal cells stop proliferating, become

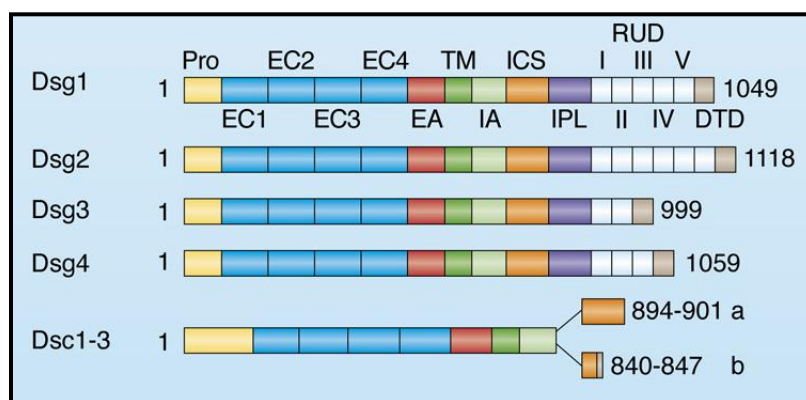


Figure 1.3. Structural domains, isoforms and splice variants of desmosomal cadherins.

Each of the four DSG genes and three DSC genes encode separate desmosomal cadherin

isoforms. All DSC isoforms are alternatively spliced to “a” and “b” forms. The “b” form has a shorter ICS domain. Abbreviations: Pro= propeptide, EC= extracellular cadherin, EA= extracellular anchor, TM= transmembrane, IA= intracellular anchor, ICS= intracellular catenin binding site, IPL= intercellular proline rich linker, RUD= repeat unit domain [51].

flattened, develop into the first layers of the cornified epithelium and are eventually shed off. The basal cells give rise to the three layers of the epidermis namely the spinous layer, the granular layer and the cornified layer (stratum corneum). During this process, the highly proliferating stem like cells of the basal layer gradually migrates to the upper layers undergoing differentiation at each layer of the epidermis. These cells undergo terminal differentiation just before entering into the stratum corneum [77-79]. During epidermal morphogenesis, desmosomal cadherins undergo stratification dependent alterations in gene expression (Figure1.4). DSG1 expression increases while DSC2 level decreases as cells move from the basal layer to the granular layer. DSG2 is only expressed in the basal layer. DSG3 and DSC3 levels decrease as cells move from basal layer to spinous layer. Both these proteins are not expressed in the granular layer. DSG4 is expressed only in the granular layer. DSC1 is not expressed in the basal layer but its expression increases as cells move from the spinous layer to the granular layer [80]. The differentiation dependant expression of desmosomal cadherins raised the possibility that DSGs and DSCs may have direct or indirect roles in epidermal differentiation. To understand the function of different DSG and DSC isoforms, individual gene knockout mice models were generated and the phenotypes were analyzed (Table 1.1). While, DSG3 knockout mice have hair loss, acantholysis of the suprabasal layers of the oral and acantholysis of skin epidermis resulting in skin crusting [81]; the DSC1 knockout mice develop acantholysis of the granular layer of the skin epidermis leading to flaky skin and skin barrier

defects [82]. DSG2 knockout mice die as embryos just after implantation into the uterus [83] while DSC3 mice die at embryonic day (E2.5) stage even before formation of mature desmosomes [84]. The phenotypes observed in DSG2 and DSG3 mice, show that these desmosomal cadherins may play desmosome independent roles and may also regulate stem cell functions.

Desmosomal cadherins are very important regulators of epidermal differentiation (reviewed in [60]). DSG1, which is present abundantly in the granular layer of the epidermis, promotes terminal differentiation. DSG1 binds to the protein, Erbin at the cell surface of differentiating cells. The membrane localized Erbin binds to SHOC2 (a scaffolding protein which allows the formation of RAS/RAF complexes, thus activate the ERK signaling pathway). The DSG1-Erbin-SHOC2 interactions deplete the availability of SHOC2 to bind to RAS/RAF, thus inhibiting ERK activation. ERK inhibition in turn leads to terminal differentiation of keratinocytes. DSG1 loss due to haplo-insufficiency in patients suffering from Striate palmoplantar keratoderma (SPPK) (Table 1.2), lead to less Erbin-SHOC2 interactions and strong ERK activation [85]. DSG3, which is expressed maximally in the basal layers of the skin epidermis and absent in the upper layers, inhibit keratinocyte terminal differentiation. To analyze the role of DSG3 in epidermal differentiation, transgenic mice having keratin 1 promoter driven over-expression of DSG3 was generated. Since keratin 1 is expressed in the spinous and granular layers of the epidermis, DSG3 expression was forced to be expressed in these layers. The skin and hair follicles of these transgenic mice showed phenotypes of hyper-proliferation and abnormal differentiation [86]. DSG3 expression driven by involucrin promoter (expression in stratum corneum) exhibited lack of terminal differentiation in the skin epidermis [87]. Thus desmosomal cadherins regulate epidermal differentiation.

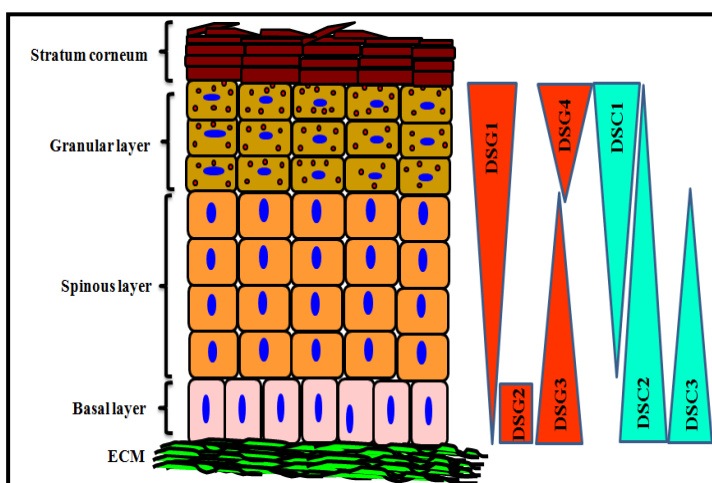


Figure 1.4. Differential expression of desmosomal cadherins in skin epidermis. Desmoglein and desmocollin isoforms show stratification specific expression in the different layers of the epidermis.

Genes encoding desmosomal cadherin	Type of knockout	Phenotypes
DSG2	Global knockout	Embryos die shortly after implantation. Desmosomal independent changes are believed to occur during embryonic stem cell proliferation in the DSG2 knockout mice because at desmosome formation takes place at least 4 weeks after embryonic gene activation in mice [83].
DSG3	Global knockout	Normal at birth, but develop acantholysis of the sub-basal layer of the oral mucosa leading to oral lesions. Crusting and acantholysis of traumatized skin. Hair loss in telogen from postnatal day 20 [81].
DSC1	Global knockout	Embryos born with eyes open and develop flaky skin with punctuate barrier defects. Acantholysis in the granular layer, resulting in epidermal fragility. Develop ulcerating lesions resembling chronic dermatitis. Exhibit local hair loss from 6 weeks of age [82].
DSC3	Global knockout	Embryos die before E2.5, even before formation of the mature desmosome [84].

Table 1.1. Phenotypes of mice having knockout of individual desmosomal cadherin genes.

The table represents the phenotypes associated with global knockout or tissue specific knockout of different desmosomal cadherins in mice models.

Desmosomal cadherins are associated with multiple human diseases (Table 1.2). DSG2 and DSC2 are the only desmosomal cadherins expressed in the myocardium, thus mutations in DSG2 and DSC2 genes lead to severe heart defects like Arrhythmogenic right ventricular dystrophy/cardiomyopathy (ARVD/C) [88, 89]. ARVD/C is a heritable heart disease that affects the myocardial cells of the right ventricle leading to right ventricular enlargement, irregular heartbeats and life threatening cardiac arrests. ARVD/C starts with loss of function mutants in cardiac desmosomes of the right ventricle which leads to detachment of cardiac myocytes and subsequent death of the myocytes. The damaged muscle is replaced by fibro-fatty tissue (reviewed in [90]). DSC2 mutations also cause the wooly hair syndrome in which the hair of the scalp appears wiry and frizzled like wool [91]. In the skin, haplo-insufficiency of DSG1 results in SPPK characterized by thickening of the stratum corneum of the palm, knees, soles, ankles and finger knuckles [92]. Mutations in DSC2 are also known to cause SPPK [91]. Mutations in DSC3 and DSG4 (a major component of the inner root sheath of the hair follicles) leads to hair loss or hypotrichosis [93, 94].

Circulating autoantibodies against DSG1 and DSG3 are known to cause severe skin blistering diseases like pemphigus vulgaris (PV) and pemphigus foliaceus (PF) [62, 95, 96]. Both PV and PF cause acantholysis (disruption of cell to cell adhesion) and internalization of desmosomal components from the cell surface leading to loss of desmosomes [97-99], but differ in two ways: PV antibodies target both DSG1 and DSG3 proteins while PF antibodies only target the DSG1 protein ; PV antibodies lead to supra-basal skin blistering and blistering of the oral mucosa, while PF antibodies lead to only superficial skin blistering (Figure 1.5). The reason behind this is; In PF, antibodies target only DSG1, the other desmosomal isoform DSG3 (which is the major desmosomal cadherin of the basal layers), compensates for the loss of DSG1. In PV, antibodies

target both DSG1 and DSG3, other DSG isoforms cannot compensate for the loss and this causes severe suprabasal blistering of the skin (reviewed in [100, 101]).

Skin blistering and acantholysis can also be caused by proteolytic action of exfoliative toxins (ETs) produced by bacteria like *Staphylococcus aureus*. If the skin blisters appear to localize only to the arms, legs or trunk, then the disease is called Bullous impetigo, but if the skin blisters occur extensively throughout the body and cause superficial blistering and exfoliation, then the disease is called Staphylococcal scalded skin syndrome (SSSS) (reviewed in [102-104]). Three homologous ETs have been successfully cloned till date and characterization of these ETs have increased our knowledge about these diseases [105, 106]. These staphylococcal ETs are serine proteases [107, 108] and have been demonstrated to cleave the extracellular region of the DSG1 protein [109, 110] at glutamate 381 residue which lies between EC3 and EC4 domains of DSG1 [111]. The cleavage mechanism is not only dependent on the amino acid sequence but also on the conformation of DSG1. The ETs can cleave DSG1 only when it exists in a calcium bound conformation [112, 113]. Thus alterations of desmosomal cadherins can lead to multiple heart and skin related diseases. A thorough understanding of the mechanisms regulating PV, PF, Bullous disease and SSSS can help develop ways to combat these diseases.

One excellent example when understanding the mechanism of a disease has helped in developing strategies for treatment of the disease is in PV. The PV antibodies targeting DSG3 (the most common target in PV) has been shown to activate the p38MAPK pathway. Active p38MAPK in turn phosphorylates Hsp27 (heat shock protein 27) and causes keratin filament retraction and actin re-organization. To inhibit the p38MAPK signaling pathway, a specific inhibitor SB202190 [114] was used. These were able to prevent PV disease in mice [115] and block keratin filament retraction and actin cytoskeleton reorganization [116]. The p38MAPK signaling

pathway has been considered to be a good target in developing treatment modalities for PV patients (reviewed in [117]).

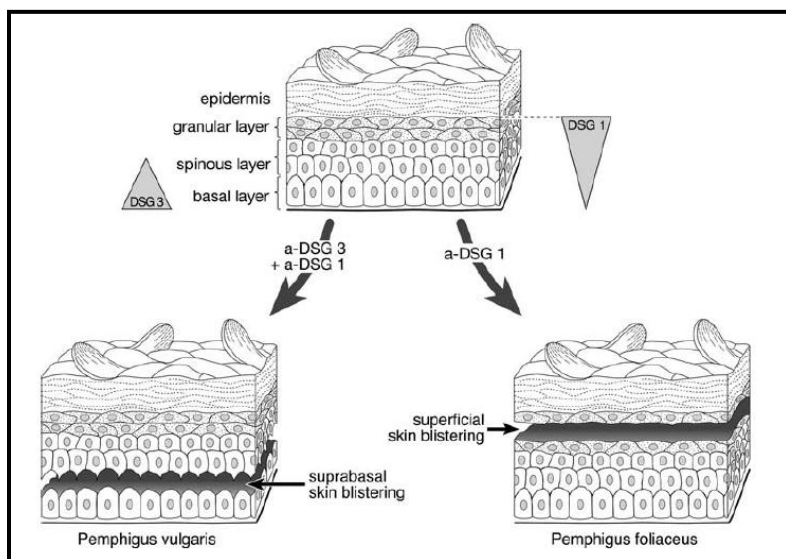


Figure 1.5. The desmoglein compensation hypothesis. In the disease PF, auto-antibodies against DSG1 can only cause superficial skin blistering (the cleavage plane of the epidermis is at the granular layer). In PV, auto-antibodies targeted against both DSG1 and 3 lead to supra-basal skin blistering (the cleavage plane is just above the basal layer) [101].

Expression levels of desmosomal cadherins also get altered in multiple cancers (Table 1.3). Decrease in mRNA/protein expression of DSG1 is associated with pancreatic cancer and anal cancer. In colon and skin cancers, DSG2 levels increase while in pancreatic and gastric cancer, DSG2 level decreases. Similarly, increase in DSG3 levels lead to head and neck squamous cell carcinoma (HNSCC) and esophageal carcinoma while its decrease is associated with breast cancer. DSC isoforms are known to be tumor suppressors (reviewed in [118]).

Decrease in DSC1 expression is associated with lung cancer and anal cancer, while decrease in DSC2 is associated with colon cancer. In a manner similar to DSC1; a decrease in DSC3

expression is associated with lung cancer and prostate cancer. Loss of DSC2 in colon cancer cells lead to activation of the AKT/ β catenin signaling pathway which in turn leads to increased neoplastic progression [119]. DSC2 loss in sporadic colorectal adenocarcinoma is also associated with a phenomenon called desmocollin switching [120].

Desmosomal cadherin	Disease name (cause of disease)
DSG1	Pemphigus foliaceus (Auto-antibodies) [96] Pemphigus vulgaris (Auto-antibodies) [121] Bullous impetigo (Exfoliative toxin) [109, 110] SSSS (Exfoliative toxin) [109, 110] SPPK (haplo-insufficiency) [92]
DSG2	ARVC/D (Frame shift/ splicing/nonsense/missense mutations/ compound heterozygosity) [89]
DSG3	Pemphigus vulgaris (Auto-antibodies) [122-124]
DSG4	Hypotrichosis (intragenic deletion/ missense mutations) [93]
DSC2	ARVC/D (Missense mutations) [88] Wooly hair syndrome with cardiomyopathy and SPPK (Frame shift mutations) [91]
DSC3	Hypotrichosis with skin vesicles (nonsense mutations) [94]

Table 1.2. Diseases associated with desmosomal cadherins. The table represents the diseases associated with desmosomal cadherin alterations and the experimentally validated causes of the disease.

DSC2 is the only isoform of DSCs found in normal colon epithelium. But upon DSC2 loss in colon cancers, de novo expression of DSC1 and DSC3 is observed. This desmocollin switching is postulated to promote neoplastic progression. Loss of DSG2 in colon cancers decreases neoplastic progression [125]. Investigation of the mechanism regulating this process revealed that DSG2 knockdown leads to increased DSC2 expression. Increased DSC2 in turn activated the EGFR pathway and inhibited cell proliferation [125]. These experiments showed that DSG2 has

a pro-tumorigenic role while DSC2 acts as a tumor suppressor protein in colon cancer via activating the EGFR pathway. Thus, alterations in mRNA/protein expression of desmosomal cadherins are associated with various signaling pathways which may either lead to increase or decrease in neoplastic progression.

Desmosomal cadherin	Types of cancers associated with:	
	Increased expression	Decreased expression
DSG1		Pancreatic cancer [126], Anal cancer [127]
DSG2	Colon cancer [125], skin cancer [128]	Pancreatic cancer [126], gastric cancer [129]
DSG3	Head and neck cancers [130], esophageal squamous cell carcinoma [131]	Breast cancer [132]
DSC1		Lung cancer [133], Anal cancer [127]
DSC2		Colon cancer [119]
DSC3		Lung cancer [133], Prostate cancer [134]

Table 1.3. Cancers associated with alterations in desmosomal cadherins. The table represents the type of cancers associated with alterations in expression of desmosomal cadherins.

1.2.3. Plakin family of proteins:

The plakin family consists of proteins having long polypeptide sequences. They join the intermediate filaments to membrane associated desmosomal plaque proteins thus playing the role of anchor proteins for both the desmosomes (cell to cell adhesion) and hemi-desmosomes (cell to ECM adhesion). The plakin family proteins present in most desmosomes are desmoplakin and plectin. The proteins periplakin , envoplakin and epiplakin are present only in cornified layers of the stratified epithelia [135].

1.2.3.1. Desmoplakin (DP):

DP is an essential component of the desmosomal plaque. It is important for desmosomal functioning and adhesion [136]. Two alternative splice variants of DP exist namely DPI and DP II. DP II has a shorter rod domain than DPI and has been proposed to exist even as monomers [137, 138] (Figure 1.6).

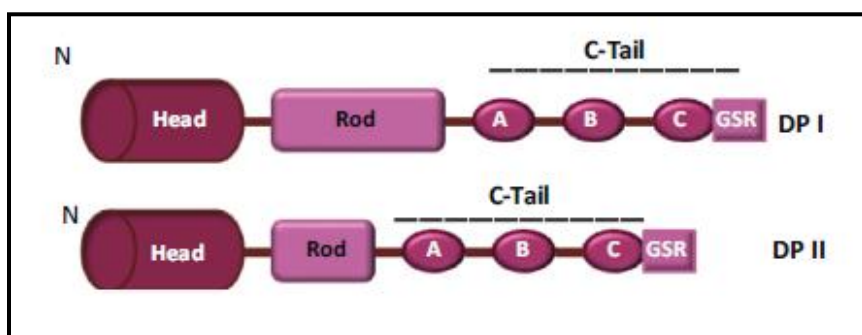


Figure 1.6. Alternative splice variants of DP and their domain structure. The figure represents the two splice variants of DP: DPI and DP II. It also depicts the domain structure of DP. DP is made up of the N terminus head domain, the rod domain, the plakin repeat domains (A, B, C) followed by the glycine-serine-arginine (GSR) domain. DP II has a shorter rod domain [139].

The structure of DP is considered to be the best model for plakin family proteins. DP is made up of a head domain, a plakin domain followed by three plakin repeat domains (PRDs) and a glycine-serine-arginine domain (GSR) [140] (Figure 1.6). The N terminus head domain, also known as the plakin domain, is a long α helical coiled coil domain and is a characteristic feature of the plakin family of proteins. The plakin domain is made of spectrin repeats and a putative SH3 domain (Figure 1.7). DP binds to other desmosomal proteins like DSC1a, PG and PKPs via the plakin domain and is needed for recruitment of DP to the membrane associated desmosomal

plaques [141, 142]. In the DP protein structure, the plakin domain is followed by the central coiled coil rod domain which is important for protein dimerization. At the C terminal domain of DP, multiple plakin repeat domains exist followed by the GSR domain. These act as binding sites for intermediate filaments [143, 144].

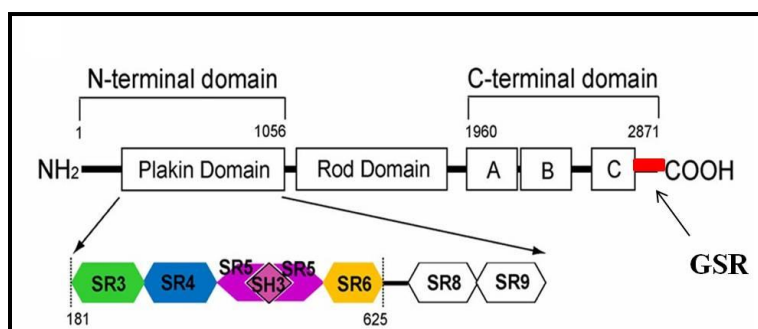


Figure 1.7. The spectrin repeats in plakin domain of DP. The plakin domain at the N terminus of DP has 6 spectrin repeats (SRs) and consists of an Src homology region (SH3) within spectrin repeat 5 (SR5) (adapted from [140]).

Both DPI and DPII are present in all stratified and simple epithelial tissues [145]. In stratified epithelium, DP expression is highest in the granular layer and least in the basal layer (Figure 1.8) [146]. In non-epithelial cells like the human umbilical vein endothelial cells, both DPI and DPII are expressed. In myocardial and Purkinje fiber cells of the heart, only DPI is expressed where it associates with the intermediate filament component desmin [147]. DPI is also exclusively found in the meningeal cells and follicular dendritic cells where it associates with the intermediate filament component vimentin [148]. DPI mediates endothelial cell to cell adhesion by interacting with VE-cadherin, PG, p0071 and vimentin. These types of junctions are called complexus adhaerentes [33, 149-151].

The importance of DP in vivo was demonstrated by performing genetic knockout of the DP gene in mice (Table 1.4). The DP-null embryos do not survive for more than embryonic day 6.5 (E6.5). In these mice there is a significant loss of desmosomes and the structure of the desmosomes were also impaired. It was also demonstrated that in the DP-null embryos, keratin 8 (K8) / keratin 18 (K18) were not able to form the characteristic filamentous meshwork [152]. A similar phenotype was observed in mouse having epidermal specific knockout of the DP gene. In this case, the desmosomes lacked attachment to IFs and were susceptible to mechanical stress induced disruption [153]. Thus DP is an important desmosomal component that is required to maintain tissue integrity.

DP is important for maintaining tissue integrity because it is a cytolinker protein which joins the desmosome to the intermediate filaments (IFs) and this allows desmosomes to withstand mechanical stress (reviewed in [154]). It had been demonstrated that the C terminal domain of DP is required for association of DP with IF proteins like keratin and vimentin. Upon expression of the C terminal domain of DP (DP CT) in cultured cells like COS-7 and NIH3T3 cells, it was observed that the DP CT co-localizes with IFs. Desmosomes in cells having DP CT expression did not show filamentous meshwork of IFs, instead they were disrupted. It was postulated that when the expression of DP CT was high, it led to disruption of IFs [155]. Unlike DP CT, an N terminus deleted mutant of DP (DP Δ N) was able to form the filamentous meshwork of IFs [155]. The interaction of IFs with the C terminal domain of DP was also found to be important for determining the spatial distribution of DP in to desmosomes, because expression of an N terminal fragment of DP (DP NTP) in cells led to DP NTP forming complexes with both desmosomal proteins and adherens junctions proteins [156]. Thus the C terminal domain of DP

is essential for both IF binding and to maintain separation of the spatial distribution of desmosomal and adherens junction proteins.

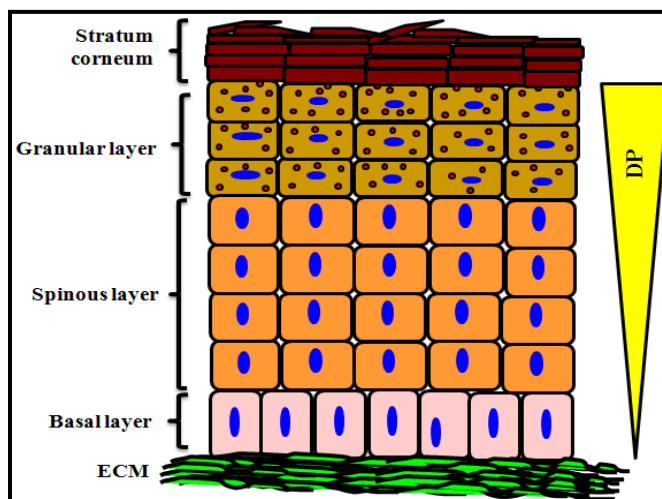


Figure 1.8. Expression of DP in the different layers of the stratified epithelium. DP expression is highest in the granular layer of the epidermis and decreases gradually in the lower layers.

DP binds to both keratin and vimentin IFs but their binding sites in DP protein were found to be different. The last 68 amino acids (which does not include the A, B and C domains) at the C terminus of DP was essential and sufficient for interaction with keratins, but for the interaction with vimentin, the C terminal plakin repeat domains A, B, C and the rod domain of DP was needed [144].

Gene encoding	Type of knockout	Phenotypes
DP	Global knockout	Embryos die at E6.5. Display abnormalities in desmosomal assembly and stability. Cells show a reduction in cell proliferation [152].
DP	Conditional knockout under the control of K14 promoter	Embryos show epidermal separation upon mechanical stresses and is most prominent in the basal layer. Desmosomes lack attachment to intermediate filaments [153].

Table 1.4. Phenotypes of mice having knockout of DP. The table represents the phenotypes associated with global knockout or tissue specific knockout of DP.

Component	Disease name (cause of disease)
DP	ARVC/D (Missense mutation) [157] Wooly hair syndrome with or without cardiomyopathy (C terminal truncation) [158] SPPK (Haplo insufficiency, Nonsense mutations) [159, 160] Lethal acantholytic epidermolysis bullosa (C terminal truncation/ nonsense mutation) [161] Carvajal syndrome (C terminal truncation) [162] Paraneoplastic pemphigus (Auto-antibodies) [163]

Table 1.5. Diseases associated with DP. The table represents the diseases associated with DP and the experimentally validated causes of the disease.

The N terminal domain of DP interacts with the head domains of both plakophilin 1 (PKP1) [141, 164] and plakoglobin (PG) [142] and these interactions are important for localization of DP to desmosomes at the cell border [144]. High DP NTP expression was found to disrupt endogenous DP localization at the cell to cell border [156].

DP is an essential component of both epidermal and myocardial desmosomes (reviewed in [154]). Thus, loss of DP or mutations that cause loss of function of DP leads to many diseases

(Table 1.5). Genetic haploinsufficiency of DP leads to SPKK [159]. Since C terminal of DP is essential for binding of desmosomes to IFs, truncation of the C terminal domain of DP lead to many diseases like the wooly hair syndrome with or without cardiomyopathy [158], lethal acantholytic epidermolysis bullosa [161] and Carvajal syndrome (a syndrome in which patients suffer from dilated cardiomyopathy, SPKK and wooly hair syndrome)) [162] . A missense mutation at the N terminal of DP causes the heart disease ARVC/D [157] while a heterozygous nonsense mutation in DP caused SPKK and was found to be associated with abnormal epidermal differentiation and alteration in keratin filament organization [160]. Auto-antibodies targeting DP has been known to cause diseases like the paraneoplastic pemphigus vulgaris [163].

Desmosomal component	Types of cancers associated with:		
	Increased expression	Decreased expression	LOH
DP		Uterine adenocarcinoma [165], OSCC [166], breast cancer [167], lung cancer [168]	

Table 1.6. Cancers caused by alterations in DP. The table represents the type of cancers associated with alterations in expression of DP.

Since DP expression is obligate components of the desmosomes. Decreased expression of DP leads to loss of desmosome number and impairment of desmosomal structure (a characteristic feature of many cancers). Thus DP loss is associated with neoplastic progression in multiple cancers (Table 1.6) like uterine adenocarcinoma [165], oral squamous cell carcinoma OSCC [166], breast cancer [167] and lung cancer [168]. One of the mechanisms by which loss of DP is known to cause neoplastic progression is by activation of the Wnt/ β catenin signaling [168]. In the non-small cell lung carcinoma cell line, NSCLC, it was demonstrated that DP loss leads to activation of the Wnt/ β catenin signaling which resulted in increased TCF/LEF transcriptional

activity and increased expression of Wnt target genes MMP14 and plakoglobin. As a consequence of this signaling the DP knockdown clones were demonstrated to have increased cell proliferation, migration and decreased sensitivity to drug induced apoptosis [168]. In the skin keratinocyte cell line, HaCaT, loss of DP was also shown to increase cell proliferation but by increasing activation of ERK and AKT signaling pathway. [169]. Thus different signaling pathways are activated in different cell types upon loss of DP leading to increased cell proliferation, migration and increased neoplastic progression.

1.2.4. The Armadillo repeat proteins

The founding member of the Armadillo protein family is named because embryos hemizygous for the armadillo gene resembled the placental mammal, armadillo [170, 171]. β catenin (a component of the adherens junction) is known to be the human homologue of the Armadillo protein. Its amino acid sequence is 71% identical to the *Drosophila* Armadillo protein [172]. The armadillo repeat proteins contain multiple repeats of armadillo domains. These armadillo domains are made up of similar but non-identical sequences of 42 amino acids. Each repeat forms three alpha helices and these alpha helices are coiled together to form a superhelix (Figure 1.9). Non-helical insert sequences can bend these super helices to different degrees to form negatively or positively charged grooves which form binding sites for other proteins [173]. Two members of the armadillo repeat family namely the plakoglobin (PG) and the plakophilins (PKPs) are important constituents of the desmosome (reviewed in [51]).

1.2.4.1. Plakoglobin (PG):

PG, also known as γ catenin, is an important component of the desmosomal junctions and is also found in adherens junctions [174]. In the adherens junction, PG interacts with α catenin, E-cadherin, N cadherin and P cadherin [175-178] while in desmosomes, PG binds to desmogleins and desmocollins, plakophilins and desmoplakin. [142, 179-181]. The PG protein has 65% similarity to β catenin at the amino acid level [182]. It has a central arm repeat domain (13 repeats) and are flanked by long N terminal and C terminal domains (Figure 1.10) [183]. The arm domain forms a positively charged groove which serves as binding sites for desmosomal cadherins, adherens junction cadherins, members of the Wnt/ β catenin signaling pathway like Adenomatous polyposis coli (APC) [184, 185], transcription factors like T cell factor (TCF) and Lymphoid enhancer binding factor (LEF) [186].

PG is found in all cell and tissue types including the skin epidermis and the myocardium. In the stratified epithelium, expression of PG increases as cells move from the basal layer to the granular layer (Figure 1.11) [187]. The importance of PG in the skin epidermis and myocardium can be understood upon examining the phenotypes of the PG knockout mice made in C57B/L6 strain of mice (Table 1.7). PG-null embryos die sometime in between E10.5 till before birth [188]. Most embryos die due to heart defects at about E10.5, but some survive and after E17.5 (the time when the adult pattern of epidermal differentiation starts), these embryos have very fragile skin and show severe skin blistering phenotypes

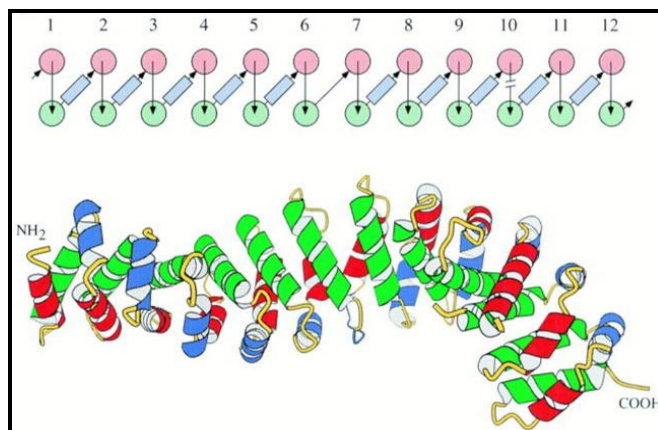


Figure 1.9. Secondary structure of a typical armadillo protein, β catenin. The secondary structure of β catenin consists of 12 repeats of three alpha helices which coils together to form a superhelix [173]



Figure 1.10. Structural domains of PG. PG is made up of armadillo repeats flanked by a head and a tail domain at N and C terminus respectively [51].

like acantholysis and apoptosis of cells of the granular layer and loss of the stratum corneum [189]. In vivo cytochemical and immuno-histochemical studies of the skin of PG^{-/-} mice [189] and in vitro studies by culturing the PG^{-/-} skin keratinocytes [190] have demonstrated that although PG^{-/-} keratinocytes form cadherin clusters due to a compensatory effect of β catenin binding to the desmosomal cadherins, they lack effective binding to intermediate filaments and are more susceptible to cell rupture than those of PG^{+/+} cells. The reason behind this effect was found to be decreased localization of plakophilin1 (PKP1) and DP to the desmosomes. Thus,

presence of PG in the desmosome is essential to withstand normal mechanical stresses generated during stratification of epidermis because PG regulates intermediate filament binding to the desmosome via DP and PKP1 [189].

PG is also important for initiating desmosome assembly and function in skin keratinocytes [188-190]. It has been demonstrated that PG binding to E-cadherin or P cadherin in the adherens junction is essential for initiation of desmosome formation [191]. In the myocardium, PG has been shown to regulate cell differentiation by regulating the Wnt signaling pathway. It has been demonstrated that nuclear plakoglobin can interact with the transcription factor, c-kit, in the cardiac progenitor cells (CPCs) to inhibit the canonical Wnt signaling pathway and activate a pro-adipogenic gene expression. This causes CPCs to differentiate into adipocytes leading to ARVC/D [192]. Since PG is an important component of the desmosome in both the epidermis and myocardium, mutations that cause loss of function of PG lead to many skin and heart diseases (Table 1.8). A C terminal truncation mutation in PG gene has been documented to cause Naxos disease (a cardiocutaneous disease consisting of the heart disease ARVC/D and cutaneous abnormalities like the palmoplantar keratoderma (PPK) and wooly hair) [193]. A novel dominant mutation involving addition of one Serine at amino acid position 39 was found to cause only ARVC/D without cutaneous abnormalities [194]. Nonsense mutations in the PG gene has been known to cause diseases like cardiomyopathy with PPK and Alopecia totalis (total baldness) [195] and also lethal congenital epidermolysis bullosa [196]. Auto-antibodies against PG are known to cause the skin blistering pemphigus vulgaris [197, 198].

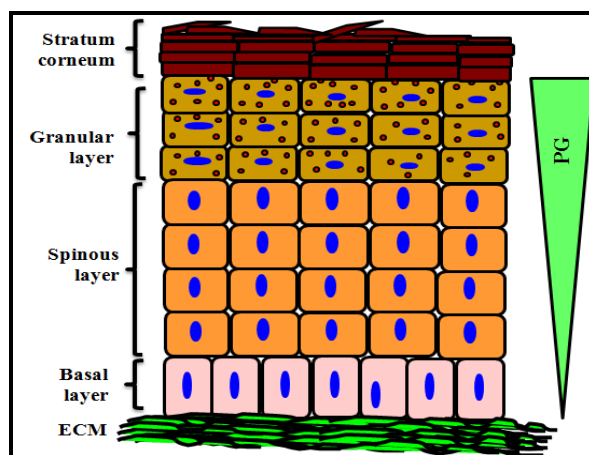


Figure 1.11. Expression of PG in the different layers of the stratified epithelium. An expression gradient of PG exists in the epidermis where PG expression increases in the upper layers of the epidermis.

PG is a tumor suppressor (reviewed in [199]). PG expression at the mRNA/protein level decreases in thyroid cancer [200], bladder cancer [201, 202], neuroblastoma [203], lung cancer [204], oral cancers [205] and renal cancer [206]. Decrease in PG expression can also occur due to LOH like in the cases of prostate cancer [207], ovarian cancer and breast cancer [208] (Table 1.9). Some of the tumor suppressor activities of PG have been correlated to its role in competing with β -catenin for binding to the TCF/LEF transcription factors ([186] and reviewed in [199]). It has been demonstrated that in NSCLC cell line (where PG levels are very low or absent), exogenous expression of PG decreased the β catenin/TCF signaling and consequently decreased the anchorage independent growth of the NSCLC clones [209]. Thus, in addition to regulating tissue integrity, PG also regulates the Wnt/ β -catenin signaling pathway and acts as a tumor suppressor in multiple cancers.

Gene encoding armadillo repeat protein	Type of knockout	Phenotypes
PG	Global knockout	Embryos die between E10.5 and birth. Develop severe heart defects, skin blistering and sub-corneal acantholysis. The embryos also show defects in desmosome number and morphology [188].
PKP2	Global knockout	Embryos die at E11 due to altered heart morphogenesis [210].
PKP3	Global knockout	Normal at birth. Hair coat pelage occurrence was delayed and the resulting hair follicles were morphologically abnormal. In the stages P8 to P10, PKP3 null mice showed increased cell proliferation of basal keratinocytes, thus leading to increased thickness of the suprabasal layers of the epidermis. But, in epidermis of adult PKP3 null mice, no such changes were observed. The number of desmosomes in the basal layers of the epidermis was decreased to half, while in the suprabasal cells, desmosome numbers were unaltered. PKP3 null mice also had increased susceptibility to cutaneous inflammation and showed phenotype similar to atopic dermatitis [211].

Table 1.7. Phenotypes of mice having knockout of individual armadillo repeat protein encoding genes. The table represents the phenotypes associated with global knockout or tissue specific knockout of different armadillo repeat protein encoding genes in mice models.

Desmosomal component	Disease name (cause of disease)
PG	Naxos disease (C terminal truncation mutation) [193] ARVC/D without cutaneous abnormalities (Addition of one Serine at amino acid position 39) [194] Cardiomyopathy with PPK and Alopecia totalis(Nonsense mutation) [195] Lethal congenital epidermolysis bullosa (Nonsense mutation) [196] Pemphigus vulgaris (Auto-antibodies) [197, 198]

Desmosomal component	Disease name (cause of disease)
PKP1	Skin fragility ectodermal dysplasia syndrome (Frameshift/ Nonsense mutations/ Splicing/ compound heterozygosity) [212, 213]
PKP2	ARVC/D (Frameshift/ Missense/Nonsense mutations/ Splicing) [214]
PKP3	Paraneoplastic pemphigus (Auto-antibodies) [215]

Table 1.8. Diseases associated with desmosomal proteins. The table represents the diseases associated with desmosomal alterations and the experimentally validated causes of the disease

1.2.4.2. Plakophilins (PKPs):

PKPs belong to the p120 catenin (ctn) family of armadillo proteins. The p120ctn is further classified into two classes: the plakophilins and the p120ctn related proteins [216, 217]. Three isoforms of plakophilins exist, namely PKP1 (earlier known as the “band 6” protein), PKP2 and PKP3 [218-220]. A protein called p0071 is sometimes classified into the PKP sub-family and is called PKP4 although p0071 is more related to the p120ctn related proteins (Figure 1.9) [221]. PKPs have a central nine armadillo repeats flanked by a long N terminal and a very short C terminal domains. Between the 5th and the 6th arm repeat PKPs have a polypeptide sequence which causes a kink in the protein structure [222]. The N terminal domain of the PKP isoforms is majorly non-conserved except for a highly conserved small region near the amino terminus called the homologous region 2 (HR2) (Figure 1.9).

Desmosomal component	Types of cancers associated with:		
	Increased expression	Decreased expression	LOH
PG		Thyroid cancer [200], bladder cancer [201, 202], neuroblastoma [203], lung cancer [204], Oral cancers [205], renal cancer [206]	Prostate cancer [207], ovarian and breast cancer [208]
PKP1		Oropharyngeal SCC, colon and pancreatic adenocarcinoma [223], prostate cancer [224]	
PKP2	Bladder cancer [225], breast cancer [226]	Colon cancer, gastric cancer [227],	
PKP3	Breast cancer [228], lung cancer [229], prostate cancer [224]	Oropharyngeal SCC [230], colon cancer [231-233], gastric cancer [227], bladder cancer [225]	

Table 1.9. Cancers caused by alterations in armadillo repeat proteins. The table represents the type of cancers associated with alterations in expression of armadillo repeat proteins.

1.2.4.2.1. PKP1

Two splice variants of PKP1 are formed due to alternative splicing of the respective gene transcripts (Figure 1.12), the shorter form called “a” variant and the longer form called variant “b”. The PKP1 “b” variant has an addition of 22 amino acids. PKP1b localizes exclusively to the nucleus while PKP1a has been found to localize to both the desmosomes and nucleus [234]. PKP1 is expressed only in the stratified and complex epithelia [219, 235]. In the epidermis, PKP1 expression increases from the basal to the granular layer [235] (Figure 1.13).

PKP1 exhibits dual localization in cell cultures, it can either be desmosomal or nuclear [234].

The in-vivo role of PKP1 has not been deciphered because no knockout mice models of PKP1 are available. But in vitro, PKP1 plays an important role in desmosomal assembly. While the C

terminus (686-726 amino acids) of PKP1 is required for its own localization to the cell-cell border, the N terminal domain of PKP1(1-235 amino acids) binds to multiple desmosomal proteins like DSG1, DSC1, DP and keratins and increases recruitment of these proteins to the desmosome in cultured keratinocytes [164, 236, 237].

PKP1, at the cell border, also regulates actin cytoskeleton re-organization. The armadillo domain of PKP1 (235-686 amino acids) has been demonstrated to indirectly bind to actin filaments and induce the formation of lamellipodia and filopodia of skin keratinocyte cells [237].

PKP1 also localizes to the nucleus (except the nucleolus) in both epithelial and non-epithelial cell lines [234]. Localization of PKP1 protein to the nucleus is regulated by two nuclear localization signals present in its N terminal and armadillo domains. Using the human squamous carcinoma derived A431 cell line, it was demonstrated that PKP1 binds

to chromatin and single stranded DNA. It was also observed that upon treatment with DNA damaging agents like etoposide, the nuclear PKP1 partially redistributed to the nucleolus. In the same cell line, PKP1 knockdown resulted in increased cell survival in response to DNA damage [238]. Thus although the nuclear function of PKP1 was not established directly, it was postulated that it may be important in regulating cell survival after DNA damage.

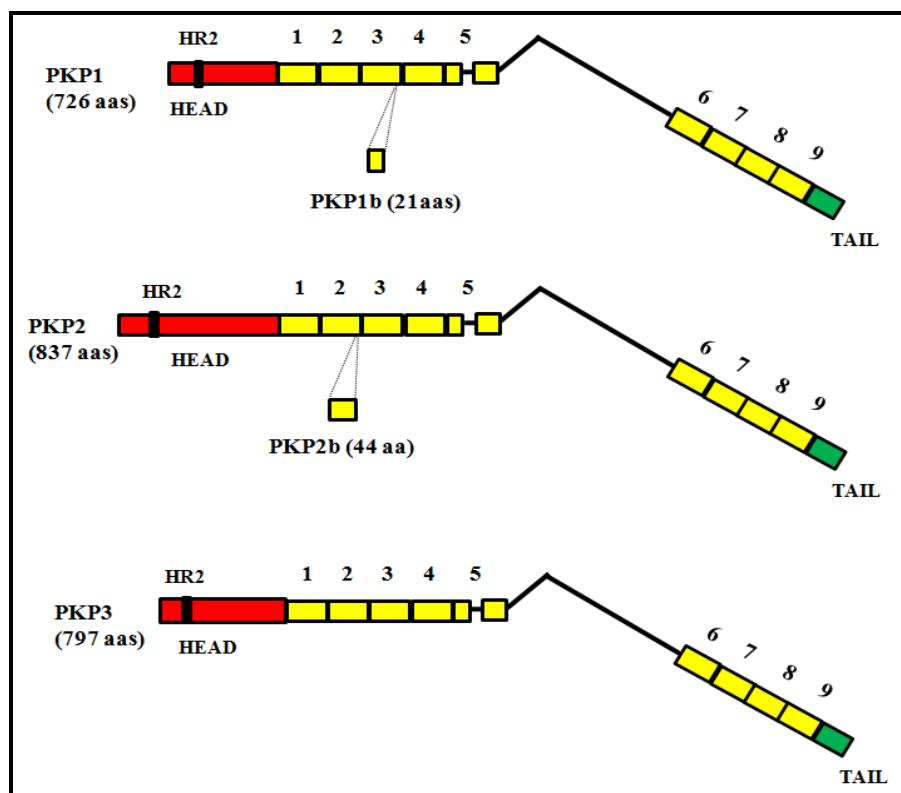


Figure 1.12. Structural domains of PKPs and alternative splice variants of PKP1 and PKP2. All PKPs have armadillo repeat domains flanked by N and C terminal domains but the PKP subfamily proteins have a distinctive kink due to the presence of a polypeptide sequence in between their armadillo repeat domain 5 and 6. The homology region 2 (HR2) is a highly conserved region in the N terminal domain of all the PKPs. Spliced variants PKP1b and PKP2b are formed by alternative splicing of the gene transcripts involving insertion of 21 amino acids between exons 3 and 4 in the PKP1 protein and 44 amino acids between exons 2 and 3 in the PKP2 protein (adapted from [51]).

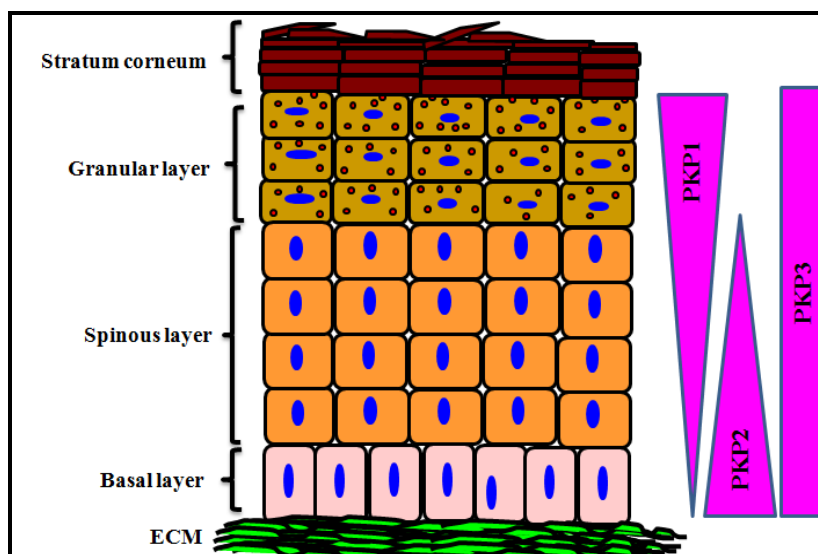


Figure 1.13. Expression of PKP isoforms in the different layers of the stratified epithelium.

Different expression gradients of PKP isoforms exist in the epidermis.

PKP1 and PKP3, but not PKP2, has also been found to localize to stress granules (sites for stalled mRNA-protein complexes). It was postulated that PKP1 may regulate mRNA translation [239]. Later, PKP1 was also shown to increase eIF4A dependent translation by binding to the eukaryotic initiation factor (eIF4A1) and promote the adenosine triphosphate (ATP) activity of eIF4A1. PKP1 was also shown to increase eIF4A dependent translation [240]. Thus, PKP1 is not just an important component of the desmosome, it also regulates desmosomal assembly, actin cytoskeleton organization, cell survival and eIF4A dependent translation.

Since PKP1 regulates multiple processes in the epidermis, loss of function mutations like frameshift mutations, nonsense mutations or compound heterozygosity of the PKP1 gene, cause the disease called skin fragility ectodermal dysplasia syndrome characterized by thickening of skin on the palms and soles, abnormal nails and fragile, blistering skin [212, 213] (Table 1.8). Loss of PKP1 has also been reported in multiple cancers (Table 1.9) like the oropharyngeal SCC,

colon and pancreatic adenocarcinoma [223] and prostate cancer [224]. Thus PKP1 acts as a tumor suppressor just like PG.

1.2.4.2.2. PKP2

The PKP2 gene transcript undergoes alternative splicing to produce two splice variants (Figure 1.12), the shorter form called “a” variant and the longer form called variant “b”. The “b” variant for PKP2 has addition of 44 amino acids in between arm repeats 3 and 4. Both PKP2a and 2b variants show dual localization, they localize to the nucleus and desmosomes [218].

PKP2 is expressed in all simple, complex and stratified epithelium and is also expressed in some non-epithelial tissues like cardiomyocytes (of the heart) and follicle cells of the lymph node [218, 241]. In the epidermis, PKP2 expression decreases as keratinocytes differentiate and move from the basal layer to the spinous layer [241] (Figure 1.13). PKP2, like PKP1 localizes to the both the desmosomes and nucleus (except the nucleolus) of all cell lines derived from stratified or simple epithelium, while in non-epithelial derived cell lines that lack desmosomes like SV80 fibroblasts, PKP2 localizes only to the nucleus [218].

PKP2 is the only plakophilin isoform expressed in the heart, so upon loss of PKP2, no other plakophilin can compensate its function. The importance of PKP2 in the heart was understood while trying to generate the PKP2 knockout mice. No transgenic mice were generated. It was observed that the PKP2 null embryos died at E11 due to altered heart morphogenesis [210] (Table 1.7). Analysis of the developing heart of the PKP2 null mice showed altered cytoskeletal organization, ruptures of the cardiac walls, and blood leakage into the pericardiac cavity. It was also found that DP of the embryonic myocardium did not localize to the cell border but formed granular aggregates in the cytoplasm. DP was also found to co-localize with adherens junction

proteins, thus making it difficult to distinguish the adherens junction and the desmosomal junction. Surprisingly, the ultra structure of desmosomes of the epidermis and the stomach mucosa were found to be unaltered. Therefore, it was demonstrated that PKP2 is essential for cardiac junction formation and also for recruitment of DP to the desmosomes [210]. Consequently frameshift, missense or nonsense mutations in the PKP2 gene lead to the heart disease ARVC/D [214] (Table 1.8).

PKP2 has been shown to play a very important role in the formation of the desmosome by recruiting DP to the cell border. PKP2 performs this function by interacting with protein kinase $C\alpha$ (PKC- α). PKP2 binds to PKC- α and recruits it to the cytoplasmic pool of DP. PKC- α phosphorylates DP at Ser 2849 and this phosphorylation causes DP to interact with intermediate filaments and initiate nascent desmosome formation. Since PKP2 recruits PKC- α to the cytoplasmic complexes consisting of DP and other desmosomal proteins, it prevents PKC α to interact with other substrates. In absence of PKP2, PKC- α was shown to phosphorylate its downstream targets more effectively. [242]. Thus, although PKP2 positively regulates desmosome assembly by regulating PKC α activity, it negatively regulates the global PKC α activity.

PKP2 localizes to the nucleus and it was demonstrated that Cdc25C associated kinase 1 (C-TAK1) and the 14-3-3 family proteins regulate the nuclear localization of PKP2. C-TAK1 phosphorylates PKP2 at serine 82 residue, thus forming a 14-3-3 binding site. Binding of 14-3-3 proteins sequester PKP2 to the cytoplasm and prevent its nuclear localization. The mechanism regulating the upstream C-TAK1 activation is not known [243].

The functions of nuclear PKP2 are unclear but it has been demonstrated that PKP2 associates with the DNA directed RNA polymerase III subunit C155 (RPC155), which is the largest subunit of the RNA polymerase III holoenzyme. PKP2 was also found to be associated with other subunits of the RNA polymerase III, RPC39, RPC82 and transcription factor IIIB (TFIIIB) but not TFIIC. Due to the absence of TFIIC, the PKP2-RPC155 complexes were postulated to be inactive RNA polymerase complexes [244]. Another important function of nuclear PKP2 is its regulation of the WNT signaling pathway. PKP2 can bind to β catenin (a central member of the canonical WNT signaling pathway) and inhibit the association of β catenin with E-cadherin (of the adherens junction). This allows more β catenin to move into the nucleus and activate the transcription factors TCF and LEF.

PKP2 plays a dual role in cancer (Table 1.9). In the case of bladder cancer [225] and breast cancer [226], increase in PKP2 is associated with increased neoplastic progression, while in case of colon cancer and gastric cancer [227], PKP2 functions as a tumor suppressor. One of the mechanisms by which PKP2 regulates breast cancer progression is by associating with EGFR and activating EGFR in a ligand dependent and ligand independent manner which in turn promotes tumor formation in breast cancer [226]. Thus, PKP2 functions not just as a desmosomal protein but regulates multiple signaling pathways like WNT/ β catenin, PKC α and the EGFR signaling pathways.

1.2.4.2.3. PKP3

Alternative splice variants of PKP3 have recently been reported. In the case of PKP3, the known variant is called PKP3a while the new variant is called PKP3b (Figure 1.14). The PKP3b variant utilizes a new 1st exon upstream of the known gene. This new exon contains a functional

translation start site which is used during translation of PKP3b protein. PKP3a is expressed in most epithelial cells while PKP3b variant is expressed predominantly in stratified epithelial cells and absent or heterogeneous in simple epithelial cells [245].

PKP3 is ubiquitously expressed in most simple and stratified epithelial tissues with the exception of hepatocytes [220]. PKP3 is also expressed uniformly in all the layers of the epidermis [220] (Figure 1.13). PKP3 binds to multiple proteins like all isoforms of DSGs and DSCs. It is the first protein found to bind to the “b” splice variant of all DSC isoforms. It also binds to PG, DP [246] and cytokeratin 18 (K18) [232, 246].

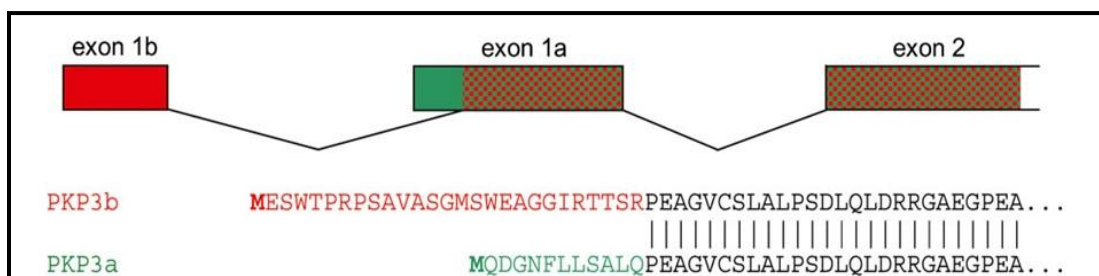


Figure 1.14. Alternative splice variants of PKP3. The alternate spliced variant of PKP3 mRNA is generated by introduction of a new exon at the N terminal (exon 1b). This leads to the splice variant protein having an alternate N terminal amino acid sequence [245]

PKP3, along with PG and E-cadherin play a crucial role in the initiation of desmosome formation. To analyze the process of initiation of desmosomes in cell cultures, calcium switch assays were performed. This assay is used to analyze cell junction disassembly and reassembly. It is based on the concept that desmosomes and adherens junctions are calcium dependent junctions and decreasing calcium concentrations (low calcium) or EDTA treatment to cells (for chelating calcium) from the culture media may lead to disruption or internalization of desmosomes. Thereafter, adding media having normal calcium concentrations lead to formation

of nascent desmosomes [247, 248]. Calcium switch assays were performed in PKP3 knockdown clones derived from the skin keratinocyte cell line, HaCaT and the colon carcinoma cell line HCT116, along with their respective vector control clones. It was observed that PKP3, PG and E-cadherin stayed at the cell border even after 16 to 18 hours incubation in low calcium conditions, while other desmosomal proteins like DSC2/3, DP and PKP2 disassembled from the desmosome both in the vector control and PKP3 knockdown clones. Upon addition of normal calcium, DSC2/3, DP and PKP2 showed a time dependent increase in localization to the cell border in the vector control clones but in the PKP3 knockdown clones, these proteins did not localize to the cell border. The cell border localization of PKP3, PG and E-cadherin were found to increase with time after addition of normal calcium medium in the vector control and PKP3 knockdown clones. Thus PKP3, PG and E-cadherin were proposed to be involved in initiation of desmosome formation and presence of PKP3 was demonstrated to be essential for desmosome formation. It was observed that in the PKP3 knockdown clones, PG and E-cadherin localization at the cell border was not hampered but localization of DSC2/3, DP and PKP2 were altered. Thereafter PG knockdown clones derived from HCT116 were generated. In the PG knockdown cells it was observed that cell border localization of PKP3 was decreased. Localization of DSC2/3, DP and PKP2 were also decreased but E-cadherin localization was unaltered. To analyze the role of E-cadherin in desmosome formation, three HCT116 derived E-cadherin knockdown clones were generated. In these E-cadherin knockdown clones, cell border localization of PKP3, DP and PKP2 were decreased but localization of PG remained unaltered. It was proposed that since PG can bind to both E-cadherin and P cadherin [249], E-cadherin loss may allow PG to bind to P cadherin and thus stay at the cell border. It was also shown that PKP3 co-localizes with both PG and E-cadherin at the cell border. All these experiments proved that

both PG and E-cadherin recruits PKP3 to the cell border and PKP3 is essential for initiation of desmosome formation because only in the presence of PKP3, the other desmosomal proteins like DP, DSC2/3 and PKP2 are recruited to the cell border [250].

Recently, PKP3 has been shown to collaborate with PKP2 for desmosome formation in the squamous cell carcinoma 9 (SCC9) and HaCaT cell lines. It has been demonstrated that while PKP3 assembles the cytoplasmic population of DP bound desmosomal proteins (precursors for desmosome formation); PKP2 is required to transfer these precursors to the membrane. One of the mechanisms by which PKP3 promotes desmosome assembly is by physically binding to and activating the Rap1 GTPase protein. A calcium switch assay was performed to analyze the activation of Rap1GTPase at different time intervals after addition of normal calcium to the medium. Rap1 GTPase activity was found to increase with time in the vector control clones as reported earlier [251], but it did not increase in the SCC9 and HaCaT derived PKP3 knockdown clones. Thus, it was demonstrated that PKP3 is required for activation of Rap1GTPase and expression of wild type Rap1GTPase in the PKP3 knockdown clones were able to efficiently localize DP to the cell border. PKP3 was also shown to govern E-cadherin maturation. It was demonstrated that the Rap1/PKP3 complex is required for formation of the Rap1/E-cadherin complex which in turn is required for adherens junction formation because upon PKP3 loss, Rap1GTPase was not able to bind to E-cadherin. To analyze if inability to bind Rap1GTPase would alter E-cadherin mediated adherens junction formation, it was observed that in the PKP3 knockdown clones, the adherens junctions formed were highly disorganized and even the cell border localization of E-cadherin was decreased as compared to the vector control clones [252]. Some of these observations are contradictory to [250]. Upon PKP3 loss, E-cadherin cell border localization was not altered in [250] but in [252], it is decreased. Thus, even though there are

some contradictions between [250] and [252], both these articles demonstrate the importance of PKP3 in desmosome formation.

Since PKP3 is very important in the formation and maintenance of desmosomal structure, loss of PKP3 was expected to decrease the ability of cells to form desmosomes. This was exactly what was observed in PKP3 knockout mice (Table 1.7). There was a decrease of approximately half of the lateral desmosomes in between the basal cells of the epidermis of PKP3-null mice [211], but desmosome numbers in the suprabasal cells were unaltered. It was demonstrated that the phenotypes of the PKP3 null mice were not as severe as those of PKP2 or PG null mice because in the PKP3 null mice, expression of PKP2 was found to increase and it was hypothesized that PKP2 may partly compensate for the loss of PKP3. The PKP3 null mice were normal at birth, but started showing abnormalities in the later stages. In these mice, hair coat pelage occurrence was delayed and the resulting hair follicles were morphologically abnormal. In the stages between postnatal day 8 (P8) to P10, PKP3 null mice showed increased cell proliferation of basal keratinocytes, thus leading to increased thickness of the suprabasal layers of the epidermis. This was ascertained to increased cell proliferation due to increased β catenin signaling in the basal keratinocytes of PKP3null mice. Unexpectedly, in the epidermis of adult PKP3 null mice, no such changes were observed. PKP3 null mice also showed increased susceptibility to cutaneous inflammation. PKP3 null mice kept in specific pathogen free environment showed less skin alterations but when kept in the conventional facilities (consisting ectoparasites), the PKP3 knockout mice developed inflammatory responses much stronger than the wild type mice [211]. Thus it was demonstrated that PKP3 is important for desmosome formation, maintaining normal hair coat structure and for preventing skin inflammation.

Supporting the role of PKP3 in prevention of inflammation, auto-antibodies that disrupt PKP3 at the cell border, causes a precancerous skin blistering disease called Paraneoplastic pemphigus [215] (Table 1.8) which is similar to the skin blistering disease PV. Interestingly, it has been recently demonstrated that PV antibodies induce Src dependent tyrosine phosphorylation of PKP3. This phosphorylation causes PKP3 detachment from the desmosome because of loss of binding to DSG3 [253]. A similar tyrosine phosphorylation of PKP3 by Src which can cause detachment of PKP3 from the desmosome has also been reported in cells subjected to oxidative stress and the tyrosine residue was found to be at position 195 [254]. A detailed understanding of the mechanisms and effects of Src mediated PKP3 phosphorylation during PV could probably help in devising ways to treat paraneoplastic pemphigus. One of the mechanisms by which Src regulates PV is by activating the downstream p38MAPK pathway. The Src/p38MAPK pathway can be an efficient target against PV because inhibition of Src has been demonstrated to block PV disease in vivo via inhibition of p38MAPK pathway [255, 256].

PKP3 loss is associated with multiple forms of cancer like oropharyngeal SCC [230], colon cancer [231-233], gastric cancer [227], bladder cancer [225]. Surprisingly, increase in PKP3 has also known to be associated with cancers like breast cancer [228], lung cancer [229], prostate cancer [224] (Table 1.9). To analyze the effect of PKP3 in colon cancer tumorigenesis, PKP3 knockdown clones were generated in the simple epithelial cell line (HCT116) and two stratified epithelial cell lines (HaCaT and FBM). It was demonstrated that PKP3 loss leads to decreased cell-cell adhesion, increased anchorage independent growth and increased in-vitro cell migration. The HCT116 and HaCaT derived PKP3 knockdown clones formed larger tumors in vivo and was shown to have a higher ability to metastasize to the lungs as compared to the vector control clones [233, 257, 258]. There were some cell type specific effects of PKP3 loss also reported. In

HaCaT, PKP3 loss increased cell growth and proliferation while in HCT116, cell growth and proliferation remained unaltered [233]. To understand the mechanisms regulating tumor formation and metastasis upon PKP3 loss, it was hypothesized that PKP3 loss may cause alterations in the normal functioning of its binding partners. Since one of the binding partners of PKP3 was cytokeratin 18 (K18) [232, 246], it was hypothesized that loss of PKP3 may regulate K18 function or stability. Since, keratins are always expressed in pairs of type I and type II keratins [259-261], and in simple epithelia K18 (type I keratin) and K8 (type II keratin) are known to form pairs [262], protein expression of K8 and K18 were analyzed in the HCT116 derived PKP3 knockdown clones and the vector control clone [232]. It was observed that both K8 and K18 protein levels were higher in the PKP3 knockdown clones than the vector control clones. Since, K8/K18 over-expression had been associated with squamous cell carcinoma progression [263-266], metastasis [267] and poor prognosis [268], it was hypothesized that increased K8 levels can regulate neoplastic progression upon PKP3 loss. To test this hypothesis, two K8 double knockdown clones (K8 knockdown clones derived from a PKP3 knockdown clone) were generated. In-vitro and in-vivo experiments were performed to compare the neoplastic potential of these double knockdown clones with the corresponding vector control clones. It was demonstrated that K8 loss causes decreased in vitro cell migration, decreased lamellopodia formation in cells. Nude mice were subcutaneously injected with the K8 double knockdown clones and its respective vector control clones and after 5 weeks, the percentage of metastasis to the lungs were analyzed. It was observed that less number of mice in K8 double knockdown group as compared to the vector controls showed greater than 30% metastasis in the lung sections of mice. Thus, it was demonstrated that elevated K8 levels were required for neoplastic transformation upon PKP3 loss. To understand the mechanism regulating increase in

K8 protein levels upon PKP3 loss, K8 mRNA levels were analyzed and it was found that K8 mRNA levels were not altered. Thus, it was hypothesized that PKP3 loss may be causing increased K8 protein stability by regulating post-translational modifications like phosphorylation or dephosphorylation. Analysis of the known phosphorylation sites of K8 [269, 270] demonstrated that K8 was dephosphorylated at Serine 473 residue in PKP3 knockdown clones. A phosphatase associated with colon cancer metastasis called Phosphatase of Regenerating Liver3 (PRL-3) had been earlier reported to increase K8 protein stability [271]. PRL-3 expression has been known to increase in colorectal cancer tissues and positively correlate with metastasis of colon cancer cells to the lung and to the liver [272-275]. PRL-3 has also been demonstrated to regulate tumor formation because in chemically induced colitis associated colon cancer model, targeted deletion of the PRL-3 encoding gene (PTP4A3) was able to decrease incidence of tumor formation [276]. Thus, since PRL-3 was known to dephosphorylate K8, it was hypothesized that PRL-3 was the phosphatase that regulates K8 protein stability upon PKP3 loss. Inhibition of PRL-3 in the PKP3 knockdown clones using a specific PRL-3 inhibitor (PRL-3i) was able to decrease K8 protein levels, K8 S473 phosphorylation and also decrease in-vitro cell migration. These experiments confirmed the above hypothesis. On analyzing PRL-3 protein and mRNA expression, it was found that PRL-3 protein levels were higher in the PKP3 knockdown clones than the vector control clones, but PRL-3 mRNA levels remain unaltered. The mechanism regulating increased PRL-3 protein levels in the PKP3 knockdown clones is not known, but it has been proposed that PKP3 may regulate translation of PRL-3 [232].

In support of the role of PKP3 regulating translation, it has been demonstrated that both PKP3 and PKP1 localize to stress granules (sites for stalled mRNA-protein complexes) and PKP3 forms complexes with RNA binding proteins like the Fragile X mental retardation autosomal

homologue 1 (FXR1), GTPase activating protein binding protein 1 (G3BP1) and the poly A binding protein Cytoplasmic 1 (PABPC1) [239]. It has also been demonstrated that binding of PKP3 to FXR1 is mRNA independent, while binding to G3BP1, PABPC1 and another RNA binding protein NMD factor up-frameshift 1 (UPF1) is mRNA dependent. A functional role of PKP3 in regulating translation was deciphered when it was shown that by virtue of binding to the RNA binding proteins, PKP3 can regulate PKP2 mRNA stability in prostate cancer cell lines [277].

1.3. Radio-resistance of cancer cells

Radiotherapy is one of the most widely used treatment modality for cancer. It can be used as a single modality treatment or in combination with surgery and chemotherapy (Table 1.10). Although, rapid progress has been made in radiotherapy due to advanced imaging technologies, computerized treatment planning and improved radiation treatment machines, yet the outcome of radiotherapy for metastatic cancers remain very poor. (reviewed in [278]). One of the major reasons for this poor outcome is the phenomenon of local recurrence and distant metastasis. Local recurrence of cancers after irradiation occurs due to a phenomenon called long term radio-resistance. This is a property of tumor cells to withstand radiotherapy and retain the ability to proliferate (i.e. clonogenic survival) ([279] and reviewed in [280]). It has been demonstrated that there are two types of radio-resistance, intrinsic resistance and radiation induced resistance [281, 282].

1.3.1. Intrinsic radio-resistance

Intrinsic radio-resistance is a property of the inbuilt genetic makeup of cells to withstand DNA damage and repair the damaged DNA after radiation exposure [283-286]. Since irradiation (both

γ and X-ray irradiation) induces double stranded breaks, the double stranded DNA damage sensing proteins like DNA-PKcs, ATM and ATR (reviewed in [287]) can bind to the damaged DNA and activate cell cycle checkpoint pathways like the G1/S and G2/M checkpoints (Figure 1.15) (reviewed in [288, 289]).

Cell cycle checkpoints are non-essential regulatory pathways that prevent cell cycle progression in response to stress such as DNA damage or incomplete S-phase [290]. Ataxia telangiectasia mutated (ATM) and Ataxia telangiectasia and Rad3 related (ATR) proteins also recruit proteins belonging to the double stranded DNA damage repair (dsDDR) mechanisms namely homologous recombination (HR) and the non-homologous end joining (NHEJ) (Figure 1.16) ([291, 292] and reviewed in [293]). HR uses an identical template for repairing DNA and thus the DNA repair is error free. HR repair is active only in late S and G2 phases of the cell cycle of mammalian cells because of the availability of sister chromatids at these stages (reviewed in [294, 295]). The NHEJ repair does not use any homologous template and is therefore error prone. NHEJ repair remains active throughout the cell cycle but is majorly important in the G1 phase of the cell cycle when no sister chromatids are available for HR to work (reviewed in [295, 296]). Thus, a coordination of the cell cycle checkpoint pathways along with the HR and NHEJ pathways ensure dsDDR (reviewed in [297]). For cancer cells to be intrinsically radio-resistant, DNA damage needs to be either repaired or tolerated before entering the M phase of the cell cycle; because in the M phase, cells have compact chromatin and in this stage, cells are more prone to DNA double stranded breaks [298].

It has been demonstrated that intrinsically radio-resistant cells show higher efficiency in DNA double stranded break repair [299]. Glioblastoma Multiforme (GBM) tumors are known to be highly radio-resistant tumors (reviewed in [300]). One of the reasons which cause radio-

resistance in GBM tumors is the presence of Glioma initiating cells (GICs). GICs have been demonstrated to have a highly efficient HR mechanism of DNA repair and an abnormal cell cycle progression due to presence of low levels of p53 protein when

Early cancers curable with radiation therapy alone	Cancers curable with radiation therapy in combination with other modalities
Skin cancers (squamous and basal cell)	Breast carcinomas
Prostate carcinomas	Anal and rectal carcinoma
Lung carcinomas	Advanced cervical carcinoma
Cervix carcinomas	Bladder carcinoma
Lymphomas (Hodgkin's and low grade Non-Hodgkin's)	Endometrial carcinoma
Head and neck carcinomas	Tumors of the central nervous system
	Soft tissue sarcomas
	Colorectal Cancer
	Pediatric tumors

Table 1.10. Some cancers can be cured with only radiation if detected early while others require combination of other modalities. The table represents cancers curable with radiation therapy alone and those requiring other modalities like surgery or chemo-radiotherapy [278, 301]

compared with neural progenitor cells but efficiency of the NHEJ pathway remains unaltered [302] Another glioma stem cell type characterized by Cluster of differentiation 133 (CD133) positivity known to be highly tumorigenic and radio-resistant as compared to the CD133- cells, was demonstrated to have a high basal activity of DNA repair signaling including presence of activated ATM, Checkpoint kinase 1 (Chk1) and Checkpoint kinase 2 (Chk2) proteins. Treatment with Chk1/Chk2 inhibitors was able to decrease the radio-resistance of the CD133

positive glioma stem cells [303]. Similar to GBMs, it has been demonstrated that efficiency of DNA repair by HR is significantly elevated in breast cancer cells as compared to the normal mammary cells [304]. Thus, abnormal cell cycle checkpoints and increased efficiency of the HR pathway regulate intrinsic radio-resistance of tumor cells.

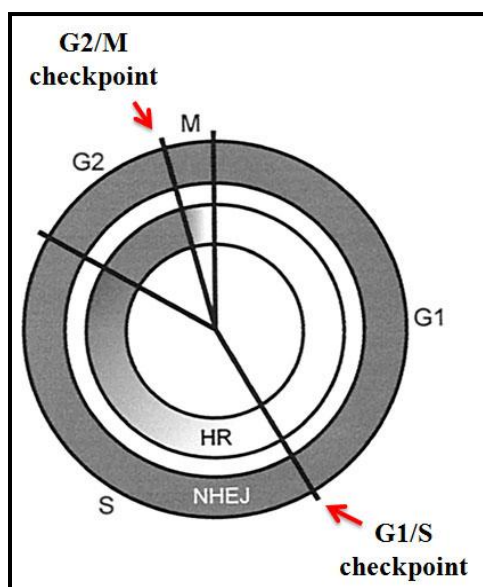


Figure 1.15. The cell cycle, the cell cycle checkpoints and the contribution of the HR and NHEJ pathways in the cell cycle. There are four phases in the cell cycle namely G1, S, G2 and M phase [305] There are two checkpoints: the G1/S checkpoint checks DNA integrity before the DNA enters replication while the G2/M checkpoint checks DNA integrity before the DNA enters the M phase. The NHEJ and the HR pathways are the main double stranded DNA repair mechanisms present in mammalian cells. The NHEJ (dark grey color) predominates in the G1 to early S phase while both NHEJ and HR (light grey color) contribute to repair DNA damage during the late G2 phase (adapted from [305]).

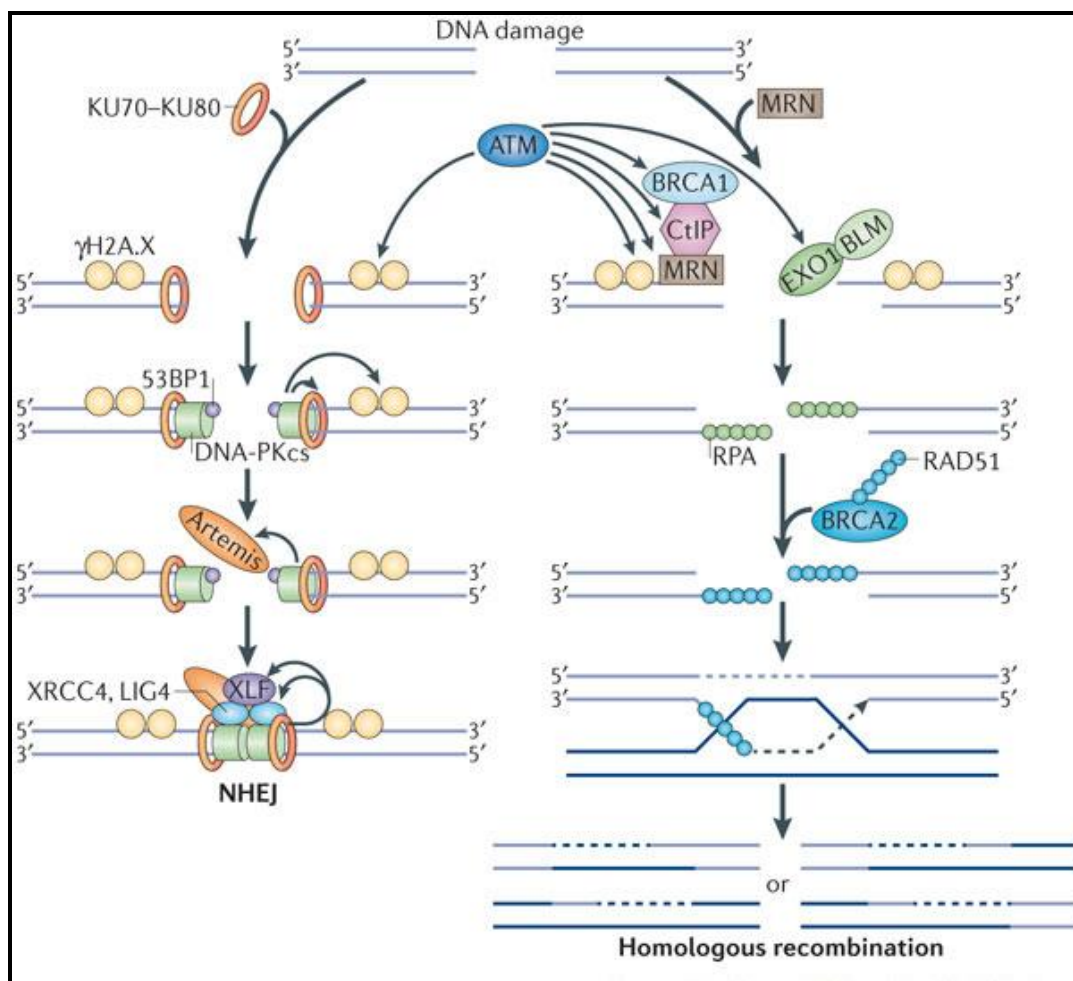


Figure 1.16. The double stranded DNA repair pathways: NHEJ and HR. The NHEJ repair pathway utilizes DNA damage sensors complexes like the Ku70-Ku80 protein complex. This complex is loaded onto the broken ends and this signals recruitment of the catalytic subunit of DNA-dependent protein kinase (DNA-PKcs) and p53-binding protein 1 (53BP1). Ataxia telangiectasia mutated (ATM)-mediated phosphorylation of histone H2A.X (γ H2A.X) and the recruitment of 53BP1 protects the broken DNA ends from being cleaved. The DNA-PKcs regulates the stability of DSB ends through phosphorylation of Artemis and other substrates. Artemis in turn facilitates the end processing and, subsequently, DNA ligase 4 (LIG4), X-ray repair cross-complementing protein 4 (XRCC4) and XRCC4-like factor (XLF) ligate the broken ends to complete repair. repair by the NHEJ pathway is error-prone (reviewed in [306]).

HR utilizes the sister chromatids (being identical to the DNA to be repaired) and repairs the double stranded break without any error. Double stranded breaks are recognized by MRN complex composed of proteins Mre11, Rad50 and Nbs1. Recognition of DNA double stranded break signals ATM and ATR proteins which rapidly phosphorylate multiple DNA repair factors including H2A.X, CtBP-interacting protein (CtIP), breast cancer type 1 susceptibility (BRCA1) and exonuclease 1 (EXO1). MRE11 induces endo-nucleolytic cleavage at double stranded breaks allowing the resection of a part of the 5' end of the damaged DNA region; this is mediated by CtIP and EXO1 in the presence of BRCA1 and Bloom's syndrome helicase (BLM). In addition, γ H2A.X spreads around the damaged site, thereby stabilizing the DNA repair complex. The single-stranded DNA generated by resection is rapidly coated by replication protein A (RPA) protein and is subsequently replaced by RAD51 in the presence of BRCA2. RAD51 coated DNA invades the sister chromatid to search for a homologous DNA strand. The fidelity of this process is maintained by anti-recombinases such as the PCNA-associated recombination inhibitor (PARI). The invading strand is extended by DNA polymerase and ligates to form D-loop structures called Holiday junctions. The final product of the homologous recombination-mediated repair is then determined by the resolution of the D-loops leading to either DNA undergoing crossover or no crossover (reviewed in [306]).

Intrinsic radio-resistance can be also be caused by constitutive activation of cell signaling pathways that in turn activates the cell cycle checkpoints, HR or NHEJ signaling pathway. Some of the key cell signaling pathways that are associated with intrinsic radio-resistance are the Epidermal growth factor receptor (EGFR) [307], Insulin growth factor receptor (IGFR) [308] and the Phosphoinositide 3-phosphate (PI3K)/AKT signaling pathways which work via

activation of the three different Mitogen activated protein kinase pathways namely the extra-cellular signal regulated kinase (ERK), p38 Mitogen activated protein kinase (p38 MAPK) and the Janus kinase (JNK) pathways. The N terminal deleted constitutively active mutant of EGFR has also been demonstrated to cause increase in intrinsic radio-resistance by activation of both the MAPK pathways and the PI3K/AKT signaling pathway [309]. The hepatocyte growth factor receptor (c-Met) signaling has been shown to increase intrinsic radio-resistance by activating the downstream nuclear factor light chain enhancer of activated B cells (NF κ B) signaling pathway [310].

Mutations in pro-apoptotic proteins can also lead to intrinsic radioresistance. The best example is the transcription factor p53 protein; an essential pro-apoptotic protein in mammalian cells which mediates cell cycle checkpoint activation upon DNA damage [311]. Mutations in the p53 encoding gene, TP53, which results in loss of function of the ability of p53 to induce the expression of the pro-apoptotic protein p21 (BAX) expression has been associated with increased intrinsic radio-resistance in glioblastoma [312]. Signaling pathways that lead to epithelial mesenchymal transitions (EMT) are also known to cause intrinsic radio-resistance (reviewed in [313]). In breast cancers, HOXB9 (a transcription factor) is over-expressed and is known to increase the transcription of TGF β , thus inducing autocrine TGF β induced EMT [314]. It was demonstrated that HOXB9 induces spontaneous DNA damage, thus leading to basal activation of DNA damage response like activation of ATM, phosphorylation of histone 2AX (H2AX) and foci formation of p53 binding protein 1 (53BP1) in the nucleus of cells. Probably this selection pressure kept the cells ready for dsDDR and it was demonstrated that upon γ irradiation, the HOXB9 overexpressing cells showed hyperactivation of ATM and faster accumulation of

phospho-H2AX and 53BP1 at the DNA double stranded break. This ensured faster repair and better cell survival.

The radio-resistance of these HOXB9 overexpressing cells was shown to depend on TGF β mediated EMT because inhibition of the TGF β signaling pathway inhibited both EMT and dsDDR responses [315]. Thus, activation of the EMT pathway can increase intrinsic radio-resistance. Supporting this hypothesis, loss of E-cadherin mediated EMT has also been demonstrated to increase intrinsic radio-resistance [316]. In this work, it was shown that treatment of MCF7 (non transformed mammary epithelial cell line) and A549 (lung carcinoma derived cell line) cells with hypoxia, TGF β or EGFRvIII can induce EMT and radio-resistance. In all three cases E-cadherin expression was lost and vimentin expression was increased. It was hypothesized that loss of cell to cell adhesion during EMT due to E-cadherin loss may be regulating radio-resistance. To assess this hypothesis, cells were seeded at high and low confluences, irradiated at different doses of γ irradiation and cell survival analysis was performed. It was demonstrated that at high confluences, E-cadherin showed extensive border staining and when these cells were subjected to irradiation, they were more radiosensitive while sparsely seeded cells were more radio-resistant. As controls, the E-cadherin levels were analyzed and it was shown that in the densely and sparsely seeded cells, E-cadherin levels did not change. To test whether E-cadherin restoration can decrease radio-resistance, E-cadherin was stably expressed in the highly metastatic cell line MDA-MB-231 (breast carcinoma derived cell line with very less endogenous E-cadherin expression). E-cadherin restoration caused reversion of cells from mesenchymal (shown by parental MDA-MB-231 cells) to epithelial phenotype and the E-cadherin restored clones were more radio-sensitive as compared to the mock transfected MDA-MB-231 clones [316]. Thus, cell to cell adhesion was demonstrated to be important for

regulation of regulate cell death and survival upon radiation treatment because loss of cell to cell adhesion can lead to in intrinsic radio-resistance in cancer cells.

1.3.2. Radiation induced radio-resistance

Radiation induced radio-resistance develops only after radiation exposure and involves activation of signaling pathways that induce cell survival and alterations in gene expression of anti-apoptotic and radio-protective genes in cells that has been exposed to radiation [317] (Figure 1.17).Some of the mechanisms that lead to radiation induced radio-resistance are enrichment of cancer stem cells, oxidative stress and activation of cell signaling pathways activated as a consequence of the DNA damage by irradiation (reviewed in [318-320]).

Cancer stem cells (CSCs) are defined as cells within a tumor that possesses the capacity to self-renew and to cause the heterogeneous lineages of cancer cells that comprise the tumor (reviewed in [321]). Intrinsically cancer stem cells possess the ability of accelerated DNA repair and less production of ROS which ,makes them intrinsically radio-resistant ([322] and reviewed in [323]).

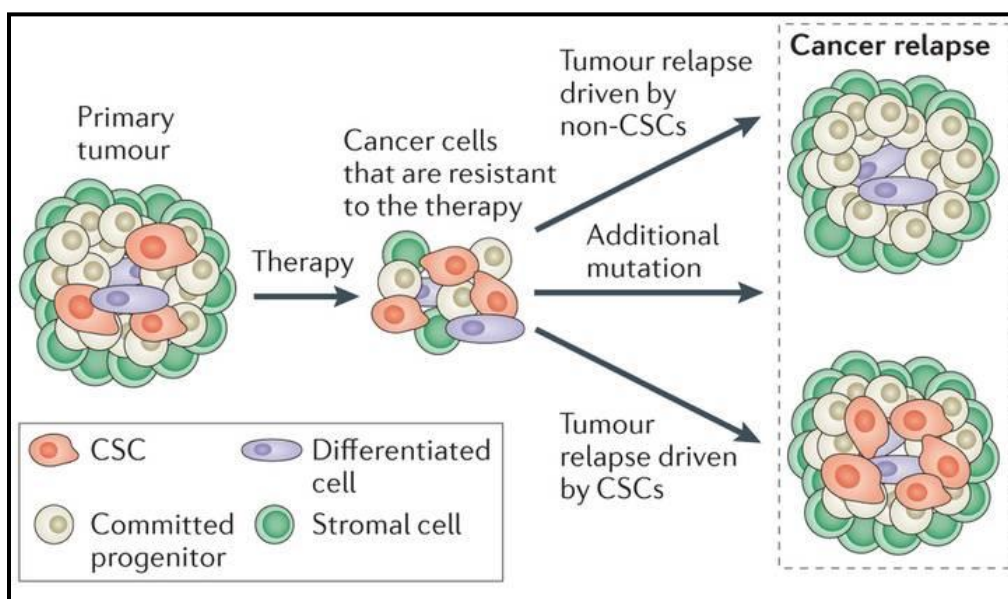


Figure 1.17. Radiation induced radio-resistance. Radiation therapy kills most cells but CSCs and some residual non-CSCs survive. The CSCs undergo enrichment while non CSCs undergo mutations, phenotypic plasticity mediated changes or radiation induced activation of signaling pathways leading to repopulation of these cells thus causing cause cancer relapse [324].

Radiation therapy kills cancer cells and causes an apparent decrease of tumor cell mass. This causes a survival pressure on the cancer cells to select radiation resistant CSCs, thus leading to CSC enrichment (Figure 1.18). These enriched CSCs differentiate into cancer cells which are more radio-resistant and aggressive leading to tumor recurrence (reviewed in [325]). The hypothesis of CSC selection has been validated by treatment of non small cell like lung carcinoma (NSCLC) derived cells to 5 Grays of irradiation and grown in ultra low adherent plates to form spheres. As controls, the un-irradiated cells were also grown in the same type of plates. It was demonstrated that the cells that formed spheres in the irradiated group had higher expression of stem cell markers, Oct4, Sox2, CD44, Snail and PDGF-beta and were more radio-resistant than the control cells [326].

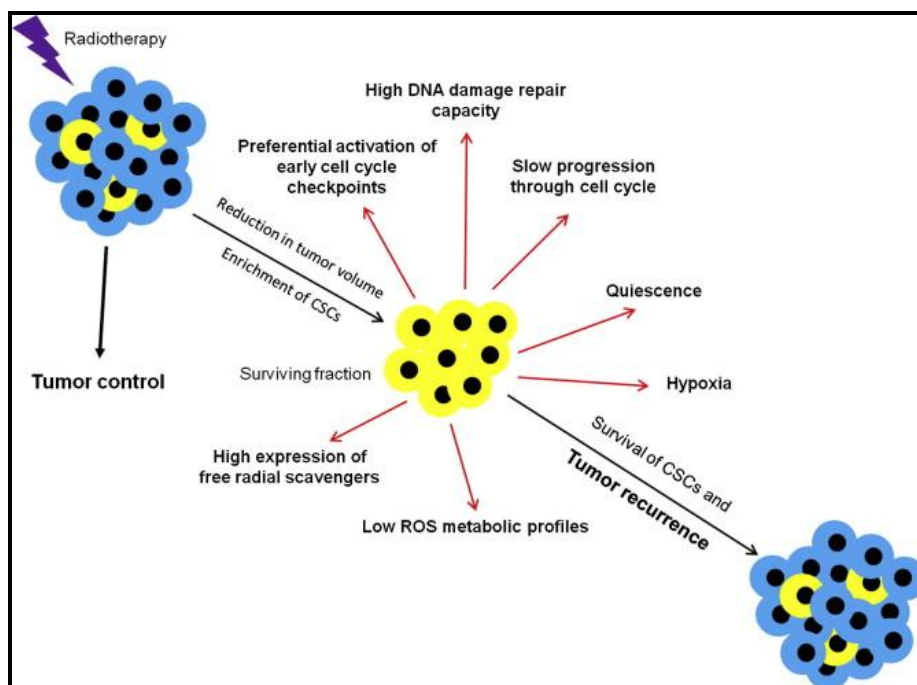


Figure 1.18. Radiation induced resistance is caused by CSC enrichment. Upon, radiation treatment, most tumor cells get destroyed causing reduction in tumor volume, but CSCs are not killed due to their intrinsic property of faster DNA damage repair. These CSCs undergo enrichment under the selection pressure of hypoxia. Enrichment causes proliferation of CSCs, increased hypoxia, quiescence, high DNA damage repair capacity, low ROS production, slow progression through the cell cycle and high expression of antioxidant or scavenger proteins. Moreover, during proliferation, CSCs undergo asymmetric division and differentiate into all cell types that make up the tumor [325].

Thus selection of CSC upon irradiation seemed to be an important mechanism of radiation induced radio-resistance. Radiation is also known to induce formation of CSCs or induce phenotypic plasticity in tumor cells which have survived radiation treatment. This theory was built on the consideration that the cells in any tumor are heterogeneous populations of clones having different phenotypes and can exhibit phenotype plasticity upon alterations in tumor

microenvironment. Thus, even non-CSCs tumor cells can dedifferentiate into CSC cells or into cell types that are more radio-resistant (reviewed in [327-329]). Phenotypic plasticity allows tumor cells to acquire a resilient, stress coping state and since this process does not require selection process, it occurs very early after irradiation and can cause tumor recurrence (reviewed in [330]). Ionizing radiation has been demonstrated to induce CSC induction in a hepatocellular carcinoma cell lines HepG2 and Huh7 by increasing stem cell markers like Sox2 and Oct3/4 expression. This caused increase in spheroid formation (a cell biology technique to analyze stem like phenotypes) and radio-resistance [331]. Even in breast cancer cells, ionizing radiation has been demonstrated to cause radiation induced radio-resistance by inducing expression of stem cell associated markers like Oct4, Nanog and Sox2 [332]. Thus, one of the mechanisms involved in radiation induced radio-resistance is the dedifferentiation of non-CSCs into CSCs.

Irradiation also activates many cell signaling pathways which are involved in conferring intrinsic radio-resistance to cells and are implicated to be involved in radiation induced radio-resistance [318]. Radiation induced activation of the PI3K/AKT pathway has been demonstrated to cause radioresistance in glioblastomas [333] and prostate cancer [334]. In medulloblastomas, radiation induced activation of the Wnt/ β catenin signaling pathway has been shown to cause radioresistance. This signaling was demonstrated to be mediated by the increase in expression of the urokinase plasminogen activator receptor (uPAR) [335]. Low dose clinically relevant radiation exposure of 1 to 2 grays can cause activation of the EGFR (also called ErBb1) and human epidermal growth factor receptor 3 (HER3, also known as ErBb3) pathway leading to activation of the downstream kinases Raf, MEK, ERK [336].

Radiation induced radio-resistance can also be developed in neighboring cells which have not been directly exposed to radiation treatment by the bystander effect. In this phenomenon, the

cells exposed to radiation secrete cytokines that act in a paracrine manner to activate cell signaling pathways that increase radio-resistance in the neighboring cells (Figure 1.19). Thus, when these neighboring cells are exposed to radiation, they would be more radio-resistant than their counterparts (reviewed in [337, 338]). This mechanism of radio-resistance utilizes cell communicating junctions like gap junctions for cells attached to each other or secretion of cytokines, hormones and other soluble factors in a paracrine or endocrine manner to activate radio-protective signals in distant cells [337]. Bystander effects can cause either radio-resistance or radio-sensitivity based on the cytokine profile of the secretome and also probably on the relative concentration of the cytokines. Most bystander effects are carried out in cell cultures by transferring conditioned medium (CM) from irradiated cells to non-irradiated cells, followed by incubation and analysis of radio-sensitivity [337]. To identify proteins involved in the CM, mass spectrometric analysis is performed. Using the above techniques, cytokines Interleukin 6 (IL6) and Interleukin 8 (IL8) have been found to be associated in bystander effect signaling in glioblastoma cells after treatment with γ irradiation. A similar study in multiple human tumor cell lines HT1080, U373MG, HT29, A549 and MCF-7 showed that these cell lines endogenously secreted cytokines IL-1 β , IL-6, IL-8, GMCSF and VEGF in the CM and correlated with the relative radio-resistivity of these tumor cell lines. On the basis of the order of radio-resistance, the HT1080 was the most radio-resistant followed by U373MG, HT29, A549 and MCF-7 cell lines. In all other cell lines used in this study except in the MCF7 cells, irradiation using acute doses of 2 and 6 grays (Gy) caused increased secretion of these cytokines in the CM but irradiation using fractionated doses of radiation (2 Gy given three times) did not change secretion of the cytokines. When bystander A549 cells were treated with the CM obtained from irradiated A549 cells, the cells showed decrease in clonogenic survival. Thus, the bystander effect on the

A549 cells was demonstrated to result in radio-sensitivity and may be caused due to the presence of less concentration of the radio-protective cytokines [339].

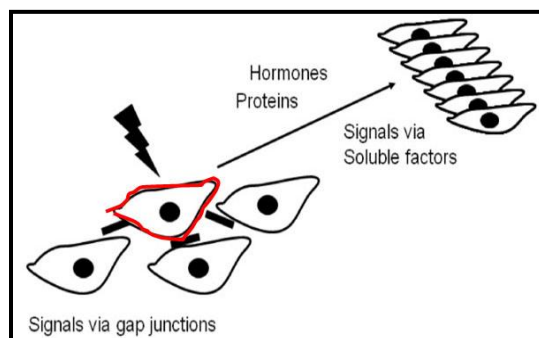


Figure 1.19. Schematic representation of the bystander effect. Chemical signals produced in an irradiated cell (with red borderline) are passed on to the neighboring cells through gap junctions. The irradiated cells also secrete hormones, proteins (cytokines) and other soluble factors that can act in a paracrine or endocrine manner to transfer radio-protective signals to distant cells or organs (adapted from [337]).

Thus, although radiation therapy has been used in treatment of cancers, there are multiple mechanisms by which radio-resistance can be induced by the same radiation treatment leading to local recurrence and poor prognosis of cancer.

1.4. PKP3 loss and radio-resistance

PKP3 loss causes decrease in cell to cell adhesion and loss of cell adhesion in EMT and metastatic cancers has been known to cause both intrinsic and radiation induced radio-resistance ([316, 340-342] and reviewed in [325]). To analyze if PKP3 loss can cause radio-resistance, HCT116 derived vector control and PKP3 knockdown clones were subjected to 4 Gy of γ irradiation or left un-irradiated. Twenty four hours post-irradiation, cells were trypsinized and 10,000 cells of each clone were plated onto 10cm plates and allowed to grow for 14 days. During

this time cells formed visible colonies which were stained with crystal violet and images of the plates were taken. It was demonstrated semi-quantitatively that irradiated PKP3 knockdown clones formed more colonies as compared to the irradiated vector control clones [257].

Thus, multiple mechanisms may exist by which PKP3 loss can regulate tumor formation and metastasis. PRL-3 mediated K8 de-phosphorylation leading to K8 protein stability and increase in K8 protein levels is just one of the mechanisms by which PKP3 loss in HCT116 cells can regulate neoplastic progression. But it still does not explain all the phenotypes found in HCT116 derived PKP3 knockdown clones like even though cell proliferation was not altered, what causes increased anchorage independent growth in vitro and increased size of tumors in vivo. More work is also required to understand the cell type specific effects of PKP3 loss in HaCaT, HCT116 and FBM cell lines. Further, as the mechanisms regulating radio-resistance observed upon PKP3 loss were not clear, experiments needed to be performed to identify the mechanisms underlying the acquisition of radio-resistance in cells lacking PKP.

2. AIMS AND OBJECTIVES

- 1. To determine the alterations in the transcriptome of cells lacking PKP3 and their relevance to neoplastic progression.**
- 2. To determine if PKP3 loss leads to radio-resistance and to identify the mechanisms regulating increase in radio-resistance upon PKP3 loss.**

3. MATERIALS AND METHODS

3.1. Plasmids and constructs.

The shRNAs against Δ Np63 α , LCN2, p38 α MAPK, p38 β MAPK, ELK1 and MMP7 were cloned in the multi-cloning site (MCS) of pLKO.1 EGFP-f-puro vector [343, 344] using AgeI and EcoRI restriction sites. The sequences for the oligonucleotides are in Table 3.1. The luciferase reporter assays were performed using the pGL3 basic vector and the pRL-TK vector. The pGL3 basic vector has a MCS region just upstream of a firefly luciferase reporter gene while the pRL-TK has a constitutively active thymidine kinase vector driving a Renilla luciferase reporter gene. Overlapping fragments of the LCN2 promoter were cloned into the MCS in the KpnI and XhoI sites. The sequences of the oligonucleotides used for cloning these promoter fragments are in Table 3.2.. The pRL-TK vector was used as a transfection control. The wild type (WT) p38 β and C terminal deletion mutants (V345 and F348) of p38 β were cloned in the pCEFL vector and was a kind gift from Dr. Engelberg's laboratory (National University of Singapore).

shRNA to target gene	Sequence (5' to 3')
shRNA Δ Np63 Forward	CCGGAATGCCAGACTCAATTTAGTCTCGAGACTA AATTGAGTCTGGGCATTTTTTTG
shRNA Δ Np63 Reverse	AATTCAAAAAAATGCCAGACTCAATTTAGTACTA AATTGAGTCTGGGCATT
shRNA LCN2.X forward	CCGGAAGATGTATGCCACCATCTATCTCGAGATAG ATGGTGGCATAACATCTTTTTTTG
shRNA LCN2.X reverse	AATTCAAAAAAAGATGTATGCCACCATCTATCTCG AGATAGATGGTGGCATAACATCTT
shRNA LCN2.Y Forward	CCGGAACTACAACCAGCATGCTATGCTCGAGCATA GCATGCTGGTTGTAGTTTTTTG
shRNA LCN2.Y reverse	AATTCAAAAAAACTACAACCAGCATGCTATGCTCG AGCATAGCATGCTGGTTGTAGTT

shRNA to target gene	Sequence (5' to 3')
shRNA Forward p38 α 1	CCGGAAATTCTCCGAGGTCTAAAGTCTCGAGACTTTAACCTCGGA GAATTTTTTTTGG
shRNA Reverse p38 α 1	AATTCAAAAAAAAAATTCTCCGAGGTCTAAAGTCTCGAGACTTTAGA CCTCGGAGAATTT
shRNA Forward p38 α 2	CCGGAACAGGATGCCAAGCCATGAGCTCGAGCTCATGGCTTGGCA TCCTGTTTTTTTGG
shRNA Reverse p38 α 2	AATTCAAAAAAAAACAGGATGCCAAGCCATGAGCTCGAGCTCATGGC TTGGCATCCTGTT
shRNA Forward p38 β 1	CCGGAAGCACCTGAAGCACGAGAACCTCGAGGTTCTCGTGCTTC AGGTGCTTTTTTTTGG
shRNA Reverse p38 β 1	AATTCAAAAAAAAAGCACCTGAAGCACGAGAACCTCGAGGTTCTCG TGCTTCAGGTGCTT
shRNA Forward p38 β 2	CCGGAACAACATCGTCAAGTGCCAGCTCGAGCTGGCACTTGACG ATGTTGTTTTTTTGG
shRNA Reverse p38 β 2	AATTCAAAAAAAAACAACATCGTCAAGTGCCAGCTCGAGCTGGCAC TTGACGATGTTGTT
shRNA Forward ELK1	CCGGAACATCATCCGCAAGGTGAGCCTCGAGGCTCACCTTGCGG ATGATGTTTTTTTGG
shRNA Reverse ELK1	AATTCAAAAAAAAACATCATCCGCAAGGTGAGCCTCGAGGCTCACCC TTGCGGATGATGTT
shRNA1 Forward MMP7	CCGGAACAGGCTCAGGACTATCTCACTCGAGTGAGATAGTCCTG AGCCTGTTTTTTTGG
shRNA1 Reverse MMP7	AATTCAAAAAAAAACAGGCTCAGGACTATCTCACTCGAGTGAGATA GTCCTGAGCCTGTT

Table 3.1. List of oligonucleotides used for generating shRNA constructs in pLKO.1 EGFP-f puro vector. The table represents name of the shRNA made against the indicated gene and the corresponding oligonucleotides used for cloning these oligonucleotides into the pLKO.1 EGFP-f puro vector.

Promoter region	Sequence (5' to 3')
- 1138 LCN promoter Forward	TAGGTACCCAAGCAGCACGTAGGCAGAG
-417 LCN promoter Forward	AAGGTACCCAGGAAACAGCACATGATCT
-153 LCN2 promoter Forward	TAGGTACCCTGTCTTGCCCAATCCTGAC
LCN2 promoter Reverse	ATCTCGAGTCAGGGCCGAGGAAGCAGGC

Table 3.2. List of oligonucleotides used for generating LCN2 overlapping promoter fragments. The table represents the oligonucleotides used to generate overlapping fragments of the LCN2 promoter: -1138 to +64 bps (L1), -417 to +64 bps (L2) and -153 to +64 bps (L3).

3.2. Cloning of oligonucleotides encoding shRNAs into pLKO.1 EGFP-f-puro vector

The oligonucleotides encoding shRNAs were designed using the Addgene pLKO.1 TRC cloning protocol. The oligonucleotides were designed to have sticky ends for AgeI and EcoRI sites so that the annealed oligonucleotides could be cloned into pLKO.1 based vectors digested with AgeI and EcoRI. The oligonucleotides were synthesized by Integrated DNA technologies (IDT) or Eurofins Scientific and delivered as high purity salt free (HPSF) oligonucleotides in a lyophilized form. The final concentration of the oligonucleotide stock solutions was 100pM in water as mentioned in the manufacturer's protocol and the stock solutions were stored at -20°C for further use.

For oligonucleotide annealing, 9µl each of the Forward and Reverse oligonucleotides were mixed with 2µl of Polynucleotide kinase Buffer (PNK Buffer, New England Biosciences). This mixture was then incubated at 95°C for 4 minutes followed by an incubation at 70°C for 10 minutes. Both these incubations were performed in a PCR machine. Thereafter, these oligonucleotides were transferred to a 70°C water bath and the water bath was switched off and

during the gradual cooling,, the oligonucleotide pairs anneal to each other. The annealed oligonucleotides can be stored at -20°C or used for cloning.

The next step in the cloning of shRNA is the phosphorylation of the annealed oligonucleotides. For this step, 2µl of the annealed oligonucleotides are mixed with 2µl of PNK Buffer, 1µl of 10mM ATP, 1µl of T4 PNK enzyme and 4µl distilled water (autoclaved MilliQ water as mentioned in 3.17). This reaction mixture was incubated in a 37°C water bath for 30 minutes and heat inactivated at 70°C for 10 minutes. The resultant solution of annealed and phosphorylated oligonucleotides was diluted 1:5 with sterile distilled water and used for ligation reactions.

The plasmid, pLKO.1 EGFP-f-puro was digested with AgeI and EcoRI and run on a 1% agarose gel. The band corresponding to the vector backbone was cut using a new scalpel

Reagents	control	Dilution of annealed oligonucleotide mix	
		undiluted	1:5 dilution
Vector backbone (100ng)	2 µl	2 µl	2 µl
Annealed oligonucleotides	0 µl	1 µl	1 µl
T4 DNA ligase buffer	2 µl	2 µl	2 µl
T4 DNA ligase	1 µl	1 µl	1 µl
Distilled water	15 µl	14 µl	14µl
Total volume		20 µl	20 µl

Table 3.3. Reaction mix for ligation of oligonucleotides to the pLKO.1 EGFP-f-puro vector backbone. The table lists the reagents and volumes required for ligation of the phosphorylated and annealed oligonucleotide pairs with the pLKO.1 EGFP-f-puro vector.

and eluted using the Qiagen Gel Elute Kit. Thereafter ligation of the phosphorylated and annealed oligonucleotides with the pLKO.1 EGFP-f-puro vector backbone was performed using the reaction mentioned in Table 3.3.

3.3. Cell lines, Transfections and Inhibitors.

Human colon carcinoma derived cell line, HCT116 (ATCC CCL-247), Human immortalized keratinocyte cell line, HaCaT [345] and Human embryonic kidney cell line, HEK293 (ATCC CRL-1573), were cultured in Dulbecco's modified Eagles medium (DMEM) (GIBCO), while the Fetal buccal mucosa, FBM [346] cells were cultured in Iscove's modified DMEM (GIBCO). Both the DMEM and IMDM media were supplemented with 10% Fetal bovine Serum (FBS) (JRH/GIBCO). Both types were media were supplemented with 100U of penicillin (Nicholas Piramal), 100 μ g/ml of streptomycin (Nicholas Piramal) and 2 μ g/ml of amphotericin B (HiMedia) [232, 233, 250]. The HCT116 and HaCaT derived PKP3 knockdown clones and the respective vector control clones were maintained in selection media containing 5 μ g/ml of blasticidin, while the FBM derived PKP3 knockdown and the vector control clones were maintained in media containing 0.5 μ g/ml puromycin as described [233]. Transient transfection of pLKO.1 EGFP-f-puro Δ Np63 shRNA vector in the HEK293 cells or FBM cells were performed using the calcium phosphate precipitation method [347] or by using Lipofectamine LTX reagent (Life Technologies). Transfection of the pCEFL p38 β MAPK wild type and C terminus truncated mutants in the HCT116 cells were performed using Lipofectamine LTX reagent.

For calcium phosphate mediated transient DNA transfection, the total amount of DNA, distilled water (D/W) and calcium phosphate required has been mentioned in Table 3.4. The composition

of the reagents used for calcium phosphate based transfection is described in the reagents section. Sterile D/W and a working aliquot of Calcium chloride

Diameter of culture dish	Volume of DNA (concentration 1µg/µl)	Amount of D/W	Amount of 0.5 M CaCl ₂	Amount of 2X BBS	Total Volume
35mm	5µl	45µl	50µl	100µl	200µl
60mm	10µl	90µl	100µl	200µl	400µl
100mm	25µg	225µl	250µl	500µl	1000ul

Table 3.4. Calcium phosphate transfection mix. The table mentions the volume of the reagents required to be mixed for transfection of DNA into cells grown in different culture dishes.

for transfection were stored at 4°C for not more than a month. BES buffered saline (BBS) was stored at -20°C. About half an hour prior to use, calcium chloride and D/W were warmed to 37°C and BBS was thawed at room temperature (RT) just prior to use. The reagents were mixed and added to cell culture plates maintained at 50 to 70% confluency. The plates were then kept in an incubator maintained at 37°C and 5% CO₂ for 16 hours. Thereafter, the media of the plates were removed and the cells were washed with phosphate buffered saline (PBS) two times and fresh media was added. The cells were incubated further for 48 hours and thereafter cell lysates were either prepared for Western blotting or for immuno-precipitation experiments.

For Lipofectamine mediated transient transfection, the total amount of DNA, Lipofectamine Plus reagent, Optimum Minimum Essential Media (OPTI-MEM) and Lipofectamine LTX required has been mentioned in Table 3.5. The DNA and Lipofectamine Plus reagent was added in OPTI-MEM and incubated at RT for five minutes. This was followed by addition of Lipofectamine

LTX reagent and incubation for thirty minutes. This transfection mix was added to the cells (at 50 to 70% confluency) having been newly fed with OPTI-MEM+10% FBS. The cells were then kept in an incubator maintained at 37°C and 5% CO₂ for 16 hours.

Diameter of culture dish	Volume of DNA (concentration 1µg/µl)	Amount of OPTI-MEM	Amount of Lipofectamine Plus reagent	Amount of Lipofectamine LTX
35mm	5µl	450µl	5µl	12.5 µl

Table 3.5. Lipofectamine LTX transfection mix. The table mentions the volume of the reagents required to be mixed for lipofectamine mediated transfection of DNA into cells grown in 35mm culture dishes.

Thereafter, the media of the plates were removed and the cells were washed with phosphate buffered saline (PBS) two times and fresh media was added. The cells were incubated further for 24 hours, trypsinized and re-plated into a 100mm plate. The cells were again incubated for 24 hours and thereafter cell lysates were either prepared for Western blotting or for immunoprecipitation experiments.

Lentivirus mediated transduction was also performed to analyze if the pLKO.1 EGFP-f-puro vector could be transduced into the FBM cells. The lentiviral vector pLKO.1.EGFP-f-puro was co-transfected with the lentiviral packaging vectors p-PAX2 (Addgene plasmid number: 12260) and p-MD2.G (Addgene plasmid number: 12259) into HEK293-T cells and the virus containing cell supernatant were harvested after 24 and 48 hours. The media were filtered using 0.45µM filters to remove the cell debris and added to FBM cells maintained at 50-70% confluency.

Thereafter the transduced FBM cells were incubated for 24 to 48 hours to analyze for expression of EGFP under a fluorescence microscope.

To generate HCT116 derived stable double knockdown clones for PKP3+LCN2; the PKP3 knockdown clone, shpkp3-2 was transfected with the pLKO.1 EGFP-f-puro vector expressing an shRNA targeting LCN2 using Lipofectamine LTX reagent. The protocol followed was the same as for transient transfection; however, 48 hours post transfection the transfected cells were trypsinized and re-plated into 100mm culture dishes in DMEM media containing 5µg/ml blasticidin and 0.5µg/ml puromycin to obtain single cell clones. Similarly, double knockdown clones derived from shpkp3-2 for p38α MAPK, p38β MAPK, ELK1 and MMP7 were generated using shRNAs against p38α MAPK, p38β MAPK, ELK1 and MMP7 respectively.

To assay the contribution of p38MAPK to LCN2 expression and PRL-3 to MMP7 expression, the p38MAPK inhibitor SB203580 (catalogue number 8307, Sigma) was added to cells at 1µM concentration for 24 hours and the PRL-3 inhibitor-1 (catalogue number P0108, Sigma) was added to cells in culture at a concentration of 5µM or 10µM for 24 hours. For treatment with different inhibitors, cells at 50 to 70% confluency were washed twice with PBS and then fresh media containing either the inhibitor or DMSO (solvent for the inhibitor) were added to the cells. The cells were incubated at 37°C and 5% CO₂ till the indicated time points and thereafter RNA or protein or cell supernatants were harvested from the treated cells.

3.4. Microarray analysis

RNA isolated from the FBM derived vector control and PKP3 knockdown cells and HCT116 derived vector control and PKP3 knockdown cells were Cy3 labeled and processed for the Sureprint G3 Human GE 8x60k microarray by single color hybridization. The results obtained

from the microarray were analyzed using the Agilent Feature Extraction software. Using normalized signal intensities (g-processed signal) obtained from the microarray, the fold changes of genes altered in FBM derived PKP3 knockdown clone (shpkp3-2) has been compared to the vector control clone (vec). Similarly, the HCT116 derived PKP3 knockdown clone (shpkp3-2) has been compared to the vector control clone (vec). A functional classification of the differentially regulated genes was performed using GeneSpring GX 11.0 software and gene ontology browser. The significant pathway list for differentially regulated genes was obtained using the GeneSpring GX 11.0 and Bioinformatics software (Genotypic, Bangalore, India). The data for the FBM derived clones has been deposited in the NCBI GEO database (Accession number GSE61512), while the data for the HCT116 derived clones have been deposited in the NCBI GEO database (Accession number GSE64580). Functional classification of genes altered upon PKP3 loss was performed using the PANTHER Classification System software [348, 349].

3.5. Semi-quantitative reverse transcriptase coupled PCR reaction (sqRT-PCR) and real time PCR or quantitative RT-PCR (qRT-PCR) reactions.

Cells were collected in RLT buffer and total RNA isolated using the Qiagen RNeasy Kit, following the manufacturer's protocol and 2 μ g of RNA was reverse transcribed to cDNA using the Applied Biosystems (ABI) High Capacity Reverse Transcriptase Kit (Life Technologies). The cDNA obtained was used for sqRT-PCR or SYBR Green based qRT-PCR. The sqRT-PCRs were performed using 500ng cDNA per reaction and Taq DNA polymerase (Fermentas, Thermo Scientific or New England Biolabs) for amplification of the PCR product. The qRT-PCRs were performed using 10ng cDNA per reaction and the ABI SYBR Green PCR Master mix (Applied Biosystems, Life Technologies) as per the manufacturer's protocol. The forward and reverse oligonucleotides used for sqRT-PCR and qRT-PCR in this study are shown in Table 3.6.

Common sqRT-PCR and qRT-PCR primers were generated using the Oligo explorer software (GeneLink). A few parameters were followed in making the primers:

- 1) Primers were designed between exon boundaries.
- 2) The melting temperature (T_m) value of the primers were between 60°C to 65°C.
- 3) The T_m difference between these primers was not be more than 5°C.
- 4)The self annealing and loop formation within the primers were minimum or none.
- 5) Primer dimer formation was minimum or none.
- 6) Primers were designed in such a way that the PCR product size was not more than 200 bps and was normally kept between 80 to 150 bps.
- 7) The primer length ranged between 19 to 25 bps.
- 8) The Gibb's free energy (ΔG) value for primer dimer interactions or for primer looping should be preferably positive and should not be less than -5 kilo calories/moles. A negative value of ΔG indicates a thermodynamically favourable reaction, thus if primer dimer formation or primer looping or primer self annealing has a negative ΔG , then the primers will have a greater tendency to form dimers or loop or self anneal than to bind to the template cDNA provided in the reaction mixture. This leads to failure of RT-PCR reactions. Thus, primers were selected such that the ΔG value for primer dimerization, looping and self annealing was either 0 or +ve.

The primers obtained with this criteria was verified using the BiSearch software [350] to ensure that the PCR product obtained is specific for the mRNA and doesnot amplify any part of the chromosome and by Primer BLAST [351] to ensure that the primers amplify only the specific

target cDNA. The primers were synthesized by Integrated DNA technologies (IDT) or Eurofins Scientific and delivered as High purity salt free (HPSF) oligonucleotides in a lyophilized form. The concentration of the primers were made up to 100pM by adding the required amount of water as mentioned by the manufacturer's protocol and stored for further use. A primer concentration of 20pM was required for sqRT-PCR while a primer concentration of 10pM was used for qRT-PCR.

Name of gene	Sequence (5' to 3')
GAPDH Forward	TGCACCACCAACTGCTTAGC
GAPDH Reverse	GGCATGGACTGTGGTCATGAG
PKP3 Forward	TGATGAGCTTCGCAAAAATG
PKP3 Reverse	CTGAGAGGCTGAGCTGAGGT
IL6 Forward	GCCACTCACCTCTTCAGAACGAATTG
IL6 Reverse	CCAGATTGGAAGCATCCATC
SAA1 Forward	CTGCAGAAGTGATCAGCG
SAA1 Reverse	ATTGTGTACCCTCTCCCC
S100A8 Forward	CAGTATATCAGGAAAAAGGGTGC
S100A8 Reverse	GCCACGCCCATCTTTATCA
S100A9 Forward	TCATCAACACCTTCCACCAA
S100A9 Reverse	TTTGTGTCCAGGTCCTCCAT
CCL2 Forward	GTCTCTGCCGCCCTTCTGTGC
CCL2 Reverse	AACAGCAGGTGACTGGGGCAT
CBS Forward	AAGTTGGCAAAGTCATCTACA
CBS Reverse	CAGCAAGTCAATGGCGGTG
SAA4 Forward	GTTCGTTTTTCAAGGAGGCT
SAA4 Reverse	TCCCTGAAGATAGACCCTGG

EPPK1 Forward	AGCTGGTGAGGATGTATAGAACACAC
EPPK1 Reverse	TGTTTGTGCTGGTTTCCTGC
ARHGEF5 Forward	GCCAACAAGCACAAGGGCTGGA
ARHGEF5 Reverse	AGCTGGGAGGAGTTGATGAGTTTGG
MMP9 Forward	GGGGGAAGATGCTGCTGTT
MMP9 Reverse	GGCTTCTCTCGGTACTGGA
MOBKL2B Forward	GTTCTGCACCGAGCGGACCTG
MOBKL2B Reverse	GGGAACACCCACGCATGTTGGA
Δ Np63 Forward	CTGGAAAACAATGCCAGAC
Δ Np63 Reverse	GGGTGATGGAGAGAGAGCAT
NR2F1 Forward	CATCGTGCTGTTACGTCAGACGCC
NR2F1 Reverse	GGGCAGTCGCAGCAGCAGTTT
IGFBP3 Forward	TGACGTGCGCACTGAGCGAG
IGFBP3 Reverse	GCTCACCTGGAGCTGGCGG
TAp63 Forward	TGGTGCGACAAACAAGATTG
TAp63 Reverse	ATAGGGACTGGTGGACGAGG
Pan p63 Forward	GACAGGAAGGCGGATGAAGATAG
Pan p63 Reverse	TGTTTCTGAAGTAAGTGCTGGTGC
LCN2 Forward	CCTCTACGGGAGAACCAAGGAGC
LCN2 Reverse	ACCTGTGCACTCAGCCGTCG
MMP7 Forward	ACAGTGGGAACAGGCTCAGGACT
MMP7 Reverse	TCTGGCACTCCACATCTGGGC
ELK1 Forward	TCCTACGCATACATTGACCC
ELK1 Reverse	CACTGGATGGAAACTGGAAG

Table 3.6. List of oligonucleotides used for sqRT-PCRs and qRT-PCRs. The table represents name of the genes and the corresponding oligonucleotides used for determining the expression of these genes by sqRT-PCR or qRT-PCR.

The reaction mix and PCR cycling conditions of a typical sqRT-PCR has been mentioned in Table 3.7 while the reaction mix for qRT-PCR using SYBR Green has been mentioned in Table 3.8 and in the following text.

(A) sqRT-PCR reaction mix		(B) PCR CONDITIONS		
Template cDNA (500ng/μl)	1 μl	Step	Temperature (°C)	Time (mins)
Taq Buffer	2 μl	1	94	3
Taq Polymerase	0.5 μl	2	94	1
10 mM dNTP	1 μl	3	T _{annealing}	1
20 pM forward primer	1 μl	4	72	1
20 pM reverse primer	1 μl	5	GO TO STEP 2- 35 times	
Autoclaved MilliQ water	18.5 μl	6	72	10
Total volume per reaction	25 μl	7	4	forever

Table 3.7. Reaction mix and PCR conditions for sqRT-PCR. The table represents all the volumes and concentrations of the different components required to set up a sqRT-PCR (A) and the PCR conditions that can be used (B). The annealing temperature (T_{annealing}) can be varied on the basis of the primers used.

Reagents	Volume	For duplicates	Total volume
2X SYBR Green Master mix	2.5μl	x 2	5 μl
Forward primer (10pM)	0.25 μl	x 2	0.5 μl
Reverse primer (10pM)	0.25 μl	x 2	0.5 μl
Total volume			6 μl

Table 3.8. Reaction mix of SYBR green and primers used for qRT-PCR. The table represents volumes and concentrations of SYBR Green master mix and the primers required to set up a sqRT-PCR.

The 6 μ l (SYBR Green Master mix + primers) solution was mixed with 4 μ l of cDNA (concentration 10ng/ μ l) to make a total volume of 10 μ l. This 10 μ l was divided equally and added into two wells of a ABI MicroAmp^R Optical 384 well Reaction plate. After adding the reaction mixes (of all the genes needed to be analyzed) into the wells of the Reaction plate, the plate was covered using the ABI MicroAmp^R Optical adhesive film. Thereafter the adhesive film was smoothed on top of the plate using the MicroAmp^R Optical adhesive film applicator. All these above steps were performed in low light conditions because SYBR green is sensitive to light. The plate was finally wrapped with a cling wrap and then in an aluminium foil and centrifuged for 2 minutes at 2500 rpm (1139xg). Multiple rounds of centrifugation followed by tapping of the wells from the bottom was done (if required) to ensure that no bubbles were present in the wells before setting up the qRT-PCR reaction. The thermal cycling conditions used for the qRT-PCR can be standardized in the 7900HT Fast Real time PCR system or in the QuantStudioTM12K Flex Real-Time PCR System (Life Technologies). As an example, the Thermal cycling protocol for a primer pair having annealing temperature (T_{anneal}) of 60°C has been shown in Figure 3.1 (Life technologies). The T_{annealing} can vary according to the primers designed for qRT-PCR.

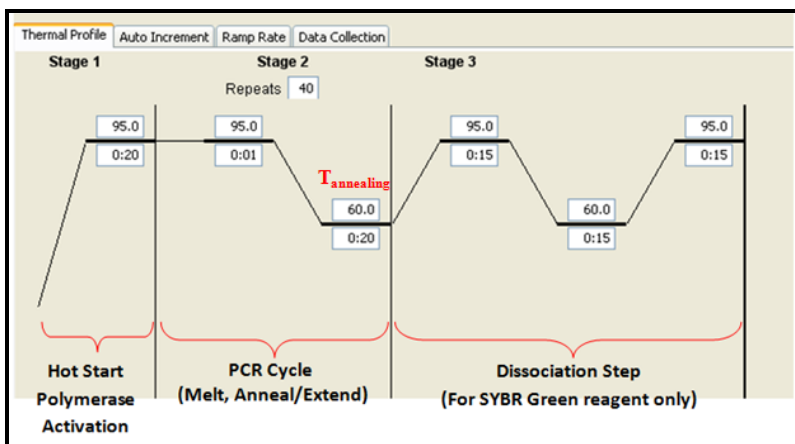


Figure 3.1. Thermal cycling conditions for a typical qRT-PCR. The figure represents the PCR conditions required for qRT-PCR in the 7900HT Fast Real time PCR system.

SYBR Green based qRT-PCR is based on principle of SYBR Green I being an intercalating agent like ethidium bromide (ETBR). SYBR Green intercalates with double stranded DNA. The resulting DNA-dye-complex absorbs blue light ($\lambda_{max} = 497 \text{ nm}$) and emits green light ($\lambda_{max} = 520 \text{ nm}$). The emitted light can be captured using a sensitive fluorescence detector and quantitated [352, 353].

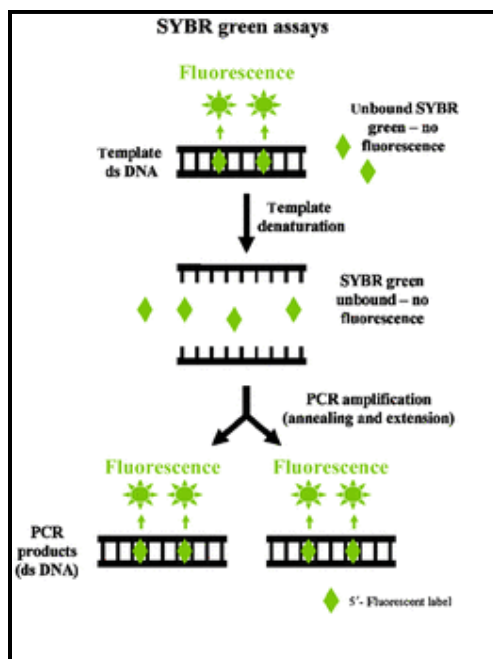


Figure 3.2. Principle of SYBR green based qRT-PCR. SYBR Green binds to double-stranded DNA and emits a fluorescent signal. SYBR green does not fluoresce when it is in the unbound state. Therefore amplification of the template DNA is measured in each thermal cycle by the corresponding increase in fluorescence intensity [354].

The fluorescence intensity for every gene in the SYBR Green assay increases per cycle as shown in Figure 3.2. The qRT-PCR machine sets an arbitrary threshold fluorescent intensity value (or cut-off value). The time taken for the fluorescence intensity to surpass this threshold value is called the Ct value. For a target gene it is represented as $Ct_{\text{target gene}}$ while for the control gene (used for normalization), it is called the $Ct_{\text{control gene}}$. The difference between the Ct values (ΔCt) of $Ct_{\text{target gene}}$ and $Ct_{\text{control gene}}$ determines the relative expression of any target gene. When the relative expression of a target gene is analyzed within two different clones (suppose 1 and 2), then the measure of $\Delta\Delta Ct$ is used:

$$\Delta\Delta Ct = \Delta Ct_{\text{clone2}} - \Delta Ct_{\text{clone1}}.$$

The fold change in expression of any target gene in clone 2 relative to the expression of the same gene in clone 1 can be calculated by using the $2^{(-\Delta\Delta Ct)}$ method [355] where:

$$\text{Fold change} = 2^{(-\Delta\Delta Ct)} = 2^{-(\Delta Ct_{\text{clone2}} - \Delta Ct_{\text{clone1}})}.$$

In the qRT-PCRs, a change in expression of two-fold either way was considered significant.

3.6. Antibodies and Western blot analysis.

For Western blots, the mouse monoclonal β actin antibody (clone AC74, catalogue number A5316, Sigma) was used at a dilution of 1:5000, the mouse monoclonal PKP3 antibody (clone 23E34, catalogue number 35-7600, Invitrogen) at a dilution of 1:2000, rabbit polyclonal P-

cadherin antibody (clone H-105, catalogue number sc-789, Santa Cruz) was used at a dilution of 1:500, mouse monoclonal Δ Np63 antibody (clone 4A4, catalogue number sc8431, Santa Cruz) was used at a dilution of 1:500, goat polyclonal LCN2 antibody (catalogue number AF1757, R&D Systems) was used at a dilution of 1:2000 (made in 5% milk), rabbit monoclonal phospho-p38MAPK (Threonine 180/Tyrosine 182) antibody (clone D3F9, catalogue number 4511, Cell Signaling technology) was used at a dilution of 1:1000, rabbit polyclonal p38MAPK antibody (catalogue number 9212, Cell Signaling technology) was used at a dilution of 1:1000, rabbit monoclonal phospho-p44/42 (ERK1/2) (Threonine 202/ Tyrosine 204) antibody (clone D13.14.4E, catalogue number 4370, Cell Signaling technology) was used at a dilution of 1:1000, rabbit polyclonal p44/42 (ERK1/2) antibody (catalogue number 9102, Cell Signaling technology) was used at a dilution of 1:3000, rabbit polyclonal p38 α MAPK antibody (catalogue number 9218, Cell Signaling technology) was used at a dilution of 1:1000, rabbit monoclonal p38 β MAPK antibody (clone C28C2, catalogue number 2339, Cell Signaling technology) was used at a dilution of 1:1000, rabbit monoclonal phospho-ATF2 (Threonine 71) antibody (catalogue number 9221, Cell Signaling technology) was used at a dilution of 1:1000, rabbit monoclonal ATF2 antibody (clone 20K1, catalogue number 9226, Cell Signaling technology) was used at a dilution of 1:1000, rabbit polyclonal phospho-MSK1 (Threonine 581) antibody (catalogue number 9595, Cell Signaling technology) was used at a dilution of 1:1000, rabbit polyclonal phospho-ELK1 antibody (Serine 383) (catalogue number 9181, Cell Signaling technology) was used at a dilution of 1:1000, rabbit polyclonal ELK1 antibody (catalogue number sc-22804, Santa Cruz Biotechnology) was used at a dilution of 1:1000 (made in 2% BSA), mouse monoclonal haemagglutinin (HA) antibody (clone 12CA5, purified cell supernatant) was used at a dilution of 1:50, rabbit polyclonal phospho-PKC α/β II (Threonine

638/641) (catalogue number 9375, Cell Signaling technology) was used at a dilution of 1:1000, rabbit polyclonal PKC α antibody (catalogue number 2056, Cell Signaling technology) was used at a dilution of 1:1000, rabbit polyclonal phospho-EGFR (Tyrosine 845) antibody (catalogue number 2231, Cell Signaling technology) was used at a dilution of 1:1000, rabbit monoclonal phospho-EGFR (Tyrosine 1068) antibody (clone D7A5, catalogue number 3777, Cell Signaling technology) was used at a dilution of 1:1000, rabbit monoclonal EGFR antibody (clone 15F8, catalogue number 4405, Cell Signaling technology) was used at a dilution of 1:1000, rabbit monoclonal phospho-MEK1/2 (Serine 217/221) antibody (clone 41G9, catalogue number 9154, Cell Signaling technology) was used at a dilution of 1:1000, rabbit monoclonal MEK1/2 antibody (clone 30C8, catalogue number 9146, Cell Signaling technology) was used at a dilution of 1:1000, mouse monoclonal MMP7 antibody (clone JL07, sc-80205, Santa Cruz,) at a dilution of 1:100; Lamin A antibody (Abcam, ab26300) at a dilution of 1:500 and α -tubulin (Abcam, ab7291) at a dilution of 1:500. For detection of phosphorylation of proteins, Western blots were performed using cell lysates made in EBC lysis buffer containing protease inhibitor mix (as mentioned in 3.17) while for total proteins, cell lysates made in either EBC lysis buffer containing protease inhibitor mix or 1X sample buffer was used. Goat anti-mouse secondary antibody (catalogue number 31430, Life Technologies) was used at a dilution of 1:2500, goat anti-rabbit secondary antibody (catalogue number G-21234, Life Technologies) was used at a dilution of 1:2500 while donkey anti-goat secondary antibody (catalogue number sc2020, Santa Cruz) was used at a dilution of 1: 250. The blots were developed using Supersignal West Pico Chemiluminescent Substrate (Pierce) according to the manufacturer's instructions.

Cells were lysed in 1X sample buffer as described [233] and protein concentration quantitated using Folin-Lowry's method. 75 μ g of the extract was resolved on 10% SDS-PAGE gels and

transferred to nitrocellulose membranes (Mdi, Membrane Technologies) followed by Western blotting with the indicated antibodies. Western blots for LCN2 and MMP7 were performed as follows. The cell supernatant from plates having cells growing in serum containing media with or without any inhibitor (PRL-3 inhibitor or p38MAPK inhibitor) were harvested and centrifuged for 10 mins at 5000 rpm (7500xg) to remove any cell debris. Three volumes of acetone were added to the supernatant and the reaction incubated at -20°C for 24 hours and then centrifuged at 3000rpm (4500xg) for 15 minutes at 4°C. The precipitate obtained was washed twice with acetone and the pellet air dried at RT for 16 hours. The precipitate was boiled in 1X SDS lysis buffer (2% SDS, 50mM Tris pH 6.8), then diluted ten-fold in 1X SDS lysisbuffer and the protein concentration was measured using Folin-Lowry's method. 100µg of the lysate was resolved on 12% SDS-PAGE gels and transferred to nitrocellulose followed by Western blots with antibodies to LCN2 or MMP7. The blot was stained with Ponceau-S (Sigma) to demonstrate equal loading.

3.7. Immuno-flourescence assays

Immuno-flourescence assays were performed to determine intracellular localization of p38MAPK in the HCT116 derived PKP3 knockdown clones and the vector control clones. The cells were cultured on glass coverslips at 50-70% confluency. The cells were washed carefully twice with 1X PBS followed by fixation in 4% paraformaldehyde for 20 minutes at room temperature or overnight at 4°C. Thereafter the cells were washed thrice or more with PBS till the smell of paraformaldehyde gets removed. The cells were then permeabilized using 0.3% Triton-X100 in 1X PBS for 20 minutes at room temperature. Primary antibodies were prepared in 3% BSA in 1X PBS + 0.1% NP-40 solution. The p38MAPK antibody was used at 1:50 dilution for immuno-flourescence. 50µl of the primary antibody solution was added on a parafilm and the coverslips were inverted onto the solution. These parafilms with the coverslips

were then kept inside a humidified chamber for 16 hours (overnight) at 4°C for incubation. Thereafter the coverslips were inverted to have the cells facing upwards. The cells were then washed with 1X PBS and 1X PBS + 0.1% NP-40 four times alternatively. Secondary antibodies were prepared in 3% BSA in 1X PBS + 0.1% NP-40 solution. The secondary antibody, Alexa Alexa 488 conjugated anti rabbit IgG (Invitrogen) was used at a dilution of 1:100. 50µl of secondary antibody was placed on a fresh piece of parafilm and the coverslips were inverted onto it and incubated for half hour at room temperature in a humidifying container. The coverslips were re-inverted followed by six alternate washes of 1X PBS and 1X PBS + 0.1% NP-40. Thereafter 50µl of DAPI was placed on a fresh piece of parafilm and the coverslips were inverted onto it and incubated for exactly 1 minute at room temperature. The coverslips were re-inverted followed by four washes of 1X PBS. The coverslips were then mounted on chromic acid treated, clean glass slides using 10-20 µl of Vectashield mounting agent (Vector Laboratories). Confocal images were obtained by using a LSM 510 Meta Carl Zeiss Confocal system with an Argon 488 nm and Helium/Neon 543 nm lasers. The intensity of staining for the p38MAPK in the nucleus was measured using the Axiovision software.

3.8. Immuno-precipitation assays

To analyze if PKP3 binds to p38β MAPK, pCEFL vectors encoding the HA tagged wild type p38β MAPK and the C terminal truncated mutants of p38β MAPK were transiently transfected in HCT116 cells. As a control for HA tag, HA-pcDNA3 vector was also transfected. For each plasmid, transfection was performed in two 100mm plates. 48 hours after transfection, the cell culture medium was decanted from both the plates and 1ml of cold PBS (pre-cooled to 4°C) was added to each plate. The cells on each plate were scraped using a cell scraper and collected in separate 1.5 ml eppendorfs kept on ice. The cells were then pelleted down by centrifugation at

2500 rpm for 2 minutes and the PBS was decanted. 500 μ l PBS was again added and the cells from both the eppendorfs were pooled, centrifuged again and PBS removed. Thereafter, 1ml of EBC lysis buffer containing protease inhibitors (as mentioned in 3.17) was added to the cells and incubated for 15 minutes on ice. This was followed by centrifugation at 10,000 rpm for 15 minutes at 4°C. The supernatant was transferred to a new 1.5 ml eppendorf. 100 μ l of this supernatant was kept separately and represented as 10% whole cell extract. To this 50 μ l of 3X sample buffer (mentioned in 3.17) was added, boiled in a water bath for 7 minutes and stored in -80°C. To the remainder of the supernatant, 200 μ l of the anti-HA antibody (clone 12CA5, purified cell supernatant) was added and the eppendorfs were kept on a rocker for two hours at 4°C. Next, 30 μ l of Protein G Sepharose (GE Healthcare) was added to the reaction mixture and the reactions were incubated at 4°C for one hour on a rocking platform. Thereafter the eppendorfs were centrifuged at 3000rpm for 1 minute. The supernatant was removed and the immuno-precipitates were washed with NET-N buffer. The eppendorfs were centrifuged at 3000rpm for 15 seconds and the supernatant was removed. Two more NET-N washes were given in the same manner followed by addition of 50 μ l of 3X sample buffer and boiling. These immunoprecipitated samples and the 5% whole cell extracts were then resolved on a SDS-PAGE gel and Western blotting was performed to detect HA and PKP3.

3.9. Scratch wound healing assays

Scratch wound healing assays were performed as described [232]. Briefly, in each well of a 6 well plate, cells were grown to 90% confluency, followed by treatment with 10 μ g/ml of mitomycin C (Sigma) for three hours. Mitomycin C inhibits cell proliferation, thus the rate of wound healing will only depend on the migration rate of cells and not on cell proliferation [356]. Three hours after the addition of mitomycin C, the cells were washed and a linear scratch wound

was made on the bottom of plate per well. The wells of this plate were then visualized under an Axiovert 200M Inverted microscope (Carl Zeiss) fitted with a cell incubator stage maintained at 37°C and 5% CO₂. Cells were observed by time lapse microscopy and images taken every 10 minutes for 20 hours using the AxioCamMRm Camera (Zeiss) with a 10X phase I objective. Axiovision software version 4.8 (Zeiss) was used to measure the cell migration. Three independent experiments were performed in triplicates for each clone.

3.10. Matrigel invasion assays.

Matrigel invasion assays were performed as described [357, 358]. Briefly, 2×10^5 cells resuspended in 200µl of serum free media were added to the upper chambers and 400µl of serum containing media was added in the lower chamber. The inner side of the insert was pre-coated with 5µg of Matrigel (BD Biosciences). After 24 hours, cell culture inserts were then removed from the wells and the cells attached to the inner side of the insert were removed using cotton buds. The inserts with cells on the outer side of the membrane were fixed with 4% para-formaldehyde, stained with 1% crystal violet and mounted on slides using DPX mountant (Qualigens). Images were taken using Olympus SZ61 stereo microscope using a 10X objective lens. Three independent experiments were performed for each clone.

3.11. Soft agar colony formation assays

The soft agar colony formation assay determines the anchorage independent growth property of cells [233]. Briefly, low melting point (LMP) agarose of two different concentrations were prepared, 1.6% and 0.8%, and autoclaved to maintain sterility. After autoclaving, both the LMP agarose solutions were kept on a float in a water bath set at 40°C to prevent the agarose from forming a gel. The 1.6% LMP agarose was then mixed with equal volumes of 2X DMEM + antibiotic +FBS mix (a mixture of sterile 2X concentrated DMEM solution, 2X concentrated relevant antibiotic and 20% FBS). Upon mixing, the final concentration of agarose became 0.8%, the concentration of DMEM and antibiotic becomes 1X and concentration of FBS became 10% (which is the concentration required for optimal growth of cells). Now 2 ml of this solution was poured onto 35mm cell culture plates slowly and allowed to form a thick solid layer on the plate. This was called the lower layer of the soft agar plate. Next, the cells of the relevant clones were trypsinized and resuspended in 1ml of 2X DMEM media. The cells are then counted using a haemocytometer to determine the concentration of the cells in the solution. Meanwhile, the 0.8% LMP agarose was mixed with equal volumes of the 2X DMEM + antibiotic + FBS mix to make a final volume of 0.4% LMP agarose + DMEM solution. To 1 ml of this solution, 2500 cells were resuspended slowly to form a homogenous suspension and spread evenly on top of the lower layer of soft agar plate and allowed to settle down and form a semi-solid upper layer. Thereafter, the plates were kept in a tissue culture incubator maintained at 37°C, 5% CO₂, for three weeks. A volume of 150µl to 200µl of fresh DMEM media with the relevant antibiotics were added on top of the soft agar plates every 2 days during these three weeks of incubation. Thereafter the total number of colonies formed on the soft agar plate was counted by making

grids at the bottom of the soft agar plate. Three independent experiments were performed in triplicates for each clone.

3.12. Growth Curves

2×10^5 cells were plated in 35mm dishes and fed every two days during the course of the experiment. At various intervals, the cells were harvested by trypsinization and counted in triplicate using a haemocytometer. The number of cells obtained at different time points was plotted against time to generate the growth curves.

3.13. Luciferase reporter assays

Luciferase reporter assays were used to determine the promoter activity of the overlapping fragments of LCN2 promoter (mentioned in Table 3.2) in the HCT116 derived PKP3 knockdown clones and the vector control clone. These assays were also used to determine if LCN2 promoter activity could be altered upon ELK1 knockdown (See Results section). The reagents required for the luciferase assay was provided in the Dual Luciferase reporter assay system (Promega). The major components of this kit were the LARII reagent (the substrate for firefly luciferase), Stop and Glo reagent (a mixture of the inhibitor of luciferase and coelentraine (the substrate for Renilla luciferase) and Passive lysis buffer (required for cell lysis). The luciferase reporter assay was performed according to the manufacturer's protocol (Promega). Briefly, cells were grown in 12 well plates to 50 to 70% confluence. Thereafter the cell culture media was decanted and cells were washed two times with 1X PBS. 100 μ l of passive lysis buffer was added to the cells and the plate was placed on a rocker for 15 minutes for cell lysis. The lysed cells were then pipetted out into a 1.5ml eppendorf tube and centrifuged to 13,000 rpm for 30 seconds at 4°C to remove the cell debris. The supernatant was collected in a fresh eppendorf tube. The supernatant was then

used for protein estimation by Bradford's method and luciferase reporter assay by the Dual luciferase reporter assay kit (Promega).

Bradford's method uses the property of the Bradford's dye which can bind to proteins specifically causing a shift of the absorption maximum of the dye from 465 to 595nm. Briefly, 5 μ l of the cell lysate was added to different wells of a 96 well plate. Five standard solutions (with known protein concentrations) containing 0, 10, 20, 30, 40 and 50 μ g/ml of Bovine serum albumin (BSA) were also made and 5 μ l of these solutions were added to new wells of the same 96 well plate as above. Thereafter 250 μ l of the Bradford's reagent was added to these wells. The plate was then placed inside an ELISA plate reader and readings were taken at 595nm. The readings obtained were used for determining the protein concentration of the cell lysates.

For luciferase reporter assays, 50 μ l of the LARII reagent was added into the required number of wells of 96-well plate and 10 μ l of cell lysates were aliquoted into these wells. The LARII reagent was also added in a well with no lysate and was designated as a Blank well. These cell lysates and the LARII solutions were mixed properly with pipette tips and the plate was inserted into a luminometer (Berthold). The chemiluminescence intensity for each of the luciferase reactions were measured for a period of 1 minute per well. This value was the measurement for the firefly luciferase intensity and designated as FL. The FL value for the blank well was used for normalization of the FL values for the cell lysates. Thereafter the plate was ejected out of the luminometer and 50 μ l of the Stop and Glow reagent was added immediately to all the wells in use. This plate was inserted back into the luminometer and chemiluminescence intensity was measured for 1 minute per well. This value was the Renilla luciferase intensity and designated as RL. The RL value for the blank well was used for normalization of the RL values for the cell lysates. Finally the ratio of the FL value to the RL value of the cell lysates were calculated and

divided by the amount of protein concentration of the corresponding cell lysate. The value of the (FL/RL)/Protein concentration so obtained was plotted on the Y axis and the name of the corresponding clones were plotted on the X axis of a histogram.

3.14. Nuclear cytoplasmic fractionation:

Nuclear and cytoplasmic fractions were isolated from HCT116 derived PKP3 knockdown clones and the vector control clone as per the manufacturer's instructions using the NE-PER kit from Promega. Total cell lysates obtained from the above cell lines were used as controls for the experiment.

3.15. Tumor formation in nude mice

BALB/c Nude mice (CAnN.Cg-Foxn1nu/Crl) of 6-8 weeks old, provided by the ACTREC animal house facility, was used for the study. 1×10^6 cells of the HCT116 based shpkp3-2 derived vector control and double knockdown clones were resuspended in 100 μ l of PBS and injected sub-cutaneously in the dorsal flank of mice. Six mice were injected for each clone. Tumor formation was monitored at intervals of 2 to 3 days and tumor size was calculated weekly for 5 weeks using the formula $(0.5 \times LV^2)$ where L is the largest dimension and V its perpendicular dimension [233]. The maximum tumor volume of 1045.421 mm³ was obtained 5th week post-injection for a mouse injected with shpkp3-2+vec. No surgical procedure was involved in the present study and therefore no anesthetic or analgesic was employed during these experiments. During injections, the animals were handled by trained, certified animal technicians and were injected by their in-house veterinarian with minimum distress to animals. Mice were sacrificed 5 weeks post injection. Animals were euthanized as per in-house Standard Operating

Procedure (SOP) approved by the attending veterinarian (AV) of the ACTREC animal house facility. Carbon dioxide (CO₂), an inhalant euthanasia agent recommended by the Committee for the Purpose of Control and Supervision of the Experiments on Animals (CPCSEA), Government of India, was used for euthanasia of mice. Euthanasia was performed under the supervision of the attending veterinarian and according to the American Veterinary Medical Association (AVMA) guidelines for the euthanasia of animals (2013 Edition). Briefly, a compressed CO₂ cylinder was used as a source for carbon dioxide to control the inflow of gas, which was connected to a euthanasia chamber. The mice were kept in the chamber and an optimal flow rate was maintained to fill 20% of the chamber volume. After keeping the mice in the chamber, the CO₂ cylinder supply valve was turned on to deliver the gas in the chamber so that animals were exposed to the gas slowly and steadily. After sufficient exposure like for 2 to 3 minutes, mice showed cessation of respiration and heart beats. The chamber was not prefilled with CO₂ and was vented out post sacrifice and before the next animal was introduced into the chamber. Thereafter, the mice were removed from the chamber and a cervical dislocation performed to ensure that the mice were dead.

3.16. Ethics statement

Animals were maintained in the ACTREC animal house facility following the national guidelines mentioned by the Committee for the Purpose of Control and Supervision of the Experiments on Animals (CPCSEA), Ministry of Environment and Forest, Government of India. A controlled environment was provided to the animals with a temperature of $22\pm 2^{\circ}\text{C}$ and relative humidity maintained at 40-70%. A 12 hours day night cycle was maintained (7:00 to 19:00 day and 19:00 to 7:00 night). The animals were given autoclaved balanced diet prepared in house and sterile water. Individually ventilated Cage system (IVC, M/S Citizen, India) was used to house mice used in the experiments. These IVCs were provided with autoclaved corn cob as bedding for the mice. Animal euthanasia was done under the guidelines of AVMA as mentioned above using CPCSEA recommended euthanizing agent, carbon dioxide. The Institutional Animal Ethics Committee (IAEC) of the Advanced Centre for Treatment Research and Education in Cancer (ACTREC) approved all the protocols used in this report. The project number for the study is 16/2008 and was approved in November 2008.

3.17. Clonogenic survival assays

For all radiation experiments, the source used for irradiation is the radioactive Cobalt 60 isotope ($^{60}\text{Co}_{27}$), a clinically used radiation source [359]. $^{60}\text{Co}_{27}$ is not a naturally occurring element because of its high reactivity, but it can be generated when the nucleus of the naturally occurring cobalt isotope, cobalt-59 ($^{59}\text{Co}_{27}$) is bombarded with a photon. The resultant $^{60}\text{Co}_{27}$ is a highly unstable isotope, it decays to Nickel-60, ($^{60}\text{Ni}_{28}$) by the emission of beta particle. The activated nickel nucleus emits two γ ray photons (γ irradiation) with an average energy of 1.35 mega-electron-volts (MeV). This energy is used to kill cancer cells. To determine if PKP3 loss leads to increased radio-resistance, PKP3 knockdown clones derived from different cell types and their respective vector control clones or double knockdown clones derived from the HCT116 derived

PKP3 knockdown clones and the vector control clones were grown to 75% confluency in 35mm cell culture plates. For radiation treatment, the sides of these plates were wrapped in parafilms and taken carefully to the BHABHATRON facility at the Department of Radiation Oncology, TMC-ACTREC. The BHABHATRON machine (an indigenous telecobalt machine developed by Bhabha Atomic Research Centre) was used for irradiating cells to 0, 2, 4 and 8 Gy of γ irradiation. The time of exposure to the $^{60}\text{Co}_{27}$ source, required for the cells to receive the required doses, was determined by radiation physicists of the Department of Radiation Oncology, TMC-ACTREC. Thereafter the cell culture plates with irradiated cells were brought into the tissue culture hood, the parafilms were removed and the cells were kept in a tissue culture incubator maintained at a temperature of 37°C and having CO₂ level of 5%. After 8 hours incubation, the cells were trypsinized and counted. As indicated in the Results section, different number of cells for the different γ irradiation doses was seeded into 60mm plates. These plates were incubated into the tissue culture incubators. Colonies were allowed to be formed for 21 days. Thereafter, these colonies were fixed using 4% paraformaldehyde. Thereafter the cells were washed thrice or more with PBS till the smell of paraformaldehyde gets removed. The cells were then stained with 1% crystal violet for 1 hour. The plates were then washed with tap water to remove the excess crystal violet dye. The individual colonies that had been formed got stained with crystal violet. Thereafter the plates were inverted and left to dry. On the next day, the number of colonies were counted and used to generate the survival curves for each clone. The survival curves were plotted using the values obtained for the survival fraction on the Y axis (log scale) and the corresponding irradiation doses on the X axis [360] where :

Survival fraction (SF) = (number of colonies formed after treatment)/(number of colonies seeded x Plating efficiency)

In this equation Plating efficiency (PE) = number of colonies formed from un-irradiated cells/ number of un-irradiated cells seeded.

The p value for the assays was calculated using the ANOVA analysis feature of the SPSS software as mentioned in [360].

3.17. Reagents for different experiments

(a) Calcium phosphate transfection

i. 2X BBS (BES-buffered solution), pH6.95

Component	Final concentration required	Amount
BES (Sigma)	50mM	1.066g
Sodium chloride (NaCl) (HiMedia)	250mM	1.636g
Sodium phosphate dibasic dihydrate (Na ₂ HPO ₄ .2 H ₂ O) (Sigma)	1.5mM	0.0267g
MilliQ water		Make up volume to 100ml

In this reaction, MilliQ water was used. MilliQ water is the name given to double distilled water obtained from the MilliQ Integral Water Purification System (EMD Millipore) installed in ACTREC. After ensuring that all the components added had mixed completely, the pH of the BBS solution was carefully adjusted to exactly 6.95 with 5N NaOH (SD Fine Chemicals) and then filtered using a 0.22µM membrane filter. BBS solution was divided into multiple aliquots and stored in -20°C.

ii. 0.5M Calcium Chloride (CaCl₂) solution for transient transfection

18.375g of CaCl₂ was dissolved in 250ml of distilled water. This was filter-sterilized into sterile 50 ml tubes and stored at -20°C. Only one vial was assigned for immediate use and kept at 4°C.

iii. Distilled water

MilliQ water was autoclaved in glass bottles and kept at room temperature (for regular use) or stored at 4°C. This autoclaved sterile MilliQ water is called distilled water and used for molecular biology reactions like PCR ligation reactions and for transfection.

(b) For bacterial growth and selection

i. Luria Bertoni (LB) media

LB media is required for optimal bacterial growth. For 1 litre of LB media, the reagents required are:

Component	Volume or Amount
Tryptone (HiMedia)	10g
Yeast extract (HiMedia)	5g
NaCl	10g
1M Tris pH 7.5	10ml
MilliQ water	make up volume to 1litre

The LB media was divided into multiple 50 ml conical tubes and autoclaved. After autoclaving these tubes were either kept at room temperature for immediate use or stored at 4°C.

ii. Ampicillin

Ampicillin was used as a selection antibiotic for bacteria transformed with plasmids having the ampicillin resistant gene along with the gene or shRNA coding sequence of interest. 100mg of Ampicillin (Sigma) was dissolved in 1 ml of distilled water to make a stock concentration of 100mg/ml. Ampicillin is added to the LB media or while making LB plates for bacterial antibiotic selection. The final working concentration for ampicillin required in an LB broth is 100µg/ml.

iii. LB Agar plates.

Component	Volume or Amount
Tryptone (HiMedia)	10g
Yeast extract (HiMedia)	5g
NaCl	10g
1M Tris pH 7.5	10ml
MilliQ water	make up volume to 1litre

After these components were completely mixed, the solution was added into a plastic or glass beaker containing 20g Agar. These components were then autoclaved. After autoclaving the solution was allowed to cool to about 37°C and 1ml ampicillin was added for 1 litre of LB Agar solution so that the final concentration of ampicillin becomes 100µg/ml. This solution was now poured slowly onto plastic bacterial culture plates to form a thick layer of LB agar. These LB agar plates were then allowed to cool at room temperature.

(c) Protein Estimation**i. Copper tartarate carbonate (CTC) Solution**

CTC solution is a mixture of 0.4% hydrated copper sulphate ($\text{CuSO}_4 \cdot 5\text{H}_2\text{O}$), 0.4% potassium sodium tartarate and 20% sodium carbonate. To make the CTC solution, first, 0.1g of potassium sodium tartarate was dissolved in 25 ml MilliQ water in a small beaker. Thereafter, 0.1g of copper sulphate was dissolved in 25ml MilliQ water, separately in another beaker. Now in a glass bottle, 10g of sodium carbonate was added to 50ml of MilliQ water and dissolved. After the sodium carbonate got dissolved completely, the potassium sodium tartarate solution and the copper sulphate solution was added at the same time, but slowly and with stirring. This reaction is light sensitive, so it is better to do all make these solutions in dark or in low light. After all the

reagents got dissolved, the glass bottle was wrapped with aluminum foil and labeled as CTC solution. This solution was stored at room temperature and not used for more than a month.

ii. 10 % Sodium Dodecyl Sulphate (SDS)

10g SDS was dissolved in 50ml MilliQ water and the volume was made up to 100ml.

iii. 0.8 N Sodium hydroxide (NaOH)

3.2g Sodium hydroxide was dissolved in 50ml of MilliQ water and make volume to 100ml.

iv. Folin’s Solution A

For any given volume of Folin’s solution A, half of the volume was made of a mixture of CTC solution, 0.8N NaOH, 10% SDS and MilliQ water mixed in 1:1:1:1 ratio. The second half of the volume was made up with MilliQ water.

v. Folin’s Solution B

The commercially available Folin-Ciocalteu reagent (SD Fine Chemicals) was mixed with MilliQ water in 1:4 ratios.

vi. Bradford’s reagent

The commercially available Bradford’s reagent (Sigma) was used.

(d) SDS PAGE and Western Blotting

i. 10X Running buffer (10X Electrode buffer)

Component	Final concentration required	Volume
Tris base (Sigma)	250mM	30g
Glycine (Sigma)	2.5M	187.7g
SDS (Sigma)	10%	10g
Heated MilliQ water/ Reverse osmosis (RO) water		750ml

After all the components were mixed, the volume of the solution was increased to 1 litre by adding more heated MilliQ water.

ii. Transfer buffer

Component	Final amount
Tris base (Sigma)	12.1g
Glycine (Sigma)	57.6g
10% SDS	4ml
Methanol	800ml
RO water	1000 ml

After the components were mixed, the volume was made up to 4 litres using MilliQ water and stored at 4°C. It can be reused at least for 10 mini-SDS PAGE gels and 5 maxi-SDS PAGE gels.

iii. Tris buffered saline with Tween-20 (TBS-T)

Component	Final concentration	Volume
1M Tris pH8.0 (Sigma)	10mM	10ml
2.5M NaCl	150mM	60ml
Tween-20		1ml
MilliQ water		930ml

The components are mixed by vigorous stirring either manually or by a magnetic stirrer.

iv. 2.5M NaCl

146.1 grams of NaCl was added to 950ml of MilliQ or Reverse osmosis (RO) water.

v. 30% Acrylamide

Dissolve 29.2g of acrylamide (Sigma) and 0.8g of Bis-acrylamide (Sigma) in 100ml of MilliQ water. The pH of the solution was maintained at less than 7.0. Thereafter, the solution was filtered and stored in a dark bottle at room temperature or kept at 4°C for long term storage.

(e) Immunofluorescence**i. 1X PBS**

Component	Volume or Amount
NaCl (HiMedia)	8g
Potassium di-hydrogen phosphate (KH_2PO_4) (SD Fine Chemicals)	0.2g
Potassium chloride (KCl) (SD Fine Chemicals)	0.2g
Sodium phosphate dibasic anhydrous (Na_2HPO_4)	2.18g
MilliQ water	make up volume to 1litre

After mixing all the components, the 1X PBS was poured into glass bottles and autoclaved before use.

Potassium di-hydrogen phosphate (KH_2PO_4) (SD Fine Chemicals)

ii. 4% paraformaldehyde in PBS

Four grams of paraformaldehyde (Sigma) was added in 90ml 1X PBS kept in a glass bottle. This mixture is now heated at 70°C in a water bath and stirred manually till the paraformaldehyde gets dissolved. Only when the paraformaldehyde gets completely dissolved, the volume of the solution was made up to 100ml with PBS and filtered through a filter paper. This solution of 4% paraformaldehyde can be stored at 4°C for about a month.

iii. 0.3% Triton X-100 in PBS

0.3ml Triton-X-100 (Sigma) was dissolved in 100ml PBS and filtered through a filter paper.

iv. 4', 6-diamidino-2- phenylindole (DAPI)

5µg of DAPI (Sigma) was dissolved in 2 ml of 1X PBS to make a concentration of 2.5µg/ml of DAPI and stored in a dark bottle at 4°C. Just prior to use, this solution was diluted 1: 5 times with 1X PBS in a 1.5ml eppendorf and centrifuged for 2 minutes at room temperature to remove debris.

(f) Co-immuno-precipitation experiments

i. EBC lysis buffer

Component	Final concentration required	Volume
1M Tris pH 8.0	0.50M	50ml
2.5M NaCl	125mM	50ml
NP-40 (or Igepal) (Sigma)	0.5%	5ml
MilliQ water		895ml

The EBC lysis was stored at 4°C. Just before use, protease inhibitors were added to it.

iii. Protease Inhibitors (per 10 ml EBC lysis buffer)

Inhibitor	Stock concentration	Final concentration	Volume
Leupeptin	1mg/ml	10µg/ml	100µl
Aprotinin	2mg/ml	20µg/ml	100µl
Sodium fluoride (NaF)	1M	50mM	500µl
Sodium orthovanadate (Van)	0.2M	1mM	50µl
Ethylenediaminetetraacetic acid (EDTA)	0.5M	1mM	20µl
Pepstatin A	10mg/ml	10µg/ml	10µl
Phenylmethanesulfonylfluoride (PMSF)	500mM	1mM	20µl

These protease inhibitors are stored at -20°C for long term storage and thawed before use. These inhibitors have target different proteases and phosphatases like Leupeptin is a Serine and Threonine protease inhibitor while Aprotinin is a Serine protease inhibitor. NaF is an inhibitor of Serine/Threonine and acidic phosphatases, Van is an inhibitor of Tyrosine and alkaline phosphatases while EDTA chelates cations and is thus a good metalloprotease inhibitor. Pepstatin A is an inhibitor of aspartic acid proteases and PMSF is an inhibitor of Serine proteases. A cocktail of these proteases is added to EBC lysis buffers to ensure that during the lysis or storage of cell lysates in EBC buffer, none of the proteins get degraded and all proteins retain their original post-translational modifications.

iv. NET-N

Component	Final concentration required	Volume
1M Tris pH 8.0	20mM	20ml
2.5M NaCl	100mM	40ml
0.5M EDTA pH 8.0	1mM	2ml
NP-40 (or Igepal) (Sigma)	0.5%	5ml
MilliQ water		933ml

v. 3X Laemmli's buffer

Component	Final concentration required	Volume or Amount
1M Tris pH 6.8	150mM	15ml
Glycerol (Sigma)	30%	30ml
SDS	6%	6g
Bromophenol blue (Sigma)	0.3%	0.3g
MilliQ water		Make up volume to 85ml

(g) Clonogenic survival assays.

i. Crystal violet (1%)

1g of crystal violet was dissolved in 100ml methanol. The crystal violet solution can be stored at room temperature and reused multiple times.

4. RESULTS

4.1. PKP3 loss leads to alterations in transcriptome of multiple cell types.

Earlier studies from our laboratory have demonstrated that PKP3 knockdown clones derived from HaCaT, HCT116 and FBM cell lines show increased neoplastic progression as compared to the vector control clones both *in vitro* and *in vivo*. To identify mechanisms governing neoplastic progression upon PKP3 loss, single hybrid gene expression microarray analysis was performed to compare the transcriptomic profiles of the PKP3 knockdown clones derived from the HCT116 and FBM cell lines with the transcriptomic profiles of the respective vector control clones. The microarray for each cell line was performed in duplicates and the average values of the two sets of data were used for analysis. The raw data and the analyzed microarray datasets for FBM derived clones and HCT116 derived clones were uploaded to NCBI GEO (Accession numbers GSE61512 and GSE64580 respectively). Upon PKP3 loss in FBM cells, 428 genes were found to be up-regulated more than 2 fold while 430 genes were down-regulated more than 2 fold. The list of these altered genes has been provided in **Annexure I** and functional classification for the genes up-regulated or down-regulated upon PKP3 loss has been represented as Venn diagrams in Figure 4.1 and Figure 4.2 respectively. Loss of PKP3 in the HCT116 cell line caused 1.5 folds up-regulation of 92 genes and 1.5 folds down-regulation of 65 genes. The list of these altered genes has been provided in **Annexure II** and functional classification of the genes up-regulated and down-regulated upon PKP3 loss have been represented as Venn diagrams in Figure 4.3 and Figure 4.4 respectively. The microarray data demonstrated that expression of PKP3 was more than two folds lower in the FBM and HCT116 derived PKP3 knockdown clones as compared to their respective vector control clones, thus confirming the previously reported results [233].

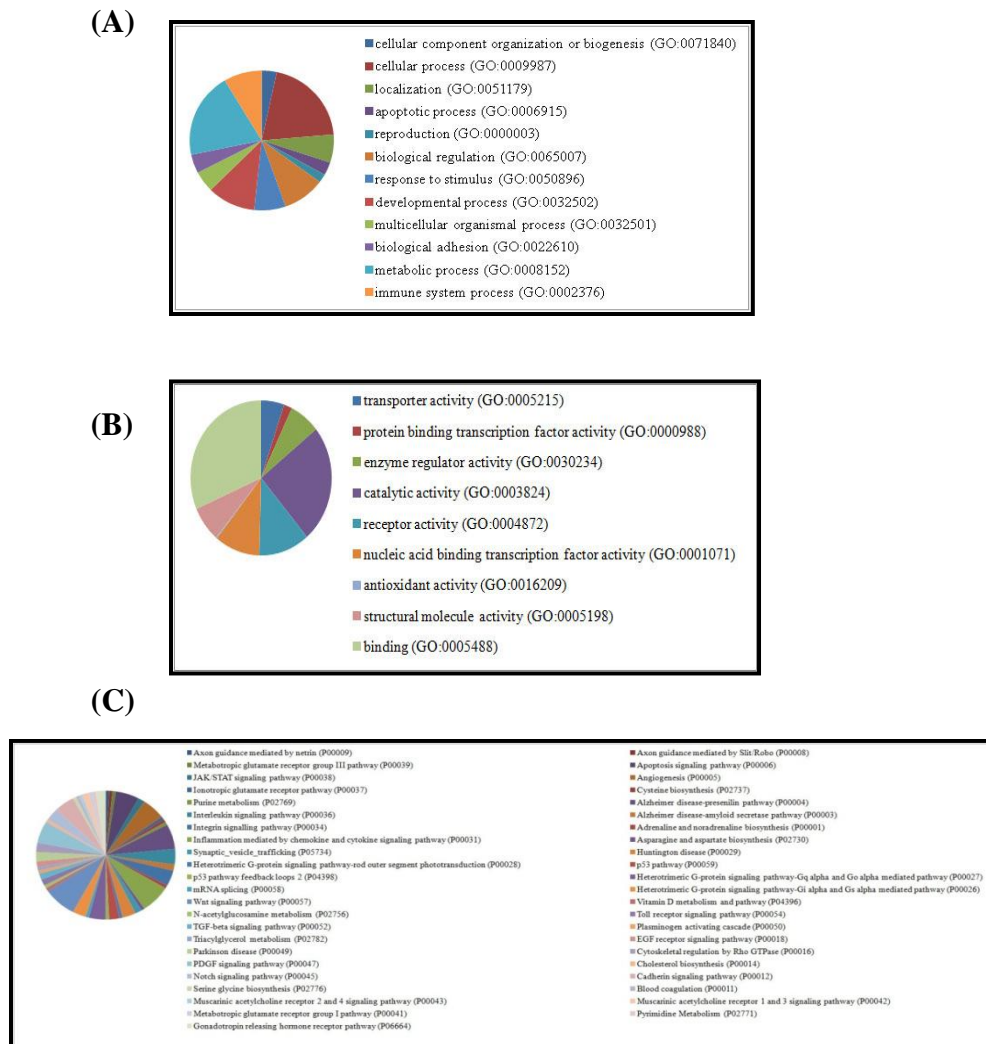


Figure 4.1 Functional classification of the genes up-regulated upon PKP3 loss in FBM cells.

Genes found to be up-regulated in the FBM derived PKP3 knockdown clones as compared to the vector control clones in the microarray dataset has been classified on the basis of their association with different biological processes (A), molecular functions (B) and cell signaling pathways (C). (Note: Only genes with well defined gene ontologies (GO) has been considered for analysis)

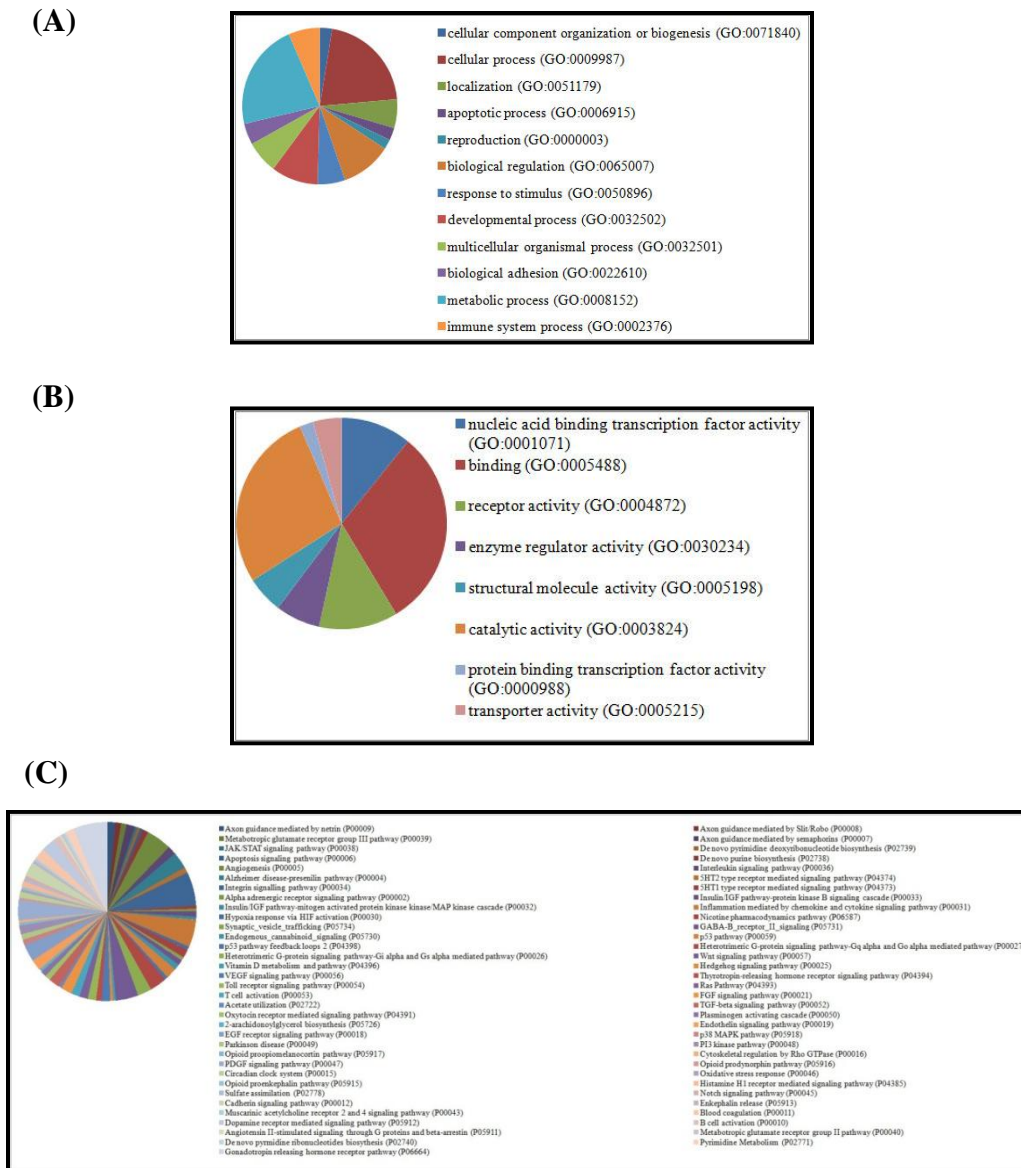


Figure 4.2 Functional classification of the genes down-regulated upon PKP3 loss in FBM cells. Genes found to be down-regulated in the FBM derived PKP3 knockdown clones as compared to the vector control clones in the microarray dataset has been classified on the basis of their association with different biological processes (A), molecular functions (B) and cell signaling pathways (C). (Note: Only genes with well defined gene ontologies (GO) has been considered for analysis)

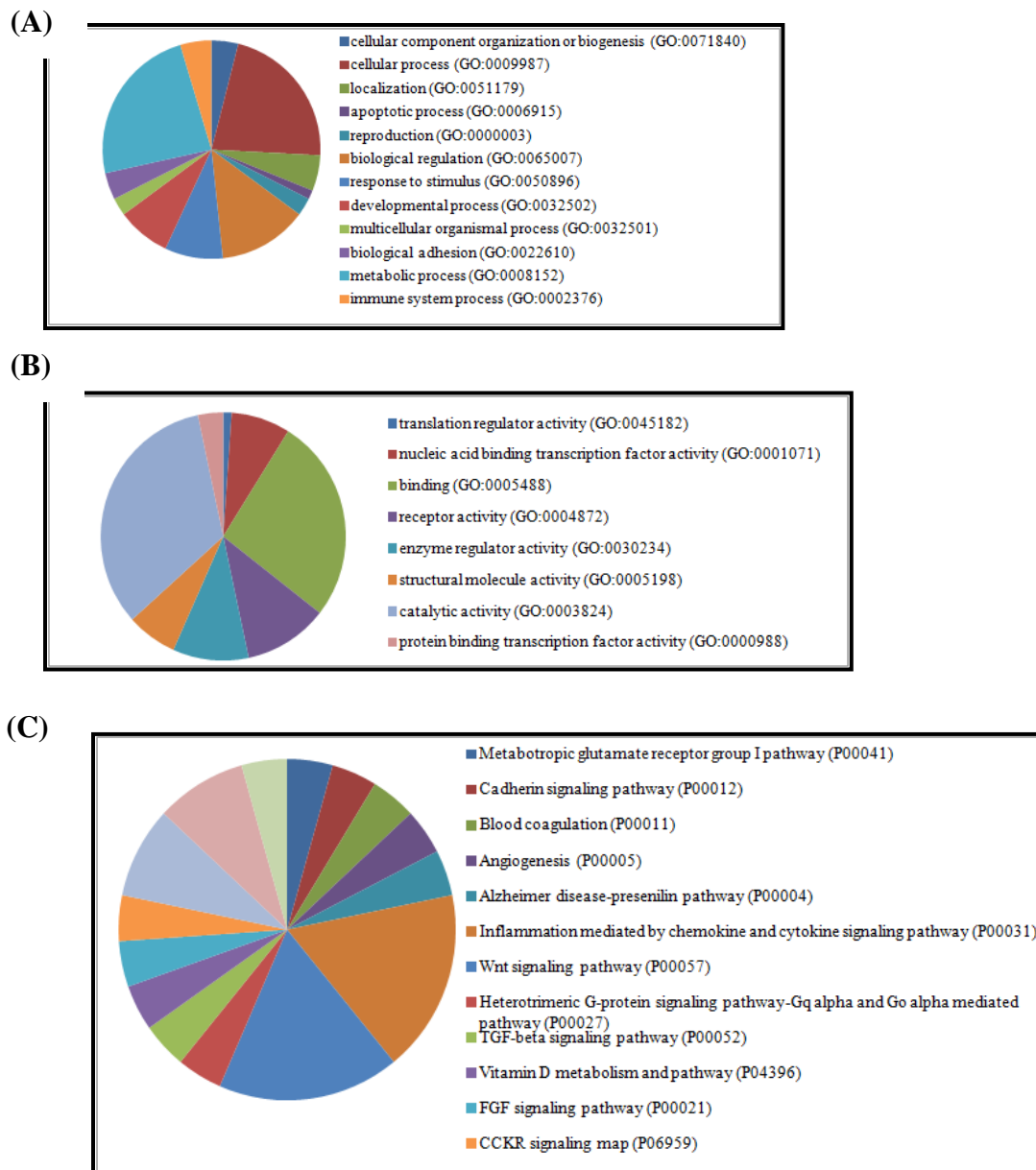
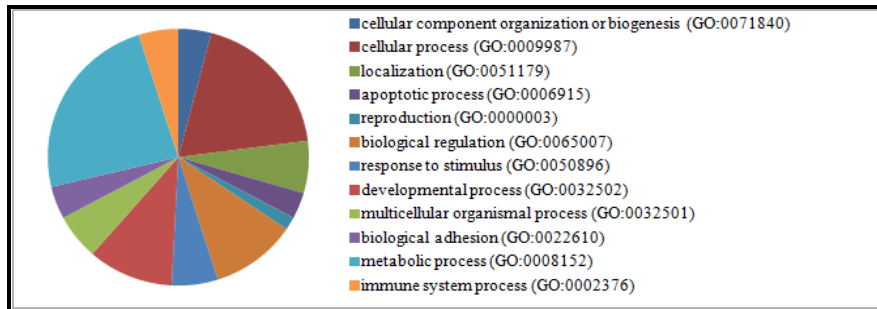
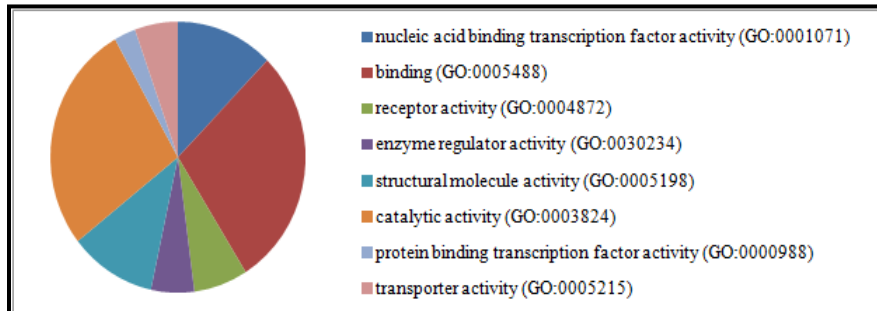


Figure 4.3 Functional classification of the genes up-regulated upon PKP3 loss in HCT116 cells. Genes found to be up-regulated in the HCT116 derived PKP3 knockdown clones as compared to the vector control clones in the microarray dataset has been classified on the basis of their association with different biological processes (A), molecular functions (B) and cell signaling pathways (C). (Note: Only genes with well defined gene ontologies (GO) has been considered for analysis)

(A)



(B)



(C)

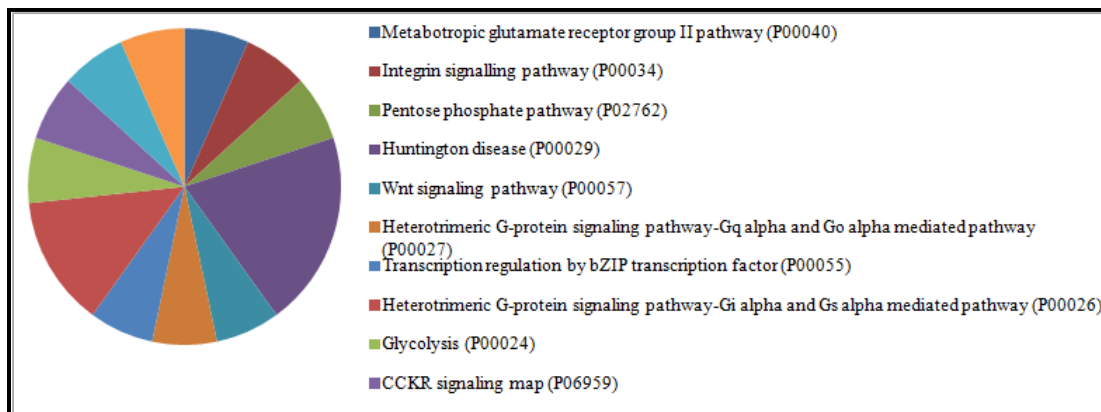


Figure 4.4 Functional classification of the genes down-regulated upon PKP3 loss in HCT116 cells. Genes found to be down-regulated in the HCT116 derived PKP3 knockdown clones as compared to the vector control clones in the microarray dataset has been classified on the basis of their association with different biological processes (A), molecular functions (B) and cell signaling pathways (C). (Note: Only genes with well defined gene ontologies (GO) has been considered for analysis)

To validate this data, expression of PKP3 was analyzed in the HaCaT, HCT116 and FBM derived PKP3 knockdown clones and the respective vector control clones by performing semi-quantitative RT-PCRs (sqRT-PCRs) (Figure 4.5 (A)) and Real time PCRs or quantitative RT-PCRs (qRT-PCRs) (Figure 4.5 (B)). It was observed that PKP3 expression was decreased in all PKP3 knockdown clones as expected. These experiments also confirmed the results of the microarray.

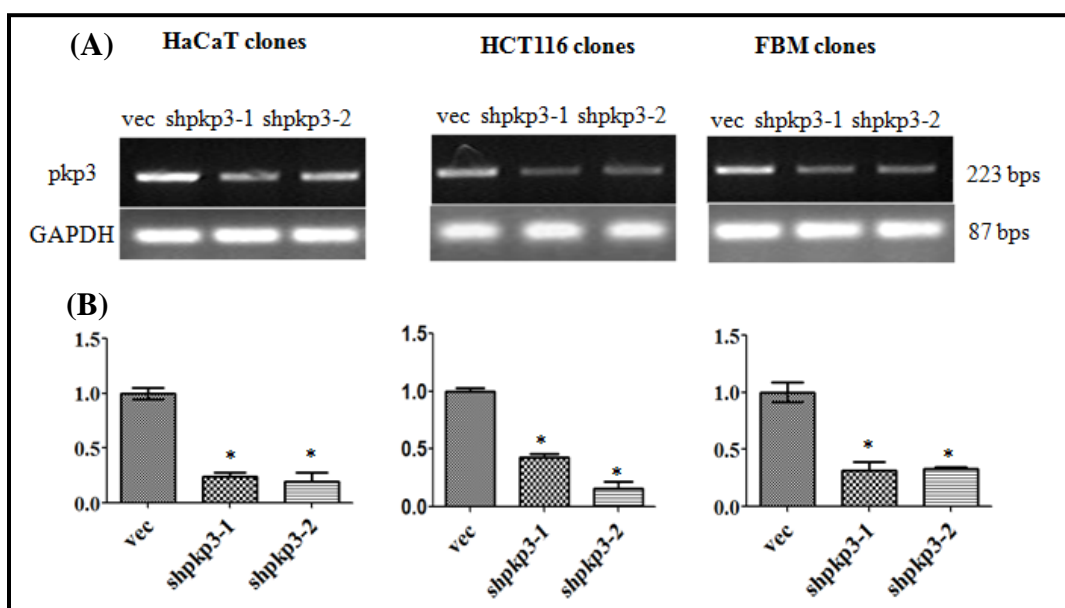


Figure 4.5. Validation of the HaCaT, HCT116 and FBM derived PKP3 knockdown clones. mRNA was prepared from the vector controls (vec) or PKP3 knockdown clones (sh-pkp3-1 and shpkp3-2) derived from either HaCaT, HCT116 or FBM cells as indicated. (A) sqRT-PCRs and (B) qRT-PCRs were performed using oligonucleotides specific to PKP3 and GAPDH. Relative expression of PKP3 in the HaCaT, HCT116 and FBM derived PKP3 knockdown clones (shpkp3-1 and shpkp3-2) was compared to the respective vector control clones (vec). Expression of GAPDH has been used for normalization. The PCR product size has been indicated in base pairs. The Y-axis in the qRT-PCR panels reflects the fold change in transcription, which is calculated

as described in the Materials and Methods. The X-axis indicates the clone name. The PCR product size in sqRT-PCR panels has been indicated in base pairs.

The expression of genes which were found to be altered more than two-fold in the FBM derived PKP3 knockdown clone was assessed using sqRT-PCRs and qRT-PCRs to validate the results of the microarray and to analyze if the same genes were altered upon PKP3 knockdown in the HCT116 and HaCaT cell lines. A change in expression of two-fold either way was considered significant. A set of genes which included inflammation associated genes such as Interleukin 6 (IL6), Serum amyloid A1 (SAA1), Chemokine (C-C Motif) Ligand 2 (CCL2), S100A8, S100A9 and CBS, were found to be up-regulated in HaCaT and FBM derived PKP3 knockdown clones by sqRT-PCR (Figure 4.6 (A)) and qRT-PCR analysis (Figure 4.6 (B)). None of these genes were expressed in HCT116 cells (data not shown for qRT-PCRs). The expressions of all the genes were normalized using the expression of GAPDH as a control. Thus, PKP3 loss leads to the generation of an inflammation associated signature in cell lines derived from stratified epithelia, which is consistent with the observation that inflammation is observed in the epidermis of mice lacking PKP3 [211]. By performing sqRT-PCR, some genes were found to be altered specifically in the FBM derived PKP3 knockdown clones while their expression was not altered in the HaCaT and HCT116 derived PKP3 knockdown clones. The genes which up-regulated in this group were Epiplakin (EPPK1), Rho Guanine Nucleotide Exchange Factor (ARHGEF5), Matrix metalloprotease 9 (MMP9) and MOB kinase activator 3B (MOBKL2b) while expression of Nuclear receptor subfamily-2 group-F member-1 (NR2F1) and Insulin like growth factor binding protein 3 (IGFBP3) were found to be down-regulated (Figure 4.7). Expression of GAPDH was used as a loading control. These results suggested that PKP3 loss leads to varying alterations in the transcriptome in the three cell types studied.

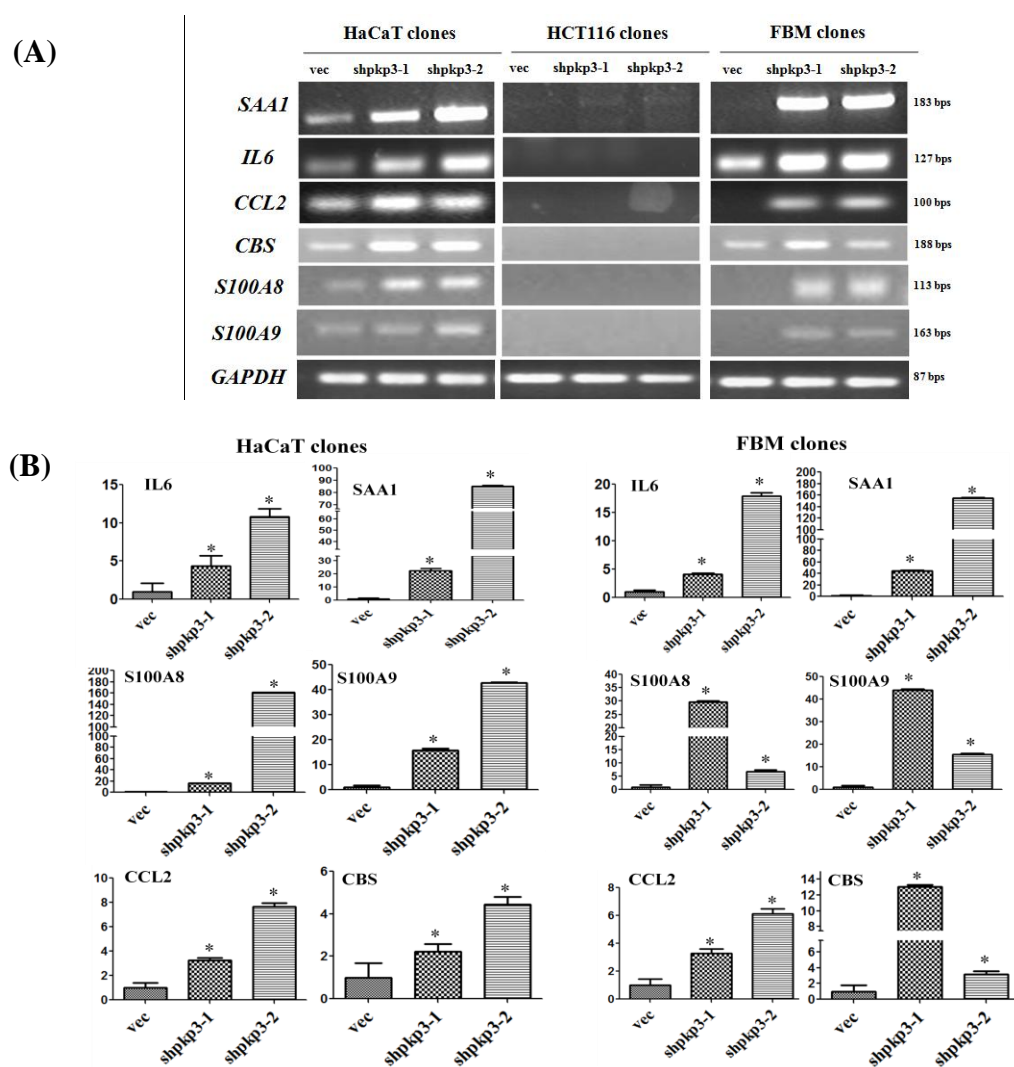


Figure 4.6. PKP3 loss in HaCaT and FBM cells leads to up-regulation of inflammation associated genes. (A) sqRT-PCRs and (B) qRT-PCRs were performed using oligonucleotides specific for IL6, SAA1, S100A8, S100A9, CCL2, CBS and GAPDH in HaCaT and FBM derived PKP3 knockdown clones and the respective vector controls. Expression of GAPDH has been used for normalization. The Y-axis in the qRT-PCR panels reflects the fold change in transcription, which is calculated as described in the Materials and Methods. The X-axis indicates the clone name. The standard errors are plotted and student's t test was performed (* indicates a p value<0.01). The PCR product size in sqRT-PCR panels has been indicated in base pairs.

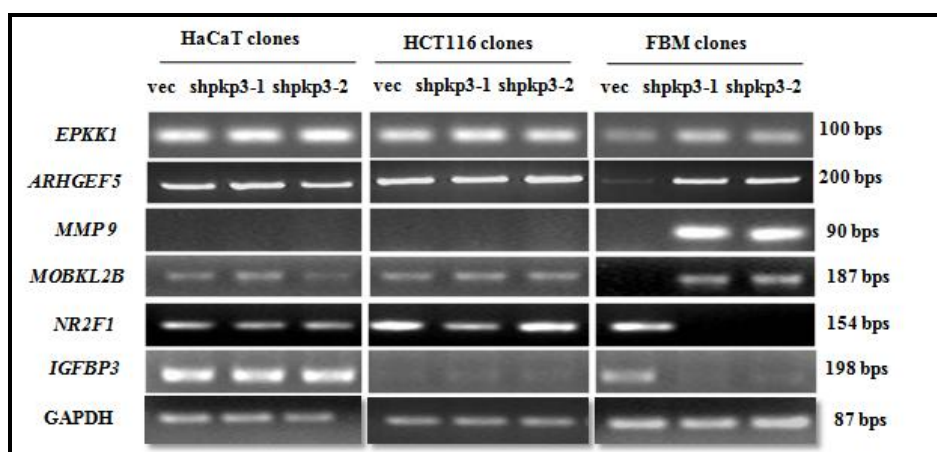


Figure 4.7. Cell type specific alterations in FBM derived PKP3 knockdown clones. sqRT-PCRs were performed using oligonucleotides specific for EPPK1, MOBKL2b, MMP9, NR2F1, Δ Np63, IGFBP3, ARHGEF5 and GAPDH, in HaCaT, HCT116 and FBM derived PKP3 knockdown clones and the respective vector controls. Expression of GAPDH has been used for normalization. The PCR product size has been indicated in base pairs.

4.2. PKP3 loss in FBM cells lead to cell type specific alterations of Δ Np63 target genes.

Upon PKP3 loss in FBM cells, there were a group of genes identified in the microarray data, which are regulated by a transcription factor named, N terminal deleted p63 alpha (Δ Np63 α). These genes have been listed in Table 4.1. Among these genes, expression of IGFBP3 (Figure 4.7) and P cadherin (Figure 4.8 (A)) were up-regulated upon PKP3 loss in FBM cells. Expression of P cadherin was increased at the protein level (Figure 4.8 (B)). Thus, it was hypothesized that Δ Np63 α may be regulating IGFBP3 and P cadherin expression upon PKP3 loss in FBM cells leading to increased neoplastic progression.

Gene symbol	Gene Name	Average fold change
IGFBP3	Homo sapiens insulin-like growth factor binding protein 3 (IGFBP3)	-7.7
FRAS1	Homo sapiens Fraser syndrome 1 (FRAS1)	6.9
CDH3	Homo sapiens cadherin 3, type 1, P-cadherin (placental) (CDH3)	3.79
CD54	Homo sapiens intercellular adhesion molecule 1 (CD54),	2.26
KRT5	Homo sapiens keratin 5 (KRT5)	2.091
KRT14	Homo sapiens keratin 14 (KRT14)	3.75
IRF6	Homo sapiens interferon regulatory factor 6 (IRF6)	4.23

Table 4.1. Δ Np63 α target genes were up-regulated upon PKP3 loss in FBM cells. List of known Δ Np63 α target genes found to be altered upon PKP3 loss in the gene expression microarray data.

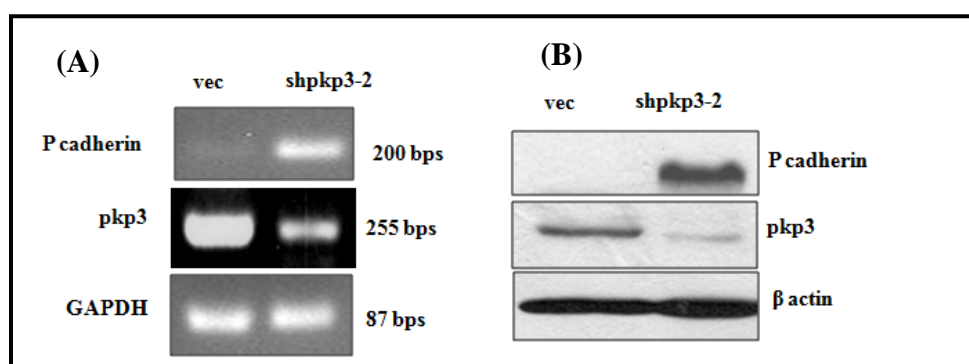


Figure 4.8. P cadherin RNA expression levels and protein expression levels are higher in FBM derived PKP3 knockdown clones. RNA and protein lysates were obtained from FBM derived vector control (vpTU6) and PKP3 kd clone (P2). (A) sqRT-PCR was performed with P cadherin, pkp3 and GAPDH (loading control) primers. The PCR product size has been indicated

in base pairs. **(B)** Western blot was performed loading 100 μ gs of the cell lysates and probing with antibodies against p63, P cadherin and β actin (loading control).

Δ Np63 α is one of the six isoforms of p63. There are two major isoforms: trans-activating (TA)p63 and Δ Np63 (transcribed from an alternate promoter). The gene transcript of each of these two isoforms undergo alternative splicing at the C terminus to give to three new splice variants named alpha, beta and gamma variants. Thus there are a total of six isoforms of p63 (Figure 4.9) [361].

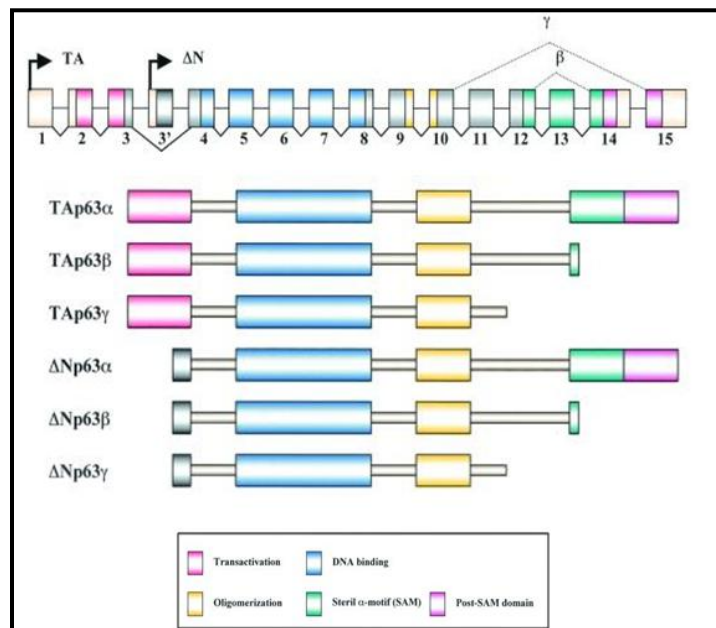


Figure 4.9. Schematic representation of p63 isoforms encoded by the *TP73L* gene by alternate promoter usage and alternate splicing. This figure is a cartoon representing the various types of alternative splicing that can occur in the *TP73L* gene transcript. Alternate promoter usage gives rise to the TA and Δ N isoforms of p63 while alternative exon splicing at the C terminus generates the alpha, beta and gamma variants. This figure also depicts the structural domains of the p63 protein and the distribution of these domains in each of the p63 isoforms. The trans-activation domain is a characteristic feature of the TAp63 isoforms. Other

structural domains are the DNA binding domain, the oligomerization domain, the Steril α -motif (SAM) and the post-SAM domain [361].

Since the microarray was not able to distinguish between the different isoforms of p63, isoform specific sqRT-PCRs for the two major p63 isoforms were performed. In the FBM derived PKP3 knockdown clones, the expression of Δ Np63 increased while TAp63 expression decreased, while total p63 levels increased. GAPDH was used as the loading control (Figure 4.10(A)).

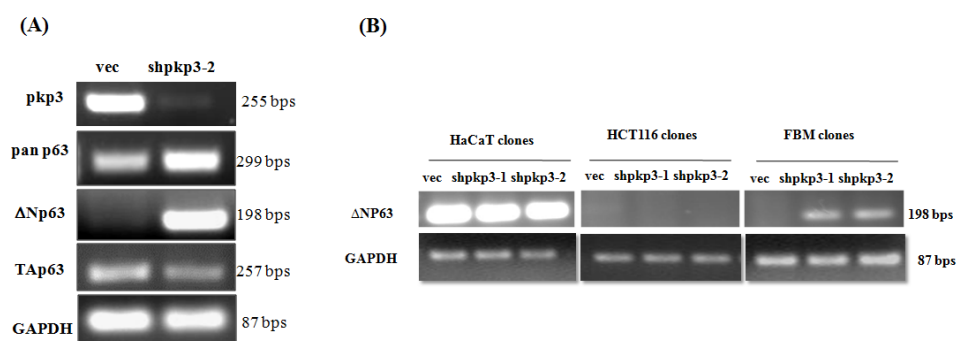


Figure 4.10. Cell type specific alterations of Δ Np63 in FBM derived PKP3 knockdown clones. (A) sqRT-PCRs were performed using oligonucleotides specific for p63, pan p63, Δ Np63, TAp63 and GAPDH in FBM derived PKP3 knockdown clones and the respective vector controls. Expression of GAPDH has been used for normalization. The PCR product size has been indicated in base pairs. (B) sqRT-PCRs were performed using oligo-nucleotides specific for Δ Np63 and GAPDH, in HaCaT, HCT116 and FBM derived PKP3 knockdown clones and the respective vector controls. Expression of GAPDH has been used for normalization. The PCR product size has been indicated in base pairs.

When mRNA expression of Δ Np63 was analyzed in the HaCaT and HCT116 cells, it was found that Δ Np63 was not altered upon PKP3 loss in HaCaT cells while there was no endogenous

Δ Np63 detected in the HCT116 cells. The expression of Δ Np63 was found to increase in the FBM derived PKP3 knockdown clones as compared to its vector control clone (Figure 4.10(B)), thus validating the results of the microarray. To analyze the expression of Δ Np63 at the protein level, Western blots were performed using cell lysates of the HaCaT and HCT116 derived PKP3 knockdown clones and their respective vector controls (Figure 4.11). It was demonstrated that Δ Np63 expression was unaltered in the HaCaT cells upon PKP3 loss, while Δ Np63 was not present in HCT116 cells supporting our sqRT-PCR data (Figure 4.7) and earlier reports showing absence of Δ Np63 in normal colon tissues and colon carcinomas [362].

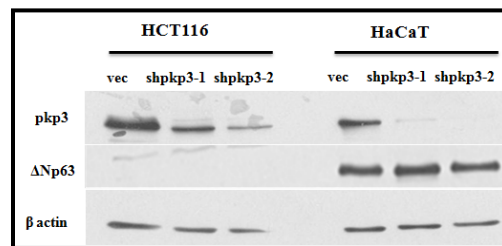


Figure 4.11. PKP3 loss does not alter Δ Np63 expression in HaCaT cells, while in HCT116, Δ Np63 is not expressed. Western blots were performed using the Δ Np63, pkp3 and β actin antibodies. It was found that that Δ Np63 expression was unaltered upon PKP3 knockdown in the HaCaT cells but HCT116 cells did not express Δ Np63. β actin was used as the loading control.

Since Δ Np63 expression was increased in the FBM derived PKP3 knockdown clones and increased Δ Np63 is associated with poor prognosis and radio-resistance in oral squamous carcinomas [363], it was hypothesized that Δ Np63 may be mediating increased neoplastic progression and radio-resistance in FBM cells upon PKP3 loss. Thus, oligonucleotides encoding shRNA against Δ Np63 were made and cloned downstream of the U6 promoter in pLKO.1-EGFP-f-puro vector (Figure 4.12(A)), a modified version of the commercial pLKO.1-puro vector [343, 344]. Three clones of this plasmid were transfected into the easy-to-transfect human

embryonic kidney cell line (HEK293) to analyze for expression of farnesylated enhanced green fluorescent protein (EGFP-F) under a fluorescence microscope. Farnesylation allows GFP to be expressed at the plasma membrane of cells [364]. It was demonstrated that the three clones expressed efficiently in the HEK 293 cells showing green fluorescence at the cell membrane. As controls, the HEK293 cells were transfected with a positive control plasmid (pLKO.1-EGFP-f-puro) and a negative control plasmid (pLKO.1 puro) (Figure 4.12(B)). These pLKO.1-EGFP-f-puro Δ Np63 shRNA constructs were thereafter transiently transfected in FBM derived PKP3 knockdown cells, but the transfection was not successful. Since pLKO.1 based plasmids are lentiviral plasmids [344], so lentivirus mediated infection of the pLKO.1-EGFP-f-puro plasmid DNA was performed but this again was unsuccessful. Further, experiments need to be performed to determine the contribution of Δ Np63 to the tumor progression observed upon PKP3 loss in FBM cells.

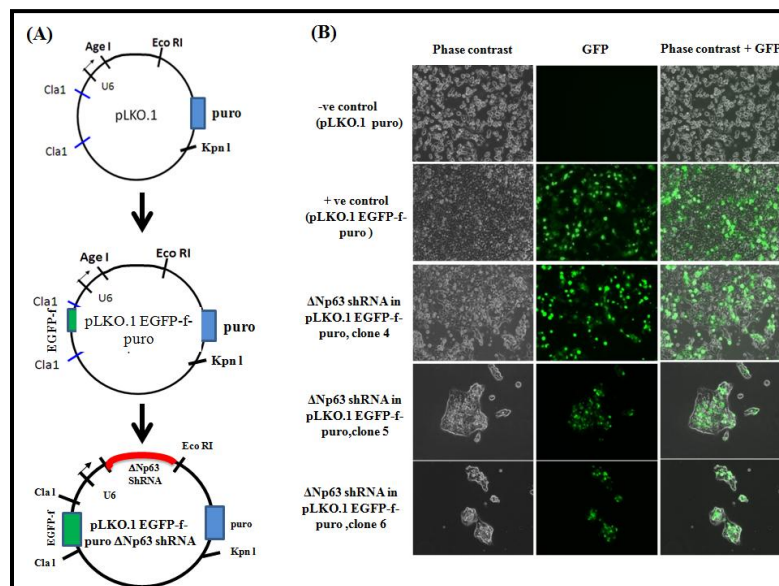


Figure 4.12. Cloning of Δ Np63 shRNA in pLKO.1 EGFP-f-puro vector and analysing EGFP-f expression. (A) Schematic representation of the cloning strategy used to clone a shRNA

against Δ Np63 into the pLKO.1 EGFP-f-puro vector (a vector generated from pLKO.1 puro containing a farnesylated EGFP reporter gene) using the AgeI and EcoRI cloning sites. (B) HEK293 cells were transiently transfected with the negative control plasmid, pLKO.1 puro and the positive control plasmid for EGFP-f expression, pLKO.1 EGFP-f-puro. EGFP-f expression was visualized under a fluorescence microscope and images were obtained. Similarly, three plasmid clones of pLKO.1 EGFP-f-puro Δ Np63 shRNA vector named clone 4, 5 and 6 were individually transfected transiently in HEK293 cells and analyzed for expression of EGFP-F under a fluorescence microscope and images were obtained. Note that the positive control and all the three clones showed green fluorescence confirming that these clones can be used for generating Δ Np63 knockdown clones using EGFP-F expression as a marker for selecting positive clones. The negative control did not show EGFP-F expression.

4.3. PKP3 loss leads to up-regulation of Lipocalin2 (LCN2) and Matrix metalloprotease7 (MMP7) in three different cell lines.

Upon thorough analysis of the microarray data, followed by its validation by sqRT-PCR and qRT-PCR, it was demonstrated that PKP3 loss in HaCaT, HCT116 and FBM cells leads to up-regulation of mRNA expression of two genes: LCN2 (Figure 4.13) and MMP7 (Figure 4.14). For both sqRT-PCR and qRT-PCR, the expression of GAPDH was used as for normalization.

LCN2 also known as NGAL (neutrophil gelatinase associated lipocalin) is a secreted glycoprotein and also an iron binding protein, which regulates iron homeostasis in cells (reviewed in [365, 366]). It was discovered as a component of natural immunity in mice [367] where LCN2 was found to bind bacterial siderophores. Siderophores, such as enterobactin, are proteins that carry Fe^{3+} as a soluble Fe^{3+} -protein complex and distribute iron to cells. Bacteria

secrete siderophores to sequester iron from the intracellular pools of their host organisms. LCN2 can bind to bacterial siderophores as well as human siderophores like ferritin and transferrin to sequester iron from the intracellular pool and transport iron into the cells via the LCN2 receptor (Megalin) [368-370].

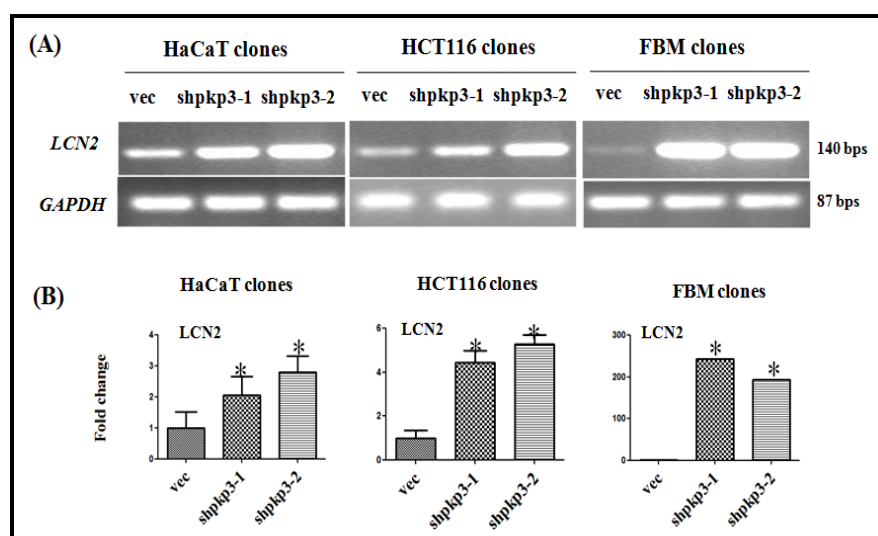


Figure 4.13. PKP3 loss leads to up-regulation of LCN2 in multiple cell types. (A) sqRT-PCRs and (B) qRT-PCRs were performed using oligonucleotides specific for LCN2 and GAPDH, in HaCaT, HCT116 and FBM derived PKP3 knockdown clones and the respective vector controls. Expression of GAPDH has been used for normalization. The Y-axis in the qRT-PCR panels reflects the fold change in transcription, which is calculated as described in the Materials and Methods. The X-axis indicates the clone name. The standard errors are plotted and student's t test was performed (* indicates a p value < 0.01). The PCR product size in sqRT-PCR panels has been indicated in base pairs.

LCN2 is often over-expressed in many types of cancers (reviewed in [365, 371]). LCN2 up-regulation has also found in patients suffering from colorectal carcinoma in multiple clinical studies and is an indicator of colon cancer progression from adenoma to carcinoma [372-374]

and is also known to increase tumor formation in xenograft mouse models of colon cancer [373]. Increased expression of LCN2 is also associated with human papillomavirus mediated cutaneous squamous cell carcinoma [375]. LCN2 also associated with both radiation induced and intrinsic radio-resistance. Its expression is known to be increased in radio-resistant cancer cell lines established by continuous fractionated γ irradiation [376] and is also associated with radio-resistance against X-ray irradiation in oral cancer and lung cancer [377].

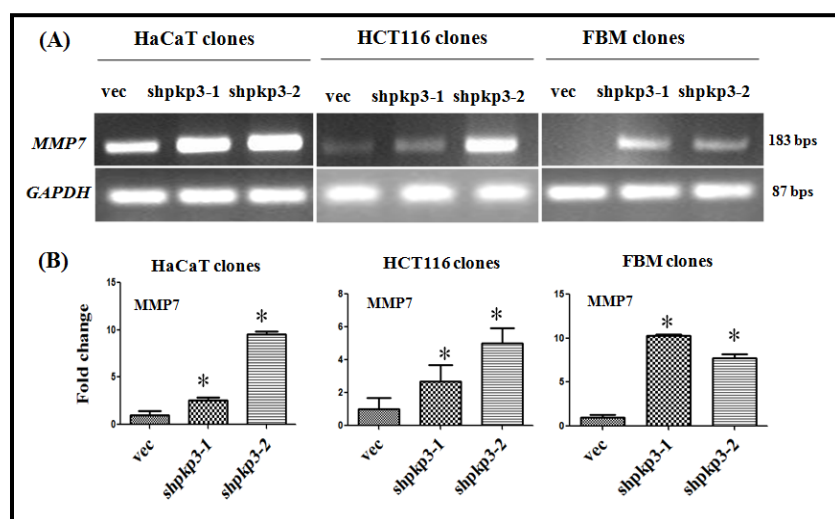


Figure 4.14. PKP3 loss leads to up-regulation of MMP7 in multiple cell types. (A) sqRT-PCRs and (B) qRT-PCRs were performed using oligonucleotides specific for MMP7 and GAPDH, in HaCaT, HCT116 and FBM derived PKP3 knockdown clones and the respective vector controls. Expression of GAPDH has been used for normalization. The Y-axis in the qRT-PCR panels reflects the fold change in transcription, which is calculated as described in the Materials and Methods. The X-axis indicates the clone name. The standard errors are plotted and student's t test was performed (* indicates a p value < 0.01). The PCR product size in sqRT-PCR panels has been indicated in base pairs.

Matrilysin (MMP7) is one of the smallest members of the MMP family. It is a highly potent metallo-protease which can degrade fibronectin, collagen III/IV/V/IX/X/XI, type gelatins type I/II/IV/ V, casein, laminin, elastin and proteoglycans [378, 379]. It is secreted from salivary glands, skin epithelia and the glandular epithelial cells of the intestine, liver, pancreas, breast, and urino-genital tract [380-383]. In the intestine, MMP7 and the matrix metalloprotease MT1-MMP are exclusively produced by the epithelial cells of the colon while the rest of the matrix metalloproteases like MMP9 and MMP11 are produced by the colonic stroma [384-387]. In non-pathogenic conditions, MMP7 is important for repair of wounded epithelial tissues ([388] and reviewed in [389]), while in pathogenic conditions MMP7 serves as a very important anti-bacterial agent produced by epithelial cells as it can cleave and convert pro-alpha-defensins into active alpha-defensins ([390] and reviewed in [391]). MMP7 expression is increased in cystic fibrosis [392], gastro-intestinal ulcers [393] and upon bacterial infections [394].

MMP7 up-regulation has also been associated with poor prognosis and metastasis in many cancers like colorectal cancer [395-397], gastric cancer [398], oral cancer [399] and bladder cancer [400]. It has been demonstrated that down-regulation of MMP7 either by knockdown in colorectal cancer cell lines or by knockout in APC min/+ mice leads to decreased tumor incidence [401, 402], while an increase in MMP7 expression in colorectal cancer cell lines causes increased tumor formation [403]. MMP7 is also known to be associated with increasing intrinsic radio-resistance because knockdown of MMP-7 enhances sensitivity to 5FU and X-ray irradiation in SW480 colon cancer cell line [404].

Since both LCN2 and MMP7 are individually known to be associated with increased neoplastic progression, metastasis and radio-resistance in cancers, it was hypothesized that up-regulation of

LCN2 or MMP7 or both may regulate increased neoplastic progression and radio-resistance upon PKP3 loss.

4.4. LCN2 is required for neoplastic transformation upon PKP3 loss.

To determine whether the increase in LCN2 levels is required for tumor formation upon PKP3 loss, double knockdown clones were generated where LCN2 was knocked down in the PKP3 knockdown clone shpkp3-2 using vector driven RNA interference. Two separate shRNAs were used and named X and Y. The oligonucleotides sequences of these shRNAs are available in Materials and Methods. Two double knockdown clones were obtained from each of these shRNAs. The clones shpkp3-2+shlcn2-1 and shpkp3-2+shlcn2-2 were obtained from shRNA X while the shRNA Y yielded two clones: shpkp3-2+shlcn2-3 and shpkp3-2+shlcn2-4. The vector control clone (shpkp3-2+vec) was generated by transfection of the empty vector in the shpkp3-2 clone (Figure 4.15).

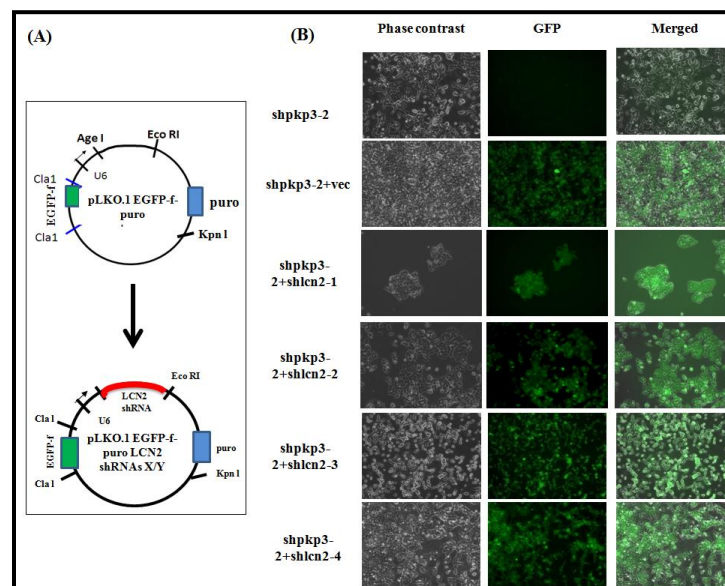


Figure 4.15. Cloning of 2 different LCN2 shRNAs (A and B) in pLKO.1 EGFP-f-puro vector and generation of stable double knockdown clones of LCN2 derived from the HCT116 based PKP3 knockdown clone shpkp3-2. (A) Schematic representation of the cloning

strategy used to clone two shRNAs (X and Y) against LCN2 into the pLKO.1 EGFP-f-puro vector using the AgeI and EcoRI cloning sites. (B) HCT116 derived PKP3 knockdown clone, shpkp3-2 was transfected with two clones each of pLKO.1 EGFP-f-puro LCN2 shRNA, A and B plasmids. The cells were maintained in media containing 5 μ g/ml blasticidin and 0.5 μ g/ml puromycin to obtain single cell clones thus generating two clones shpkp3-2+shlcn2-1 and 2 (from X) and two more clones shpkp3-2+shlcn2-3 and 4 (from Y). Similarly, the pLKO.1 EGFP-f-puro plasmid was transfected in shpkp3-2 cells and selected in blasticidin and puromycin to generate the vector control clone. All clones cells were analyzed for expression of EGFP-F under a fluorescence microscope and images were obtained. The shpkp3-2 cells served as a negative control for the EGFP-F expression. Note that all double knockdown clones and vector control clones except the negative control clone showed EGFP-F expression at the cell border.

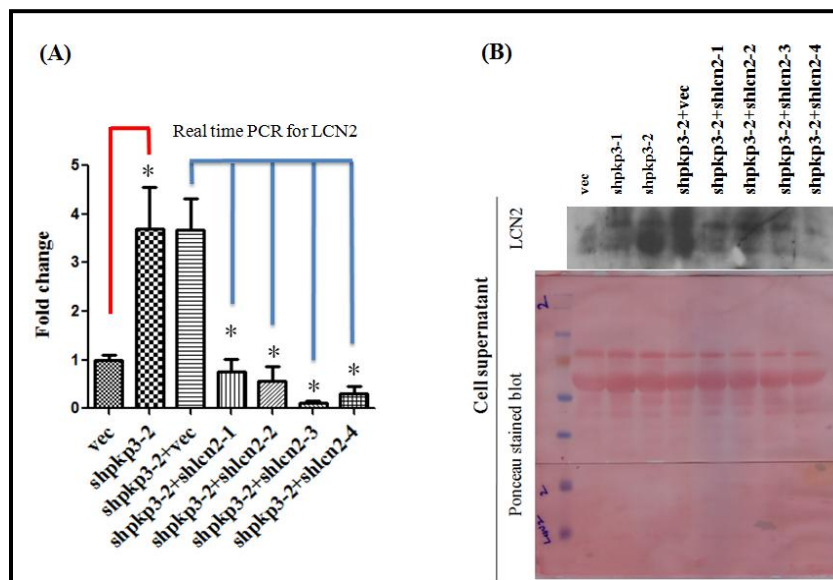


Figure 4.16. Validation of LCN2+PKP3 double knockdown clones by qRT-PCR and Western blotting (of acetone precipitated cell supernatant). (A) mRNA prepared from HCT116 derived PKP3 knockdown clone (shpkp3-2), its vector control clone (vec), the LCN2+PKP3 double knockdown clones (shpkp3-2 + shlcn2-1, shpkp3-2 + shlcn2-2, shpkp3-2

+sh lcn2-3 and shpkp3-2 + shlcn2-4) and the corresponding vector control clone (shpkp3-2 + vec) was used as a substrate for reverse transcriptase followed by real time PCR reactions using oligonucleotides specific for LCN2. All expression was normalized to the levels of GAPDH. The fold change is graphed on the Y-axis and the clone name is on the X-axis. Note that LCN2 levels are higher in the PKP3 knockdown clones as compared to its vector control clone, while LCN2 expression is decreased in the LCN2+PKP3 double knockdown clones as compared to the corresponding vector control. The standard errors are plotted and student's t test was performed (* indicates a p value<0.01).**(B)** 100µg of acetone precipitated cell supernatants were resolved on 12% SDS PAGE gels followed by Western blotting with antibodies specific to LCN2. Note that LCN2 levels are higher in supernatants prepared from the PKP3 knockdown cells as compared to the vector controls and the levels are lower in the double knockdown clones. The same blot was stained with Ponceau stain to demonstrate equal loading of proteins (lower panels).

The expression of LCN2 in the vector control and the double knockdown clones was validated by qRT-PCR (Figure 4.16 (A)). Since LCN2 [405-407] is a secreted protein, cells were grown in the absence of serum and the supernatant collected for the indicated cell types. The proteins in the supernatant were precipitated using acetone as described in the Materials and Methods and a Western blot performed for LCN2. It was demonstrated that PKP3 knockdown led to an increase in the expression of LCN2 while knockdown of LCN2 causes a decrease in the expression of LCN2 as expected (Figure 4.16 (B)). The blot was stained with Ponceau-S to show equal protein loading for the cell supernatants. To determine if PKP3 loss in HaCaT cells also leads to increased LCN2 secretion, the HaCaT derived PKP3 knockdown clones and vector control clones were grown in the absence of serum and the supernatant was collected followed by

Western blotting for LCN2. It was observed that like in HCT116, PKP3 loss in HaCaT also leads to an increase in expression of LCN2 (Figure 4.17).

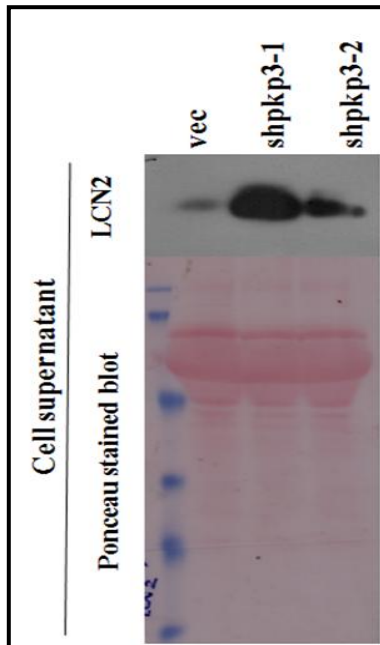


Figure 4.17. PKP3 loss in HaCaT cells lead to increased protein expression of the secreted protein LCN2. 100 μ g of acetone precipitated cell supernatants from HCT116 derived PKP3 knockdown clones shpkp3-1 and shpkp3-2, and its vector control clone (vec) were resolved on 12% SDS PAGE gels followed by Western blotting with antibodies specific to LCN2. Note that LCN2 levels are higher in supernatants prepared from the PKP3 knockdown. The same blot was stained with Ponceau stain to demonstrate equal loading of proteins (lower panels).

PKP3 loss in HCT116 cells lead to increased cell migration as assayed by scratch wound healing assay [233]. To determine if LCN2 knockdown in the PKP3 knockdown clone shpkp3-2 can decrease cell migration, scratch wound healing assays were performed and it was demonstrated that loss of LCN2 decreased cell migration (Figure 4.18 (A) and (B)). PKP3 loss has also been demonstrated to increase metastasis which indicated that it may increase cell invasion [233]. *In vitro* cell invasion was analyzed using the Matrigel invasion assay for two PKP3 knockdown clones (shpkp3-1 and shpkp3-2). It was demonstrated that loss of PKP3 leads to an increase in invasion as shown in Figure 4.19. The increase in invasion observed upon PKP3 loss was reversed when LCN2 expression was inhibited (Figure 4.19). These results suggested that LCN2

is required for the increased cell migration and invasion observed upon PKP3 knockdown in HCT116 cells.

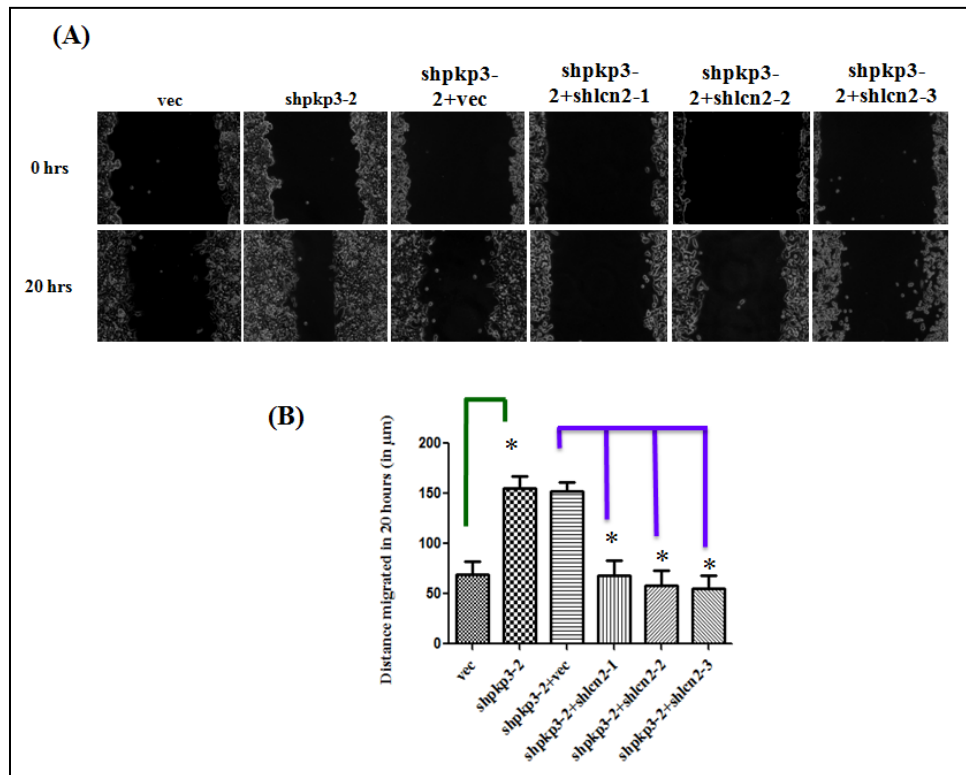


Figure 4.18. LCN2 loss leads to a decrease in migration. Scratch wound healing assays were performed on the HCT116 derived vector control (vec), PKP3 knockdown clone shpkp3-2, shpkp3-2 derived vector control clone (shpkp3-2+vec) and shpkp3-2 derived LCN2 knockdown clones (shpkp3-2+shlcn2-1, shpkp3-2+shlcn2-2 and shpkp3-2+shlcn2-3) as described. Phase contrast images of wound healing at 0 hours (start) and 20 hours (end of experiment) have been shown (A). The mean and standard deviation of the distance migrated in 20 hours has been plotted in Y axis. The p value was calculated using student's t test (* indicates a p value < 0.01) (B). Note that migration is increased in the pkp3 knockdown clones, while it is decreased in the double knockdown clones.

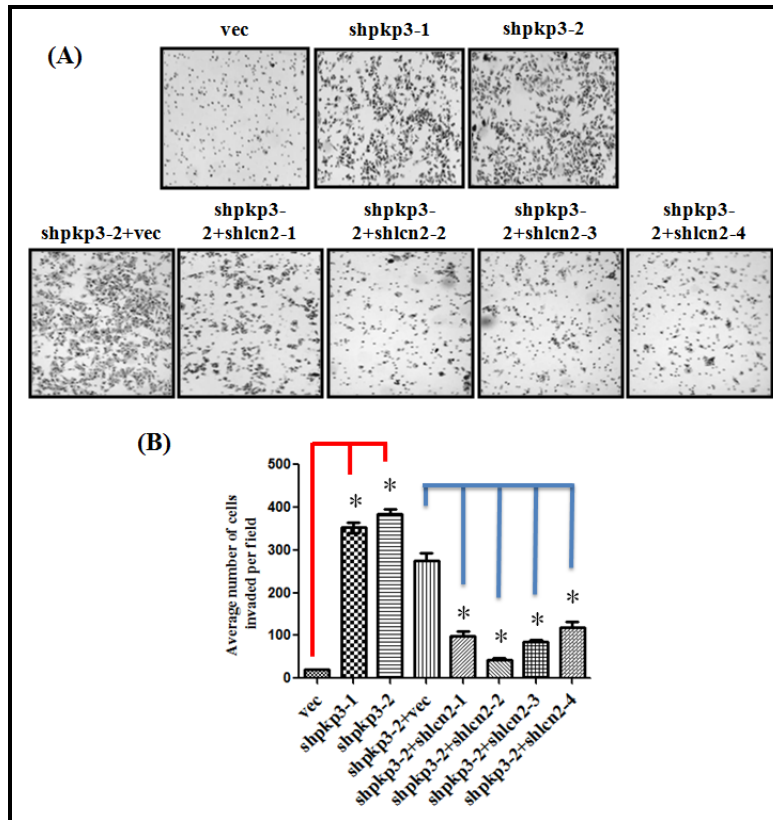


Figure 4.19. LCN2 loss leads to a decrease in cell invasion. Matrigel invasion assays were performed in Boyden's chambers for HCT116 derived vector control cells, PKP3 knockdown clones and the LCN2 double knockdown clones. The number of cells observed in ten random fields of the membrane for each clone was determined as described in Materials and Methods, representative images for each clone are shown. The mean and standard deviation of three independent experiments are plotted. The p value was calculated using a student's t-test (* indicates a p value < 0.01). Note that loss of PKP3 leads to an increase in invasion as compared to the vector control and this phenotype is reversed in the double knockdown clones.

PKP3 loss leads to an increase in anchorage independent growth and an increase in tumor formation and metastasis *in vivo* [233]. To determine if loss of LCN2 can reverse the phenotype of anchorage independent growth, soft agar assays were performed on the HCT116 derived

PKP3 knockdown clones, LCN2+PKP3 double knockdown clones (shpkp3-2+shlcn2-1, shpkp3-2+shlcn2-2, shpkp3-2+shlcn2-3 and shpkp3-2+shlcn2-4) and the corresponding vector control clones vec and shpkp3-2+vec respectively. It was demonstrated that while pkp3 loss increased anchorage independent growth, knockdown of LCN2 reversed the phenotype (Figure 4.20).

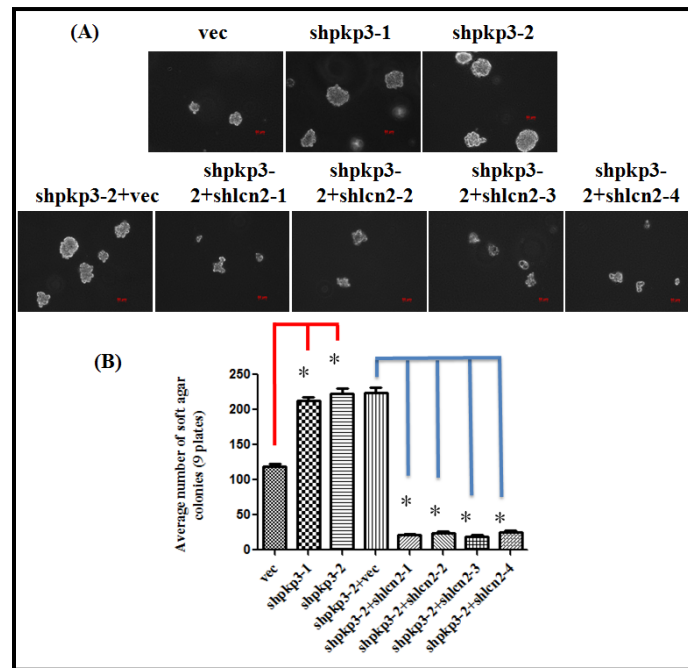


Figure 4.20. LCN2 loss leads to a decrease in anchorage independent growth. Soft agar colony formation assay was performed with the HCT116 derived vector control and pkp3 knockdown clones, the shpkp3-2 derived LCN2+PKP3 double knockdown clones and the shpkp3-2 derived vector control clone. Representative differential interference contrast (DIC) images were taken of the soft agar colonies (A). The number of soft agar colonies formed in three plates each of three independent experiments (total nine plates) was counted and the mean and standard error plotted. The p value was calculated using a student's t-test and was found to be <0.05. Note that loss of PKP3 leads to an increase in anchorage independent growth as compared to the vector control and this phenotype is reversed in the double knockdown clones.

It has been reported earlier that HCT116 derived pkp3 knockdown clones form larger tumors and show increased metastasis *in vivo* [233]. The vector control, shpkp3-2+vec and the PKP3+LCN2 double knockdown clones were injected subcutaneously in nude mice as previously described [232, 233]. The mice were observed for 5 weeks and tumor size was measured at regular intervals. Five of the six mice injected with the vector control developed large tumors. In contrast, only one out of six mice injected with shpkp3-2+shLCN2-3 and none of the six mice injected with shpkp3-2+shLCN2-4 were able to develop tumors at the site of injection (Figure 4.21). The average volume of the tumor formed in the mice was analyzed using the formula mentioned in Materials and Methods.

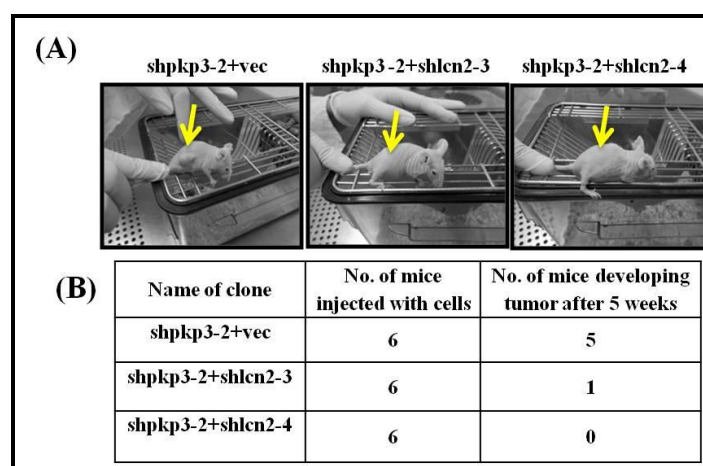


Figure 4.21. Tumor formation is inhibited in the PKP3 knockdown cells upon LCN2 knockdown. 1×10^6 cells of the shpkp3-2 derived vector control or LCN2+PKP3 double knockdown clones were injected sub-cutaneously into nude mice and allowed to develop tumors. Representative images of mice have been shown (A). The table shows the number of mice injected with the respective clones and the number of mice among them which were able to develop tumors (B).

To determine whether ectopic expression of LCN2 in HCT116 cells can increase neoplastic progression, the cDNA of LCN2 was cloned into pcDNA3, a mammalian expression vector along with 2 time hemagglutinin (HA) tag. Stable LCN2 over-expressing clones were generated [408, 409] and validation was done by performing sqRT-PCR using oligonucleotides specific to LCN2 and GAPDH (loading control) and Western blotting using antibody specific to HA and β actin (loading control) [408].

4.5. LCN2 up-regulation upon PKP3 loss is regulated by p38MAPK

To determine whether LCN2 up-regulation upon PKP3 loss was regulated at the transcriptional level, three overlapping regions of the LCN2 promoter [410, 411] containing promoter regions -1138 to+64, -417 to +64 and -153 to +64 were named L1, L2 and L3 respectively were PCR amplified from HCT116 genomic DNA and cloned into the pGL3 basic vector using Kpn1 and Xho1 sites present in the MCS (Multiple cloning site) region of the pGL3 vector (Figure 4.22(A)) [409].

The pGL3 basic vector has the MCS region just upstream of a firefly luciferase reporter gene. Firefly luciferase is a 61kDa monomeric protein that does not require posttranslational processing for enzymatic activity. Thus, it functions as a genetic reporter immediately upon translation [412, 413]. In addition to the reporter plasmids, a control for transfection, pRL-TK, is included in these assays. The plasmid, pRL-TK has a constitutively active thymidine kinase vector driving a Renilla luciferase reporter gene. The Renilla luciferase is a 36 kDa monomeric protein and like firefly luciferase, post- translational modification is not required for its activity. The enzyme functions as a genetic reporter immediately following translation [414, 415].

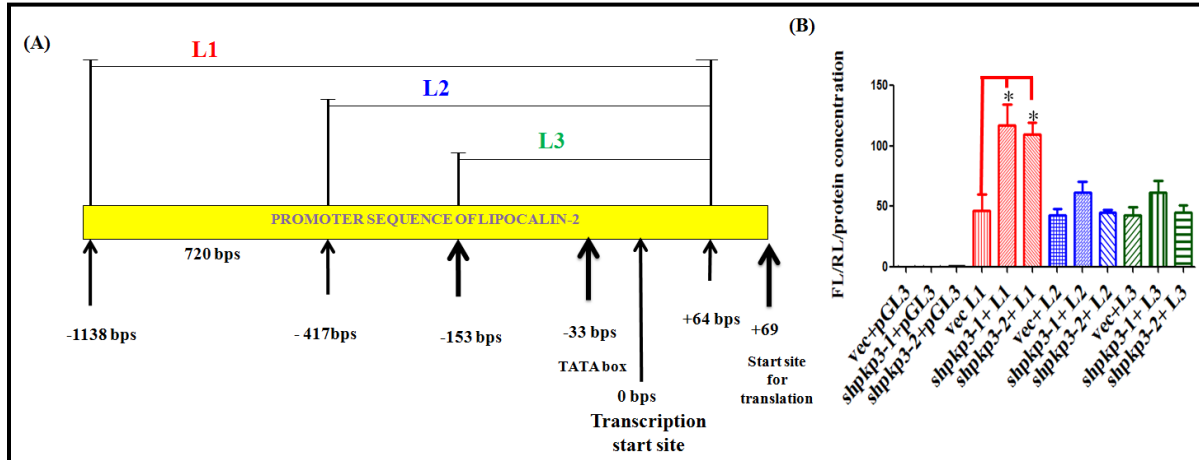


Figure 4.22. LCN2 promoter activity is higher in PKP3 knockdown clones. (A) Schematic representation of the overlapping promoter fragments (L1, L2 and L3) of the LCN2 promoter which were cloned in pGL3 vector (encodes firefly luciferase). The + ve or – ve sign indicates the position of the nucleotide base relative to the transcription start site (TSS) which has been denoted as 0. The translation start site is at position +69 relative to TSS. The location of the promoter fragments on the actual LCN2 promoter has been indicated in base pairs. (B) The LCN2 promoter driven luciferase reporter vectors were transiently transfected in vector control and PKP3 knockdown clones and luciferase reporter assay was performed. CMV promoter driven renilla luciferase encoding vector pRLTK was used as transfection control. The promoterless pGL3 basic vector has been used as a negative control. In the graph, FL represents Firefly luciferase activity based luminescence while RL represents Renilla luciferase activity based luminescence. The ratio of FL/RL/protein concentration of the different promoter constructs in the corresponding cells has been plotted in Y axis. The p value was calculated using a student's t-test and plotted (* indicates p value <0.01).

The Luciferase reporter assays (reviewed in [416]) demonstrated that promoter activity of only the L1 fragment is higher in the PKP3 knockdown clones than the vector control. For the L2 and L3 fragments although there was an increase in the basal luciferase promoter activity compared to the pGL3 basic vector, the increase was observed in both the vector control and PKP3 knockdown clones. Thus the non-overlapping region of the L1 promoter, i.e. -1138 to -417 was hypothesized to have the enhancer elements required for increased transcriptional activity upon PKP3 loss (Figure 4.21(B)). The L1 fragment of 720 bases between -1138 and -417 was named as the region of interest (ROI). A prediction of transcription factor binding sites on the ROI using JASPAR and ALLGEN PROMO software at stringency levels of 95% and 90% respectively suggested that among the most potential transcription factors having binding affinity to this sequence are the Activator protein1 (AP1), GATA binding protein 2 (GATA2), Ying Yang1 (YY1), V-Ets Avian Erythroblastosis Virus E26 Oncogene homolog 1 (ETS1) and ETS1 like protein (ELK1) (data shown later). Since the common upstream kinases of AP1, ETS1 and ELK1 are the p38 Mitogen activated protein kinase (MAPK) and Extracellular signal regulated kinase (ERK)1/2 and previous reports suggested that activation of p38 MAPK and ERK1/2 signaling can up-regulate LCN2 expression [417, 418], the degree of activation of p38 MAPK or ERK1/2 was determined in the PKP3 knockdown clones by Western blotting with antibodies against phospho-p38 MAPK, total p38 MAPK, phospho-ERK1/2 and total ERK1/2 in HCT116 derived PKP3 knockdown clones and the vector control. These experiments demonstrated that PKP3 loss in HCT116 cells result in increased p38MAPK phosphorylation (Figure 4.23 (A)) but not ERK1/2 activation (Figure 4.23 (B)).

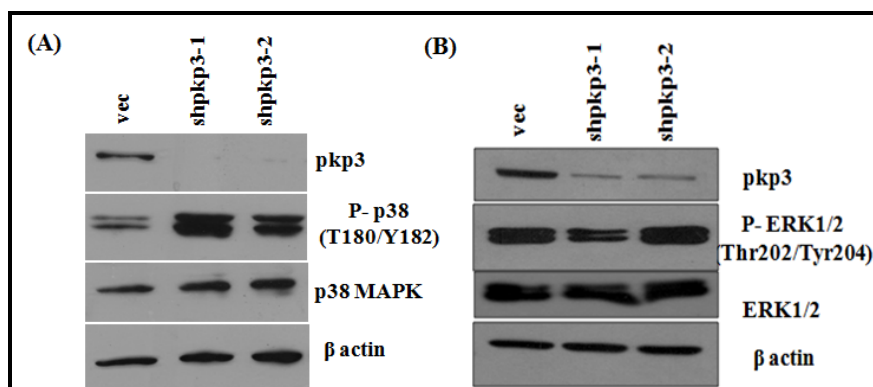


Figure 4.23. Phosphorylation of p38MAPK increases while ERK phosphorylation is not altered in HCT116 derived PKP3 knockdown clones. 75 μ g of a whole cell extract (WCE) was resolved on 12% SDS PAGE gels followed by Western blotting with antibodies specific to PKP3, phospho-p38MAPK (Threonine180/ Tyrosine 182) and total p38MAPK in (A) and PKP3, phospho-ERK1/2 (Threonine202/ Tyrosine 204) and total ERK1/2 in (B). Note that PKP3 levels are lower in clones with a PKP3 knockdown. also note that p38MAPK phosphorylation increases upon PKP3 loss. Western blots for β actin served as a loading control (upper panels).

Since phosphorylation leads to activation of p38MAPK and also stimulates its translocation into the nucleus [419], immuno-flourescence assays were performed using antibodies specific to p38MAPK to analyze localization of p38MAPK in the HCT116 derived PKP3 knockdown and vector control clone. It was observed that PKP3 loss resulted in an increase in the nuclear localization of p38MAPK as determined (Figure 4.24). Nuclear cytoplasmic fractionation was performed using the HCT116 derived vector control and PKP3 knockdown clones. The results of the fractionation experiment demonstrated that nuclear p38MAPK levels were higher in PKP3 knockdown clones as compared to the vector control clones (Figure 4.25). Thus PKP3 loss leads to increased phosphorylation of p38MAPK as well as increased nuclear localization of p38MAPK in the nucleus.

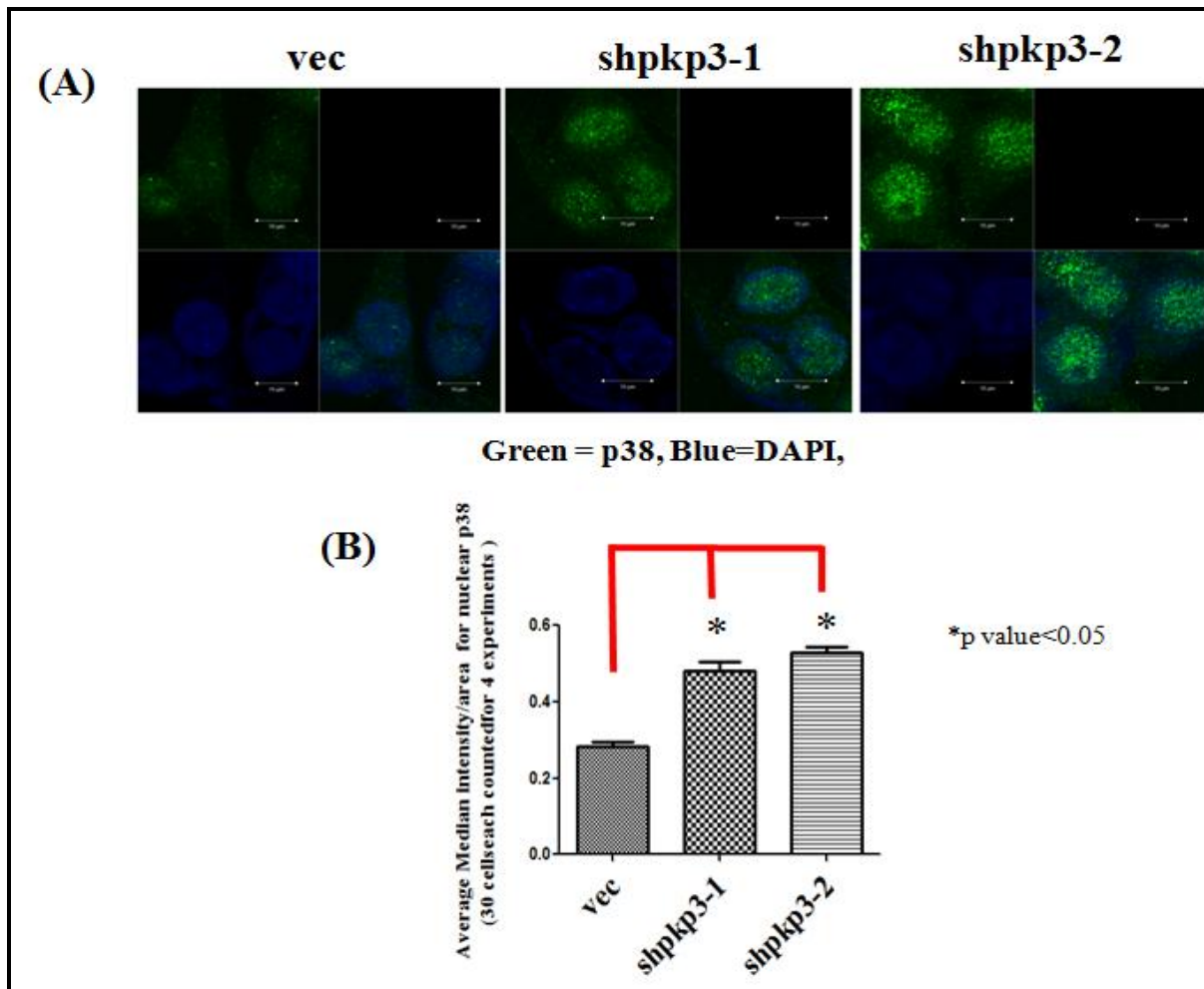


Figure 4.24. Nuclear localization of p38MAPK increases upon PKP3 knockdown in HCT116 cells. Immuno-flourescence for p38MAPK was performed on HCT116 derived vector control and PKP3 knockdown clones. Images were taken in a confocal microscope. The representative images have been shown in (A). The intensity of p38MAPK in the nucleus was quantitated for a 30 cells each in four independent experimets using LSM software and the ratio of the average median intensity to the total area of the nuleus has been plotted. The p value was calculated using a student's t-test and was found to be <0.05 and indicated as *.

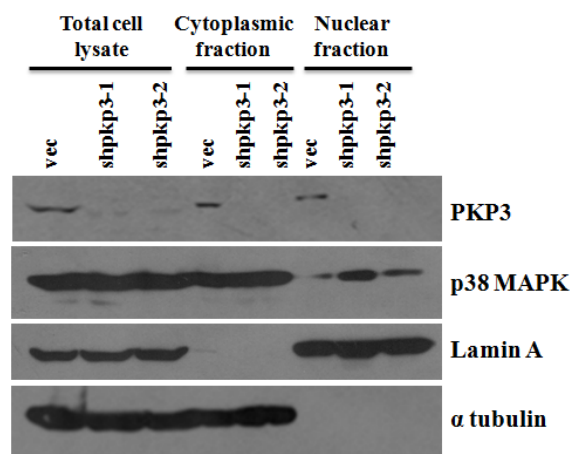


Figure 4.25. Localization of p38MAPK in the nucleus increases upon PKP3 loss: Nuclear cytoplasmic fractionation. 50 μ g of total cell lysate, 50 μ g of cytoplasmic extract and 25 μ g of nuclear extract were resolved on 10% SDS PAGE gels followed by Western blotting with antibodies specific to PKP3, p38MAPK, LaminA (marker for nuclear fraction) and α tubulin (marker for cytoplasmic fraction). Note that p38MAPK levels in the nuclear fraction are higher in the PKP3 knockdown clones as compared to the vector control clone.

Four isoforms of p38 MAPK exist in mammalian cells: p38 α , p38 β , p38 γ and p38 δ . The p38 α and β isoforms are ubiquitously expressed while the γ and δ isoforms show tissue specific expression. These isoforms share high structural homologies: p38 α and β are 75% homologous [420]. The p38 γ and δ have 62% and 61% homology to p38 α respectively; while p38 γ and δ share approximately 70% homology ([421] and reviewed in [422]). Another major difference between the isoforms is that p38 α and β are inhibited by the small concentrations of the pyridinyl imidazol compounds like SB203580, while p38 γ and δ are unaffected [423, 424]. Most of the knowledge about p38 α and β has been derived using SB203580 or its derivatives. Unfortunately, isoform specific effects of p38 α or β cannot be delineated by use of such inhibitors, so additional studies involving knockdown and knockout of the individual isoforms are needed for this

purpose. To determine if PKP3 loss leads to alteration in expression of p38 MAPK isoforms, sqRT-PCR was performed (Figure 4.26) [408]. It was demonstrated that expression of p38 MAPK isoforms were not altered upon PKP3 loss in HCT116 cells.

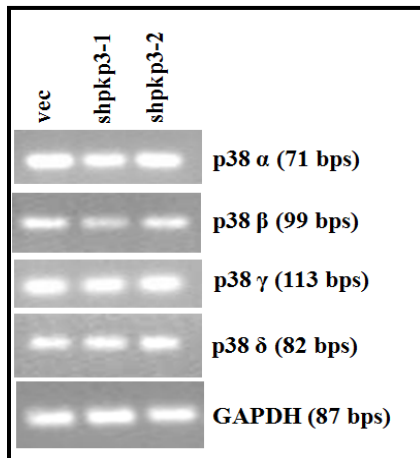


Figure 4.26. PKP3 loss in HCT116 cells doesnot alter expression of any of the p38MAPK isoforms. Four isoforms of p38MAPK exists namely p38 α , p38 β , p38 γ and p38 δ . SqRT-PCRs were performed using oligonucleotides specific for each individual isoforms and GAPDH in HCT116 derived PKP3 knockdown clones and the vector control clone. Expression of GAPDH has been used as a loading control. The PCR product size has been indicated in base pairs.

Since, p38 MAPK activation was higher in PKP3 knockdown clones; it was hypothesized that at least one of the four isoforms of p38MAPK may get phosphorylated upon PKP3 loss, which may in turn cause an increase in LCN2 expression. To identify which p38 isoform is activated upon PKP3 loss, HCT116 derived PKP3 knockdown and vector control clones were treated with 1 μ M SB203580 (the specific inhibitor for p38 α and p38 β isoforms). It was demonstrated that inhibition of p38 α / β MAPK activity was able to decrease LCN2 expression in PKP3 knockdown clones (Figure 4.27 (A)) but MMP7 expression was not altered (Figure 4.27 (B)). Thus either one or both p38 α / β MAPK may be important for LCN2 up-regulation upon PKP3 loss in HCT116 cells.

To determine whether p38 α or p38 β are required for the increase in LCN2 expression upon PKP3 loss, their expression was inhibited in the PKP3 knockdown clone shpkp3-2 using vector

driven RNA interference. Two separate shRNAs were used for each isoform and cloned into the pLKO.1-EGFP-f-puro vector. The oligonucleotides sequences of these shRNAs are available in Materials and Methods. Three p38 α MAPK+PKP3 double knockdown clones were generated using the shRNAs p38 α 1 and p38 α 2. Two clones shpkp3-2+shp38 α 1.1 (validated positive by Western blotting but not used in the further experiments) and shpkp3-2+shp38 α 1.2 was obtained from shRNA p38 α 1 while the shRNA p38 α 2 yielded two clones: shpkp3-2+shp38 α 2.2 and shpkp3-2+shp38 α 2.4 [408].

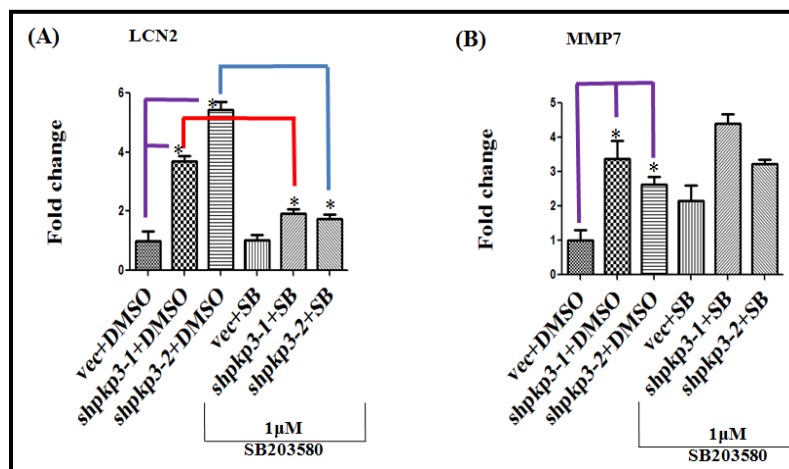


Figure 4.27. Inhibition of the activity of p38 α / β results in a decrease in LCN2 but not MMP7 expression in PKP3 knockdown cells. Real time PCR for LCN2 (A) and MMP7(B) was performed using cDNA obtained from vector control and PKP3 knockdown clones after treatment with 10 μ M SB203580 (p38MAPK inhibitor) or DMSO (solvent control) for 24 hours. All expression was normalized to the levels of GAPDH. The fold change is graphed on the Y-axis and the clone name is on the X-axis. The standard errors are plotted and student's t test was performed (* indicates a p value<0.01).

Four p38 β MAPK+PKP3 double knockdown clones were generated using the shRNAs p38 β 1 and p38 β 2. Two clones designated shpkp3-2+shp38 β 1.1 and shpkp3-2+shp38 β 1.4 were obtained

from shRNA p38 β 1 while the shRNA p38 β 2 yielded two clones: shpkp3-2+shp38 β 2.4 and shpkp3-2+ shp38 β 2.5. The clone shpkp3-2+vec was used as the vector control. The expression of p38 α and p38 β MAPKs in the HCT116 derived vector control, PKP3 knockdown clones and p38 α or p38 β double knockdown clones were validated by Western blotting (Figure 4.28) and qRT-PCR (Figure 4.29).. It was demonstrated that p38 α +PKP3 double knockdown clones showed decrease in expression of p38 α MAPK but p38 β levels remained unaltered. Correspondingly, p38 β +PKP3 double knockdown clones showed decrease in expression of p38 β MAPK but p38 α levels remained unaltered.

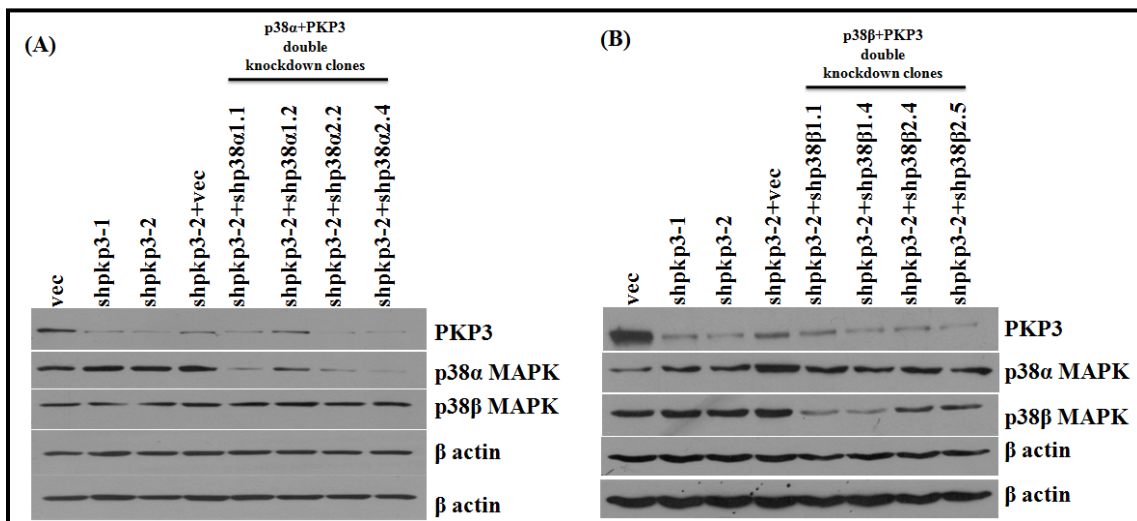


Figure 4.28. Validation of p38 α +PKP3 double knockdown clones and p38 β +PKP3 double knockdown clones by Western blotting. 75 μ g of a whole cell extract (WCE) was resolved on 12% SDS PAGE gels followed by Western blotting using antibodies specific for the p38 α , p38 β MAPK isoform and β actin (loading control) in HCT116 derived PKP3 knockdown clones (shpkp3-1 and shpkp3-2), its vector control clone (vec), the shpkp3-2 derived vector control clone (shpkp3-2 + vec), the p38 β α +PKP3 double knockdown clones (shpkp3-2 + shp38 α 1.1, shpkp3-2 + shp38 α 1.2, shpkp3-2 + shp38 α 2.2 and shpkp3-2 + shp38 α 2.4) (A), and the p38 β

+PKP3 double knockdown clones (shpkp3-2 + shp38 β 1.1, shpkp3-2 + shp38 β 1.4, shpkp3-2 + shp38 β 2.4 and , shpkp3-2 + shp38 β 2.5) (B). Note that p38 α expression decreases while p38 β expression is unchanged in the p38 α +PKP3 double knockdown clones, while in the p38 β +PKP3 double knockdown clones p38 β expression decreases and p38 α expression is not altered.

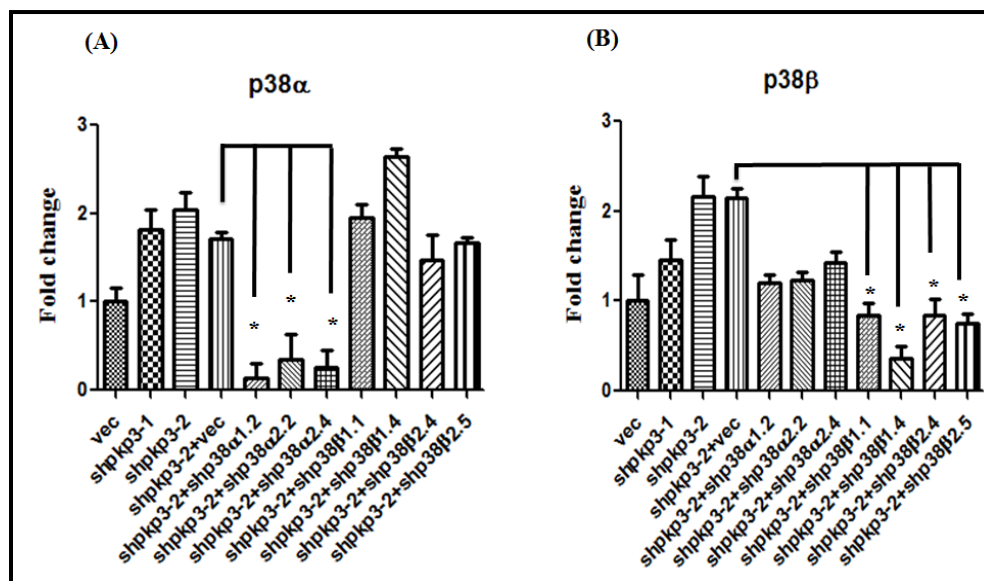


Figure 4.29. Validation of p38 α +PKP3 double knockdown clones and p38 β +PKP3 double knockdown clones by qRT-PCR. qRT-PCRs were performed using oligonucleotides specific for p38 α MAPK isoform (A), p38 β MAPK isoform (B) and GAPDH in HCT116 derived PKP3 knockdown clones (shpkp3-1 and shpkp3-2), its vector control clone (vec), the shpkp3-2 derived p38 α +PKP3 double knockdown clones (shpkp3-2 + shp38 α 1.2, shpkp3-2 + shp38 α 2.2 and shpkp3-2 + shp38 α 2.4) , p38 β +PKP3 double knockdown clones (shpkp3-2 + shp38 β 1.1, shpkp3-2 + shp38 β 1.4, shpkp3-2 + shp38 β 2.4 and , shpkp3-2 + shp38 β 2.5) and the corresponding vector control clone (shpkp3-2 + vec). All expressions were normalized to the levels of GAPDH. The fold change is graphed on the Y-axis and the clone name is on the X-axis. The standard errors are plotted and student's t test was performed (* indicates a p value<0.01).

Note that p38 α expression decreases in the p38 α +PKP3 double knockdown clones while it is unchanged in the p38 β +PKP3 double knockdown clones, while p38 β expression decreases in the p38 α β +PKP3 double knockdown clones while it is unchanged in the p38 β α +PKP3 double knockdown clones.

To determine if LCN2 expression is altered upon loss of p38 α or p38 β MAPK in PKP3 knockdown clones, qRT-PCR was performed in the HCT116 derived PKP3 knockdown clones, its vector control clone, p38 α +PKP3 double knockdown clones, p38 β +PKP3 double knockdown clones and their vector control clone shpkp3-2. As expected, LCN2 expression was increased upon PKP3 loss in HCT116 cells but upon p38 α loss in the PKP3 knockdown clone, LCN2 expression was further increased while upon p38 β loss, LCN2 expression was reduced more than two fold (Figure 4.30). These experiments suggest that p38 β activation regulated LCN2 up-regulation upon PKP3 loss in HCT116 cells.

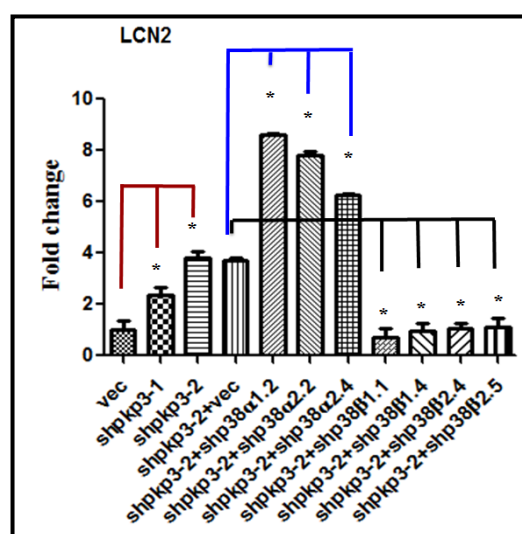


Figure 4.30. p38 β knockdown in HCT116 derived PKP3 knockdown clones decreases LCN2 expression but p38 α knockdown highly increases LCN2 expression. qRT-PCRs were performed using oligonucleotides specific for LCN2 and GAPDH, in PKP3 knockdown clones,

its vector control, the p38 α +PKP3 double knockdown clones, the p38 β +PKP3 double knockdown clones and the respective vector control clone. Expression of GAPDH has been used for normalization. The Y-axis in the qRT-PCR panels reflects the fold change in transcription, which is calculated as described in the Materials and Methods. The X-axis indicates the clone name. The standard errors are plotted and student's t test was performed (* indicates a p value<0.01).The PCR product size in sqRT-PCR panels has been indicated in base pairs.

p38MAPK is activated by environmental stress, oxidative stresses and inflammatory cytokines. The p38MAPK signaling pathway involves phosphorylation and activation of transcription factors like Activating transcription factor 2 (ATF2) [425], Nuclear Mitogen- And Stress- Activated Protein Kinase (MSK1) [425], ETS1 [426] and ELK1[427] (Figure 4.31).

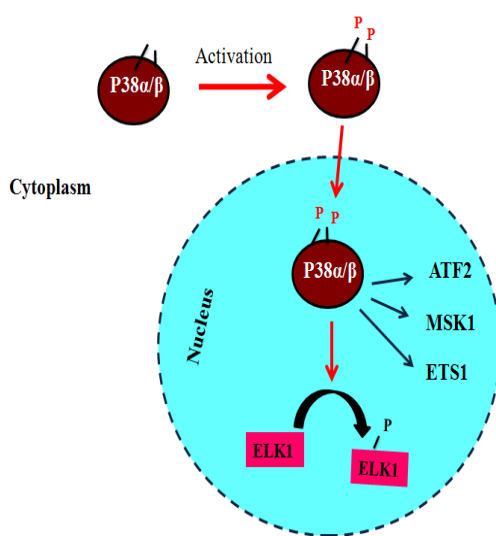


Figure 4.31. The p38MAPK signaling pathway.

Schematic representation of the p38MAPK regulating ELK1 activation upon PKP3 loss. Note that p38MAPK enters the nucleus upon phosphorylation mediated activation and this in turn activates transcription factors like ATF2, MSK1, ETS1 and ELK1.

To determine if PKP3 loss leads to alterations in phosphorylation status and total protein levels of these transcription factors, Western blotting was performed using specific antibodies to these proteins. Phosphorylation of ATF2 and MSK1 was unaltered (Figure 4.32) but phosphorylated ELK1 and total ELK1 protein levels were increased upon PKP3 loss (Figure 4.33 (A)). Subsequently, qRT-PCR for ELK1 was performed

in the HCT116 derived PKP3 knockdown clones and the vector control clones and it was demonstrated that the mRNA expression of ELK1 was also increased (Figure 4.33 (B)).

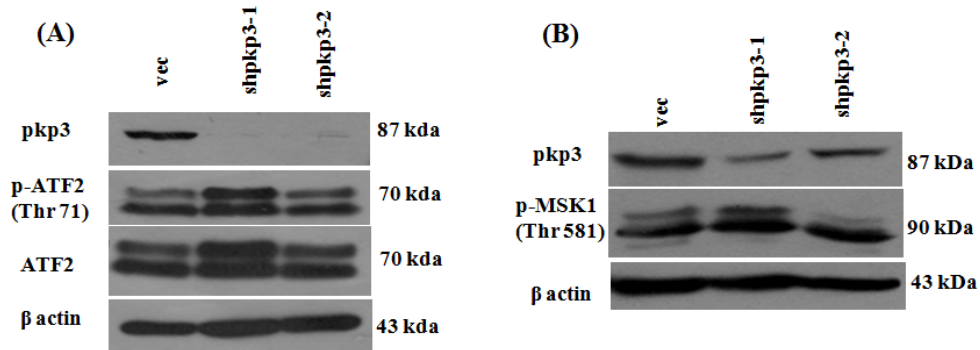


Figure 4.32. No alteration in activation of ATF2 and MSK1 upon PKP3 loss. 75µg of a whole cell extract (WCE) was resolved on 12% SDS PAGE gels followed by Western blotting with antibodies specific to PKP3, phospho-ATF2 (Threonine 71), total ATF2 and β actin in (A) and PKP3, phospho-MSK1 (Threonine 581) and β actin in (B). In both Western blots β actin has been used as the loading control. The molecular weights of the proteins analyzed by Western blotting have been indicated as kilo Daltons (kDa).

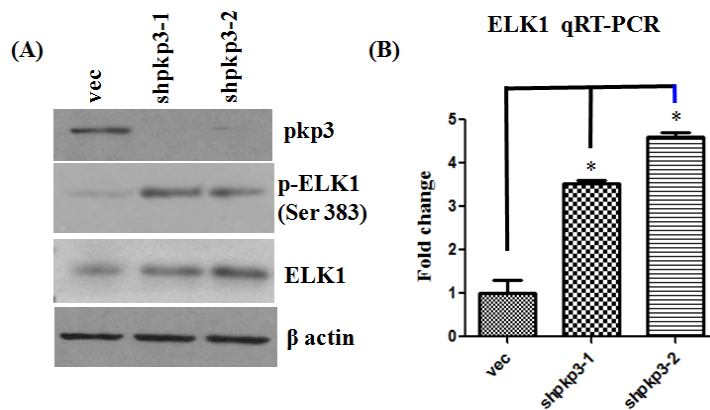


Figure 4.33. ELK1 expression and activation increases upon PKP3 loss in HCT116 cells.

(A) 75µg of a whole cell extract (WCE) was resolved on 10% SDS PAGE gels followed by

Western blotting with antibodies specific to PKP3, phospho-ELK1 (Ser 383), total ELK1 and β actin (loading control). Note that both phospho-ELK1 and ELK1 levels are higher in the PKP3 knockdown clones. (B) qRT-PCRs were performed using oligonucleotides specific for ELK1 and GAPDH, in HCT116 derived PKP3 knockdown clones and the vector control clone. Expression of GAPDH has been used for normalization. The standard errors are plotted and student's t test was performed (* indicates a p value < 0.01).

4.6. ELK1 is required for the increase in LCN2 expression observed upon PKP3 loss.

ELK1 is a member of the Ets family of transcription factors and of the ternary complex factor (TCF) subfamily (Figure 4.34). Proteins of the TCF subfamily form a ternary complex by binding to the serum response factor (SRF) ([428] and reviewed in [429]). ELK1 is a downstream target of p38 MAPK [427, 430, 431]. Since ELK1 is a well studied transcription factor, its consensus binding sites on promoters are known [432, 433] and thus can be predicted using transcription factor binding site prediction software such as ALLGEN PROMO [434, 435] and JASPAR [436, 437] which can detect the consensus binding motif of many transcription factors including ELK1. ELK1 can also bind to ETS1 binding sites on promoter sequences [438] and can also collaborate with Serum Response Factor (SRF) to bind to certain promoters [439].

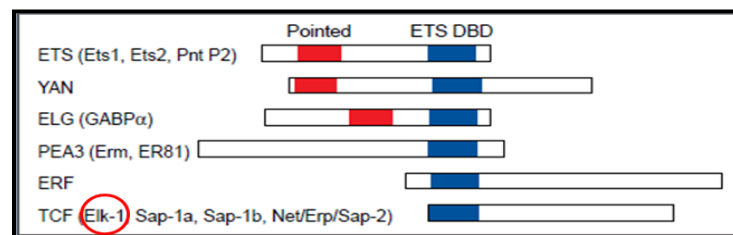


Figure 4.34. ELK1 is a member of the ETS family of transcription factors. A schematic representation of the different members of the ETS1 family proteins and its structural domains.

ELK1 belongs to the T cell factor (TCF) subfamily of the ETS family of transcription factors. It has the same DNA binding domain as ETS1 (ETS DBD represented as blue box) [429].

To determine if the ROI of the LCN2 promoter has any ELK1 or ETS1 binding sites, the ROI sequence was submitted to the ALLGEN-PROMO and JASPAR analysis softwares. Five ETS1 sites and one consensus ELK1 site was detected in the ROI sequence (Figure 4.35). To analyze if ELK1 regulates LCN2 over-expression upon PKP3 loss, ELK1 was

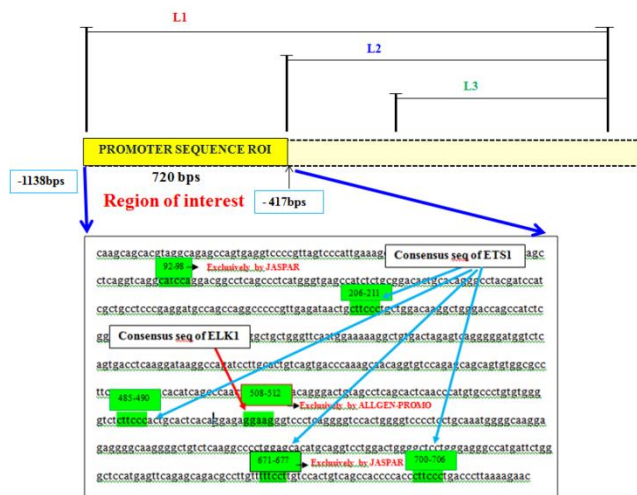


Figure 4.35. ELK1 and ETS1 binding sites are present in the LCN2 promoter region of interest (ROI). JASPAR and ALLGEN-PROMO software analysis of transcription factor binding sites in the LCN2 promoter ROI identified presence of multiple ETS1 binding sites and one ELK1 binding site. The positions of these sites have been indicated (highlighted green) on the promoter sequence of ROI depicted in the box.

knocked down in a HCT116 derived PKP3 knockdown clone generating ELK1 double knockdown clones (shpkp3-2+shelk1-3 and shpkp3-2+shelk1-5). ELK1 knockdown in these clones at the mRNA and protein levels were validated using qRT-PCR (Figure 4.36 (A)) and Western blotting (Figure 4.36 (B)) respectively.

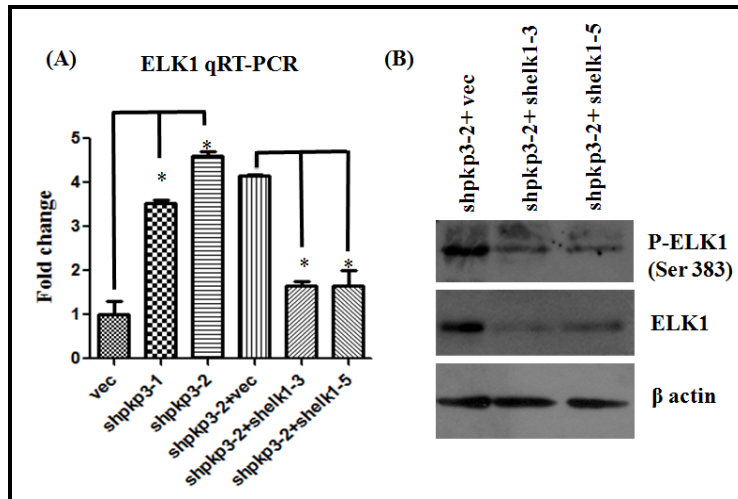


Figure 4.36. Validation of ELK1+PKP3 double knockdown clones by qRT-PCR and Western blotting. qRT-PCRs were performed using oligonucleotides specific for ELK1 and GAPDH in the HCT116 derived PKP3 knockdown clones, the vector control clone (vec), the shpkp3-2 derived ELK1+PKP3 double knockdown clones and the corresponding vector control clone (shpkp3-2 + vec). All expressions were normalized to the levels of GAPDH. The standard errors are plotted and student's t test was performed (* indicates a p value<0.01). (B) 75 μ g of a whole cell extract (WCE) was resolved on 10% SDS PAGE gels followed by Western blotting with antibodies specific to PKP3, phospho-ELK1 (Serine 383), total ELK1 and β actin (loading control). Note that ELK1 expression decreases in the ELK1+PKP3 double knockdown clones both at mRNA and protein level.

Subsequently, qRT-PCR assays were performed to determine if LCN2 expression was altered upon ELK1 knockdown in the PKP3 knockdown clones. It was demonstrated that LCN2 levels were indeed decreased in the ELK1+PKP3 double knockdown clones than their corresponding vector control clone (Figure 4.37). Thereafter, luciferase reporter assays were performed to analyze if the decrease in LCN2 upon ELK1 loss in the PKP3 knockdown clones was due to

decreased transcription of LCN2. It was demonstrated that ELK1 was required for increased LCN2 promoter activity in the PKP3 knockdown clones (Figure 4.38). As the knockdown of both p38 β and ELK1 resulted in a decrease in LCN2 transcription and p38MAPK is known to phosphorylate and activate ELK1 [427], it was hypothesized that probably p38 β activates ELK1 and this in turn regulates LCN2 up-regulation.

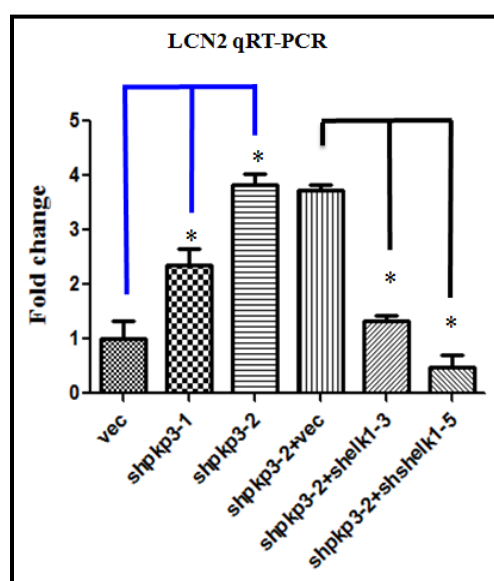


Figure 4.37. ELK1 regulates LCN2 expression upon PKP3 loss in HCT116 cells. (A) qRT-PCRs were performed using oligonucleotides specific for ELK1 and GAPDH, in HCT116 derived PKP3 knockdown clones, its vector control clone, shpkp3-2 derived ELK1+PKP3 knockdown clones and its respective vector control shpkp3-2+vec. Expression of GAPDH has been used for normalization. The standard errors are plotted and student's t test was performed (* indicates a p value<0.01). Note that both LCN2 levels are higher in the PKP3 knockdown clones but decreases upon ELK1 knockdown.

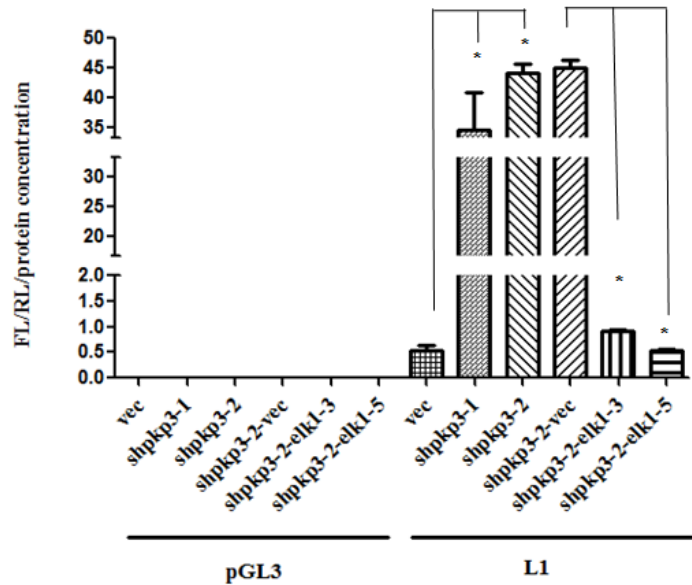


Figure 4.38. LCN2 promoter activity is decreased upon ELK1 knockdown in PKP3 knockdown cells. The LCN2 promoter driven luciferase reporter vector L1 was transiently transfected in HCT116 derived vector control, PKP3 knockdown clones, ELK+PKP3 double knockdown clones and the corresponding vector control clone. The cells were lysed after 24 hours using the prescribed lysis buffer (Promega). The lysates were collected and luciferase reporter assay was performed along with protein estimation. CMV promoter driven renilla luciferase encoding vector pRLTK was used as transfection control. The promoterless pGL3 basic vector has been used as a negative control. The ratio of FL/RL/protein concentration of the L1 in the corresponding cells has been plotted in Y axis. The p value was calculated using a student's t-test and plotted (* indicates p value <0.01).

Since ELK1 expression was higher in the PKP3 knockdown clones and was found to be important in up-regulating expression of LCN2 upon PKP3 loss, it was hypothesized that some other targets of ELK1 may also be increased in the PKP3 knockdown clones. It has been demonstrated that ELK1 (upon activation by the nuclear factor of activated T cells (NFAT)

pathway) can cause activation of the c-myc promoter thus causing increase in c-myc expression and promote c-myc induced growth in pancreatic cancer cells [440]. To determine if ELK1 can regulate increased c-myc expression in HCT116 derived PKP3 knockdown clones, Western blotting was performed using cell lysates obtained from HCT116 derived vector control clones, PKP3 knockdown clones, the ELK1+PKP3 double knockdown clones and the corresponding vector control clone. It was demonstrated that c-myc expression was higher in the PKP3 knockdown clones than the vector control clones but its expression did not decrease upon ELK1 knockdown [441]. Thus, ELK1 mediated transcriptional activation upon PKP3 loss is specific to the LCN2 promoter.

4.8. p38 β MAPK and ELK1 independently regulates increase in LCN2 expression upon PKP3 loss.

As the loss of both p38 β and ELK1 resulted in a decrease in LCN2 transcription and p38MAPK is known to phosphorylate and activate ELK1⁴⁵, it was hypothesized that the increased activity of p38 β results in an increase in ELK1 levels and ELK1 activation leading to an increase in LCN2 expression. Western blotting was also performed to analyze the expression and phosphorylation of ELK1 in the p38 β +PKP3 double knockdown clones. It was demonstrated that ELK1 expression and phosphorylation was unaltered upon p38 β loss in the PKP3 knockdown clones. As controls, Western blotting experiments demonstrated that the levels of ELK1 and phosphorylated ELK1 were diminished in the ELK1 knockdown cells (Figure 4.39 (A)). Western blotting was also performed to analyze if p38MAPK activity can be regulated by ELK1 and it was demonstrated that p38 β activity was not altered upon ELK1 knockdown (Figure 4.39 (B)). Thus, PKP3 loss leads to an increase in both ELK1 expression and p38 β activation and both events independently regulate LCN2 activity.

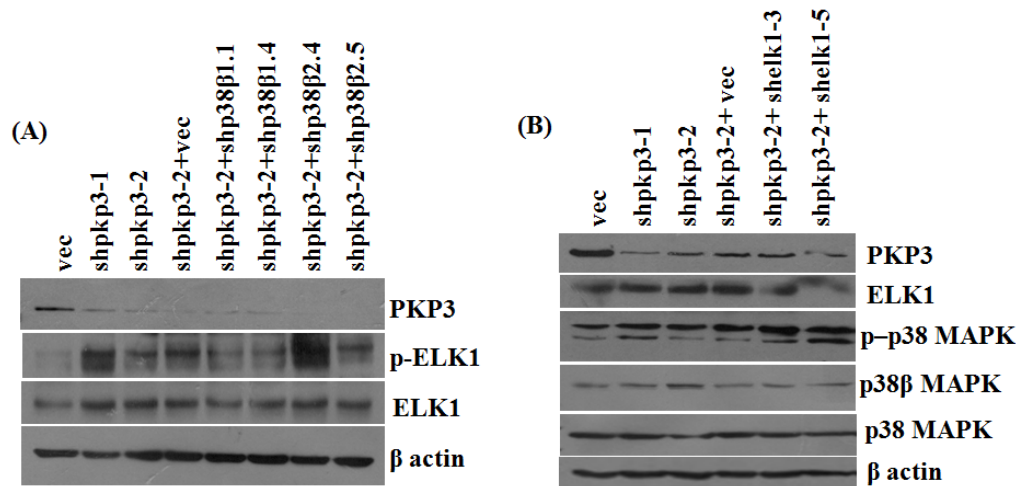


Figure 4.39. Activation of p38 β MAPK and ELK1 upon PKP3 loss is independent of each other. (A) 75 μ g of a whole cell extract obtained from HCT116 derived PKP3 knockdown clones, its vector control, the p38 β +PKP3 double knockdown clones and the respective vector control clone was resolved on 10% SDS PAGE gels followed by Western blotting with antibodies specific to PKP3, phospho-ELK1 (Serine 373), total ELK1 and β actin (loading control). Note that both phospho-ELK1 and ELK1 levels are higher in the PKP3 knockdown clones but remain unaltered when p38 β is knocked down in the PKP3 knockdown clones (B) 75 μ g of a whole cell extract obtained from HCT116 derived PKP3 knockdown clones, its vector control, the ELK1 +PKP3 double knockdown clones and the respective vector control clone was resolved on 10% SDS PAGE gels followed by Western blotting with antibodies specific to PKP3, phospho- p38 MAPK (Threonine 180/ Tyrosine 182), total p38MAPK, p38 β MAPK and β actin (loading control). Note that p38MAPK phosphorylation increases upon PKP3 loss but remain unaltered when ELK1 is knocked down in the PKP3 knockdown clones.

4.8. PKP3 binds to p38 β MAPK.

It has been demonstrated that PKP3 loss leads to activation of the p38 β MAPK and/or activation and up-regulation of ELK1 which in turn up-regulates LCN2 expression in HCT116 cells, but the mechanism regulating p38 β activation upon PKP3 loss is not known. It has been hypothesized that PKP3 may bind to p38 β thus inhibiting phosphorylation and activation of p38 β . Thus, when PKP3 is lost, p38 β MAPK gets activated which leads to LCN2 upregulation probably via ELK1 mediated increase in transcription of LCN2.

p38 β MAPK (p38 β), one of the four isoforms of p38MAPK,. Although p38 β shares 75% homology with p38 α [420], a comparison between the structures of p38 α and p38 β showed a difference in the orientation of the N and C terminal lobes (domains) in p38 β . This caused a reduction in the size of its ATP binding pocket [442]. p38 β gets phosphorylated by MAPK kinase 4 (MKK4) and MAPK kinase 6 (MKK6) at residues Threonine180 and Tyrosine182 present as the dual phosphorylation motif characteristic of all p38MAPKs [420]. Unlike all other p38MAPK isoforms, p38 β can be auto-phosphorylated *in vitro*, but *in vivo*, its auto-phosphorylation is inhibited by the interaction of its C terminal domain and an N terminal lobe. This interaction is strengthened by interaction of some unknown p38 β regulatory proteins [443]. It was hypothesized that PKP3 may bind to the C terminal domain of p38 β and inhibit its auto-activation *in vivo*. A model for this hypothesis has been shown in Figure 4.40. To address this hypothesis, cDNA encoding p38 β MAPK wild type and C terminal truncated mutants V345 and F348 cloned into the mammalian expression vector pCEFL and containing 3 times HA tag [443] was obtained as a kind gift from Dr. Engelberg's laboratory (National University of Singapore).

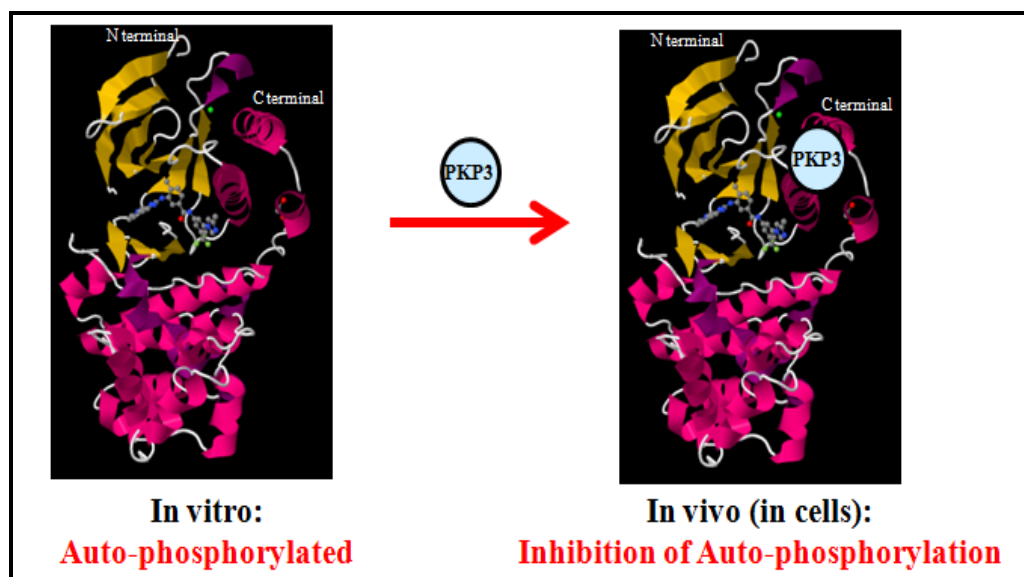


Figure 4.40. PKP3 may inhibit auto-phosphorylation of p38 β MAPK by binding its C terminus. The figure is a cartoon of the PKP3 protein superimposed on the three dimensional secondary structure of p38 β MAPK. It has been hypothesized that in human cells PKP3 may bind to the C terminal of p38 β MAPK and inhibit its auto-phosphorylation.

	P38 β MAPK protein	No. of amino acids	3XHA tag (1 kDa each)	Mol. Wt.
	N	C		
WT			364	~ 43 kDa + 3 kDa = 46 kDa
F348			348	~ 41 kDa + 3 kDa = 44 kDa
V345			345	~ 41 kDa + 3 kDa = 44 kDa

Figure 4.41. Schematic representation of the wild type (WT) and C terminal truncated mutants of p38 β MAPK. The figure is a cartoon representing the protein structure of the WT and the C terminal deletion mutants of p38 β MAPK. Since the cDNA encoding these constructs has been cloned in pCEFL vector with 3 times HA tag, and each HA tag protein is 1kDa in size, the figure also indicates the molecular weight of the protein and its mutants before and after addition of three HA tags.

A schematic representation of the wild type and truncated mutants of p38 β has been shown in Figure 4.41. These cDNA encoding plasmids were transiently transfected into HCT116 cells and immuno-precipitation experiments were performed using an antibody specific to the HA tag. The immuno-precipitated samples and 5% input whole cell lysates were run on a 10% SDS PAGE gel and probed for PKP3. It was observed that PKP3 co-immuno-precipitated with the HA tagged wild type p38 β as well as with the C terminal truncated mutants of p38 β (Figure 4.42). Thus, it was demonstrated that PKP3 physically binds to p38 β but not at the C terminal regions that had been truncated.

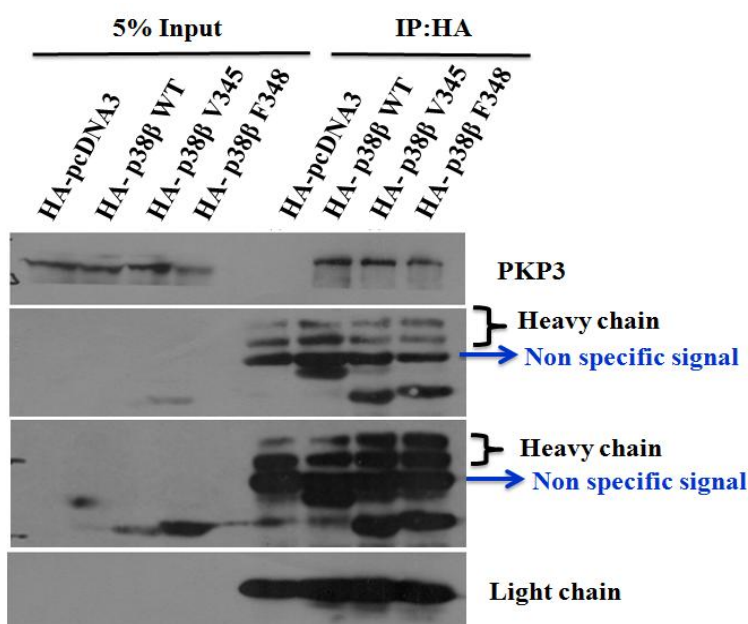


Figure 4.42. PKP3 binds to p38 β but not via the C terminus of p38 β MAPK. Plasmid vectors encoding HA tagged WT p38 β MAPK, HA tagged C terminal deletion mutants of p38 β MAPK and HA pcDNA3 (negative control) were transiently transfected in HCT116 cells. Immuno-precipitation experiments were performed using HA antibody. The immune-precipitated samples along with 5% input of the whole cell extracts (collected before immune-precipitation) were run on 10% SDS PAGE gel followed by Western blotting using PKP3 and HA antibodies. The heavy

chain and light chain of the antibody used for immune-precipitation has been indicated. Note that in the uppermost panel, PKP3 binds to both the WT and C terminal deletion mutants of p38 β MAPK.

To determine if endogenous p38 β MAPK binds to the endogenous PKP3, cell lysates obtained from HCT116 derived vector control and PKP3 knockdown clones were used for immunoprecipitation experiments using an antibody specific to p38 β MAPK. The immuno-precipitated samples and 5% input whole cell lysates were run on a 7.5% SDS PAGE gel and probed for PKP3 (Figure 4.43 (A)). A similar immuno-precipitation experiment was also performed using an antibody specific to p38 α MAPK and again the immuno-precipitated samples and 5% input whole cell lysates were run on a 7.5% SDS PAGE gel and probed for PKP3 (Figure 4.43 (B)). Thus PKP3 binds to both p38 β and p38 α MAPK and thus it can be postulated that PKP3 may prevent phosphorylation of p38MAPK by preventing its interaction with its upstream kinases like MKK3/4/6.

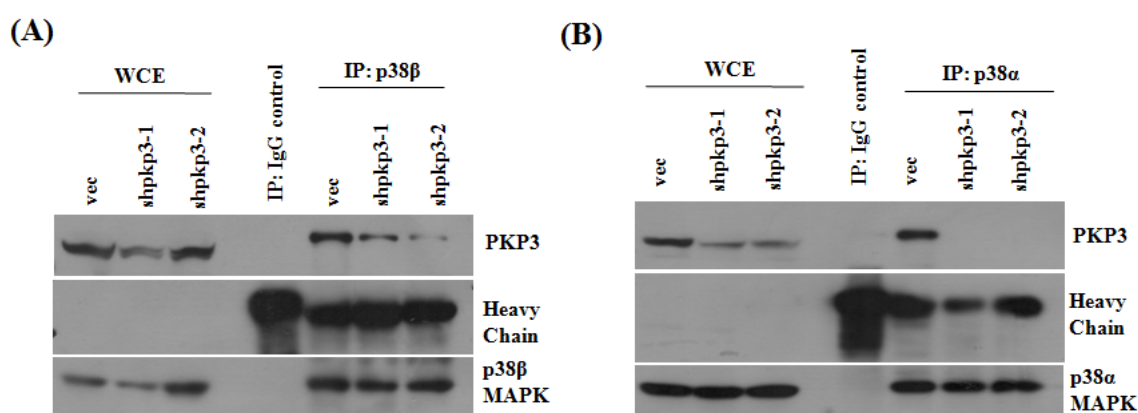


Figure 4.43. PKP3 interacts with both p38 β and p38 α MAPK. (A) Whole cell extracts were collected from HCT116 derived PKP3 knockdown and vector control clones and immunoprecipitation experiments were performed using p38 β MAPK antibody. The immuno-

precipitated samples along with 5% input of the whole cell extracts (collected before immune-precipitation) were run on 7.5% SDS PAGE gel followed by Western blotting using PKP3 and p38 β MAPK antibodies. The heavy chain of the antibody used for immune-precipitation has been indicated. Note that PKP3 immuno-precipitates out with p38 β and in PKP3 knockdown cells, co-immuno-precipitation of PKP3 decreases. (B) Whole cell extracts were collected from HCT116 derived PKP3 knockdown and vector control clones and immuno-precipitation experiments were performed using p38 α MAPK antibody. The immuno-precipitated samples along with 5% input of the whole cell extracts (collected before immune-precipitation) were run on 7.5% SDS PAGE gel followed by Western blotting using PKP3 and p38 α MAPK antibodies. The heavy chain of the antibody used for immune-precipitation has been indicated. Note that PKP3 co-immuno-precipitates with p38 α and in PKP3 knockdown cells, co-immuno-precipitation of PKP3 decreases.

4.8. MMP7 is necessary for neoplastic transformation upon PKP3 loss.

Similar to LCN2, PKP3 loss leads to increase in expression of MMP7 across all three cell types tested (Figure 4.14). To determine whether the increase in MMP7 levels is also required for tumor formation upon PKP3 loss, shpkp3-2 derived MMP7+PKP3 double knockdown clones were generated using the pLKO.1-EGFP-f puro vector driven RNA interference. The oligonucleotides sequences of these shRNAs are available in Materials and Methods. Two double knockdown clones were generated and named shpkp3-2+shmp7-1 and shpkp3-2+mmp7-2 (Figure 4.44). The clone shpkp3-2+vec was used as the vector control clone. The expression of MMP7 in the vector control and the double knockdown clones was analyzed by qRT-PCR (Figure 4.45 (A)). Since MMP7 [444-446] is a secreted protein, cells were grown in the absence of serum and the supernatant collected for the HCT116 derived PKP3 knockdown

clones shpkp3-1 and shpkp3-2, the vector control clone vec, the shpkp3-2 derived MMP7 knockdown clones shpkp3-2+shmp7.1 and shpkp3-2+shmp7.2. The proteins in the supernatant were precipitated using acetone as described in the Materials and Methods and a Western blot performed for MMP7. It was demonstrated that PKP3 knockdown led to an increase in the expression of MMP7 while knockdown of MMP7 causes a decrease in MMP7 expression of as expected (Figure 4.45 (B)). The blot was stained with ponceau-S to show equal protein loading for the cell supernatants.

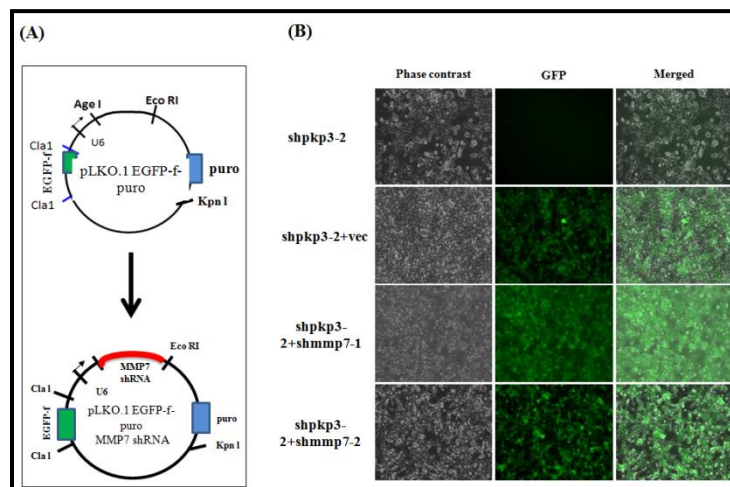


Figure 4.44. Cloning of MMP7 shRNA in pLKO.1-EGFP-f-puro vector and generation of stable double knockdown clones of MMP7 derived from the HCT116 based PKP3 knockdown clone shpkp3-2. (A) Schematic representation of the cloning strategy used to clone a shRNA against MMP7 into the pLKO.1 EGFP-f-puro vector. The sites AgeI and EcoRI cloning were used for this purpose. (B) HCT116 derived PKP3 knockdown clone, shpkp3-2 was transfected with two clones each of pLKO.1 EGFP-f-puro LCN2 shRNA, A and B plasmids. The cells were maintained in media containing 5µg/ml blasticidin and 0.5µg/ml puromycin to obtain single cell clones thus generating two clones shpkp3-2+shLCN2-1 and 2 (from A) and two more clones shpkp3-2+shLCN2-3 and 4 (from B). Similarly, the pLKO.1 EGFP-f-puro plasmid was transfected in shpkp3-2 cells and selected in blasticidin and puromycin to generate

the vector control clone. All clones cells were analyzed for expression of EGFP-f under a fluorescence microscope and images were obtained. The shpkp3-2 cells served as a negative control for the EGFP-f expression. Note that all double knockdown clones and vector control clones except the negative control clone showed EGFP-F expression at the cell border.

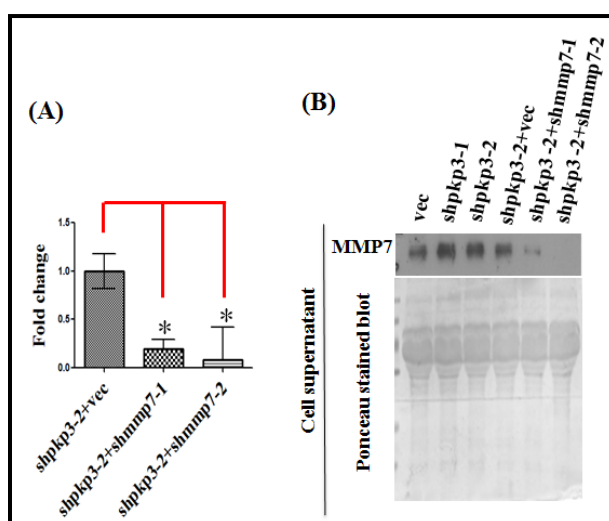


Figure 4.45. Validation of MMP7+PKP3 double knockdown clones by qRT-PCR and Western blotting (of acetone precipitated cell supernatant). (A) qRT-PCR was performed using oligonucleotides specific for MMP7 and GAPDH, in the MMP7+PKP3 double knockdown clones (shpkp3-2 + shmp7-1, shpkp3-2 + mmp7-2) and the vector control (shpkp3-2 + vec). All expression was normalized to the levels of GAPDH. The standard errors are plotted and student's t test was performed (* indicates a p value<0.01). Note that MMP7 levels are decreased in the MMP7+PKP3 double knockdown clones as compared to the corresponding vector control. (B) 100 μ g of acetone precipitated cell supernatants of the HCT116 derived vector control (vec), PKP3 knockdown clones shpkp3-1 and shpkp3-2, the MMP7+PKP3 double knockdown clones and its vector control clone were resolved on 12% SDS PAGE gels followed by Western blotting with antibodies specific to MMP7. Note that MMP7 levels are higher in supernatants prepared from the PKP3 knockdown cells as compared to the vector controls while the MMP7 levels are

lower in the double knockdown clones. The same blot was stained with Ponceau stain to demonstrate equal loading of proteins (lower panels).

To determine if MMP7 knockdown in the PKP3 knockdown clone shpkp3-2 can decrease cell migration, scratch wound healing assays were performed and it was demonstrated that loss of MMP7 indeed decreased cell migration (Figure 4.46 (A) and (B)).

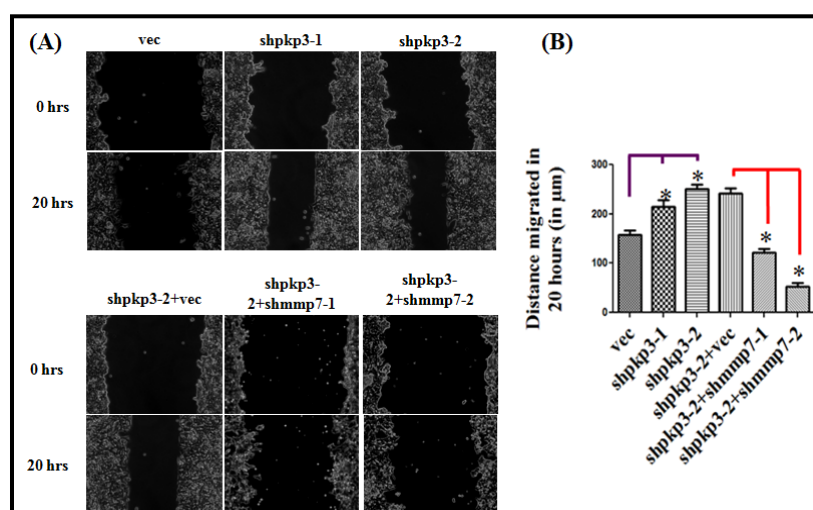


Figure 4.46. MMP7 loss leads to a decrease in cell migration. Scratch wound healing assays were performed on the HCT116 derived vector control(vec), PKP3 knockdown clones (shpkp3-1 and shpkp3-2), shpkp3-2 derived vector control clone (shpkp3-2+vec) and shpkp3-2 derived MMP7 knockdown clones(shpkp3-2+shmp7-1 and shpkp3-2+shmp7-2) as described. Phase contrast images of wound healing at 0 hours (start) and 20 hours (end of experiment) have been shown. The mean and standard deviation of the distance migrated in 20 hours has been plotted. Note that migration is increased in the pkp3 knockdown clones, while it is decreased in the double knockdown clones.

Matrigel invasion assays using Bowden's chambers demonstrated that the increase in invasion observed upon PKP3 loss can be reversed by MMP7 knockdown (Figure 4.47). These results suggested that MMP7 is required for the increased migration and invasion observed upon PKP3 knockdown in HCT116 cells. The HCT116 derived PKP3 knockdown clones have been reported to grow to higher saturation densities in culture due to loss of contact inhibition but without change in cell proliferation [233] unlike in HaCaT cells where PKP3 loss leads to increased cell proliferation. Interestingly MMP7 over-expression has also been shown to increase growth of cells to higher saturation densities [447]. Thus to analyze if MMP7 down-regulation can reverse the phenotype of loss of contact inhibition, a growth curve analysis was performed for the shpkp3-2+vec and the MMP7+PKP3 double knockdown clones. It was demonstrated that MMP7 knockdown indeed decreased the phenotype of growth to high density in cell cultures (Figure 4.48) and thus MMP7 may regulate loss of contact inhibition in PKP3 knockdown clones.

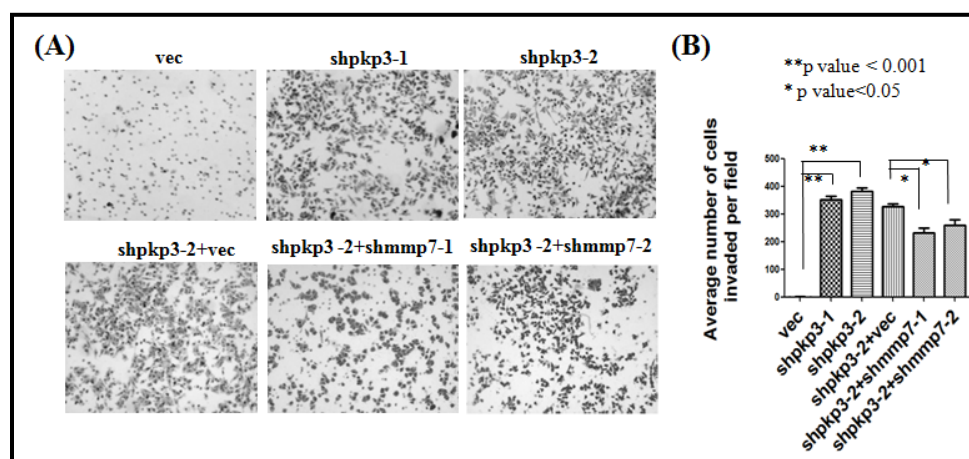


Figure 4.47. MMP7 loss leads to a decrease in cell invasion. Matrigel invasion assays were performed in Boyden's chambers for HCT116 derived vector control cells, PKP3 knockdown clones and the MMP7+PKP3 double knockdown clones. The number of cells observed in ten random fields of the membrane for each clone was determined as described in Materials and

Methods, representative images of for each clone are shown. The mean and standard deviation of three independent experiments are plotted. The p value was calculated using a student's t-test (* indicates a p value < 0.01). Note that loss of PKP3 leads to an increase in invasion as compared to the vector control and this phenotype is reversed in the double knockdown clones.

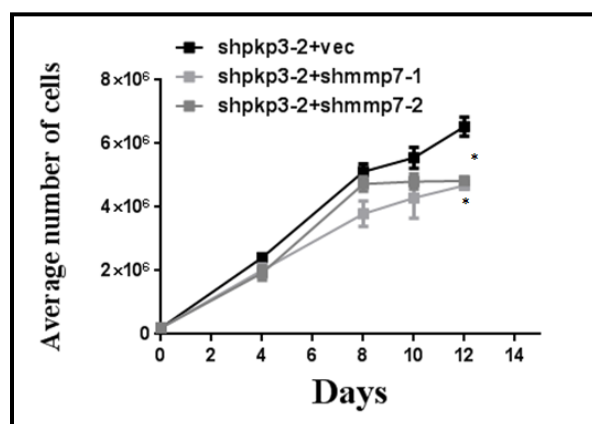


Figure 4.48. MMP7 loss leads to a decrease in cell growth to higher density. HCT116 derived vector control cells, PKP3 knockdown clones and the MMP7+PKP3 double knockdown clones were plated in 35 mm dishes. At various times, cells were counted in triplicate and the mean and standard deviation plotted on the Y-axis and the number of days on the X-axis (* p < 0.05 by students t-test)

One of the mechanisms by which MMP7 decreases contact inhibition is by cleavage of the transmembrane protein E-cadherin [447]. Since E-cadherin regulates contact inhibition by modulating the Hippo signaling pathway ([448] and reviewed in [449]), loss of E-cadherin at the cell border (due to cleavage by MMP7) causes decrease in contact inhibition and increased cell proliferation at higher densities [447]. To determine the expression of E cadherin upon MMP7 knockdown, Western blotting was performed using antibodies specific for E-cadherin and β actin (loading control). It was observed that E cadherin expression increased upon MMP7 loss in the

PKP3 knockdown clones [450]. Thus it was hypothesized that increased E-cadherin levels may increase contact-inhibition upon MMP7 knockdown and decrease cell proliferation in high density cultures. Further work is needed to validate this hypothesis.

To determine if loss of MMP7 can reverse the phenotype of anchorage independent growth, soft agar colony formation assays were performed for the HCT116 derived PKP3 knockdown clones, MMP7+PKP3 double knockdown clones (shpkp3-2+shmp7-1 and shpkp3-2+shmp7-2) and the corresponding vector control clones, vec and shpkp3-2+vec.

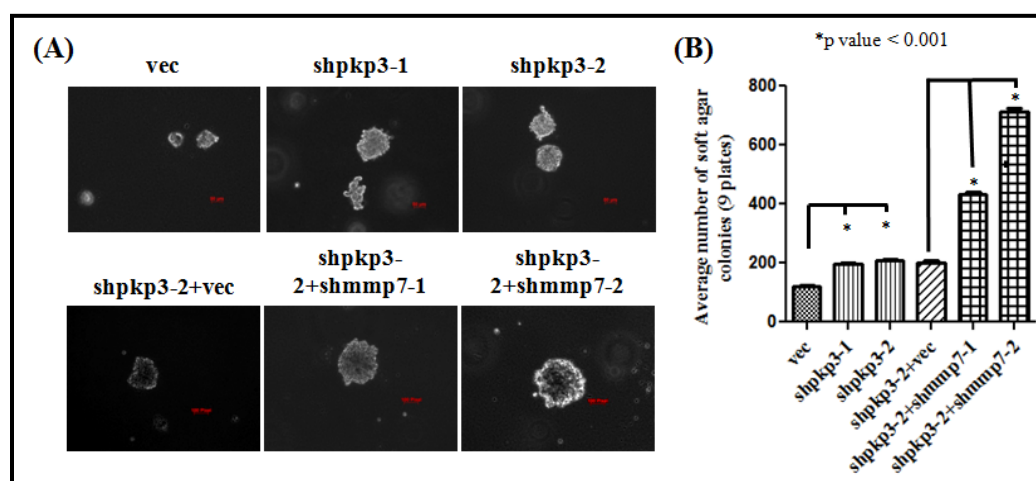


Figure 4.49. MMP7 loss leads to an increase in anchorage independent growth. Soft agar colony formation assay was performed with the HCT116 derived vector control and pkp3 knockdown clones, the shpkp3-2 derived MMP7+PKP3 double knockdown clones and the shpkp3-2 derived vector control clone. Representative DIC images were taken of the soft agar colonies (A). The number of soft agar colonies formed in three plates each of three independent experiments (total nine plates) was counted and the mean and standard error plotted. The p value was calculated using a student's t-test and was found to be <0.05 . Note that loss of PKP3 leads to an increase in anchorage independent growth as compared to the vector control and this phenotype is increased even more in the double knockdown clones.

As reported earlier, PKP3 loss causes increased anchorage independent growth but surprisingly MMP7+PKP3 double knockdown clones formed more colonies in soft-agar than the vector control clones (Figure 4.49). Since this result was in contrast to the results obtained in the migration and invasion assays, it was proposed that some pathway was being activated in MMP7 +PKP3 double knockdown clones which could specifically increase anchorage independent growth of cells.

To rule out the possibility of a crosstalk between MMP7 and LCN2 in regulating this increased anchorage independent growth, sqRT-PCRs and qRT-PCRs were performed for LCN2 in the MMP7+PKP3 double knockdown clones and for MMP7 in the LCN2+PKP3 double knockdown clones (Figure 4.50).

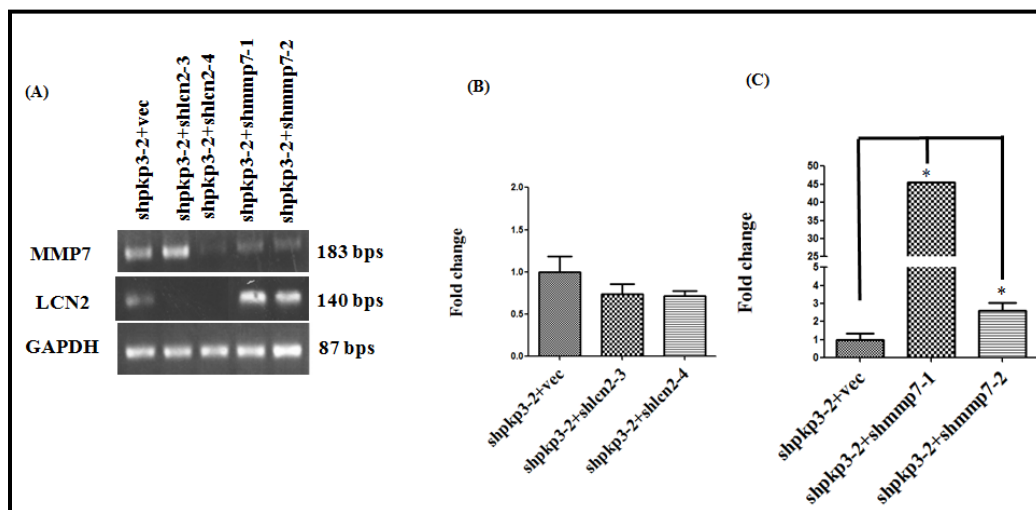


Figure 4.50. MMP7 loss leads to a huge increase in LCN2 levels but LCN2 loss does not alter MMP7 levels. (A) sqRT-PCRs were performed using oligonucleotides specific for MMP7, LCN2 and GAPDH, in the HCT116 derived PKP3 knockdown clone shpkp3-2, the LCN2+PKP3 double knockdown clones and the MMP7+PKP3 double knockdown clones (B) qRT-PCR were performed using oligonucleotides specific for MMP7 and GAPDH in LCN2+PKP3 double knockdown clones and the vector control clone shpkp3-2+vec. (C). qRT-PCR were performed

using oligonucleotides specific for LCN2 and GAPDH in LCN2+PKP3 double knockdown clones and the vector control clone shpkp3-2+vec. Expression of GAPDH has been used for normalization. The Y-axis in the qRT-PCR panels reflects the fold change in transcription, which is calculated as described in the Materials and Methods. The X-axis indicates the clone name. The standard errors are plotted and student's t test was performed (* indicates a p value<0.01). The PCR product size in sqRT-PCR panels has been indicated in base pairs. Note that in MMP7+PKP3 double knockdown clones, expression of LCN2 is higher than the PKP3 knockdown clone shpkp3-2.

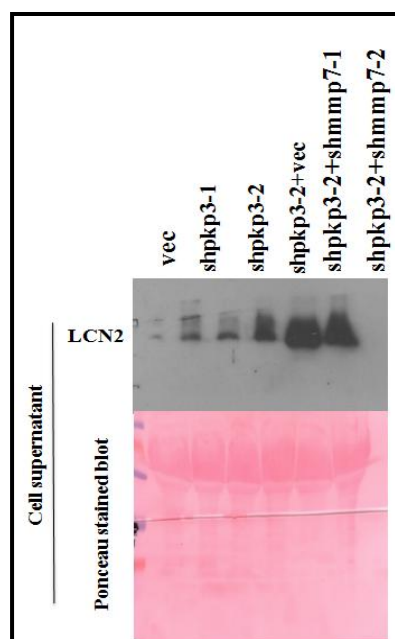


Figure 4.51. MMP7 loss leads to a huge increase in LCN2 levels even at the protein level. 100 μ g of acetone precipitated cell supernatants of the HCT116 derived vector control (vec), PKP3 knockdown clones shpkp3-1 and shpkp3-2, shpkp3-2+vec) and the MMP7+PKP3 double knockdown clones were resolved on 12% SDS PAGE gels followed by Western blotting with antibodies specific to LCN2. Note that LCN2 levels are higher in supernatants prepared from the PKP3 knockdown cells as compared to the vector controls and the levels are higher in

the MMP7+PKP3 double knockdown clones. The same blot was stained with Ponceau stain to demonstrate equal loading of proteins (lower panels).

It was demonstrated that although LCN2 knockdown did not alter MMP7 expression levels, MMP7 knockdown increased LCN2 levels to even higher levels compared to that of shpkp3-2+vec clone. Similarly, the protein levels of LCN2 were also found to be increased (Figure 4.51).

Thus it was hypothesized that the increased LCN2 levels may regulate the increased anchorage independent growth in MMP7+PKP3 double knockdown clones.

To determine whether MMP7 loss can cause any alteration in tumor formation *in vivo*, the shpkp3-2+vec and the double knockdown clones were injected subcutaneously in nude mice as previously described [232, 233]. The mice were observed for 5 weeks and tumor size measured at regular intervals. Five of the six mice injected with the vector control developed large tumors. In contrast, only two out of six mice injected with shpkp3-2+shMMP7-1 and one of the six mice injected with shpkp3-2+shMMP7-2 were able to develop tumors at the site of injection and the tumors formed were much smaller in size than those formed in mice injected with the vector control clone (shpkp3-2+vec) (Figure 4.52). The average volume of the tumor formed in the mice was analyzed using the formula mentioned in Materials and Methods. Thus MMP7 up-regulation is needed for neoplastic progression upon PKP3 loss [451].

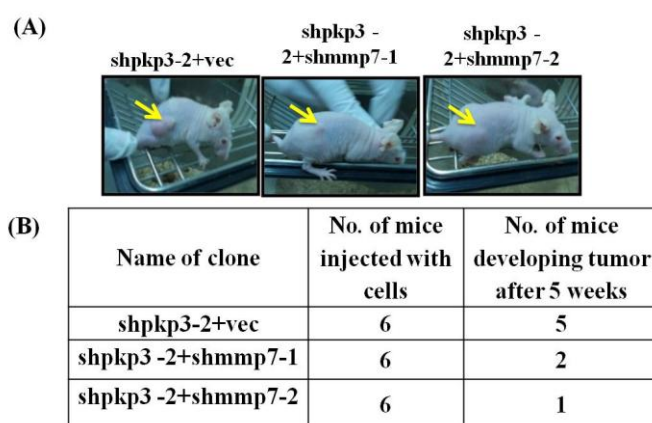


Figure 4.52. Tumor formation is inhibited in the PKP3 knockdown cells upon MMP7 knockdown. 1×10^6 cells of the shpkp3-2 derived vector control or MMP7+PKP3 double knockdown clones were injected sub-cutaneously into nude mice and allowed to develop tumors. Representative images of mice have been shown (A). The table shows the number of mice

injected with the respective clones and the number of mice among them which were able to develop tumors (B).

4.9. MMP7 up-regulation upon PKP3 loss is regulated by PRL-3 activity

Previous data from our laboratory has demonstrated that an elevation in the levels of Keratin 8 is observed in the HCT116 derived PKP3 knockdown clones and that this increase is due to an increase in the levels of the phosphatase of regenerating liver 3 (PRL-3) and inhibition of PRL-3 activity using a chemical inhibitor resulted in a decrease in cell migration [232]. An inhibition of PRL-3 activity using a chemical inhibitor of PRL-3 resulted in a decrease in cell migration in the HCT116 derived PKP3 knockdown clones [232]. A previous report also demonstrated that PRL-3 activity regulates MMP7 expression via the PI3K/AKT and ERK signaling pathway in the colon cancer derived cell line DLD1 [452]. Therefore, we hypothesized that the increase in MMP7 levels observed upon PKP3 knockdown was due to the increase in PRL-3 levels. To test this hypothesis the HCT116 derived vector control and PKP3 knockdown clones were treated with 5 or 10 μ M of the PRL-3 inhibitor for 24 hours. A qRT-PCR analysis demonstrated that the levels of MMP7 mRNA in the PKP3 knockdown clones were decreased upon treatment with the PRL-3 inhibitor in a concentration dependent manner (Figure 4.53(A)). The mRNA levels of Lipocalin2 (LCN2) which increases upon PKP3 knockdown in HCT116 cells did not decrease upon treatment with the PRL-3 inhibitor (Figure 4.53(B)) suggesting that PRL-3 activity does not regulate the expression of LCN2 in these cells.

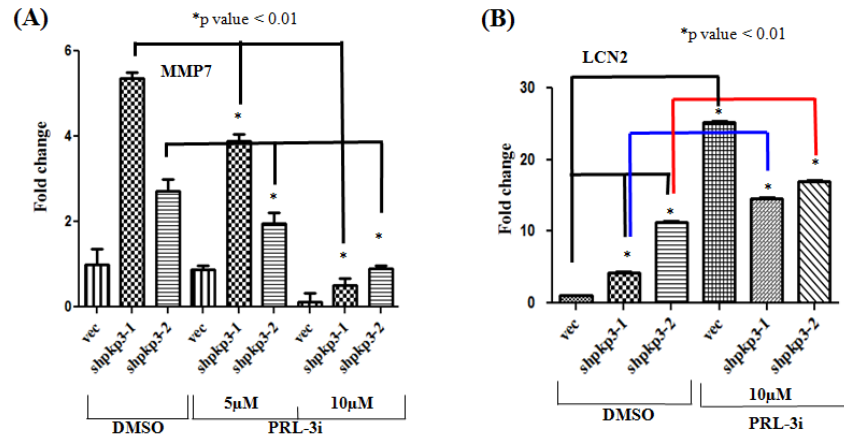


Figure 4.53. MMP7 but not LCN2 expression decreases upon inhibition of PRL-3 activity.

The HCT116 derived PKP3 knockdown clones (shpkp3-1 and shpkp3-2) or the vector control (vec) were treated with either the vehicle control (DMSO) or 5 or 10 μ M PRL-3 inhibitor-1 (PRL-3i) (as indicated) for 24 hours. qRT-PCR was performed using oligonucleotides specific for MMP7 (A) and LCN2 (B) in the treated cells. All expression was normalized to the levels of GAPDH. The fold change is graphed on the Y-axis and the clone name is on the X-axis. The standard errors are plotted and student's t test was performed. Note that MMP7 levels are lowered upon treatment with PRL-3 inhibitor. Note that MMP7 levels decrease while LCN2 levels increase upon PRL-3 inhibition.

To determine if MMP7 protein levels can also be down-regulated upon PRL-3 inhibition, Western blot analysis using antibodies specific to MMP7 demonstrated that the levels of MMP7 protein were decreased upon treatment with the inhibitor at 24 hours in HCT116 cells (Figure 4.54 (A)) as expected. In HaCaT cells, PKP3 knockdown clones showed higher LCN2 expression than the vector control but PRL-3 inhibition did not decrease MMP7 expression in these cells (Figure 4.54 (B)).

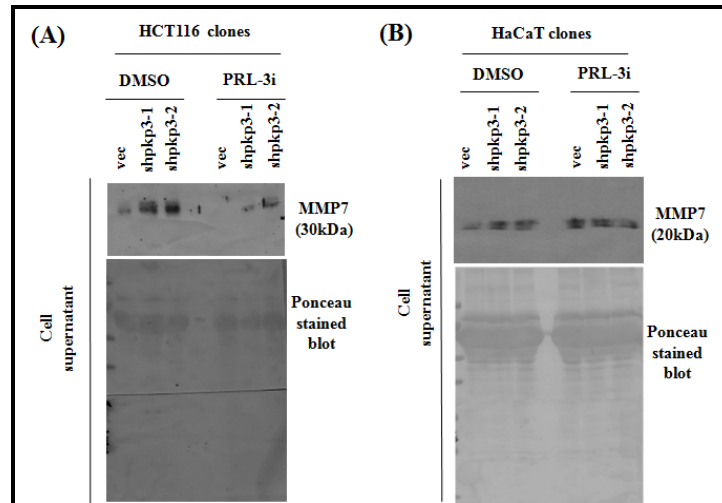


Figure 4.54. MMP7 protein expression decreases upon PRL-3 inhibition only in HCT116 cells but not in HaCaT cells. The HCT116 derived (A) or the HaCaT derived (B) PKP3 knockdown clones (shpkp3-1 and shpkp3-2) and their respective vector control (vec) clones were treated with either DMSO or 10 μ M PRL-3 inhibitor-1(PRL-3i) for 24 hours or 48 hours. The cell supernatants were collected and a100 μ g of acetone precipitated protein was resolved on 12% SDS PAGE gels followed by Western blotting with antibodies to MMP7. The same blot was stained with Ponceau stain to indicate equal loading. Note that in both HCT116 and HaCaT cells, PKP3 loss causes increase in MMP7 protein levels but MMP7 levels decrease upon PRL-3 inhibition only in HCT116 cells but not in HaCaT cells.

To determine whether PRL-3 inhibitor treatment (which inhibits the activity of PRL-3) resulted in a change in PRL-3 protein levels, a Western blot analysis was performed. It was observed that PRL-3 levels were higher in PKP3 knockdown clones as reported earlier [232], but no change in the levels of PRL-3 was observed upon treatment with the PRL-3 inhibitor (Figure 4.55). These results suggested that the increase in PRL-3 levels observed upon PKP3 loss is required for the increase in MMP7 mRNA and protein levels observed in HCT116 cells [451].

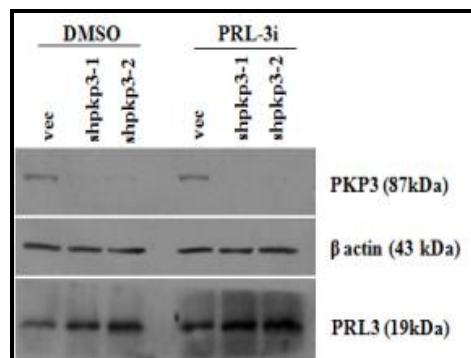


Figure 4.55. PRL-3 protein levels do not change upon inhibition of PRL-3 activity. The whole cell lysates of HCT116 derived vector control and PKP3 knockdown clones treated or untreated with 10 μ M PRL-3i for 24 hours were resolved on 12% poly-acrylamide gel. This was followed by Western blotting with antibodies to PKP3, β actin and PRL-3. The molecular weights of these proteins are indicated in brackets.

Ectopic PRL-3 over-expression is known to decrease expression of Phosphatase and tensin homologue deleted on chromosome 10 (PTEN), an inhibitor of Phosphoinositide-3- kinase (PI3K)/Protein kinase B (AKT) pathway by post-transcriptional modifications which in turn cause increased activation of the PI3K/AKT pathway [453]. This involves phosphorylation of AKT at position Serine 473 and inhibition of AKT activity was shown to decrease MMP7 expression [452]. Thus, to determine phosphorylation status of AKT, Western blots were performed using cell lysates from HCT116 derived PKP3 knockdown clones and the vector control clone. It was observed that AKT phosphorylation at Serine 473 residue was increased in the PKP3 knockdown clones [441]. Thus, upon PKP3 loss, PRL-3 protein levels increase, which may regulate AKT phosphorylation leading to increase in expression of MMP7. More experiments are required to confirm if PRL-3 regulates MMP7 expression via the PI3K/AKT signaling or by some other mechanism.

4.10. PKP3 loss in HaCaT cells lead to activation of the EGFR/ ERK1/2 signaling pathway.

PKP3 loss in HaCaT cells has been demonstrated to cause loss of cell to cell adhesion, increased cell proliferation, cell invasion, migration, anchorage independent growth *in vitro* [233] and increased tumor formation and metastasis *in vivo* [258]. The mechanism regulating these phenotypes upon PKP3 loss is not known. Probably LCN2 or MMP7 may regulate neoplastic progression upon PKP3 loss because both LCN2 and MMP7 expression levels have been found to be up-regulated in the PKP3 knockdown clones. Expression of many inflammation associated genes has also been found to be up-regulated in the HaCaT derived PKP3 knockdown clones, but the signaling pathways that can increase the expression of LCN2, MMP7 or the inflammatory associated genes upon PKP3 loss in HaCaT cells are not known. Since PKP3 loss in HCT116 cells leads to activation of the p38MAPK pathway and not the ERK1/2 pathway, the status of the phosphorylated and total levels of p38MAPK and ERK1/2 in HaCaT derived vector control and PKP3 knockdown clones were analyzed by performing Western blotting. It was observed that ERK1/2 phosphorylation increased upon PKP3 loss in HaCaT cells while p38MAPK phosphorylation decreases. The total levels of p38MAPK and ERK1/2 remained constant (Figure 4.56). To determine if PKP3 loss alters the phosphorylation status of Protein kinase C (PKC) α/β , a kinase involved in desmosome assembly [242], Western blotting was performed in HCT116 and HaCaT derived PKP3 knockdown clones and their respective vector control clones using antibodies specific to phospho-PKC α/β , total PKC α and β actin (loading control) . In HaCaT cells, but not in HCT116 cells, PKP3 loss was shown to increase phosphorylation of PKC α/β as well as increase the total levels of PKC α (Figure 4.56). Thus differential cell type specific signaling pathways are activated upon PKP3 loss in HaCaT and HCT116 cells.

Since ERK1/2 phosphorylation was increased in the HaCaT derived PKP3 knockdown clones, the phosphorylation status of the upstream kinases of ERK1/2 signaling pathway were analyzed. Western blotting for phospho-MEK1/2 and phospho-EGFR indicated that MEK1/2 phosphorylation at Serine 217/Serine 221 as well as phosphorylation of EGFR at two different sites Tyrosine 845 and Tyr 1068 was higher in HaCaT derived PKP3 knockdown clones as compared to the vector control clone (Figure 4.57(A)). Since EGFR, MEK1/2 and ERK1/2 are components of the Epidermal growth factor receptor (EGFR) signaling pathway, thus activation of these proteins upon PKP3 loss indicated that PKP3 loss in HaCaT cells lead to activation of the EGFR signaling pathway (Figure 4.57 (B)). One of the downstream effectors of ERK1/2 in the EGFR pathway is ELK1. Since ELK1 activation and expression has been shown to be increased upon PKP3 loss in HCT116 cells, it was important to determine if PKP3 loss can alter ELK1 phosphorylation even in the HaCaT cells. Western blotting using a specific antibody against phospho-ELK1 (Ser 383) and β actin demonstrated that PKP3 loss in HaCaT cells also leads to increased phosphorylation and activation of ELK1 (Figure 4.56). Thus, although two different signaling pathways are activated upon PKP3 loss in HaCaT and HCT116 cells, these pathways converge at the common effector ELK1 which in turn increases transcription of the LCN2 gene.

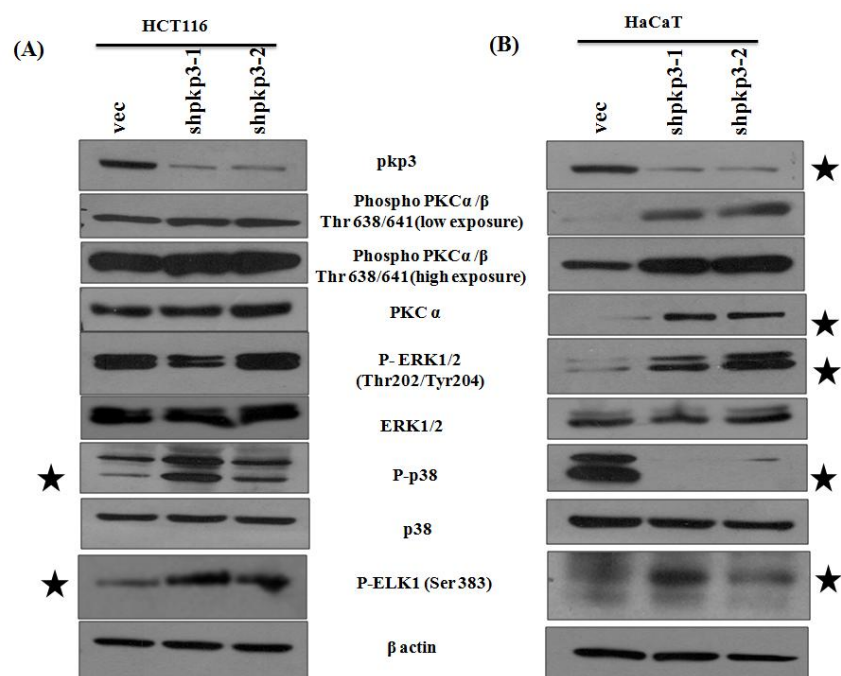


Figure 4.56. The ERK1/2 pathway and PKC α/β pathways are activated upon PKP3 loss in HaCaT cells unlike HCT116 cells. 75 μ g of a whole cell extract (WCE) from HCT116 derived and HaCaT derived PKP3 knockdown clones and their respective vector control clones was resolved on 12% SDS PAGE gels followed by Western blotting with antibodies specific to PKP3, phospho- PKC α/β (Threonine 638/ Threonine 641), total PKC α , phospho-ERK1/2 (Threonine 202/ Tyrosine 204), phospho p38MAPK (Threonine180/ Tyrosine 182), total p38MAPK, phospho ELK1 (Serine 383) and β actin. Protein levels of β actin have been used as the loading control. Note that ERK1/2 and PKC α/β phosphorylation levels increase upon PKP3 loss in HaCaT cells but not in HCT116 cells. Total PKC α levels are also higher in HaCaT derived PKP3 knockdown clones as compared to the vector control clone. Unlike HCT116, p38MAPK phosphorylation was found to decrease upon PKP3 loss in HaCaT cells. Western blotting using a specific antibody against phospho-ELK1 (Ser 383) and β actin demonstrated that PKP3 loss in HaCaT cells also leads to increased phosphorylation and activation of ELK1.

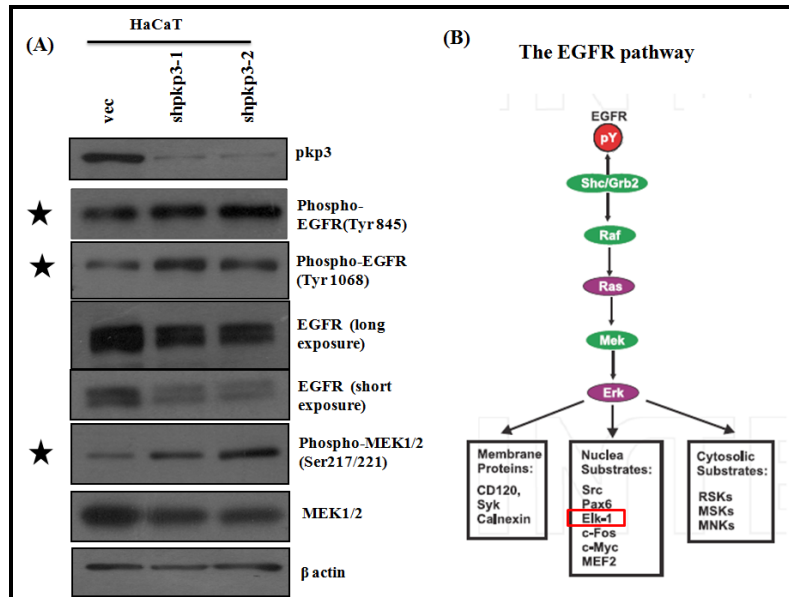


Figure 4.57. The EGFR/MEK/ERK pathway is activated upon PKP3 loss in HaCaT cells which may lead to activation of the downstream targets ERK1/2 and ELK1. (A) 75 μ g of a whole cell extract (WCE) from HaCaT derived PKP3 knockdown clones and their respective vector control clones was resolved on 12% SDS PAGE gels followed by Western blotting with antibodies specific to PKP3, phospho-EGFR (Tyrosine 845), phospho-EGFR (Tyrosine 1068), total EGFR, phospho-MEK1/2 (Serine 217/ Serine 221), total MEK1/2 and β actin. Protein levels of β actin have been used as the loading control. Note that MEK1/2 and EGFR phosphorylation levels increase upon PKP3 loss in HaCaT cells. Total EGFR levels are found to decrease upon PKP3 loss in HaCaT cells. (B) A schematic representation of the EGFR pathway indicating that EGFR activation leads to activation of the downstream Raf/Ras/MEK/ERK/ELK1 pathway. Note PKP3 loss in HaCaT cells leads to activation of EGFR, MEK1/2, ERK1/2 and ELK1. Since ELK1 regulates LCN2 expression in HCT116 cells upon PKP3 loss, it may also regulate LCN2 up-regulation in HaCaT cells upon PKP3 loss.

4.11. PKP3 loss leads to increased radio-resistance in HaCaT, HCT116 and FBM cells.

Earlier studies from our laboratory have demonstrated that PKP3 knockdown clones derived from HaCaT, HCT116 and FBM cell lines show increased radio-resistance as compared to the vector control clones [257, 258], but the clonogenic survival assays performed earlier were not quantitative but rather qualitative because the actual number of colonies formed after irradiation was never counted. Thus clonogenic survival assay [360] along with quantitative SPSS software based survival analysis was performed to determine if PKP3 loss in HaCaT, HCT116 and FBM cells led to increased radio-resistance to γ irradiation. Herein, HaCaT, HCT116 and FBM derived PKP3 knockdown clones and their respective vector control clones were subjected to 0, 2, 4 and 8 Gy of γ irradiation.

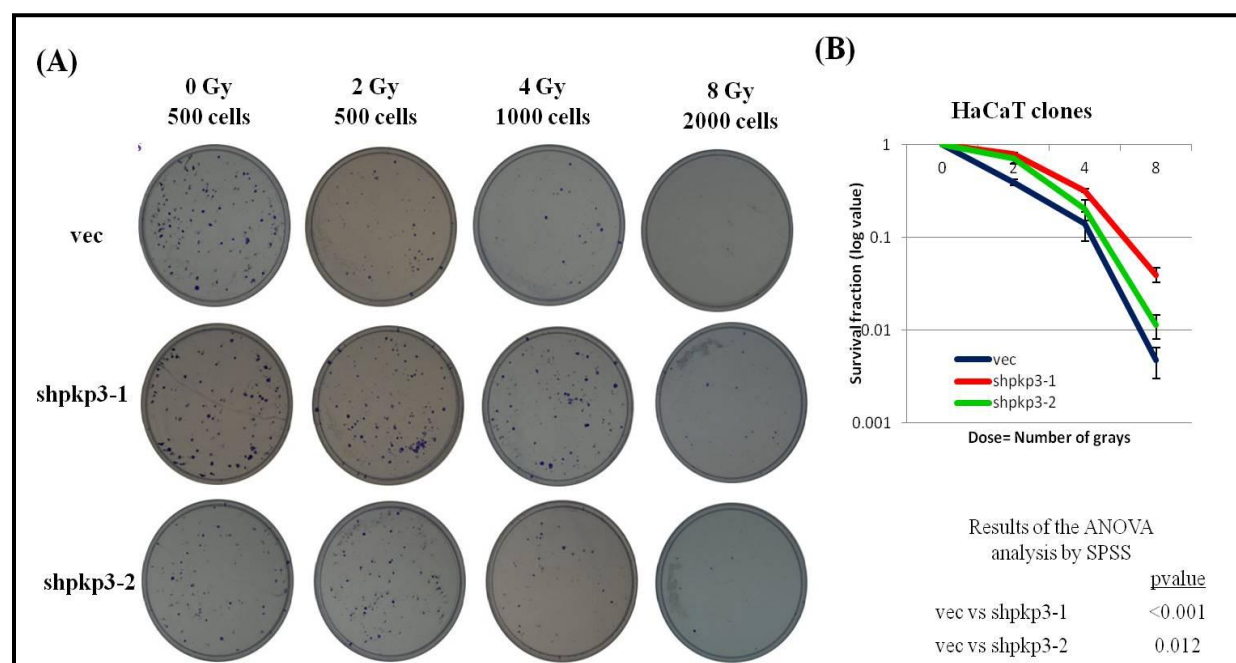


Figure 4.58. PKP3 loss causes radio-resistance in HaCaT cell line. The HaCaT derived vector control cells and PKP3 knockdown clones were subjected to 0 Gy, 2 Gy, 4 Gy and 8 Gy of gamma irradiation. Post-irradiation cells were trypsinized and 500, 1000 or 2000 cells of un-

irradiated and irradiated cells (as indicated in the figure) were plated on 60 mm plates and allowed to grow to form visible colonies for 21 days. Colonies formed were fixed with 4% paraformaldehyde and stained with crystal violet. Representative images of the plates containing the colonies have been shown (A). The survival fractions for vector control and PKP3 knockdown clones were calculated using the SPSS software. The survival fraction obtained was plotted against the corresponding radiation dose (B). The p value was found to <0.05 in all cases.

After 8 hours incubation at 37°C, 5% CO₂ conditions, the cells were trypsinized and counted. For cells subjected to 0, 2, 4 and 8 Gy of irradiation, 500, 500, 1000 and 2000 cells (for HaCaT and FBM derived clones) respectively and 2500, 2500, 5000 and 10,000 cells (for HCT116 derived clones) respectively were seeded into 60mm plates. In this assay, only those cells which survive the radiation exposure and retain the ability to proliferate, can form colonies. This is why the assay is called clonogenic survival assay. Colonies were allowed to be formed for 21 days. Thereafter, these colonies were fixed using 4% paraformaldehyde and stained with crystal violet.

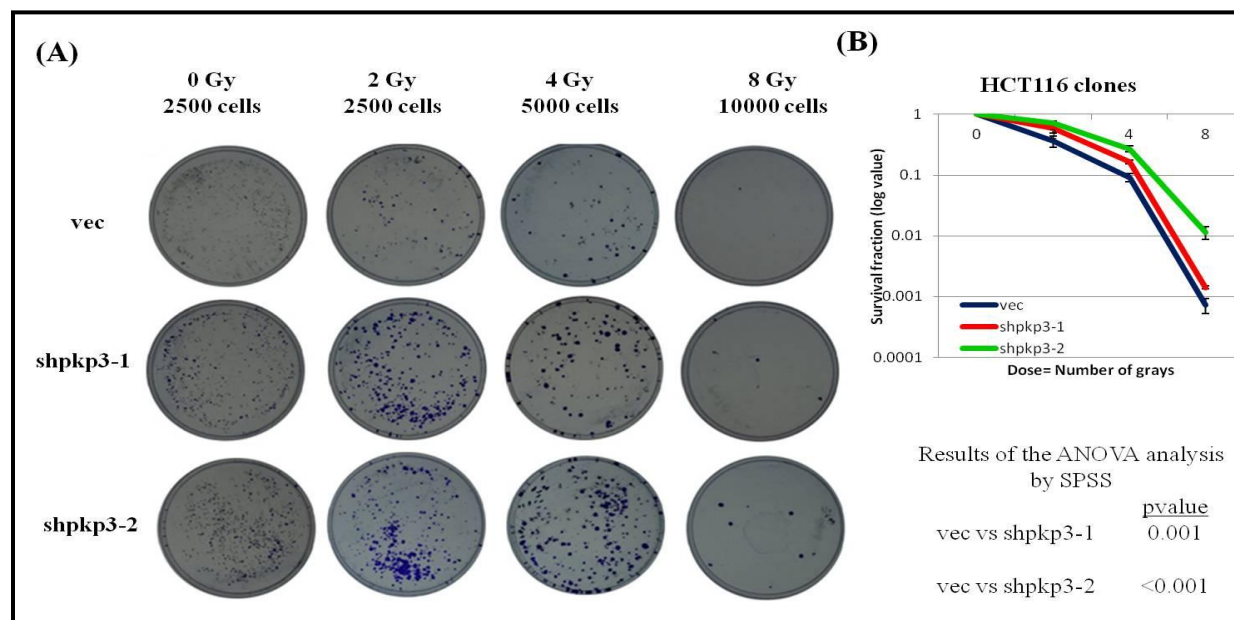


Figure 4.59. PKP3 loss causes radio-resistance in HCT116 cell line. The HCT116 derived vector control cells and PKP3 knockdown clones were subjected to 0 Gy, 2 Gy, 4 Gy and 8 Gy of gamma irradiation. Post-irradiation cells were trypsinized and 2500, 5000 or 10000 cells of un-irradiated and irradiated cells (as indicated in the figure) were plated on 60 mm plates and allowed to grow to form visible colonies for 21 days. Colonies formed were fixed with 4% paraformaldehyde and stained with crystal violet. Representative images of the plates containing the colonies have been shown (A). The survival fractions for vector control and PKP3 knockdown clones were calculated using the SPSS software. The survival fraction obtained was plotted against the corresponding radiation dose (B). The p value was found to <0.05 in all cases.

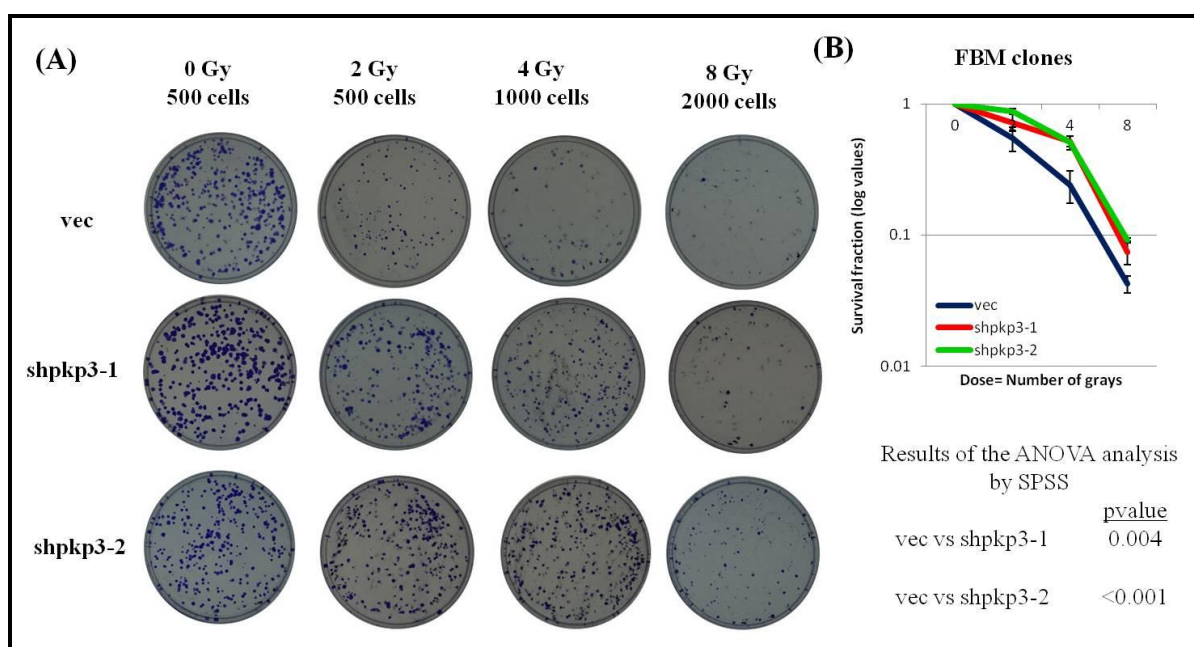


Figure 4.60. PKP3 loss causes radio-resistance in FBM cell line. The FBM derived vector control cells and PKP3 knockdown clones were subjected to 0 Gy, 2 Gy, 4 Gy and 8 Gy of gamma irradiation. Post-irradiation cells were trypsinized and 500, 1000 or 2000 cells of un-irradiated and irradiated cells (as indicated in the figure) were plated on 60 mm plates and allowed to grow to form visible colonies for 21 days. Colonies formed were fixed with 4% para-

formaldehyde and stained with crystal violet. Representative images of the plates containing the colonies have been shown (A). The survival fractions for vector control and PKP3 knockdown clones were calculated using the SPSS software. The survival fraction obtained was plotted against the corresponding radiation dose (B). The p value was found to <0.05 in all cases.

Representative images of the plates with colonies for the HaCaT, HCT116 and FBM cells are shown in Figure 4.58 (A), Figure 4.59 (A) and Figure 4.60 (A) respectively. The number of colonies formed were counted and processed for survival analysis using the SPSS software (Figure 4.58 (B), Figure 4.59 (B) and Figure 4.60 (B) respectively). The p value was obtained by the statistical ANOVA test provided by the SPSS software [360]. It was demonstrated that PKP3 knockdown clones were more radio-resistant than the corresponding control cells in all the three cell lines tested.

4.12. LCN2 is required for increased radio-resistance in HCT116 cells, upon PKP3 loss.

PKP3 loss has been demonstrated to increased expression of LCN2 and MMP7 in all three cell types under study. Since both LCN2 [377] and MMP7 [404] are known to increase intrinsic radio-resistance in cells, it was hypothesized that either LCN2 or MMP7 or both may regulate radio-resistance observed upon PKP3 loss. To analyze the role of LCN2 in regulating radio-resistance, two shpkp3-2 derived LCN2 knockdown clones (shpkp3-2+lcn2-3 and shpkp3-2+shlcn2-4) and the vector control clone shpkp3-2+vec were treated with 0, 2, 4 and 8 Gy of γ -irradiation. After 8 hours incubation at 37°C, 5% CO₂ conditions, the cells were trypsinized, counted and 5000, 5000, 10000 and 20000 cells were seeded into 60mm plates for cells subjected to 0, 2, 4 and 8 Gy of irradiation respectively. Colonies were allowed to be formed for 21 days and then these colonies were fixed using 4% paraformaldehyde and stained with crystal

violet. Representative images of the plates with colonies are shown in Figure 4.61 (A). The number of colonies formed were counted and processed for survival analysis using the SPSS software (Figure 4.61 (B)). The *p* value was obtained by the statistical ANOVA test provided by the SPSS software [360]. It was demonstrated that LCN2+PKP3 double knockdown clones were more radiosensitive as compared to the vector control clone (shpkp3-2+vec). Thus LCN2 was found to be important for regulating radio-resistance observed in PKP3 knockdown clones.

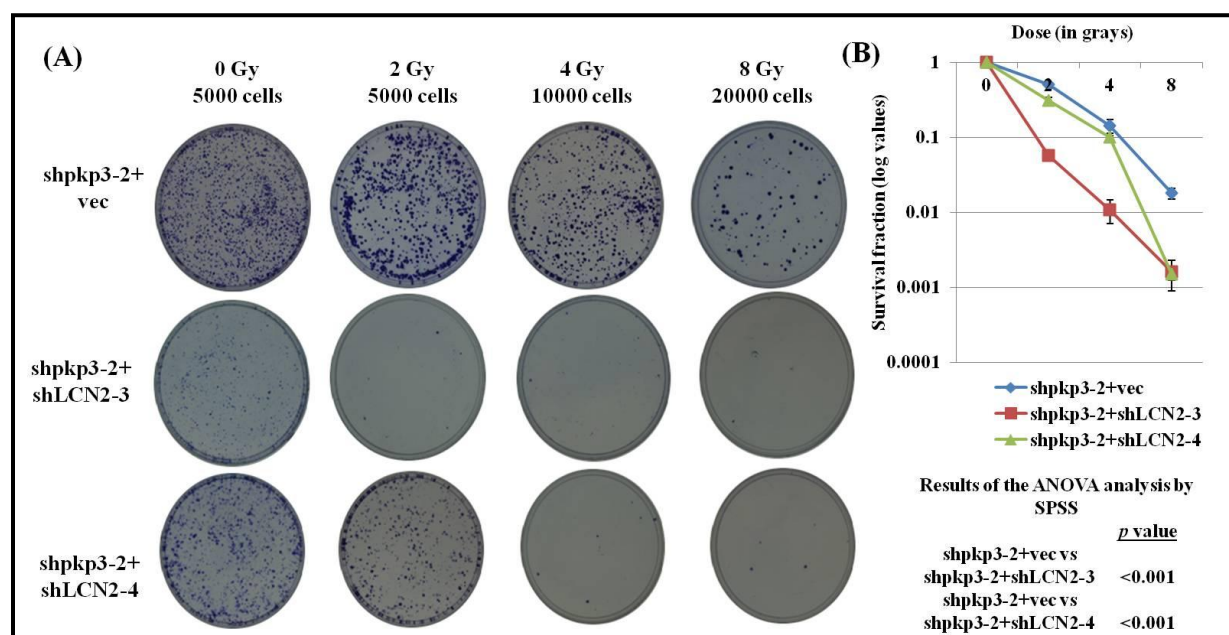


Figure 4.61. The shpkp3-2 derived LCN2 knockdown clones were more radio-sensitive than the vector control clones. Two shpkp3-2 derived LCN2 knockdown clones and the corresponding vector control clone were subjected to 0 Gy, 2 Gy, 4 Gy and 8 Gy of gamma irradiation. Post-irradiation cells were trypsinized and 5000, 10000 or 20000 cells of un-irradiated and irradiated cells (as indicated in the figure) were plated on 60 mm plates and allowed to grow to form visible colonies for 21 days. Colonies formed were fixed with 4% paraformaldehyde and stained with crystal violet. Representative images of the plates containing the colonies have been shown (A). The survival fractions for vector control and PKP3 knockdown

clones were calculated using the SPSS software. The survival fraction obtained was plotted against the corresponding radiation dose (B). The p value was found to <0.05 in all cases.

To determine if MMP7 is important in regulating radio-resistance upon PKP3 loss, two MMP7+PKP3 double knockdown clones (shpkp3-2+shmp7-1 and shpkp3-2+shmp7-2) and its vector control clone (shpkp3-2+vec) were treated with 0, 2, 4 and 8 Gy of γ -irradiation and after 8 hours the cells were trypsinized counted and 5000, 5000, 10000 and 20000 cells were seeded into 60mm plates for cells subjected to 0, 2, 4 and 8 Gy of

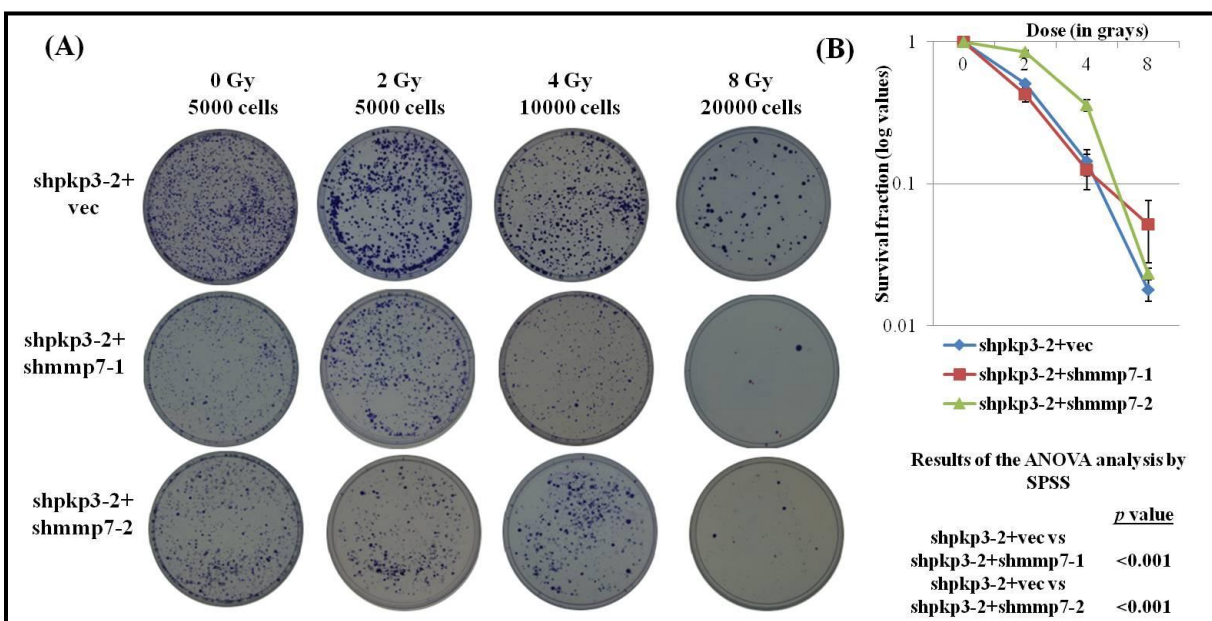


Figure 4.62. The shpkp3-2 derived MMP7 knockdown clones were more radio-sensitive than the vector control clones. Two shpkp3-2 derived MMP7 knockdown clones and the corresponding vector control clone were subjected to 0 Gy, 2 Gy, 4 Gy and 8 Gy of gamma irradiation. Post-irradiation cells were trypsinized and 5000, 10000 or 20000 cells of un-irradiated and irradiated cells (as indicated in the figure) were plated on 60 mm plates and allowed to grow to form visible colonies for 21 days. Colonies formed were fixed with 4% paraformaldehyde and stained with crystal violet. Representative images of the plates containing the

colonies have been shown (A). The survival fractions for vector control and PKP3 knockdown clones were calculated using the SPSS software. The survival fraction obtained was plotted against the corresponding radiation dose (B). The p value was found to <0.05 in all cases.

γ irradiation respectively. After 21 days incubation (to allow formation of colonies from surviving cells), the colonies were fixed using 4% paraformaldehyde and stained with crystal violet. The representative images of the plates with colonies are shown in Figure 4.62 (A). The number of colonies formed was counted and survival analysis was performed using the SPSS software Figure 4.62 (B). ANOVA analysis was used to analyze the p value for the experiments. It was demonstrated that MMP7+PKP3 knockdown clones showed no alteration in radio-resistance when compared with the vector control clone.

Thus the up-regulation of LCN2 expression is one of the mechanisms that determine radio-resistance observed upon PKP3 loss in HCT116 cells. Since p38 β has been demonstrated to regulate LCN2 up-regulation, and is also known to it remains to be seen if activation of p38 β upon PKP3 loss can regulate radio-resistance in HCT116 cells.

5. DISCUSSION

The results presented in this thesis suggest that multiple pathways determine tumor progression and metastasis upon PKP3 loss in HCT116 cells and possibly in other cell types. PKP3 loss in HCT116 cells leads to an increase in LCN2 expression due to activation of the p38MAPK pathway and an increase in MMP7 levels due to an increase in the levels of the protein phosphatase PRL-3. In addition, the work in this thesis demonstrates that loss of PKP3 leads to the acquisition of an inflammation associated signature in two cell lines, HaCaT and FBM, but not in HCT116 cells. Finally, loss of PKP3 leads to the acquisition of radio-resistance and this might be dependent on the increase in LCN2 levels observed upon PKP3 loss. Therefore, PKP3 loss leads to the activation of multiple signaling pathways that might regulate neoplastic progression and metastasis.

5.1. LCN2 is necessary for neoplastic progression upon PKP3 loss

Studies by Barresi et.al. [454, 455], Sun et. al. [373] and McLean et.al [374] demonstrated that increased levels of LCN2 correlated with tumor stage, tumor recurrence and decreased patient survival. Higher plasma levels of the secreted LCN2 was also detected in colorectal cancer patients and it correlated with increased tumor volume, higher metastasis, shorter disease free survival and higher recurrence [456]. Consistent with these reports, results from this thesis demonstrate that increase in LCN2 expression upon PKP3 loss in HCT116 cells is necessary for in vitro cell migration, invasion, anchorage independent growth and in vivo tumor formation. Since LCN2 knockdown led to a drastic decrease in tumor incidence, the role of LCN2 in metastasis could not be confirmed.

In some cancers like breast cancer [457] and bladder cancer [458], the effect of LCN2 on tumor formation depends on its ability to form a complex with MMP9 and prevent its degradation by other proteases thus increasing protein stability and activity of MMP9 [459]. Unlike breast

cancers or bladder cancers, LCN2 serves as an independent prognostic marker for colon cancers as its effect on neoplastic progression was shown to be independent of MMP9 activity [455, 460]. Consistent with these reports, results presented in this thesis demonstrate that the effect of LCN2 in increasing neoplastic progression upon PKP3 loss in HCT116 cells is independent of MMP9 levels or activity because HCT116 cells did not express MMP9 even at the mRNA level.

To determine if any correlation exists between LCN2 and PKP3 levels across colon cancers at the transcript level, the data sets in the Oncomine database (www.oncomine.org) were analyzed. When PKP3 levels in normal colon samples were compared with that in colon cancer, the levels were found to be unchanged, while LCN2 levels were higher in colon cancer samples. None of the databases present had actually validated the PKP3 levels using sq RT-PCR or qRT-PCR. It was also observed that a thorough immuno-histochemical analysis of PKP3 and LCN2 levels in a large dataset of colorectal cancer patients has never been performed. This type of analysis will be performed to determine if any correlation exists between PKP3 and LCN2 levels in colon cancers.

LCN2 over-expression has been associated with skin cancer progression [375, 461] but no studies have been performed to determine the role of LCN2 in skin cancers. The results presented in this thesis demonstrate that LCN2 was up-regulated upon PKP3 loss in the HaCaT cells both at the mRNA and protein levels. More studies are required to determine if similar to HCT116 cells, LCN2 is required for neoplastic progression in HaCaT derived PKP3 knockdown clones.

5.2. p38 β MAPK is required to increase LCN2 expression upon PKP3 loss in HCT116 cells while the EGFR/MEK/ERK pathway may increase LCN2 expression in HaCaT cells.

A study by Yoo do et.al., [418] demonstrated that activation of p38MAPK and ERK1/2 pathways can increase LCN2 expression in intestinal epithelial cells. Consistent with this report, the results from this thesis demonstrate that upon PKP3 loss in HCT116 cells, p38MAPK gets hyper activated and localizes preferentially to the nucleus while ERK1/2 activation was not altered. Since inhibition of p38MAPK activity was able to decrease LCN2 expression in PKP3 knockdown clones, it was concluded that the increased p38MAPK activation upon PKP3 loss in HCT116 cells leads to increased LCN2 expression. Conversely, in the HaCaT derived PKP3 knockdown clones, the phosphorylation of ERK1/2 were increased, while phosphorylation of p38MAPK was lower when compared to the vector control clones. It was also observed that upon PKP3 loss in HaCaT cells, phosphorylation of the upstream activators of ERK1/2 like EGFR and MEK1/2 was also increased. Thus it can be concluded that PKP3 loss in the HaCaT cell line causes activation of the EGFR pathway which leads to increased ERK1/2 phosphorylation. Since activation of the EGFR pathway has been known to increase LCN2 expression in wounded human skin [462], future experiments need to be performed to determine if inhibition of EGFR activity or ERK1/2 activity can decrease LCN2 expression in HaCaT derived PKP3 knockdown clones. For these purpose specific inhibitors that inhibit EGFR activity (Gefitinib) or ERK1/2 phosphorylation (PD98059) can be used.

Although, p38MAPK activation has been reported to increase LCN2 expression [417, 418], none of these studies have mentioned any isoform specificity of p38MAPK. Results obtained in this thesis demonstrate that while knockdown of p38 α MAPK in the HCT116 derived PKP3 knockdown clone, shpkp3-2, increased LCN2 expression; p38 β MAPK knockdown decreased

LCN2 expression. Thus, p38 β MAPK was required for increase in LCN2 expression upon PKP3 loss in HCT116 cells while p38 α MAPK inhibits LCN2 expression. Thus different p38MAPK isoforms play opposing roles in regulating LCN2 expression and may be one of the mechanisms by which p38MAPKs regulate colon cancer progression. Interestingly p38 α plays a tumor suppressive role in colon cancers [463] and knocking down p38 α increases tumor formation in aoxymethane (AOM)-DSS induced inflammation associated colon cancers [464]. The specific role of p38 β in colon cancers has not yet been studied.

5.3. PKP3 binds to p38 β MAPK and may inhibit activation of p38 β MAPK.

Beenstock et.al.[443] demonstrated that p38 β MAPK (p38 β) undergoes auto-activation in-vitro, but in mammalian cells, p38 β was not auto-activated. It was demonstrated that the interaction of its C terminal domain with the N terminal lobe decreased its auto-activation. Truncated C terminal mutants of p38 β were found to be highly auto-phosphorylated. Thus, it was proposed that some cellular protein can stabilize the inhibitory interaction of the C terminal and the N terminal lobe and prevent auto-activation [443]. As PKP3 loss leads to activation of p38 β , it was possible that PKP3 might mediate the interaction between these two domains in p38 β in HCT116 cells. The results from this thesis demonstrate that although PKP3 binds to the wild type p38 β , it can also bind to the C terminal truncated mutants of p38 β . Thus, it was concluded that the C terminal domain of p38 β does not contain the binding site for PKP3, suggesting that PKP3 might not mediate the interaction between the two p38 β domains. It is possible that PKP3 could bind to another domain in p38 β and allosterically regulates the interaction between the C terminal domain and N terminal lobe of p38 β . Alternatively, PKP3 could inhibit the activity of p38 β by other mechanisms. Truncation mutants of the different domains of p38 β can be generated and

immuno-precipitation experiments can be performed to delineate the PKP3 binding domain in p38 β and address the issue of how PKP3 loss leads to activation of p38 β .

Enslin et.al [465] and Ho et.al. [466] observed that a common feature among MAPK kinases (MAPKKs) like MAPK kinase 6 (MKK6), MKK3b (an alternative splice variant of MKK3) and MKK4 that activate p38 β was the presence of a amino acid sequence motif known as the D domain (earlier identified as a MAPK docking site present for ERK2) [467]. The consensus sequence for the D domain is (-Lysine/Arginine-Xaa₃-Leucine/Isoleucine-Xaa-Leucine/Isoleucine-). The symbol “Xaa” stands for any amino acid, while Xaa₃ stands for a series of any three amino acids. It was demonstrated that the D domain was required for binding of MAPKKs to p38 β and this binding was necessary for activation of p38 β [465]. To analyze if the amino acid sequence of PKP3 contains any D domain, a Motif Scan (<http://scansite.mit.edu/motifscan>) analysis was performed and it was found that there are two D domains in PKP3 (Figure 5.1). Since it has already been demonstrated that PKP3 binds to p38 β , future experiments will be performed to determine if the D domains of PKP3 are required for binding to p38 β .

Kinase binding site group (Kin_bind)				
Erk D-domain			Gene Card MAPK1	
Site	Score	Percentile	Sequence	SA
L284	0.5376	0.089 %	RAPS VRSLSLSI ADS	0.735
Erk D-domain			Gene Card MAPK1	
Site	Score	Percentile	Sequence	SA
L582	0.3492	0.001 %	RRLRELPI A AADALTF	0.411

Figure 5.1. Detection of D domain motifs in PKP3 amino acid sequence by Motif Scan software. The PKP3 amino acid sequence was fed into the Motif Scan software and analyzed for

presence of conserved motifs. Two D domains were predicted around the amino acid position 284 and 582. The amino acid sequence in PKP3 which matches the D domain sequence has been depicted on the right side of the figure. All amino acids are denoted as single letter amino acid codes.

5.4. ELK1 is required for the increase in LCN2 expression observed upon PKP3 loss.

A study by Yang, et.al.,[468] demonstrated that ERK1/2, JNK1/2 and p38MAPK isoforms p38 α , p38 β and p38 γ can all bind to ELK1 and activate it. Thus both p38 β and ERK1/2 can activate ELK1. Consistent with this report, the results of this thesis demonstrate that upon PKP3 loss in HCT116 cells and HaCaT cells, ELK1 phosphorylation increases and upon knocking down ELK1 in HCT116 derived PKP3 knockdown clones, the expression of LCN2 decreases. It was also observed a PKP3 loss responsive region exists in the LCN2 promoter and this DNA sequence contained one consensus ELK1 binding site and four consensus ETS1 binding sites. Knockdown of ELK1 in the HCT116 derived PKP3 knockdown clones were able to decrease the LCN2 promoter activity during luciferase reporter assays. Surprisingly, it was also observed that the total ELK1 levels were higher in the HCT116 derived PKP3 knockdown clones as compared to their vector control clones. Thus upon PKP3 loss in HCT116 cells p38 β MAPK activates ELK1, while upon PKP3 loss in HaCaT cells, ERK1/2 activates ELK1 via the EGFR pathway. ELK1 acts as the common effector for the different signaling pathways and activation of ELK1 leads to increased LCN2 expression.

5.5. MMP7 mediates cell invasion and tumor formation upon PKP3 loss

MMP7 levels are increased in colon cancer tissues [397, 444, 469] and in the serum of colon cancer patients [470]. A study by Witty et.al., demonstrated that MMP7 knockdown clones derived from the colon cancer cell line SW620 do not form tumors as efficiently as the corresponding vector controls in orthotopic xenografts of colon cancer [403]. Further, studies by Wilson et. al., [401] and Guillen-Ahlers et.al. [402] demonstrated that loss of MMP7 in the intestine of *Apc^{Min}* mice leads to a decrease in tumor incidence. The results presented in this thesis have demonstrated that PKP3 loss in HCT116 cells leads to an increase in migration, invasion, tumor formation and metastasis and that increase in MMP7 expression upon PKP3 loss is necessary for these functions.

To determine if any correlation exists between MMP7 and PKP3 levels across colon cancers at the transcript level, the data sets in the Oncomine database (www.oncomine.org) were analyzed. When MMP7 levels in normal colon samples were compared with that in colon cancer, the levels were found to be increased unlike PKP3 whose expression did not get altered. None of the databases present had actually validated the PKP3 levels using real time PCR or reverse transcriptase PCR. It was observed that a thorough immuno-histochemical analysis of PKP3 and MMP7 levels in a large dataset of colorectal cancer patients has never been performed. This type of analysis will be performed to determine if any correlation exists between PKP3 and MMP7 levels in colon cancers.

In this thesis, it has been demonstrated that MMP7 loss in the HCT116 derived PKP3 knockdown clones lead to an increase in colony formation in soft agar. It was also observed that MMP7 knockdown leads to a huge increase in LCN2 levels. The reason why this huge LCN2 expression levels does not increase cell migration or invasion in the MMP7+PKP3 knockdown

clones is not understood. Unlike many studies which have demonstrated that LCN2 acts as an oncogene in colon cancer [372, 373], a study by Lee, H.J. et.al. [471], demonstrated that LCN2 can act as a tumor suppressor in colon cancer. In these studies, over-expression of LCN2 in the KM12SM colon cancer cell line (a highly metastatic cell line) was shown to decrease cell migration and invasion both in-vitro and in-vivo. Interestingly, KM12SM was shown to have a very high endogenous expression levels of LCN2 compared to HCT116 cells [471]. Since a further increase in LCN2 levels in KM12SM cells led to a decrease in cell migration and invasion, it can be hypothesized that very high LCN2 concentrations (above some threshold) in a cell may be detrimental to cells in terms of cell migration and invasion but may still favor anchorage independent growth [451]. To address this problem, multiple HCT116 derived LCN2 over-expressing clones have been generated which have varied levels of LCN2 expression [441]. These clones can be used to analyze if the oncogenic role of LCN2 changes to a tumor suppressive role at very high concentrations.

Although MMP7+PKP3 double knockdown clones formed more colonies in soft agar, when these clones were subcutaneously injected in nude mice and allowed to form tumors, they showed decreased tumor incidence as compared to the vector control clones. These results suggest that the ability of MMP7 to induce the degradation of the extra-cellular matrix in vivo maybe essential for the ability of the PKP3 knockdown cells to form a tumor. Taken together these results suggest that the increase in MMP7 levels observed upon PKP3 loss is necessary for increased tumorigenesis in cells derived from the colon.

MMP7 over-expression has also been associated with skin cancer progression [472]. A study by Mitsui et.al. demonstrated that MMP7 is expressed in the invasive front of cutaneous squamous carcinomas and a monoclonal antibody targeting MMP7 can decrease cell migration of the

squamous carcinoma cell line A431 [473]. The results presented in this thesis demonstrate that MMP7 was up-regulated upon PKP3 loss in the HaCaT cells both at the mRNA and protein levels. More studies are required to determine if MMP7 is required for neoplastic progression upon PKP3 loss in HaCaT cells.

5.6. MMP7 over-expression upon PKP3 loss is regulated by PRL-3

PRL-3 levels have been found to be increased in colorectal cancers [474] and PRL-3 over-expression leads to metastasis in tumors derived from the colon [275]. A study by Lee, et.al., [452] demonstrated that PRL-3 increases cell migration and invasion by up-regulating expression of MMP7 in colorectal cancer cell line DLD-1, via the PI3K/AKT and ERK signaling pathway. Earlier reports from our laboratory have demonstrated that an increase in K8 levels upon PKP3 knockdown in HCT116 cells is dependent on increased levels of PRL-3 and that the inhibition of PRL-3 expression using shRNA constructs or the inhibition of PRL-3 activity using a specific inhibitor results in a reversal of the observed phenotype [232]. The results presented in this thesis demonstrate that PKP3 loss causes increase in MMP7 expression while inhibition of PRL-3 activity in the PKP3 knockdown clones results in a decrease in MMP7 levels. Since PRL-3 protein levels were found to be increased upon PKP3 loss in HCT116 cells without any increase in the levels of PRL-3 mRNA or stability [232], it was implicated that translation of the PRL-3 mRNA maybe increased upon PKP3 loss. Hofmann, et.al have demonstrated that PKP3 localizes to stress granules (sites of stalled mRNA-protein complexes) and forms a complex with RNA binding proteins like Poly (A) binding protein, Cytoplasmic 1 (PABPC1), Fragile X Mental Retardation, Autosomal Homolog 1 (FXR1), and GTPase Activating Protein (SH3 Domain) Binding Protein1 (G3BP) [239, 277]. Moreover, a study by Wang, et.al., showed that PRL-3 over-expression in cancers is not directly related to its transcript level but depend on the post-

transcriptional regulation of an RNA binding protein called Poly C binding protein 1 (PCBP1). PCBP1 binds to the a triple GCCCAG motif present at the 5' untranslated region (UTR) of the PRL-3 mRNA and suppresses translation by preventing mRNA loading into polyribosomes [475]. Thus, PKP3 may regulate the translation of PRL-3 mRNA translation by binding to different RNA binding proteins. Consistent with these observations, a PKP subfamily member, PKP1 has been reported to regulate translation initiation by directly binding to eIF4A (eukaryotic Initiation factor 4A) and promoting its activity [240].

5.7. PKP3 loss in HaCaT and FBM cells lead to increase in expression of inflammatory associated genes.

PKP3 knockout mice kept in conventional animal house conditions (environment infested with mites) but not in specific pathogen free conditions, show symptoms of severe itching, intercellular edema, neutrophil infiltration, epidermal hyperplasia, hair loss and muscle wasting [211]. Because of this dermatitis associated muscle wasting, the PKP3 null mice are smaller in size than the wild type mice and are very similar to the mouse model for atopic dermatitis, a severe form of skin inflammation [211].

It has recently been reported that in specific pathogen free conditions, the systemic cytokine profile of PKP3 knockout mice and the control mice remain unchanged but PKP3 knockout mice were more susceptible to phorbol-12-myristate-13-acetate (PMA) (also known as 12-O-tetradecanoylphorbol-13-acetate (TPA)) induced skin inflammation [476]. Using tissue specific PKP3 knockout mice, it was demonstrated that PMA induced skin inflammation was greater in hematopoietic tissue specific PKP3 knockout mice (PKP3^{-/hem}) than in the wild type counterpart (PKP3^{fl/fl} mice). No inflammation was seen in the keratinocyte specific PKP3 knockout mice

(PKP3^{-/-ker}). A systemic cytokine analysis by qRT-PCR showed that the PKP3^{-/ hem} mice expressed more pro-inflammatory cytokines like IL6, TNF α , IL1 β , IL17, iNOS and KC (or CXCL1) as compared to the wild type counterpart (PKP3^{fl/fl} mice) [476]

The results presented in this thesis demonstrate that loss of PKP3 in HaCaT and FBM cell lines lead to the over-expression of multiple genes associated with inflammation. But these results do not correlate with the observations made in PKP3^{-/ker} mice which neither showed constitutive inflammatory phenotype nor increased susceptibility to PMA induced inflammation. The difference between the inflammatory phenotypes between keratinocytes of PKP3^{-/ker} mice and HaCaT derived PKP3 knockdown clones may arise because of the differential response of cells to knockout or knockdown of PKP3. In the study by Sklyarova et.al. [211], keratinocytes of PKP3 null mice kept in specific pathogen free conditions had increased PKP1 or PKP2 protein levels as a compensatory mechanism to prevent complete loss of desmosome function. β catenin protein levels were also increased in these epidermis as compared to the control mice [211]. Since PKP2 is known to increase β catenin activity [477], it is also possible that the keratinocytes of PKP3 null mice exhibited higher β catenin activity. β catenin is known to negatively regulate NF κ B mediated inflammation in multiple cell types [478-480]. Over-expression of β catenin [479] or activation of β catenin [478] has been shown to decrease NF κ B dependant transcription of pro-inflammatory genes like IL6, TNF α , IFN γ , IL17, IL8 and iNOS [478, 479, 481]. Similar to I κ B α (a well known inhibitor of NF κ B), β catenin binds to NF κ B and sequesters it to the cytoplasm and degradation of β catenin via proteasome mediated degradation releases NF κ B which then translocates to the nucleus and activates transcription of pro-inflammatory genes [478, 482]. Moreover, NF κ B activation is essential for PMA induced skin inflammation in mouse and the resultant increase in gene expression of pro-inflammatory cytokines [483] and

inhibition of NF κ B activity decreases cytokine production during PMA induced skin inflammation [484, 485]. Thus, increase in β catenin expression and β catenin activation in the PKP3 null epidermis inhibits PMA/NF κ B mediated inflammation. Unlike the keratinocytes of PKP3 null mice, the HaCaT derived PKP3 knockdown clones show no compensatory increase in PKP2 levels and β catenin levels and activity remain unchanged. Thus, to understand the specific role of PKP3 in the skin, an epidermis specific PKP3 knockdown mouse needs to be generated.

The results presented in this thesis demonstrate that PKP3 loss in HaCaT cells lead to activation of the EGFR pathway. Since the EGFR pathway has been associated with increased inflammation and cancer ([486, 487] and reviewed in [488, 489]), it has been proposed that activation of the EGFR pathway upon PKP3 loss may be required to increase expression of inflammatory associated genes and in turn lead to increased tumor formation. Consistent with this hypothesis, over-expression of a PKP isoform, PKP2, has been shown to cause ligand dependant and ligand independent EGFR activation leading to increased neoplastic progression in breast cancer cells [226]. PKP2 has also been shown to bind to EGFR [226]. Conversely, a desmosomal cadherin, DSG1 which co-localizes with EGFR at cell to cell contacts, initiates terminal differentiation in keratinocytes by inhibiting EGFR phosphorylation at Tyrosine 1068 and leads to inhibition of the downstream EGFR signaling [490]. Thus, EGFR co-localizes with desmosomal proteins and desmosomal proteins can regulate EGFR activation. Future experiments will be done to study the role of EGFR in PKP3 loss mediated neoplastic progression and to determine the mechanism regulating EGFR activation upon PKP3 loss.

In the study by Sklyarova et.al. [476], intestinal epithelial cell specific PKP3 knockout (PKP3^{-/IEC}) mice was generated. These mice did not show any inflammatory associated phenotype when kept in specific pathogen free conditions [476]. Consistent with this observation, HCT116

derived PKP3 knockdown clones did not show any increase in the expression of inflammatory associated genes as compared to the vector control clones.

5.8. PKP3 knockdown leads to differential alterations in transcriptome of three different cell types

The mechanism of regulation of MMP7 over-expression upon PKP3 loss was found to be cell type specific. Upon treatment with the PRL-3 inhibitor, MMP7 levels did not decrease in the HaCaT cells suggesting that the increase in MMP7 in HaCaT cells occurs via mechanisms distinct from those observed in HCT116 cells and is consistent with our observations that PKP3 loss leads to cell type specific alterations in the transcriptome. The relevance of other alterations in gene expression that is specific to the FBM cell line, like increase in Δ Np63 α and its target genes is not clear. They may relate to the role of PKP3 in regulating desmosome formation in the oral cavity or these alterations in gene expression and signaling might also have a role to play in the increased migration and cellular transformation observed in the FBM cells upon PKP3 loss [233]. Thus, PKP3 loss can lead to both cell type dependent and cell type independent alterations in gene expression.

5.9. LCN2, but not MMP7, is required to increase radio-resistance of HCT116 cells upon PKP3 loss.

A study by Shiiba et.al, demonstrated that oral cancer or lung cancer derived cell lines transfected with an siRNA against LCN2 showed greater radio-sensitivity to X-ray irradiation as compared to the cells transfected with the control siRNA [377]. Thus, LCN2 was shown to regulate radio-resistance in both oral cancer cell lines and lung cancer cell lines. Consistent with

the above study, the results presented in this thesis demonstrate that knockdown of LCN2 in a HCT116 derived PKP3 knockdown clone causes increased radio-sensitivity to γ irradiation as compared to the vector control clones. Thus LCN2 is necessary for the increased radio-resistance observed upon PKP3 loss. Similar to LCN2, MMP7 was shown to be required for radio-resistance of the colon cancer derived cell line, SW480, against X ray irradiation [404]. Results from this thesis demonstrate that MMP7 loss in PKP3 knockdown clones do not alter radio-resistance of cells against γ irradiation. Thus, MMP7 was not required for the increased radio-resistance observed upon PKP3 loss in HCT116 cells.

5.10. Conclusion

The results presented in this thesis suggest that multiple pathways determine tumor progression and metastasis upon PKP3 loss in HCT116 cells and possibly in other cell types. PKP3 loss in HCT116 cells leads to an increase in LCN2 expression due to activation of the p38MAPK pathway. Expression of p38 β , but not p38 α , was required for the increase in LCN2 expression observed upon PKP3 loss. Activation of p38 β leads to an increase in ELK1 expression and activation, which were required for the increased LCN2 expression observed upon PKP3 loss in HCT116 cells. LCN2 is one of the factors necessary for the increased neoplastic progression observed upon PKP3 loss. It was demonstrated earlier that PKP3 loss in HCT116 cells leads to increase in PRL-3 protein levels leading to dephosphorylation of K8 and an increase in K8 stability. The increase in the levels of K8 is required for the increased transformation and metastasis observed upon PKP3 knockdown [232]. The results presented in this thesis demonstrate that the increase in PRL-3 protein levels upon PKP3 loss lead to an increase in MMP7 expression and MMP7 is necessary for the increased tumor formation observed upon

PKP3 loss [451]. Thus both MMP7 and LCN2 are necessary for tumor formation upon PKP3 loss in HCT116 cells (Figure 5.1).

PKP3 loss was also known to increase radio-resistance in HaCaT, HCT116 and FBM cells [257, 258]. During the course of this thesis, quantitative clonogenic survival assays were performed to re-confirm these earlier studies. It was demonstrated that the increased radio-resistance observed upon PKP3 loss in HCT116 cells was reversed upon LCN2 loss, but not upon loss of MMP7, thereby suggesting that LCN2 might be required for the increased radioresistance observed upon PKP3 knockdown (Figure 5.2).

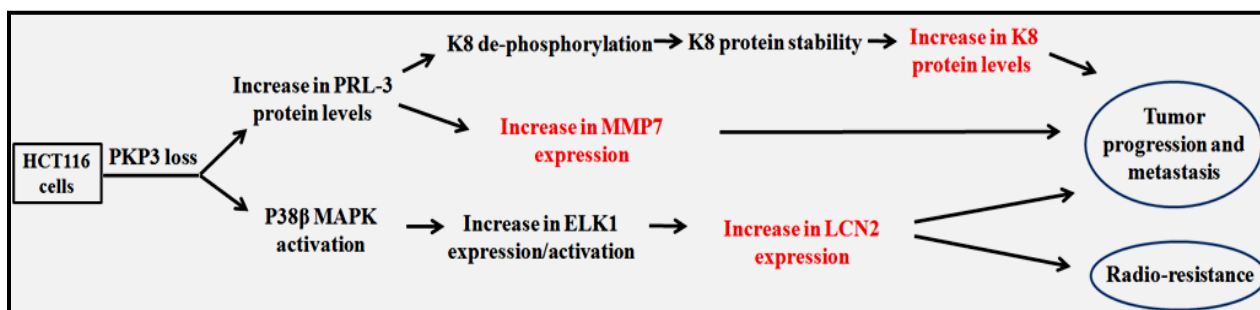


Figure 5.2. Mechanisms leading to increased tumor formation, metastasis and radioresistance upon PKP3 loss in HCT116 cells. This figure is a schematic representation of the different mechanisms that are regulated upon PKP3 loss in HCT116 cells leading to increased tumor formation, metastasis and radio-resistance. Increase in PRL-3 activity upon PKP3 loss causes increased K8 protein levels and increased expression of MMP7 while activation of the p38 β MAPK/ ELK1 pathway leads to increase in LCN2 expression. The increase in LCN2 and MMP7 expression and the increased K8 protein levels were shown to be necessary for increased tumor formation and metastasis upon PKP3 loss in HCT116 cells. Presence of LCN2 was also necessary to increase radioresistance of the PKP3 knockdown clones against γ irradiation.

In the HaCaT and FBM cells, similar to HCT116 cells, PKP3 loss led to an increase in the levels of LCN2 and MMP7. In addition to these two gene products, the loss of PKP3 in the HaCaT and FBM cell lines led to an increase in expression of many inflammatory associated genes like IL6, CCL2, SAA1, S100A8, S100A9 and CBS. These changes were not observed in the HCT116 derived PKP3 knockdown cells. PKP3 loss in the HaCaT cell line also led to activation of the EGFR/ MEK(1/2)/ ERK(1/2)/ ELK1 signaling pathway. Since ELK1 was necessary for increasing LCN2 expression upon PKP3 loss in HCT116 cells, it was proposed that ELK1 may increase LCN2 expression in HaCaT cells upon PKP3 loss. It has been proposed that activation of the EGFR pathway or increased expression of LCN2, MMP7 and inflammatory associated genes are required for increasing tumor progression, metastasis and radio-resistance observed upon PKP3 loss in HaCaT cells (Figure 5.3).

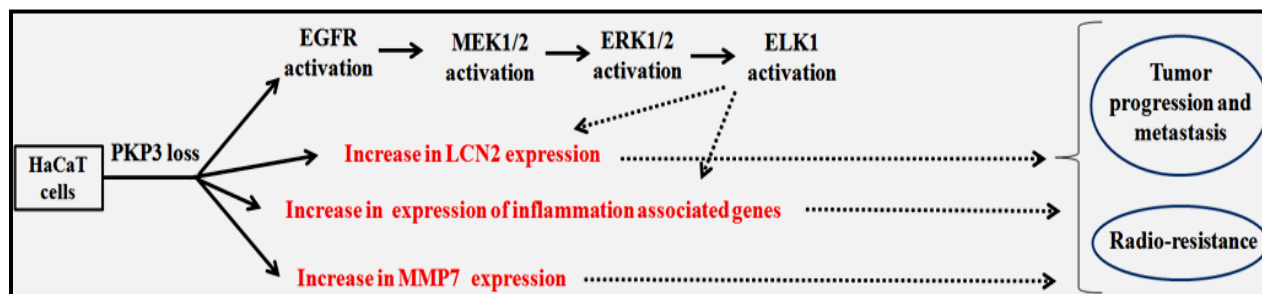


Figure 5.3. Possible mechanisms leading to increased tumor formation, metastasis and radioresistance upon PKP3 loss in HaCaT cells. PKP3 loss in HaCaT cells lead to an increase in expression of LCN2, MMP7 and some inflammatory associated genes. It has been proposed that all or some of these factors may be necessary for tumor progression, metastasis and radioresistance observed upon PKP3 loss in the HaCaT cell line. The EGFR/ MEK(1/2)/ ERK(1/2)/ ELK1 signaling pathway is also activated in the HaCaT derived PKP3 knockdown clones and ELK1 may be necessary for increasing transcriptional activation of the LCN2 gene.

The stealth arrows in this figure represent the mechanisms that have been verified in the course of this thesis, while the dashed arrows represent the proposed mechanisms.

6. BIBLIOGRAPHY

1. Giepmans BN, van Ijzendoorn SC. Epithelial cell-cell junctions and plasma membrane domains. *Biochim Biophys Acta*. 2009;1788(4):820-31.
2. Martin-Belmonte F, Perez-Moreno M. Epithelial cell polarity, stem cells and cancer. *Nat Rev Cancer*. 2012;12(1):23-38.
3. Rejniak KA. Homeostatic imbalance in epithelial ducts and its role in carcinogenesis. *Scientifica (Cairo)*. 2012;2012:132978.
4. Royer C, Lu X. Epithelial cell polarity: a major gatekeeper against cancer? *Cell Death Differ*. 2011;18(9):1470-7.
5. Roignot J, Peng X, Mostov K. Polarity in mammalian epithelial morphogenesis. *Cold Spring Harb Perspect Biol*. 2013;5(2).
6. Peterson LW, Artis D. Intestinal epithelial cells: regulators of barrier function and immune homeostasis. *Nat Rev Immunol*. 2014;14(3):141-53.
7. Poulson ND, Lechler T. Asymmetric cell divisions in the epidermis. *Int Rev Cell Mol Biol*. 2012;295:199-232.
8. Niessen MT, Iden S, Niessen CM. The in vivo function of mammalian cell and tissue polarity regulators--how to shape and maintain the epidermal barrier. *J Cell Sci*. 2012;125(Pt 15):3501-10.
9. Ellenbroek SI, Iden S, Collard JG. Cell polarity proteins and cancer. *Semin Cancer Biol*. 2012;22(3):208-15.
10. Tanos B, Rodriguez-Boulan E. The epithelial polarity program: machineries involved and their hijacking by cancer. *Oncogene*. 2008;27(55):6939-57.
11. Tervonen TA, Partanen JI, Saarikoski ST, Myllynen M, Marques E, Paasonen K, et al. Faulty epithelial polarity genes and cancer. *Adv Cancer Res*. 2011;111:97-161.

12. Jefferson JJ, Leung CL, Liem RK. Plakins: goliaths that link cell junctions and the cytoskeleton. *Nat Rev Mol Cell Biol.* 2004;5(7):542-53.
13. Wang Q, Margolis B. Apical junctional complexes and cell polarity. *Kidney Int.* 2007;72(12):1448-58.
14. Shin K, Fogg VC, Margolis B. Tight junctions and cell polarity. *Annu Rev Cell Dev Biol.* 2006;22:207-35.
15. Baum B, Georgiou M. Dynamics of adherens junctions in epithelial establishment, maintenance, and remodeling. *J Cell Biol.* 2011;192(6):907-17.
16. Hernandez S, Chavez Munguia B, Gonzalez-Mariscal L. ZO-2 silencing in epithelial cells perturbs the gate and fence function of tight junctions and leads to an atypical monolayer architecture. *Exp Cell Res.* 2007;313(8):1533-47.
17. Hoover KB, Liao SY, Bryant PJ. Loss of the tight junction MAGUK ZO-1 in breast cancer: relationship to glandular differentiation and loss of heterozygosity. *Am J Pathol.* 1998;153(6):1767-73.
18. Martin TA, Mansel RE, Jiang WG. Loss of occludin leads to the progression of human breast cancer. *Int J Mol Med.* 2010;26(5):723-34.
19. Desai RA, Gao L, Raghavan S, Liu WF, Chen CS. Cell polarity triggered by cell-cell adhesion via E-cadherin. *J Cell Sci.* 2009;122(Pt 7):905-11.
20. Runswick SK, O'Hare MJ, Jones L, Streuli CH, Garrod DR. Desmosomal adhesion regulates epithelial morphogenesis and cell positioning. *Nat Cell Biol.* 2001;3(9):823-30.
21. Schneider MR, Kolligs FT. E-cadherin's role in development, tissue homeostasis and disease: Insights from mouse models: Tissue-specific inactivation of the adhesion protein E-cadherin in mice reveals its functions in health and disease. *Bioessays.* 2015;37(3):294-304.

22. Dorudi S, Sheffield JP, Poulson R, Northover JM, Hart IR. E-cadherin expression in colorectal cancer. An immunocytochemical and in situ hybridization study. *Am J Pathol.* 1993;142(4):981-6.
23. Bae GY, Choi SJ, Lee JS, Jo J, Lee J, Kim J, et al. Loss of E-cadherin activates EGFR-MEK/ERK signaling, which promotes invasion via the ZEB1/MMP2 axis in non-small cell lung cancer. *Oncotarget.* 2013;4(12):2512-22.
24. Singhai R, Patil VW, Jaiswal SR, Patil SD, Tayade MB, Patil AV. E-Cadherin as a diagnostic biomarker in breast cancer. *N Am J Med Sci.* 2011;3(5):227-33.
25. Onder TT, Gupta PB, Mani SA, Yang J, Lander ES, Weinberg RA. Loss of E-cadherin promotes metastasis via multiple downstream transcriptional pathways. *Cancer Res.* 2008;68(10):3645-54.
26. Lu P, Weaver VM, Werb Z. The extracellular matrix: a dynamic niche in cancer progression. *J Cell Biol.* 2012;196(4):395-406.
27. Wu C. Focal adhesion: a focal point in current cell biology and molecular medicine. *Cell Adh Migr.* 2007;1(1):13-8.
28. Rozario T, DeSimone DW. The extracellular matrix in development and morphogenesis: a dynamic view. *Dev Biol.* 2010;341(1):126-40.
29. Simpson CL, Patel DM, Green KJ. Deconstructing the skin: cytoarchitectural determinants of epidermal morphogenesis. *Nat Rev Mol Cell Biol.* 2011;12(9):565-80.
30. Huttenlocher A, Horwitz AR. Integrins in cell migration. *Cold Spring Harb Perspect Biol.* 2011;3(9):a005074.
31. Vicente-Manzanares M, Choi CK, Horwitz AR. Integrins in cell migration--the actin connection. *J Cell Sci.* 2009;122(Pt 2):199-206.

32. Radisky D, Muschler J, Bissell MJ. Order and disorder: the role of extracellular matrix in epithelial cancer. *Cancer Invest.* 2002;20(1):139-53.
33. Cowin P, Kapprell HP, Franke WW. The complement of desmosomal plaque proteins in different cell types. *J Cell Biol.* 1985;101(4):1442-54.
34. Garrod DR. Desmosomes, cell adhesion molecules and the adhesive properties of cells in tissues. *J Cell Sci Suppl.* 1986;4:221-37.
35. Garrod DR. Formation of desmosomes in polarized and non-polarized epithelial cells: implications for epithelial morphogenesis. *Biochem Soc Trans.* 1986;14(1):172-5.
36. Schmelz M, Duden R, Cowin P, Franke WW. A constitutive transmembrane glycoprotein of Mr 165,000 (desmoglein) in epidermal and non-epidermal desmosomes. I. Biochemical identification of the polypeptide. *Eur J Cell Biol.* 1986;42(2):177-83.
37. Schmelz M, Duden R, Cowin P, Franke WW. A constitutive transmembrane glycoprotein of Mr 165,000 (desmoglein) in epidermal and non-epidermal desmosomes. II. Immunolocalization and microinjection studies. *Eur J Cell Biol.* 1986;42(2):184-99.
38. Parrish EP, Garrod DR, Matthey DL, Hand L, Steart PV, Weller RO. Mouse antisera specific for desmosomal adhesion molecules of suprabasal skin cells, meninges, and meningioma. *Proc Natl Acad Sci U S A.* 1986;83(8):2657-61.
39. Matthey DL, Garrod DR. Calcium-induced desmosome formation in cultured kidney epithelial cells. *J Cell Sci.* 1986;85:95-111.
40. Matthey DL, Garrod DR. Splitting and internalization of the desmosomes of cultured kidney epithelial cells by reduction in calcium concentration. *J Cell Sci.* 1986;85:113-24.
41. Watt FM, Matthey DL, Garrod DR. Calcium-induced reorganization of desmosomal components in cultured human keratinocytes. *J Cell Biol.* 1984;99(6):2211-5.

42. Garrod DR, Berika MY, Bardsley WF, Holmes D, Taberner L. Hyper-adhesion in desmosomes: its regulation in wound healing and possible relationship to cadherin crystal structure. *J Cell Sci.* 2005;118(Pt 24):5743-54.
43. Kimura TE, Merritt AJ, Garrod DR. Calcium-independent desmosomes of keratinocytes are hyper-adhesive. *J Invest Dermatol.* 2007;127(4):775-81.
44. Arnn J, Staehelin LA. The structure and function of spot desmosomes. *Int J Dermatol.* 1981;20(5):330-9.
45. Goldman RD, Goldman AE, Green KJ, Jones JC, Jones SM, Yang HY. Intermediate filament networks: organization and possible functions of a diverse group of cytoskeletal elements. *J Cell Sci Suppl.* 1986;5:69-97.
46. Smith EA, Fuchs E. Defining the interactions between intermediate filaments and desmosomes. *J Cell Biol.* 1998;141(5):1229-41.
47. Bissell MJ, Bilder D. Polarity determination in breast tissue: desmosomal adhesion, myoepithelial cells, and laminin 1. *Breast Cancer Res.* 2003;5(2):117-9.
48. Huang RY, Guilford P, Thiery JP. Early events in cell adhesion and polarity during epithelial-mesenchymal transition. *J Cell Sci.* 2012;125(Pt 19):4417-22.
49. North AJ, Bardsley WG, Hyam J, Bornslaeger EA, Cordingley HC, Trinnaman B, et al. Molecular map of the desmosomal plaque. *J Cell Sci.* 1999;112 (Pt 23):4325-36.
50. Al-Amoudi A, Castano-Diez D, Devos DP, Russell RB, Johnson GT, Frangakis AS. The three-dimensional molecular structure of the desmosomal plaque. *Proc Natl Acad Sci U S A.* 2011;108(16):6480-5.
51. Desai BV, Harmon RM, Green KJ. Desmosomes at a glance. *J Cell Sci.* 2009;122(Pt 24):4401-7.

52. Farquhar MG, Palade GE. Junctional complexes in various epithelia. *J Cell Biol.* 1963;17:375-412.
53. Odland GF. The fine structure of the interrelationship of cells in the human epidermis. *J Biophys Biochem Cytol.* 1958;4(5):529-38.
54. Kelly DE. Fine structure of desmosomes, hemidesmosomes, and an adepidermal globular layer in developing newt epidermis. *J Cell Biol.* 1966;28(1):51-72.
55. Rayns DG, Simpson FO, Ledingham JM. Ultrastructure of desmosomes in mammalian intercalated disc; appearances after lanthanum treatment. *J Cell Biol.* 1969;42(1):322-6.
56. Burdett ID. Aspects of the structure and assembly of desmosomes. *Micron.* 1998;29(4):309-28.
57. Cohen SM, Gorbsky G, Steinberg MS. Immunochemical characterization of related families of glycoproteins in desmosomes. *The Journal of biological chemistry.* 1983;258(4):2621-7.
58. Vester-Christensen MB, Halim A, Joshi HJ, Steentoft C, Bennett EP, Lavery SB, et al. Mining the O-mannose glycoproteome reveals cadherins as major O-mannosylated glycoproteins. *Proc Natl Acad Sci U S A.* 2013;110(52):21018-23.
59. Nollet F, Kools P, van Roy F. Phylogenetic analysis of the cadherin superfamily allows identification of six major subfamilies besides several solitary members. *J Mol Biol.* 2000;299(3):551-72.
60. Garrod DR, Merritt AJ, Nie Z. Desmosomal cadherins. *Current opinion in cell biology.* 2002;14(5):537-45.

61. Koch PJ, Goldschmidt MD, Walsh MJ, Zimbelmann R, Franke WW. Complete amino acid sequence of the epidermal desmoglein precursor polypeptide and identification of a second type of desmoglein gene. *Eur J Cell Biol.* 1991;55(2):200-8.
62. Amagai M, Klaus-Kovtun V, Stanley JR. Autoantibodies against a novel epithelial cadherin in pemphigus vulgaris, a disease of cell adhesion. *Cell.* 1991;67(5):869-77.
63. Wheeler GN, Buxton RS, Parker AE, Arnemann J, Rees DA, King IA, et al. Desmosomal glycoproteins I, II and III: novel members of the cadherin superfamily. *Biochem Soc Trans.* 1991;19(4):1060-4.
64. Wheeler GN, Parker AE, Thomas CL, Ataliotis P, Poynter D, Arnemann J, et al. Desmosomal glycoprotein DGI, a component of intercellular desmosome junctions, is related to the cadherin family of cell adhesion molecules. *Proc Natl Acad Sci U S A.* 1991;88(11):4796-800.
65. Whittock NV, Bower C. Genetic evidence for a novel human desmosomal cadherin, desmoglein 4. *J Invest Dermatol.* 2003;120(4):523-30.
66. King IA, Sullivan KH, Bennett R, Jr., Buxton RS. The desmocollins of human foreskin epidermis: identification and chromosomal assignment of a third gene and expression patterns of the three isoforms. *J Invest Dermatol.* 1995;105(3):314-21.
67. Theis DG, Koch PJ, Franke WW. Differential synthesis of type 1 and type 2 desmocollin mRNAs in human stratified epithelia. *Int J Dev Biol.* 1993;37(1):101-10.
68. Parker AE, Wheeler GN, Arnemann J, Pidsley SC, Ataliotis P, Thomas CL, et al. Desmosomal glycoproteins II and III. Cadherin-like junctional molecules generated by alternative splicing. *The Journal of biological chemistry.* 1991;266(16):10438-45.

69. Cheng X, Mihindukulasuriya K, Den Z, Kowalczyk AP, Calkins CC, Ishiko A, et al. Assessment of splice variant-specific functions of desmocollin 1 in the skin. *Molecular and cellular biology*. 2004;24(1):154-63.
70. Shapiro L, Fannon AM, Kwong PD, Thompson A, Lehmann MS, Grubel G, et al. Structural basis of cell-cell adhesion by cadherins. *Nature*. 1995;374(6520):327-37.
71. Shapiro L, Weis WI. Structure and biochemistry of cadherins and catenins. *Cold Spring Harb Perspect Biol*. 2009;1(3):a003053.
72. Nuber UA, Schafer S, Schmidt A, Koch PJ, Franke WW. The widespread human desmocollin Dsc2 and tissue-specific patterns of synthesis of various desmocollin subtypes. *Eur J Cell Biol*. 1995;66(1):69-74.
73. Nuber UA, Schafer S, Stehr S, Rackwitz HR, Franke WW. Patterns of desmocollin synthesis in human epithelia: immunolocalization of desmocollins 1 and 3 in special epithelia and in cultured cells. *Eur J Cell Biol*. 1996;71(1):1-13.
74. Schafer S, Koch PJ, Franke WW. Identification of the ubiquitous human desmoglein, Dsg2, and the expression catalogue of the desmoglein subfamily of desmosomal cadherins. *Exp Cell Res*. 1994;211(2):391-9.
75. Koch PJ, Goldschmidt MD, Zimbelmann R, Troyanovsky R, Franke WW. Complexity and expression patterns of the desmosomal cadherins. *Proc Natl Acad Sci U S A*. 1992;89(1):353-7.
76. Bazzi H, Getz A, Mahoney MG, Ishida-Yamamoto A, Langbein L, Wahl JK, 3rd, et al. Desmoglein 4 is expressed in highly differentiated keratinocytes and trichocytes in human epidermis and hair follicle. *Differentiation; research in biological diversity*. 2006;74(2-3):129-40.

77. Holbrook KA, Odland GF. The fine structure of developing human epidermis: light, scanning, and transmission electron microscopy of the periderm. *J Invest Dermatol.* 1975;65(1):16-38.
78. Delpech-Stewart A. An immunofluorescent study of antigenic structures in the development of human epidermis. *J Histochem Cytochem.* 1971;19(10):627-9.
79. Hentula M, Peltonen J, Peltonen S. Expression profiles of cell-cell and cell-matrix junction proteins in developing human epidermis. *Arch Dermatol Res.* 2001;293(5):259-67.
80. Arnemann J, Sullivan KH, Magee AI, King IA, Buxton RS. Stratification-related expression of isoforms of the desmosomal cadherins in human epidermis. *J Cell Sci.* 1993;104 (Pt 3):741-50.
81. Koch PJ, Mahoney MG, Cotsarelis G, Rothenberger K, Lavker RM, Stanley JR. Desmoglein 3 anchors telogen hair in the follicle. *J Cell Sci.* 1998;111 (Pt 17):2529-37.
82. Chidgey M, Brakebusch C, Gustafsson E, Cruchley A, Hail C, Kirk S, et al. Mice lacking desmocollin 1 show epidermal fragility accompanied by barrier defects and abnormal differentiation. *J Cell Biol.* 2001;155(5):821-32.
83. Eshkind L, Tian Q, Schmidt A, Franke WW, Windoffer R, Leube RE. Loss of desmoglein 2 suggests essential functions for early embryonic development and proliferation of embryonal stem cells. *Eur J Cell Biol.* 2002;81(11):592-8.
84. Den Z, Cheng X, Merched-Sauvage M, Koch PJ. Desmocollin 3 is required for pre-implantation development of the mouse embryo. *J Cell Sci.* 2006;119(Pt 3):482-9.
85. Harmon RM, Simpson CL, Johnson JL, Koetsier JL, Dubash AD, Najor NA, et al. Desmoglein-1/Erbin interaction suppresses ERK activation to support epidermal differentiation. *J Clin Invest.* 2013;123(4):1556-70.

86. Merritt AJ, Berika MY, Zhai W, Kirk SE, Ji B, Hardman MJ, et al. Suprabasal desmoglein 3 expression in the epidermis of transgenic mice results in hyperproliferation and abnormal differentiation. *Molecular and cellular biology*. 2002;22(16):5846-58.
87. Elias PM, Matsuyoshi N, Wu H, Lin C, Wang ZH, Brown BE, et al. Desmoglein isoform distribution affects stratum corneum structure and function. *J Cell Biol*. 2001;153(2):243-9.
88. Heuser A, Plovie ER, Ellinor PT, Grossmann KS, Shin JT, Wichter T, et al. Mutant desmocollin-2 causes arrhythmogenic right ventricular cardiomyopathy. *Am J Hum Genet*. 2006;79(6):1081-8.
89. Pilichou K, Nava A, Basso C, Beffagna G, Bauce B, Lorenzon A, et al. Mutations in desmoglein-2 gene are associated with arrhythmogenic right ventricular cardiomyopathy. *Circulation*. 2006;113(9):1171-9.
90. Gear K, Marcus F. Arrhythmogenic right ventricular dysplasia/cardiomyopathy. *Circulation*. 2003;107(4):e31-3.
91. Simpson MA, Mansour S, Ahnood D, Kalidas K, Patton MA, McKenna WJ, et al. Homozygous mutation of desmocollin-2 in arrhythmogenic right ventricular cardiomyopathy with mild palmoplantar keratoderma and woolly hair. *Cardiology*. 2009;113(1):28-34.
92. Rickman L, Simrak D, Stevens HP, Hunt DM, King IA, Bryant SP, et al. N-terminal deletion in a desmosomal cadherin causes the autosomal dominant skin disease striate palmoplantar keratoderma. *Hum Mol Genet*. 1999;8(6):971-6.
93. Kljuic A, Bazzi H, Sundberg JP, Martinez-Mir A, O'Shaughnessy R, Mahoney MG, et al. Desmoglein 4 in hair follicle differentiation and epidermal adhesion: evidence from inherited hypotrichosis and acquired pemphigus vulgaris. *Cell*. 2003;113(2):249-60.

94. Ayub M, Basit S, Jelani M, Ur Rehman F, Iqbal M, Yasinzai M, et al. A homozygous nonsense mutation in the human desmocollin-3 (DSC3) gene underlies hereditary hypotrichosis and recurrent skin vesicles. *Am J Hum Genet.* 2009;85(4):515-20.
95. Koulu L, Kusumi A, Steinberg MS, Klaus-Kovtun V, Stanley JR. Human autoantibodies against a desmosomal core protein in pemphigus foliaceus. *J Exp Med.* 1984;160(5):1509-18.
96. Olague-Alcala M, Giudice GJ, Diaz LA. Pemphigus foliaceus sera recognize an N-terminal fragment of bovine desmoglein 1. *J Invest Dermatol.* 1994;102(6):882-5.
97. Calkins CC, Setzer SV, Jennings JM, Summers S, Tsunoda K, Amagai M, et al. Desmoglein endocytosis and desmosome disassembly are coordinated responses to pemphigus autoantibodies. *The Journal of biological chemistry.* 2006;281(11):7623-34.
98. Cirillo N, Gombos F, Lanza A. Changes in desmoglein 1 expression and subcellular localization in cultured keratinocytes subjected to anti-desmoglein 1 pemphigus autoimmunity. *J Cell Physiol.* 2007;210(2):411-6.
99. van der Wier G, Jonkman MF, Pas HH, Diercks GF. Ultrastructure of acantholysis in pemphigus foliaceus re-examined from the current perspective. *Br J Dermatol.* 2012;167(6):1265-71.
100. Payne AS, Hanakawa Y, Amagai M, Stanley JR. Desmosomes and disease: pemphigus and bullous impetigo. *Current opinion in cell biology.* 2004;16(5):536-43.
101. Waschke J. The desmosome and pemphigus. *Histochem Cell Biol.* 2008;130(1):21-54.
102. Farrell AM. Staphylococcal scalded-skin syndrome. *Lancet.* 1999;354(9182):880-1.
103. Lyell A. The staphylococcal scalded skin syndrome in historical perspective: emergence of dermopathic strains of *Staphylococcus aureus* and discovery of the epidermolytic toxin. A review of events up to 1970. *J Am Acad Dermatol.* 1983;9(2):285-94.

104. Stanley JR, Amagai M. Pemphigus, bullous impetigo, and the staphylococcal scalded-skin syndrome. *N Engl J Med.* 2006;355(17):1800-10.
105. Lee CY, Schmidt JJ, Johnson-Winegar AD, Spero L, Iandolo JJ. Sequence determination and comparison of the exfoliative toxin A and toxin B genes from *Staphylococcus aureus*. *J Bacteriol.* 1987;169(9):3904-9.
106. Yamaguchi T, Nishifuji K, Sasaki M, Fudaba Y, Aepfelbacher M, Takata T, et al. Identification of the *Staphylococcus aureus* etd pathogenicity island which encodes a novel exfoliative toxin, ETD, and EDIN-B. *Infect Immun.* 2002;70(10):5835-45.
107. Vath GM, Earhart CA, Monie DD, Iandolo JJ, Schlievert PM, Ohlendorf DH. The crystal structure of exfoliative toxin B: a superantigen with enzymatic activity. *Biochemistry.* 1999;38(32):10239-46.
108. Vath GM, Earhart CA, Rago JV, Kim MH, Bohach GA, Schlievert PM, et al. The structure of the superantigen exfoliative toxin A suggests a novel regulation as a serine protease. *Biochemistry.* 1997;36(7):1559-66.
109. Amagai M, Matsuyoshi N, Wang ZH, Andl C, Stanley JR. Toxin in bullous impetigo and staphylococcal scalded-skin syndrome targets desmoglein 1. *Nat Med.* 2000;6(11):1275-7.
110. Amagai M, Yamaguchi T, Hanakawa Y, Nishifuji K, Sugai M, Stanley JR. Staphylococcal exfoliative toxin B specifically cleaves desmoglein 1. *J Invest Dermatol.* 2002;118(5):845-50.
111. Hanakawa Y, Schechter NM, Lin C, Garza L, Li H, Yamaguchi T, et al. Molecular mechanisms of blister formation in bullous impetigo and staphylococcal scalded skin syndrome. *J Clin Invest.* 2002;110(1):53-60.

112. Hanakawa Y, Schechter NM, Lin C, Nishifuji K, Amagai M, Stanley JR. Enzymatic and molecular characteristics of the efficiency and specificity of exfoliative toxin cleavage of desmoglein 1. *The Journal of biological chemistry*. 2004;279(7):5268-77.
113. Hanakawa Y, Selwood T, Woo D, Lin C, Schechter NM, Stanley JR. Calcium-dependent conformation of desmoglein 1 is required for its cleavage by exfoliative toxin. *J Invest Dermatol*. 2003;121(2):383-9.
114. Manthey CL, Wang SW, Kinney SD, Yao Z. SB202190, a selective inhibitor of p38 mitogen-activated protein kinase, is a powerful regulator of LPS-induced mRNAs in monocytes. *J Leukoc Biol*. 1998;64(3):409-17.
115. Berkowitz P, Hu P, Warren S, Liu Z, Diaz LA, Rubenstein DS. p38MAPK inhibition prevents disease in pemphigus vulgaris mice. *Proc Natl Acad Sci U S A*. 2006;103(34):12855-60.
116. Berkowitz P, Hu P, Liu Z, Diaz LA, Enghild JJ, Chua MP, et al. Desmosome signaling. Inhibition of p38MAPK prevents pemphigus vulgaris IgG-induced cytoskeleton reorganization. *The Journal of biological chemistry*. 2005;280(25):23778-84.
117. Mavropoulos A, Orfanidou T, Liaskos C, Smyk DS, Spyrou V, Sakkas LI, et al. p38 MAPK Signaling in Pemphigus: Implications for Skin Autoimmunity. *Autoimmune Dis*. 2013;2013:728529.
118. Dusek RL, Attardi LD. Desmosomes: new perpetrators in tumour suppression. *Nat Rev Cancer*. 2011;11(5):317-23.
119. Kolegraff K, Nava P, Helms MN, Parkos CA, Nusrat A. Loss of desmocollin-2 confers a tumorigenic phenotype to colonic epithelial cells through activation of Akt/beta-catenin signaling. *Molecular biology of the cell*. 2011;22(8):1121-34.

120. Khan K, Hardy R, Haq A, Ogunbiyi O, Morton D, Chidgey M. Desmocollin switching in colorectal cancer. *Br J Cancer*. 2006;95(10):1367-70.
121. Ding X, Diaz LA, Fairley JA, Giudice GJ, Liu Z. The anti-desmoglein 1 autoantibodies in pemphigus vulgaris sera are pathogenic. *J Invest Dermatol*. 1999;112(5):739-43.
122. Aoyama Y, Kitajima Y. Pemphigus vulgaris-IgG causes a rapid depletion of desmoglein 3 (Dsg3) from the Triton X-100 soluble pools, leading to the formation of Dsg3-depleted desmosomes in a human squamous carcinoma cell line, DJM-1 cells. *J Invest Dermatol*. 1999;112(1):67-71.
123. Sato M, Aoyama Y, Kitajima Y. Assembly pathway of desmoglein 3 to desmosomes and its perturbation by pemphigus vulgaris-IgG in cultured keratinocytes, as revealed by time-lapsed labeling immunoelectron microscopy. *Lab Invest*. 2000;80(10):1583-92.
124. Shu E, Yamamoto Y, Aoyama Y, Kitajima Y. Intraperitoneal injection of pemphigus vulgaris-IgG into mouse depletes epidermal keratinocytes of desmoglein 3 associated with generation of acantholysis. *Arch Dermatol Res*. 2007;299(3):165-7.
125. Kamekura R, Kolegraff KN, Nava P, Hilgarth RS, Feng M, Parkos CA, et al. Loss of the desmosomal cadherin desmoglein-2 suppresses colon cancer cell proliferation through EGFR signaling. *Oncogene*. 2014;33(36):4531-6.
126. Ramani VC, Hennings L, Haun RS. Desmoglein 2 is a substrate of kallikrein 7 in pancreatic cancer. *BMC Cancer*. 2008;8:373.
127. Myklebust MP, Fluge O, Immervoll H, Skarstein A, Balteskard L, Bruland O, et al. Expression of DSG1 and DSC1 are prognostic markers in anal carcinoma patients. *Br J Cancer*. 2012;106(4):756-62.

128. Brennan D, Mahoney MG. Increased expression of Dsg2 in malignant skin carcinomas: A tissue-microarray based study. *Cell Adh Migr.* 2009;3(2):148-54.
129. Biedermann K, Vogelsang H, Becker I, Plaschke S, Siewert JR, Hofler H, et al. Desmoglein 2 is expressed abnormally rather than mutated in familial and sporadic gastric cancer. *J Pathol.* 2005;207(2):199-206.
130. Chen YJ, Chang JT, Lee L, Wang HM, Liao CT, Chiu CC, et al. DSG3 is overexpressed in head neck cancer and is a potential molecular target for inhibition of oncogenesis. *Oncogene.* 2007;26(3):467-76.
131. Fang WK, Gu W, Liao LD, Chen B, Wu ZY, Wu JY, et al. Prognostic significance of desmoglein 2 and desmoglein 3 in esophageal squamous cell carcinoma. *Asian Pac J Cancer Prev.* 2014;15(2):871-6.
132. Oshiro MM, Kim CJ, Wozniak RJ, Junk DJ, Munoz-Rodriguez JL, Burr JA, et al. Epigenetic silencing of DSC3 is a common event in human breast cancer. *Breast Cancer Res.* 2005;7(5):R669-80.
133. Cui T, Chen Y, Yang L, Mireskandari M, Knosel T, Zhang Q, et al. Diagnostic and prognostic impact of desmocollins in human lung cancer. *J Clin Pathol.* 2012;65(12):1100-6.
134. Pan J, Chen Y, Mo C, Wang D, Chen J, Mao X, et al. Association of DSC3 mRNA down-regulation in prostate cancer with promoter hypermethylation and poor prognosis. *PLoS One.* 2014;9(3):e92815.
135. Holthofer B, Windoffer R, Troyanovsky S, Leube RE. Structure and function of desmosomes. *Int Rev Cytol.* 2007;264:65-163.
136. Lai Cheong JE, Wessagowit V, McGrath JA. Molecular abnormalities of the desmosomal protein desmoplakin in human disease. *Clin Exp Dermatol.* 2005;30(3):261-6.

137. O'Keefe EJ, Erickson HP, Bennett V. Desmoplakin I and desmoplakin II. Purification and characterization. *The Journal of biological chemistry*. 1989;264(14):8310-8.
138. Franke WW, Mueller H, Mittnacht S, Kapprell HP, Jorcano JL. Significance of two desmosome plaque-associated polypeptides of molecular weights 75 000 and 83 000. *EMBO J*. 1983;2(12):2211-5.
139. Nekrasova O, Green KJ. Desmosome assembly and dynamics. *Trends Cell Biol*. 2013;23(11):537-46.
140. Choi HJ, Weis WI. Crystal structure of a rigid four-spectrin-repeat fragment of the human desmoplakin plakin domain. *J Mol Biol*. 2011;409(5):800-12.
141. Bornslaeger EA, Godsel LM, Corcoran CM, Park JK, Hatzfeld M, Kowalczyk AP, et al. Plakophilin 1 interferes with plakoglobin binding to desmoplakin, yet together with plakoglobin promotes clustering of desmosomal plaque complexes at cell-cell borders. *J Cell Sci*. 2001;114(Pt 4):727-38.
142. Kowalczyk AP, Bornslaeger EA, Borgwardt JE, Palka HL, Dhaliwal AS, Corcoran CM, et al. The amino-terminal domain of desmoplakin binds to plakoglobin and clusters desmosomal cadherin-plakoglobin complexes. *J Cell Biol*. 1997;139(3):773-84.
143. Kouklis PD, Hutton E, Fuchs E. Making a connection: direct binding between keratin intermediate filaments and desmosomal proteins. *J Cell Biol*. 1994;127(4):1049-60.
144. Stappenbeck TS, Bornslaeger EA, Corcoran CM, Luu HH, Virata ML, Green KJ. Functional analysis of desmoplakin domains: specification of the interaction with keratin versus vimentin intermediate filament networks. *J Cell Biol*. 1993;123(3):691-705.
145. Angst BD, Nilles LA, Green KJ. Desmoplakin II expression is not restricted to stratified epithelia. *J Cell Sci*. 1990;97 (Pt 2):247-57.

146. Klein-Szanto AJ. Stereologic baseline data of normal human epidermis. *J Invest Dermatol.* 1977;68(2):73-8.
147. Kartenbeck J, Franke WW, Moser JG, Stoffels U. Specific attachment of desmin filaments to desmosomal plaques in cardiac myocytes. *EMBO J.* 1983;2(5):735-42.
148. Kartenbeck J, Schwechheimer K, Moll R, Franke WW. Attachment of vimentin filaments to desmosomal plaques in human meningioma cells and arachnoidal tissue. *J Cell Biol.* 1984;98(3):1072-81.
149. Valiron O, Chevrier V, Usson Y, Breviario F, Job D, Dejana E. Desmoplakin expression and organization at human umbilical vein endothelial cell-to-cell junctions. *J Cell Sci.* 1996;109 (Pt 8):2141-9.
150. Calkins CC, Hoepner BL, Law CM, Novak MR, Setzer SV, Hatzfeld M, et al. The Armadillo family protein p0071 is a VE-cadherin- and desmoplakin-binding protein. *The Journal of biological chemistry.* 2003;278(3):1774-83.
151. Kowalczyk AP, Navarro P, Dejana E, Bornslaeger EA, Green KJ, Kopp DS, et al. VE-cadherin and desmoplakin are assembled into dermal microvascular endothelial intercellular junctions: a pivotal role for plakoglobin in the recruitment of desmoplakin to intercellular junctions. *J Cell Sci.* 1998;111 (Pt 20):3045-57.
152. Gallicano GI, Kouklis P, Bauer C, Yin M, Vasioukhin V, Degenstein L, et al. Desmoplakin is required early in development for assembly of desmosomes and cytoskeletal linkage. *J Cell Biol.* 1998;143(7):2009-22.
153. Vasioukhin V, Bowers E, Bauer C, Degenstein L, Fuchs E. Desmoplakin is essential in epidermal sheet formation. *Nat Cell Biol.* 2001;3(12):1076-85.

154. Leung CL, Green KJ, Liem RK. Plakins: a family of versatile cytolinker proteins. *Trends Cell Biol.* 2002;12(1):37-45.
155. Stappenbeck TS, Green KJ. The desmoplakin carboxyl terminus coaligns with and specifically disrupts intermediate filament networks when expressed in cultured cells. *J Cell Biol.* 1992;116(5):1197-209.
156. Bornslaeger EA, Corcoran CM, Stappenbeck TS, Green KJ. Breaking the connection: displacement of the desmosomal plaque protein desmoplakin from cell-cell interfaces disrupts anchorage of intermediate filament bundles and alters intercellular junction assembly. *J Cell Biol.* 1996;134(4):985-1001.
157. Rampazzo A, Nava A, Malacrida S, Beffagna G, Baucé B, Rossi V, et al. Mutation in human desmoplakin domain binding to plakoglobin causes a dominant form of arrhythmogenic right ventricular cardiomyopathy. *Am J Hum Genet.* 2002;71(5):1200-6.
158. Norgett EE, Hatsell SJ, Carvajal-Huerta L, Cabezas JC, Common J, Purkis PE, et al. Recessive mutation in desmoplakin disrupts desmoplakin-intermediate filament interactions and causes dilated cardiomyopathy, woolly hair and keratoderma. *Hum Mol Genet.* 2000;9(18):2761-6.
159. Whittock NV, Ashton GH, Dopping-Hepenstal PJ, Gratian MJ, Keane FM, Eady RA, et al. Striate palmoplantar keratoderma resulting from desmoplakin haploinsufficiency. *J Invest Dermatol.* 1999;113(6):940-6.
160. Wan H, Dopping-Hepenstal PJ, Gratian MJ, Stone MG, Zhu G, Purkis PE, et al. Striate palmoplantar keratoderma arising from desmoplakin and desmoglein 1 mutations is associated with contrasting perturbations of desmosomes and the keratin filament network. *Br J Dermatol.* 2004;150(5):878-91.

161. Jonkman MF, Pasmooij AM, Pasmans SG, van den Berg MP, Ter Horst HJ, Timmer A, et al. Loss of desmoplakin tail causes lethal acantholytic epidermolysis bullosa. *Am J Hum Genet.* 2005;77(4):653-60.
162. Molho-Pessach V, Sheffer S, Siam R, Tams S, Siam I, Awwad R, et al. Two Novel Homozygous Desmoplakin Mutations in Carvajal Syndrome. *Pediatr Dermatol.* 2015.
163. Oursler JR, Labib RS, Ariss-Abdo L, Burke T, O'Keefe EJ, Anhalt GJ. Human autoantibodies against desmoplakins in paraneoplastic pemphigus. *J Clin Invest.* 1992;89(6):1775-82.
164. Kowalczyk AP, Hatzfeld M, Bornslaeger EA, Kopp DS, Borgwardt JE, Corcoran CM, et al. The head domain of plakophilin-1 binds to desmoplakin and enhances its recruitment to desmosomes. Implications for cutaneous disease. *The Journal of biological chemistry.* 1999;274(26):18145-8.
165. Nei H, Saito T, Tobioka H, Itoh E, Mori M, Kudo R. Expression of component desmosomal proteins in uterine endometrial carcinoma and their relation to cellular differentiation. *Cancer.* 1996;78(3):461-70.
166. Hiraki A, Shinohara M, Ikebe T, Nakamura S, Kurahara S, Garrod DR. Immunohistochemical staining of desmosomal components in oral squamous cell carcinomas and its association with tumour behaviour. *Br J Cancer.* 1996;73(12):1491-7.
167. Davies EL, Gee JM, Cochrane RA, Jiang WG, Sharma AK, Nicholson RI, et al. The immunohistochemical expression of desmoplakin and its role in vivo in the progression and metastasis of breast cancer. *Eur J Cancer.* 1999;35(6):902-7.

168. Yang L, Chen Y, Cui T, Knosel T, Zhang Q, Albring KF, et al. Desmoplakin acts as a tumor suppressor by inhibition of the Wnt/beta-catenin signaling pathway in human lung cancer. *Carcinogenesis*. 2012;33(10):1863-70.
169. Wan H, South AP, Hart IR. Increased keratinocyte proliferation initiated through downregulation of desmoplakin by RNA interference. *Exp Cell Res*. 2007;313(11):2336-44.
170. Riggelman B, Wieschaus E, Schedl P. Molecular analysis of the armadillo locus: uniformly distributed transcripts and a protein with novel internal repeats are associated with a *Drosophila* segment polarity gene. *Genes Dev*. 1989;3(1):96-113.
171. Wieschaus E, Riggelman R. Autonomous requirements for the segment polarity gene armadillo during *Drosophila* embryogenesis. *Cell*. 1987;49(2):177-84.
172. Orsulic S, Peifer M. An in vivo structure-function study of armadillo, the beta-catenin homologue, reveals both separate and overlapping regions of the protein required for cell adhesion and for wingless signaling. *J Cell Biol*. 1996;134(5):1283-300.
173. Huber AH, Nelson WJ, Weis WI. Three-dimensional structure of the armadillo repeat region of beta-catenin. *Cell*. 1997;90(5):871-82.
174. Cowin P, Kapprell HP, Franke WW, Tamkun J, Hynes RO. Plakoglobin: a protein common to different kinds of intercellular adhering junctions. *Cell*. 1986;46(7):1063-73.
175. Ozawa M, Baribault H, Kemler R. The cytoplasmic domain of the cell adhesion molecule uvomorulin associates with three independent proteins structurally related in different species. *EMBO J*. 1989;8(6):1711-7.
176. McCrea PD, Turck CW, Gumbiner B. A homolog of the armadillo protein in *Drosophila* (plakoglobin) associated with E-cadherin. *Science*. 1991;254(5036):1359-61.

177. Knudsen KA, Wheelock MJ. Plakoglobin, or an 83-kD homologue distinct from beta-catenin, interacts with E-cadherin and N-cadherin. *J Cell Biol.* 1992;118(3):671-9.
178. Sacco PA, McGranahan TM, Wheelock MJ, Johnson KR. Identification of plakoglobin domains required for association with N-cadherin and alpha-catenin. *The Journal of biological chemistry.* 1995;270(34):20201-6.
179. Cowin P, Garrod DR. Antibodies to epithelial desmosomes show wide tissue and species cross-reactivity. *Nature.* 1983;302(5904):148-50.
180. Mathur M, Goodwin L, Cowin P. Interactions of the cytoplasmic domain of the desmosomal cadherin Dsg1 with plakoglobin. *The Journal of biological chemistry.* 1994;269(19):14075-80.
181. Korman NJ, Eyre RW, Klaus-Kovtun V, Stanley JR. Demonstration of an adhering-junction molecule (plakoglobin) in the autoantigens of pemphigus foliaceus and pemphigus vulgaris. *N Engl J Med.* 1989;321(10):631-5.
182. Fouquet B, Zimbelmann R, Franke WW. Identification of plakoglobin in oocytes and early embryos of *Xenopus laevis*: maternal expression of a gene encoding a junctional plaque protein. *Differentiation; research in biological diversity.* 1992;51(3):187-94.
183. Wahl JK, Sacco PA, McGranahan-Sadler TM, Sauppe LM, Wheelock MJ, Johnson KR. Plakoglobin domains that define its association with the desmosomal cadherins and the classical cadherins: identification of unique and shared domains. *J Cell Sci.* 1996;109 (Pt 5):1143-54.
184. Rubinfeld B, Souza B, Albert I, Munemitsu S, Polakis P. The APC protein and E-cadherin form similar but independent complexes with alpha-catenin, beta-catenin, and plakoglobin. *The Journal of biological chemistry.* 1995;270(10):5549-55.

185. Ozawa M, Terada H, Pedraza C. The fourth armadillo repeat of plakoglobin (gamma-catenin) is required for its high affinity binding to the cytoplasmic domains of E-cadherin and desmosomal cadherin Dsg2, and the tumor suppressor APC protein. *J Biochem.* 1995;118(5):1077-82.
186. Miravet S, Piedra J, Miro F, Itarte E, Garcia de Herreros A, Dunach M. The transcriptional factor Tcf-4 contains different binding sites for beta-catenin and plakoglobin. *The Journal of biological chemistry.* 2002;277(3):1884-91.
187. Ishiko A, Matsunaga Y, Masunaga T, Aiso S, Nishikawa T, Shimizu H. Immunomolecular mapping of adherens junction and desmosomal components in normal human epidermis. *Exp Dermatol.* 2003;12(6):747-54.
188. Bierkamp C, McLaughlin KJ, Schwarz H, Huber O, Kemler R. Embryonic heart and skin defects in mice lacking plakoglobin. *Dev Biol.* 1996;180(2):780-5.
189. Bierkamp C, Schwarz H, Huber O, Kemler R. Desmosomal localization of beta-catenin in the skin of plakoglobin null-mutant mice. *Development.* 1999;126(2):371-81.
190. Acehan D, Petzold C, Gumper I, Sabatini DD, Muller EJ, Cowin P, et al. Plakoglobin is required for effective intermediate filament anchorage to desmosomes. *J Invest Dermatol.* 2008;128(11):2665-75.
191. Lewis JE, Wahl JK, 3rd, Sass KM, Jensen PJ, Johnson KR, Wheelock MJ. Cross-talk between adherens junctions and desmosomes depends on plakoglobin. *J Cell Biol.* 1997;136(4):919-34.
192. Lombardi R, da Graca Cabreira-Hansen M, Bell A, Fromm RR, Willerson JT, Marian AJ. Nuclear plakoglobin is essential for differentiation of cardiac progenitor cells to adipocytes in arrhythmogenic right ventricular cardiomyopathy. *Circ Res.* 2011;109(12):1342-53.

193. McKoy G, Protonotarios N, Crosby A, Tsatsopoulou A, Anastasakis A, Coonar A, et al. Identification of a deletion in plakoglobin in arrhythmogenic right ventricular cardiomyopathy with palmoplantar keratoderma and woolly hair (Naxos disease). *Lancet*. 2000;355(9221):2119-24.
194. Asimaki A, Syrris P, Wichter T, Matthias P, Saffitz JE, McKenna WJ. A novel dominant mutation in plakoglobin causes arrhythmogenic right ventricular cardiomyopathy. *Am J Hum Genet*. 2007;81(5):964-73.
195. Erken H, Yariz KO, Duman D, Kaya CT, Sayin T, Heper AO, et al. Cardiomyopathy with alopecia and palmoplantar keratoderma (CAPK) is caused by a JUP mutation. *Br J Dermatol*. 2011;165(4):917-21.
196. Pigors M, Kiritsi D, Krumpelmann S, Wagner N, He Y, Podda M, et al. Lack of plakoglobin leads to lethal congenital epidermolysis bullosa: a novel clinico-genetic entity. *Hum Mol Genet*. 2011;20(9):1811-9.
197. Caldelari R, de Bruin A, Baumann D, Suter MM, Bierkamp C, Balmer V, et al. A central role for the armadillo protein plakoglobin in the autoimmune disease pemphigus vulgaris. *J Cell Biol*. 2001;153(4):823-34.
198. de Bruin A, Caldelari R, Williamson L, Suter MM, Hunziker T, Wyder M, et al. Plakoglobin-dependent disruption of the desmosomal plaque in pemphigus vulgaris. *Exp Dermatol*. 2007;16(6):468-75.
199. Aktary Z, Pasdar M. Plakoglobin: role in tumorigenesis and metastasis. *Int J Cell Biol*. 2012;2012:189521.
200. Cerrato A, Fulciniti F, Avallone A, Benincasa G, Palombini L, Grieco M. Beta- and gamma-catenin expression in thyroid carcinomas. *J Pathol*. 1998;185(3):267-72.

201. Rieger-Christ KM, Ng L, Hanley RS, Durrani O, Ma H, Yee AS, et al. Restoration of plakoglobin expression in bladder carcinoma cell lines suppresses cell migration and tumorigenic potential. *Br J Cancer*. 2005;92(12):2153-9.
202. Syrigos KN, Harrington K, Waxman J, Krausz T, Pignatelli M. Altered gamma-catenin expression correlates with poor survival in patients with bladder cancer. *J Urol*. 1998;160(5):1889-93.
203. Amitay R, Nass D, Meitar D, Goldberg I, Davidson B, Trakhtenbrot L, et al. Reduced expression of plakoglobin correlates with adverse outcome in patients with neuroblastoma. *Am J Pathol*. 2001;159(1):43-9.
204. Pantel K, Passlick B, Vogt J, Stosiek P, Angstwurm M, Seen-Hibler R, et al. Reduced expression of plakoglobin indicates an unfavorable prognosis in subsets of patients with non-small-cell lung cancer. *J Clin Oncol*. 1998;16(4):1407-13.
205. Ueda G, Sunakawa H, Nakamori K, Shinya T, Tshako W, Tamura Y, et al. Aberrant expression of beta- and gamma-catenin is an independent prognostic marker in oral squamous cell carcinoma. *Int J Oral Maxillofac Surg*. 2006;35(4):356-61.
206. Breault JE, Shiina H, Igawa M, Ribeiro-Filho LA, Deguchi M, Enokida H, et al. Methylation of the gamma-catenin gene is associated with poor prognosis of renal cell carcinoma. *Clin Cancer Res*. 2005;11(2 Pt 1):557-64.
207. Shiina H, Breault JE, Basset WW, Enokida H, Urakami S, Li LC, et al. Functional Loss of the gamma-catenin gene through epigenetic and genetic pathways in human prostate cancer. *Cancer Res*. 2005;65(6):2130-8.

208. Aberle H, Bierkamp C, Torchard D, Serova O, Wagner T, Natt E, et al. The human plakoglobin gene localizes on chromosome 17q21 and is subjected to loss of heterozygosity in breast and ovarian cancers. *Proc Natl Acad Sci U S A*. 1995;92(14):6384-8.
209. Winn RA, Bremnes RM, Bemis L, Franklin WA, Miller YE, Cool C, et al. gamma-Catenin expression is reduced or absent in a subset of human lung cancers and re-expression inhibits transformed cell growth. *Oncogene*. 2002;21(49):7497-506.
210. Grossmann KS, Grund C, Huelsken J, Behrend M, Erdmann B, Franke WW, et al. Requirement of plakophilin 2 for heart morphogenesis and cardiac junction formation. *J Cell Biol*. 2004;167(1):149-60.
211. Sklyarova T, Bonne S, D'Hooge P, Denecker G, Goossens S, De Rycke R, et al. Plakophilin-3-deficient mice develop hair coat abnormalities and are prone to cutaneous inflammation. *J Invest Dermatol*. 2008;128(6):1375-85.
212. McGrath JA, Hoeger PH, Christiano AM, McMillan JR, Mellerio JE, Ashton GH, et al. Skin fragility and hypohidrotic ectodermal dysplasia resulting from ablation of plakophilin 1. *Br J Dermatol*. 1999;140(2):297-307.
213. McGrath JA, McMillan JR, Shemanko CS, Runswick SK, Leigh IM, Lane EB, et al. Mutations in the plakophilin 1 gene result in ectodermal dysplasia/skin fragility syndrome. *Nat Genet*. 1997;17(2):240-4.
214. Gerull B, Heuser A, Wichter T, Paul M, Basson CT, McDermott DA, et al. Mutations in the desmosomal protein plakophilin-2 are common in arrhythmogenic right ventricular cardiomyopathy. *Nat Genet*. 2004;36(11):1162-4.
215. Lambert J, Bracke S, van Roy F, Pas HH, Bonne S, De Schepper S. Serum plakophilin-3 autoreactivity in paraneoplastic pemphigus. *Br J Dermatol*. 2010;163(3):630-2.

216. Anastasiadis PZ, Reynolds AB. The p120 catenin family: complex roles in adhesion, signaling and cancer. *J Cell Sci.* 2000;113 (Pt 8):1319-34.
217. Bass-Zubek AE, Godsel LM, Delmar M, Green KJ. Plakophilins: multifunctional scaffolds for adhesion and signaling. *Current opinion in cell biology.* 2009;21(5):708-16.
218. Mertens C, Kuhn C, Franke WW. Plakophilins 2a and 2b: constitutive proteins of dual location in the karyoplasm and the desmosomal plaque. *J Cell Biol.* 1996;135(4):1009-25.
219. Hatzfeld M, Kristjansson GI, Plessmann U, Weber K. Band 6 protein, a major constituent of desmosomes from stratified epithelia, is a novel member of the armadillo multigene family. *J Cell Sci.* 1994;107 (Pt 8):2259-70.
220. Schmidt A, Langbein L, Pratzel S, Rode M, Rackwitz HR, Franke WW. Plakophilin 3--a novel cell-type-specific desmosomal plaque protein. *Differentiation; research in biological diversity.* 1999;64(5):291-306.
221. Hatzfeld M, Nachtsheim C. Cloning and characterization of a new armadillo family member, p0071, associated with the junctional plaque: evidence for a subfamily of closely related proteins. *J Cell Sci.* 1996;109 (Pt 11):2767-78.
222. Choi HJ, Weis WI. Structure of the armadillo repeat domain of plakophilin 1. *J Mol Biol.* 2005;346(1):367-76.
223. Schwarz J, Ayim A, Schmidt A, Jager S, Koch S, Baumann R, et al. Differential expression of desmosomal plakophilins in various types of carcinomas: correlation with cell type and differentiation. *Human pathology.* 2006;37(5):613-22.
224. Breuninger S, Reidenbach S, Sauer CG, Strobel P, Pfitzenmaier J, Trojan L, et al. Desmosomal plakophilins in the prostate and prostatic adenocarcinomas: implications for diagnosis and tumor progression. *Am J Pathol.* 2010;176(5):2509-19.

225. Takahashi H, Nakatsuji H, Takahashi M, Avirmed S, Fukawa T, Takemura M, et al. Up-regulation of plakophilin-2 and Down-regulation of plakophilin-3 are correlated with invasiveness in bladder cancer. *Urology*. 2012;79(1):240 e1-8.
226. Arimoto K, Burkart C, Yan M, Ran D, Weng S, Zhang DE. Plakophilin-2 promotes tumor development by enhancing ligand-dependent and -independent epidermal growth factor receptor dimerization and activation. *Molecular and cellular biology*. 2014;34(20):3843-54.
227. Demirag GG, Sullu Y, Gurgenyatagi D, Okumus NO, Yucel I. Expression of plakophilins (PKP1, PKP2, and PKP3) in gastric cancers. *Diagn Pathol*. 2011;6:1.
228. Demirag GG, Sullu Y, Yucel I. Expression of Plakophilins (PKP1, PKP2, and PKP3) in breast cancers. *Med Oncol*. 2012;29(3):1518-22.
229. Furukawa C, Daigo Y, Ishikawa N, Kato T, Ito T, Tsuchiya E, et al. Plakophilin 3 oncogene as prognostic marker and therapeutic target for lung cancer. *Cancer Res*. 2005;65(16):7102-10.
230. Papagerakis S, Shabana AH, Depondt J, Gehanno P, Forest N. Immunohistochemical localization of plakophilins (PKP1, PKP2, PKP3, and p0071) in primary oropharyngeal tumors: correlation with clinical parameters. *Human pathology*. 2003;34(6):565-72.
231. Aigner K, Descovich L, Mikula M, Sultan A, Dampier B, Bonne S, et al. The transcription factor ZEB1 (deltaEF1) represses Plakophilin 3 during human cancer progression. *FEBS letters*. 2007;581(8):1617-24.
232. Khapare N, Kundu ST, Sehgal L, Sawant M, Priya R, Gosavi P, et al. Plakophilin3 Loss Leads to an Increase in PRL3 Levels Promoting K8 Dephosphorylation, Which Is Required for Transformation and Metastasis. *PLoS One*. 2012;7(6):e38561.

233. Kundu ST, Gosavi P, Khapare N, Patel R, Hosing AS, Maru GB, et al. Plakophilin3 downregulation leads to a decrease in cell adhesion and promotes metastasis. *International journal of cancer*. 2008;123(10):2303-14.
234. Schmidt A, Langbein L, Rode M, Pratzel S, Zimbelmann R, Franke WW. Plakophilins 1a and 1b: widespread nuclear proteins recruited in specific epithelial cells as desmosomal plaque components. *Cell Tissue Res*. 1997;290(3):481-99.
235. Kapprell HP, Owaribe K, Franke WW. Identification of a basic protein of Mr 75,000 as an accessory desmosomal plaque protein in stratified and complex epithelia. *J Cell Biol*. 1988;106(5):1679-91.
236. Sobolik-Delmaire T, Katafiasz D, Wahl JK, 3rd. Carboxyl terminus of Plakophilin-1 recruits it to plasma membrane, whereas amino terminus recruits desmoplakin and promotes desmosome assembly. *The Journal of biological chemistry*. 2006;281(25):16962-70.
237. Hatzfeld M, Haffner C, Schulze K, Vinzens U. The function of plakophilin 1 in desmosome assembly and actin filament organization. *J Cell Biol*. 2000;149(1):209-22.
238. Sobolik-Delmaire T, Reddy R, Pashaj A, Roberts BJ, Wahl JK, 3rd. Plakophilin-1 localizes to the nucleus and interacts with single-stranded DNA. *J Invest Dermatol*. 2010;130(11):2638-46.
239. Hofmann I, Casella M, Schnolzer M, Schlechter T, Spring H, Franke WW. Identification of the junctional plaque protein plakophilin 3 in cytoplasmic particles containing RNA-binding proteins and the recruitment of plakophilins 1 and 3 to stress granules. *Molecular biology of the cell*. 2006;17(3):1388-98.

240. Wolf A, Krause-Gruszczynska M, Birkenmeier O, Ostareck-Lederer A, Huttelmaier S, Hatzfeld M. Plakophilin 1 stimulates translation by promoting eIF4A1 activity. *J Cell Biol.* 2010;188(4):463-71.
241. Mertens C, Kuhn C, Moll R, Schwetlick I, Franke WW. Desmosomal plakophilin 2 as a differentiation marker in normal and malignant tissues. *Differentiation; research in biological diversity.* 1999;64(5):277-90.
242. Bass-Zubek AE, Hobbs RP, Amargo EV, Garcia NJ, Hsieh SN, Chen X, et al. Plakophilin 2: a critical scaffold for PKC alpha that regulates intercellular junction assembly. *J Cell Biol.* 2008;181(4):605-13.
243. Muller J, Ritt DA, Copeland TD, Morrison DK. Functional analysis of C-TAK1 substrate binding and identification of PKP2 as a new C-TAK1 substrate. *EMBO J.* 2003;22(17):4431-42.
244. Mertens C, Hofmann I, Wang Z, Teichmann M, Sepehri Chong S, Schnolzer M, et al. Nuclear particles containing RNA polymerase III complexes associated with the junctional plaque protein plakophilin 2. *Proc Natl Acad Sci U S A.* 2001;98(14):7795-800.
245. Muhmer M, Ditthardt D, Jakel J, Wischmann V, Moll R, Schmidt A. An alternative promoter of the human plakophilin-3 gene controls the expression of the new isoform PKP3b. *Cell Tissue Res.* 2014;355(1):143-62.
246. Bonne S, Gilbert B, Hatzfeld M, Chen X, Green KJ, van Roy F. Defining desmosomal plakophilin-3 interactions. *J Cell Biol.* 2003;161(2):403-16.
247. Martinez-Palomo A, Meza I, Beaty G, Cereijido M. Experimental modulation of occluding junctions in a cultured transporting epithelium. *J Cell Biol.* 1980;87(3 Pt 1):736-45.

248. Windoffer R, Borchert-Stuhltrager M, Leube RE. Desmosomes: interconnected calcium-dependent structures of remarkable stability with significant integral membrane protein turnover. *J Cell Sci.* 2002;115(Pt 8):1717-32.
249. Kartenbeck J, Haselmann U, Gassler N. Synthesis of junctional proteins in metastasizing colon cancer cells. *Eur J Cell Biol.* 2005;84(2-3):417-30.
250. Gosavi P, Kundu ST, Khapare N, Sehgal L, Karkhanis MS, Dalal SN. E-cadherin and plakoglobin recruit plakophilin3 to the cell border to initiate desmosome assembly. *Cell Mol Life Sci.* 2011;68(8):1439-54.
251. D'Silva NJ, Mitra RS, Zhang Z, Kurnit DM, Babcock CR, Polverini PJ, et al. Rap1, a small GTP-binding protein is upregulated during arrest of proliferation in human keratinocytes. *J Cell Physiol.* 2003;196(3):532-40.
252. Todorovic V, Koetsier JL, Godsel LM, Green KJ. Plakophilin 3 mediates Rap1-dependent desmosome assembly and adherens junction maturation. *Molecular biology of the cell.* 2014;25(23):3749-64.
253. Cirillo N, AlShwaimi E, McCullough M, Prime SS. Pemphigus vulgaris autoimmune globulin induces Src-dependent tyrosine-phosphorylation of plakophilin 3 and its detachment from desmoglein 3. *Autoimmunity.* 2014;47(2):134-40.
254. Neuber S, Jager S, Meyer M, Wischmann V, Koch PJ, Moll R, et al. c-Src mediated tyrosine phosphorylation of plakophilin 3 as a new mechanism to control desmosome composition in cells exposed to oxidative stress. *Cell Tissue Res.* 2015;359(3):799-816.
255. Chernyavsky AI, Arredondo J, Kitajima Y, Sato-Nagai M, Grando SA. Desmoglein versus non-desmoglein signaling in pemphigus acantholysis: characterization of novel signaling

pathways downstream of pemphigus vulgaris antigens. *The Journal of biological chemistry*. 2007;282(18):13804-12.

256. Sanchez-Carpintero I, Espana A, Pelacho B, Lopez Moratalla N, Rubenstein DS, Diaz LA, et al. In vivo blockade of pemphigus vulgaris acantholysis by inhibition of intracellular signal transduction cascades. *Br J Dermatol*. 2004;151(3):565-70.

257. Kundu ST. Regulation of G2/M DNA damage checkpoint and neoplastic progression by 14-3-3 sigma and plakophilin3. PhD.Thesis. Advanced Centre for Treatment Research and Education in Cancer (ACTREC), Cancer Research Institute (CRI), Navi Mumbai.

[PhD thesis]. 1: 1; 2009.

258. Gosavi P. The role of plakophilin3 in regulating cellular response to DNA damage: consequences for neoplastic progression. PhD.Thesis. Advanced Centre for Treatment Research and Education in Cancer (ACTREC), Cancer Research Institute (CRI), Navi Mumbai. [Ph.D. Thesis]. 1: 1; 2010.

259. Franke WW, Schiller DL, Hatzfeld M, Winter S. Protein complexes of intermediate-sized filaments: melting of cytokeratin complexes in urea reveals different polypeptide separation characteristics. *Proc Natl Acad Sci U S A*. 1983;80(23):7113-7.

260. Steinert PM, Gullino MI. Bovine epidermal keratin filament assembly in vitro. *Biochem Biophys Res Commun*. 1976;70(1):221-7.

261. Steinert PM, Idler WW, Zimmerman SB. Self-assembly of bovine epidermal keratin filaments in vitro. *J Mol Biol*. 1976;108(3):547-67.

262. Moll R, Franke WW, Schiller DL, Geiger B, Krepler R. The catalog of human cytokeratins: patterns of expression in normal epithelia, tumors and cultured cells. *Cell*. 1982;31(1):11-24.

263. Hendrix MJ, Seftor EA, Chu YW, Trevor KT, Seftor RE. Role of intermediate filaments in migration, invasion and metastasis. *Cancer Metastasis Rev.* 1996;15(4):507-25.
264. Larcher F, Bauluz C, Diaz-Guerra M, Quintanilla M, Conti CJ, Ballestin C, et al. Aberrant expression of the simple epithelial type II keratin 8 by mouse skin carcinomas but not papillomas. *Mol Carcinog.* 1992;6(2):112-21.
265. Oshima RG, Baribault H, Caulin C. Oncogenic regulation and function of keratins 8 and 18. *Cancer Metastasis Rev.* 1996;15(4):445-71.
266. Vaidya MM, Borges AM, Pradhan SA, Bhisey AN. Cytokeratin expression in squamous cell carcinomas of the tongue and alveolar mucosa. *Eur J Cancer B Oral Oncol.* 1996;32B(5):333-6.
267. Schaafsma HE, Van Der Velden LA, Manni JJ, Peters H, Link M, Rutter DJ, et al. Increased expression of cytokeratins 8, 18 and vimentin in the invasion front of mucosal squamous cell carcinoma. *J Pathol.* 1993;170(1):77-86.
268. Fillies T, Werkmeister R, Packeisen J, Brandt B, Morin P, Weingart D, et al. Cytokeratin 8/18 expression indicates a poor prognosis in squamous cell carcinomas of the oral cavity. *BMC Cancer.* 2006;6:10.
269. Ku NO, Omary MB. Keratins turn over by ubiquitination in a phosphorylation-modulated fashion. *J Cell Biol.* 2000;149(3):547-52.
270. Woll S, Windoffer R, Leube RE. p38 MAPK-dependent shaping of the keratin cytoskeleton in cultured cells. *J Cell Biol.* 2007;177(5):795-807.
271. Mizuuchi E, Semba S, Kodama Y, Yokozaki H. Down-modulation of keratin 8 phosphorylation levels by PRL-3 contributes to colorectal carcinoma progression. *International journal of cancer.* 2009;124(8):1802-10.

272. Kato H, Semba S, Miskad UA, Seo Y, Kasuga M, Yokozaki H. High expression of PRL-3 promotes cancer cell motility and liver metastasis in human colorectal cancer: a predictive molecular marker of metachronous liver and lung metastases. *Clin Cancer Res.* 2004;10(21):7318-28.
273. Bardelli A, Saha S, Sager JA, Romans KE, Xin B, Markowitz SD, et al. PRL-3 expression in metastatic cancers. *Clin Cancer Res.* 2003;9(15):5607-15.
274. Jiang Y, Liu XQ, Rajput A, Geng L, Ongchin M, Zeng Q, et al. Phosphatase PRL-3 is a direct regulatory target of TGFbeta in colon cancer metastasis. *Cancer Res.* 2011;71(1):234-44.
275. Saha S, Bardelli A, Buckhaults P, Velculescu VE, Rago C, St Croix B, et al. A phosphatase associated with metastasis of colorectal cancer. *Science.* 2001;294(5545):1343-6.
276. Zimmerman MW, Homanics GE, Lazo JS. Targeted deletion of the metastasis-associated phosphatase Ptp4a3 (PRL-3) suppresses murine colon cancer. *PLoS One.* 2013;8(3):e58300.
277. Fischer-Keso R, Breuninger S, Hofmann S, Henn M, Rohrig T, Strobel P, et al. Plakophilins 1 and 3 bind to FXR1 and thereby influence the mRNA stability of desmosomal proteins. *Molecular and cellular biology.* 2014.
278. Baskar R, Lee KA, Yeo R, Yeoh KW. Cancer and radiation therapy: current advances and future directions. *Int J Med Sci.* 2012;9(3):193-9.
279. Touboul E, Buffat L, Belkacemi Y, Lefranc JP, Uzan S, Lhuillier P, et al. Local recurrences and distant metastases after breast-conserving surgery and radiation therapy for early breast cancer. *Int J Radiat Oncol Biol Phys.* 1999;43(1):25-38.
280. Huber SM, Butz L, Stegen B, Klumpp D, Braun N, Ruth P, et al. Ionizing radiation, ion transports, and radioresistance of cancer cells. *Frontiers in physiology.* 2013;4:212.

281. Calautti E, Cabodi S, Stein PL, Hatzfeld M, Kedersha N, Paolo Dotto G. Tyrosine phosphorylation and src family kinases control keratinocyte cell-cell adhesion. *J Cell Biol.* 1998;141(6):1449-65.
282. Schae D, McBride WH. Counteracting tumor radioresistance by targeting DNA repair. *Molecular cancer therapeutics.* 2005;4(10):1548-50.
283. Gerweck LE, Vijayappa S, Kurimasa A, Ogawa K, Chen DJ. Tumor cell radiosensitivity is a major determinant of tumor response to radiation. *Cancer Res.* 2006;66(17):8352-5.
284. Weichselbaum RR. Radioresistant and repair proficient cells may determine radiocurability in human tumors. *Int J Radiat Oncol Biol Phys.* 1986;12(4):637-9.
285. Weichselbaum RR, Dahlberg W, Little JB. Inherently radioresistant cells exist in some human tumors. *Proc Natl Acad Sci U S A.* 1985;82(14):4732-5.
286. Weichselbaum RR, Little JB. The differential response of human tumours to fractionated radiation may be due to a post-irradiation repair process. *Br J Cancer.* 1982;46(4):532-7.
287. Yang J, Yu Y, Hamrick HE, Duerksen-Hughes PJ. ATM, ATR and DNA-PK: initiators of the cellular genotoxic stress responses. *Carcinogenesis.* 2003;24(10):1571-80.
288. Kastan MB, Bartek J. Cell-cycle checkpoints and cancer. *Nature.* 2004;432(7015):316-23.
289. Abraham RT. Cell cycle checkpoint signaling through the ATM and ATR kinases. *Genes Dev.* 2001;15(17):2177-96.
290. Hartwell LH, Weinert TA. Checkpoints: controls that ensure the order of cell cycle events. *Science.* 1989;246(4930):629-34.

291. Kuhne C, Tjornhammar ML, Pongor S, Banks L, Simoncsits A. Repair of a minimal DNA double-strand break by NHEJ requires DNA-PKcs and is controlled by the ATM/ATR checkpoint. *Nucleic Acids Res.* 2003;31(24):7227-37.
292. Serrano MA, Li Z, Dangeti M, Musich PR, Patrick S, Roginskaya M, et al. DNA-PK, ATM and ATR collaboratively regulate p53-RPA interaction to facilitate homologous recombination DNA repair. *Oncogene.* 2013;32(19):2452-62.
293. Smith J, Tho LM, Xu N, Gillespie DA. The ATM-Chk2 and ATR-Chk1 pathways in DNA damage signaling and cancer. *Adv Cancer Res.* 2010;108:73-112.
294. San Filippo J, Sung P, Klein H. Mechanism of eukaryotic homologous recombination. *Annu Rev Biochem.* 2008;77:229-57.
295. Branzei D, Foiani M. Regulation of DNA repair throughout the cell cycle. *Nat Rev Mol Cell Biol.* 2008;9(4):297-308.
296. Weterings E, Chen DJ. The endless tale of non-homologous end-joining. *Cell Res.* 2008;18(1):114-24.
297. Thompson LH. Recognition, signaling, and repair of DNA double-strand breaks produced by ionizing radiation in mammalian cells: the molecular choreography. *Mutat Res.* 2012;751(2):158-246.
298. Sinclair WK, Morton RA. Variations in X-Ray Response during the Division Cycle of Partially Synchronized Chinese Hamster Cells in Culture. *Nature.* 1963;199:1158-60.
299. Kuwahara Y, Li L, Baba T, Nakagawa H, Shimura T, Yamamoto Y, et al. Clinically relevant radioresistant cells efficiently repair DNA double-strand breaks induced by X-rays. *Cancer science.* 2009;100(4):747-52.

300. Fischer U, Meese E. Glioblastoma multiforme: the role of DSB repair between genotype and phenotype. *Oncogene*. 2007;26(56):7809-15.
301. Ayanian JZ, Zaslavsky AM, Fuchs CS, Guadagnoli E, Creech CM, Cress RD, et al. Use of adjuvant chemotherapy and radiation therapy for colorectal cancer in a population-based cohort. *J Clin Oncol*. 2003;21(7):1293-300.
302. Lim YC, Roberts TL, Day BW, Harding A, Kozlov S, Kijas AW, et al. A role for homologous recombination and abnormal cell-cycle progression in radioresistance of glioma-initiating cells. *Molecular cancer therapeutics*. 2012;11(9):1863-72.
303. Bao S, Wu Q, McLendon RE, Hao Y, Shi Q, Hjelmeland AB, et al. Glioma stem cells promote radioresistance by preferential activation of the DNA damage response. *Nature*. 2006;444(7120):756-60.
304. Mao Z, Jiang Y, Liu X, Seluanov A, Gorbunova V. DNA repair by homologous recombination, but not by nonhomologous end joining, is elevated in breast cancer cells. *Neoplasia*. 2009;11(7):683-91.
305. Rothkamm K, Kruger I, Thompson LH, Lobrich M. Pathways of DNA double-strand break repair during the mammalian cell cycle. *Molecular and cellular biology*. 2003;23(16):5706-15.
306. Chowdhury D, Choi YE, Brault ME. Charity begins at home: non-coding RNA functions in DNA repair. *Nat Rev Mol Cell Biol*. 2013;14(3):181-9.
307. Liang K, Ang KK, Milas L, Hunter N, Fan Z. The epidermal growth factor receptor mediates radioresistance. *Int J Radiat Oncol Biol Phys*. 2003;57(1):246-54.

308. Yu D, Watanabe H, Shibuya H, Miura M. Redundancy of radioresistant signaling pathways originating from insulin-like growth factor I receptor. *The Journal of biological chemistry*. 2003;278(9):6702-9.
309. Lammering G, Hewit TH, Valerie K, Contessa JN, Amorino GP, Dent P, et al. EGFRvIII-mediated radioresistance through a strong cytoprotective response. *Oncogene*. 2003;22(36):5545-53.
310. De Bacco F, Luraghi P, Medico E, Reato G, Girolami F, Perera T, et al. Induction of MET by ionizing radiation and its role in radioresistance and invasive growth of cancer. *J Natl Cancer Inst*. 2011;103(8):645-61.
311. Kuerbitz SJ, Plunkett BS, Walsh WV, Kastan MB. Wild-type p53 is a cell cycle checkpoint determinant following irradiation. *Proc Natl Acad Sci U S A*. 1992;89(16):7491-5.
312. Shu HK, Kim MM, Chen P, Furman F, Julin CM, Israel MA. The intrinsic radioresistance of glioblastoma-derived cell lines is associated with a failure of p53 to induce p21(BAX) expression. *Proc Natl Acad Sci U S A*. 1998;95(24):14453-8.
313. Ansieau S, Collin G, Hill L. EMT or EMT-Promoting Transcription Factors, Where to Focus the Light? *Front Oncol*. 2014;4:353.
314. Hayashida T, Takahashi F, Chiba N, Brachtel E, Takahashi M, Godin-Heymann N, et al. HOXB9, a gene overexpressed in breast cancer, promotes tumorigenicity and lung metastasis. *Proc Natl Acad Sci U S A*. 2010;107(3):1100-5.
315. Chiba N, Comaills V, Shiotani B, Takahashi F, Shimada T, Tajima K, et al. Homeobox B9 induces epithelial-to-mesenchymal transition-associated radioresistance by accelerating DNA damage responses. *Proc Natl Acad Sci U S A*. 2011.

316. Theys J, Jutten B, Habets R, Paesmans K, Groot AJ, Lambin P, et al. E-Cadherin loss associated with EMT promotes radioresistance in human tumor cells. *Radiother Oncol.* 2011;99(3):392-7.
317. Hein AL, Ouellette MM, Yan Y. Radiation-induced signaling pathways that promote cancer cell survival (review). *Int J Oncol.* 2014;45(5):1813-9.
318. Valerie K, Yacoub A, Hagan MP, Curiel DT, Fisher PB, Grant S, et al. Radiation-induced cell signaling: inside-out and outside-in. *Molecular cancer therapeutics.* 2007;6(3):789-801.
319. Hockel M, Vaupel P. Tumor hypoxia: definitions and current clinical, biologic, and molecular aspects. *J Natl Cancer Inst.* 2001;93(4):266-76.
320. Gorrini C, Harris IS, Mak TW. Modulation of oxidative stress as an anticancer strategy. *Nat Rev Drug Discov.* 2013;12(12):931-47.
321. Clarke MF, Dick JE, Dirks PB, Eaves CJ, Jamieson CH, Jones DL, et al. Cancer stem cells--perspectives on current status and future directions: AACR Workshop on cancer stem cells. *Cancer Res.* 2006;66(19):9339-44.
322. Kim YS, Kang MJ, Cho YM. Low production of reactive oxygen species and high DNA repair: mechanism of radioresistance of prostate cancer stem cells. *Anticancer Res.* 2013;33(10):4469-74.
323. Pajonk F, Vlashi E, McBride WH. Radiation resistance of cancer stem cells: the 4 R's of radiobiology revisited. *Stem Cells.* 2010;28(4):639-48.
324. Beck B, Blanpain C. Unravelling cancer stem cell potential. *Nat Rev Cancer.* 2013;13(10):727-38.

325. Marie-Egyptienne DT, Lohse I, Hill RP. Cancer stem cells, the epithelial to mesenchymal transition (EMT) and radioresistance: potential role of hypoxia. *Cancer Lett.* 2013;341(1):63-72.
326. Gomez-Casal R, Bhattacharya C, Ganesh N, Bailey L, Basse P, Gibson M, et al. Non-small cell lung cancer cells survived ionizing radiation treatment display cancer stem cell and epithelial-mesenchymal transition phenotypes. *Mol Cancer.* 2013;12(1):94.
327. Pisco AO, Huang S. Non-genetic cancer cell plasticity and therapy-induced stemness in tumour relapse: 'What does not kill me strengthens me'. *Br J Cancer.* 2015;112(11):1725-32.
328. Tang DG. Understanding cancer stem cell heterogeneity and plasticity. *Cell Res.* 2012;22(3):457-72.
329. Marusyk A, Almendro V, Polyak K. Intra-tumour heterogeneity: a looking glass for cancer? *Nat Rev Cancer.* 2012;12(5):323-34.
330. Huang S. The war on cancer: lessons from the war on terror. *Front Oncol.* 2014;4:293.
331. Ghisolfi L, Keates AC, Hu X, Lee DK, Li CJ. Ionizing radiation induces stemness in cancer cells. *PLoS One.* 2012;7(8):e43628.
332. Lagadec C, Vlashi E, Della Donna L, Dekmezian C, Pajonk F. Radiation-induced reprogramming of breast cancer cells. *Stem Cells.* 2012;30(5):833-44.
333. Li HF, Kim JS, Waldman T. Radiation-induced Akt activation modulates radioresistance in human glioblastoma cells. *Radiat Oncol.* 2009;4:43.
334. Chang L, Graham PH, Hao J, Ni J, Bucci J, Cozzi PJ, et al. Acquisition of epithelial-mesenchymal transition and cancer stem cell phenotypes is associated with activation of the PI3K/Akt/mTOR pathway in prostate cancer radioresistance. *Cell Death Dis.* 2013;4:e875.
335. Asuthkar S, Gondi CS, Nalla AK, Velpula KK, Gorantla B, Rao JS. Urokinase-type plasminogen activator receptor (uPAR)-mediated regulation of WNT/beta-catenin signaling is

enhanced in irradiated medulloblastoma cells. *The Journal of biological chemistry*. 2012;287(24):20576-89.

336. Todd DG, Mikkelsen RB, Rorrer WK, Valerie K, Schmidt-Ullrich RK. Ionizing radiation stimulates existing signal transduction pathways involving the activation of epidermal growth factor receptor and ERBB-3, and changes of intracellular calcium in A431 human squamous carcinoma cells. *J Recept Signal Transduct Res*. 1999;19(6):885-908.

337. Baskar R. Emerging role of radiation induced bystander effects: Cell communications and carcinogenesis. *Genome Integr*. 2010;1(1):13.

338. Rzeszowska-Wolny J, Przybyszewski WM, Widel M. Ionizing radiation-induced bystander effects, potential targets for modulation of radiotherapy. *Eur J Pharmacol*. 2009;625(1-3):156-64.

339. Desai S, Kumar A, Laskar S, Pandey BN. Cytokine profile of conditioned medium from human tumor cell lines after acute and fractionated doses of gamma radiation and its effect on survival of bystander tumor cells. *Cytokine*. 2013;61(1):54-62.

340. Kim E, Youn H, Kwon T, Son B, Kang J, Yang HJ, et al. PAK1 tyrosine phosphorylation is required to induce epithelial-mesenchymal transition and radioresistance in lung cancer cells. *Cancer Res*. 2014;74(19):5520-31.

341. Kurrey NK, Jalgaonkar SP, Joglekar AV, Ghanate AD, Chaskar PD, Doiphode RY, et al. Snail and slug mediate radioresistance and chemoresistance by antagonizing p53-mediated apoptosis and acquiring a stem-like phenotype in ovarian cancer cells. *Stem Cells*. 2009;27(9):2059-68.

342. Zhang P, Wei Y, Wang L, Debeb BG, Yuan Y, Zhang J, et al. ATM-mediated stabilization of ZEB1 promotes DNA damage response and radioresistance through CHK1. *Nat Cell Biol.* 2014;16(9):864-75.
343. Sehgal L, Thorat R, Khapare N, Mukhopadhaya A, Sawant M, Dalal SN. Lentiviral mediated transgenesis by in vivo manipulation of spermatogonial stem cells. *PLoS One.* 2011;6(7):e21975.
344. Stewart SA, Dykxhoorn DM, Palliser D, Mizuno H, Yu EY, An DS, et al. Lentivirus-delivered stable gene silencing by RNAi in primary cells. *RNA.* 2003;9(4):493-501.
345. Boukamp P, Petrussevska RT, Breitkreutz D, Hornung J, Markham A, Fusenig NE. Normal keratinization in a spontaneously immortalized aneuploid human keratinocyte cell line. *J Cell Biol.* 1988;106(3):761-71.
346. Raul U, Sawant S, Dange P, Kalraiya R, Ingle A, Vaidya M. Implications of cytokeratin 8/18 filament formation in stratified epithelial cells: induction of transformed phenotype. *International journal of cancer.* 2004;111(5):662-8.
347. Sambrook J, Russell DW. Calcium-phosphate-mediated Transfection of Eukaryotic Cells with Plasmid DNAs. *CSH Protoc.* 2006;2006(1).
348. Mi H, Muruganujan A, Casagrande JT, Thomas PD. Large-scale gene function analysis with the PANTHER classification system. *Nat Protoc.* 2013;8(8):1551-66.
349. Mi H, Muruganujan A, Thomas PD. PANTHER in 2013: modeling the evolution of gene function, and other gene attributes, in the context of phylogenetic trees. *Nucleic Acids Res.* 2013;41(Database issue):D377-86.
350. Aranyi T, Varadi A, Simon I, Tusnady GE. The BiSearch web server. *BMC Bioinformatics.* 2006;7:431.

351. Ye J, Coulouris G, Zaretskaya I, Cutcutache I, Rozen S, Madden TL. Primer-BLAST: a tool to design target-specific primers for polymerase chain reaction. *BMC Bioinformatics*. 2012;13:134.
352. Leggate J, Allain R, Isaac L, Blais BW. Microplate fluorescence assay for the quantification of double stranded DNA using SYBR Green I dye. *Biotechnol Lett*. 2006;28(19):1587-94.
353. Zipper H, Brunner H, Bernhagen J, Vitzthum F. Investigations on DNA intercalation and surface binding by SYBR Green I, its structure determination and methodological implications. *Nucleic Acids Res*. 2004;32(12):e103.
354. Smith CJ, Osborn AM. Advantages and limitations of quantitative PCR (Q-PCR)-based approaches in microbial ecology. *FEMS Microbiol Ecol*. 2009;67(1):6-20.
355. Schmittgen TD, Livak KJ. Analyzing real-time PCR data by the comparative C(T) method. *Nat Protoc*. 2008;3(6):1101-8.
356. Wang YW, Ren JH, Xia K, Wang SH, Yin TF, Xie DH, et al. Effect of mitomycin on normal dermal fibroblast and HaCat cell: an in vitro study. *J Zhejiang Univ Sci B*. 2012;13(12):997-1005.
357. Kleinman HK, Jacob K. Invasion assays. *Current protocols in cell biology / editorial board, Juan S Bonifacino [et al]*. 2001;Chapter 12:Unit 12 2.
358. Albini A, Iwamoto Y, Kleinman HK, Martin GR, Aaronson SA, Kozlowski JM, et al. A rapid in vitro assay for quantitating the invasive potential of tumor cells. *Cancer Res*. 1987;47(12):3239-45.
359. Schreiner LJ, Joshi CP, Darko J, Kerr A, Salomons G, Dhanesar S. The role of Cobalt-60 in modern radiation therapy: Dose delivery and image guidance. *J Med Phys*. 2009;34(3):133-6.

360. Franken NA, Rodermond HM, Stap J, Haveman J, van Bree C. Clonogenic assay of cells in vitro. *Nat Protoc.* 2006;1(5):2315-9.
361. Ghioni P, Bolognese F, Duijf PH, Van Bokhoven H, Mantovani R, Guerrini L. Complex transcriptional effects of p63 isoforms: identification of novel activation and repression domains. *Molecular and cellular biology.* 2002;22(24):8659-68.
362. Di Como CJ, Urist MJ, Babayan I, Drobnjak M, Hedvat CV, Teruya-Feldstein J, et al. p63 expression profiles in human normal and tumor tissues. *Clin Cancer Res.* 2002;8(2):494-501.
363. Moergel M, Abt E, Stockinger M, Kunkel M. Overexpression of p63 is associated with radiation resistance and prognosis in oral squamous cell carcinoma. *Oral Oncol.* 2010;46(9):667-71.
364. Harvey KJ, Lukovic D, Ucker DS. Membrane-targeted green fluorescent protein reliably and uniquely marks cells through apoptotic death. *Cytometry.* 2001;43(4):273-8.
365. Chakraborty S, Kaur S, Guha S, Batra SK. The multifaceted roles of neutrophil gelatinase associated lipocalin (NGAL) in inflammation and cancer. *Biochim Biophys Acta.* 2012;1826(1):129-69.
366. Schmidt-Ott KM, Mori K, Kalandadze A, Li JY, Paragas N, Nicholas T, et al. Neutrophil gelatinase-associated lipocalin-mediated iron traffic in kidney epithelia. *Curr Opin Nephrol Hypertens.* 2006;15(4):442-9.
367. Kjeldsen L, Johnsen AH, Sengelov H, Borregaard N. Isolation and primary structure of NGAL, a novel protein associated with human neutrophil gelatinase. *The Journal of biological chemistry.* 1993;268(14):10425-32.

368. Yang J, Goetz D, Li JY, Wang W, Mori K, Setlik D, et al. An iron delivery pathway mediated by a lipocalin. *Mol Cell*. 2002;10(5):1045-56.
369. Borregaard N, Cowland JB. Neutrophil gelatinase-associated lipocalin, a siderophore-binding eukaryotic protein. *Biometals*. 2006;19(2):211-5.
370. Hvidberg V, Jacobsen C, Strong RK, Cowland JB, Moestrup SK, Borregaard N. The endocytic receptor megalin binds the iron transporting neutrophil-gelatinase-associated lipocalin with high affinity and mediates its cellular uptake. *FEBS letters*. 2005;579(3):773-7.
371. Rodvold JJ, Mahadevan NR, Zanetti M. Lipocalin 2 in cancer: when good immunity goes bad. *Cancer Lett*. 2012;316(2):132-8.
372. Nielsen BS, Borregaard N, Bundgaard JR, Timshel S, Sehested M, Kjeldsen L. Induction of NGAL synthesis in epithelial cells of human colorectal neoplasia and inflammatory bowel diseases. *Gut*. 1996;38(3):414-20.
373. Sun Y, Yokoi K, Li H, Gao J, Hu L, Liu B, et al. NGAL expression is elevated in both colorectal adenoma-carcinoma sequence and cancer progression and enhances tumorigenesis in xenograft mouse models. *Clin Cancer Res*. 2011;17(13):4331-40.
374. McLean MH, Thomson AJ, Murray GI, Fyfe N, Hold GL, El-Omar EM. Expression of neutrophil gelatinase-associated lipocalin in colorectal neoplastic progression: a marker of malignant potential? *Br J Cancer*. 2013;108(12):2537-41.
375. Akgul B, Bauer B, Zigrino P, Storey A, Mauch C, Pfister H. Upregulation of lipocalin-2 in human papillomavirus-positive keratinocytes and cutaneous squamous cell carcinomas. *J Gen Virol*. 2011;92(Pt 2):395-401.

376. Fukuda K, Sakakura C, Miyagawa K, Kuriu Y, Kin S, Nakase Y, et al. Differential gene expression profiles of radioresistant oesophageal cancer cell lines established by continuous fractionated irradiation. *Br J Cancer*. 2004;91(8):1543-50.
377. Shiiba M, Saito K, Fushimi K, Ishigami T, Shinozuka K, Nakashima D, et al. Lipocalin-2 is associated with radioresistance in oral cancer and lung cancer cells. *Int J Oncol*. 2013;42(4):1197-204.
378. Woessner JF, Jr., Taplin CJ. Purification and properties of a small latent matrix metalloproteinase of the rat uterus. *The Journal of biological chemistry*. 1988;263(32):16918-25.
379. Miyazaki K, Hattori Y, Umenishi F, Yasumitsu H, Umeda M. Purification and characterization of extracellular matrix-degrading metalloproteinase, matrin (pump-1), secreted from human rectal carcinoma cell line. *Cancer Res*. 1990;50(24):7758-64.
380. Rodgers WH, Matrisian LM, Giudice LC, Dsupin B, Cannon P, Svitek C, et al. Patterns of matrix metalloproteinase expression in cycling endometrium imply differential functions and regulation by steroid hormones. *J Clin Invest*. 1994;94(3):946-53.
381. Saarialho-Kere UK, Crouch EC, Parks WC. Matrix metalloproteinase matrilysin is constitutively expressed in adult human exocrine epithelium. *J Invest Dermatol*. 1995;105(2):190-6.
382. Wilson CL, Heppner KJ, Rudolph LA, Matrisian LM. The metalloproteinase matrilysin is preferentially expressed by epithelial cells in a tissue-restricted pattern in the mouse. *Molecular biology of the cell*. 1995;6(7):851-69.
383. Wilson MJ, Garcia B, Woodson M, Sinha AA. Metalloproteinase activities expressed during development and maturation of the rat prostatic complex and seminal vesicles. *Biol Reprod*. 1992;47(5):683-91.

384. Porte H, Chastre E, Prevot S, Nordlinger B, Empereur S, Basset P, et al. Neoplastic progression of human colorectal cancer is associated with overexpression of the stromelysin-3 and BM-40/SPARC genes. *International journal of cancer*. 1995;64(1):70-5.
385. McDonnell S, Navre M, Coffey RJ, Jr., Matrisian LM. Expression and localization of the matrix metalloproteinase pump-1 (MMP-7) in human gastric and colon carcinomas. *Mol Carcinog*. 1991;4(6):527-33.
386. Zeng ZS, Guillem JG. Distinct pattern of matrix metalloproteinase 9 and tissue inhibitor of metalloproteinase 1 mRNA expression in human colorectal cancer and liver metastases. *Br J Cancer*. 1995;72(3):575-82.
387. Okada A, Bellocq JP, Rouyer N, Chenard MP, Rio MC, Chambon P, et al. Membrane-type matrix metalloproteinase (MT-MMP) gene is expressed in stromal cells of human colon, breast, and head and neck carcinomas. *Proc Natl Acad Sci U S A*. 1995;92(7):2730-4.
388. Dunsmore SE, Saarialho-Kere UK, Roby JD, Wilson CL, Matrisian LM, Welgus HG, et al. Matrilysin expression and function in airway epithelium. *J Clin Invest*. 1998;102(7):1321-31.
389. Parks WC, Lopez-Boado YS, Wilson CL. Matrilysin in epithelial repair and defense. *Chest*. 2001;120(1 Suppl):36S-41S.
390. Wilson CL, Ouellette AJ, Satchell DP, Ayabe T, Lopez-Boado YS, Stratman JL, et al. Regulation of intestinal alpha-defensin activation by the metalloproteinase matrilysin in innate host defense. *Science*. 1999;286(5437):113-7.
391. Burke B. The role of matrix metalloproteinase 7 in innate immunity. *Immunobiology*. 2004;209(1-2):51-6.

392. Hajj R, Lesimple P, Nawrocki-Raby B, Birembaut P, Puchelle E, Coraux C. Human airway surface epithelial regeneration is delayed and abnormal in cystic fibrosis. *J Pathol.* 2007;211(3):340-50.
393. Saarialho-Kere UK, Vaalamo M, Puolakkainen P, Airola K, Parks WC, Karjalainen-Lindsberg ML. Enhanced expression of matrilysin, collagenase, and stromelysin-1 in gastrointestinal ulcers. *Am J Pathol.* 1996;148(2):519-26.
394. Lopez-Boado YS, Wilson CL, Hooper LV, Gordon JI, Hultgren SJ, Parks WC. Bacterial exposure induces and activates matrilysin in mucosal epithelial cells. *J Cell Biol.* 2000;148(6):1305-15.
395. Newell KJ, Witty JP, Rodgers WH, Matrisian LM. Expression and localization of matrix-degrading metalloproteinases during colorectal tumorigenesis. *Mol Carcinog.* 1994;10(4):199-206.
396. Adachi Y, Yamamoto H, Itoh F, Hinoda Y, Okada Y, Imai K. Contribution of matrilysin (MMP-7) to the metastatic pathway of human colorectal cancers. *Gut.* 1999;45(2):252-8.
397. Zeng ZS, Shu WP, Cohen AM, Guillem JG. Matrix metalloproteinase-7 expression in colorectal cancer liver metastases: evidence for involvement of MMP-7 activation in human cancer metastases. *Clin Cancer Res.* 2002;8(1):144-8.
398. Wroblewski LE, Noble PJ, Pagliocca A, Pritchard DM, Hart CA, Campbell F, et al. Stimulation of MMP-7 (matrilysin) by *Helicobacter pylori* in human gastric epithelial cells: role in epithelial cell migration. *J Cell Sci.* 2003;116(Pt 14):3017-26.
399. Vairaktaris E, Serefoglou Z, Yapijakis C, Vylliotis A, Nkenke E, Derka S, et al. High gene expression of matrix metalloproteinase-7 is associated with early stages of oral cancer. *Anticancer Res.* 2007;27(4B):2493-8.

400. Szarvas T, Becker M, vom Dorp F, Gethmann C, Totsch M, Bankfalvi A, et al. Matrix metalloproteinase-7 as a marker of metastasis and predictor of poor survival in bladder cancer. *Cancer science*. 2010;101(5):1300-8.
401. Wilson CL, Heppner KJ, Labosky PA, Hogan BL, Matrisian LM. Intestinal tumorigenesis is suppressed in mice lacking the metalloproteinase matrilysin. *Proc Natl Acad Sci U S A*. 1997;94(4):1402-7.
402. Guillen-Ahlers H, Buechler SA, Suckow MA, Castellino FJ, Ploplis VA. Sulindac treatment alters collagen and matrilysin expression in adenomas of ApcMin/+ mice. *Carcinogenesis*. 2008;29(7):1421-7.
403. Witty JP, McDonnell S, Newell KJ, Cannon P, Navre M, Tressler RJ, et al. Modulation of matrilysin levels in colon carcinoma cell lines affects tumorigenicity in vivo. *Cancer Res*. 1994;54(17):4805-12.
404. Zhang W, Li Y, Yang L, Zhou B, Chen KL, Meng WJ, et al. Knockdown of MMP-7 inhibits cell proliferation and enhances sensitivity to 5-Fluorouracil and X-ray irradiation in colon cancer cells. *Clinical and experimental medicine*. 2014;14(1):99-106.
405. Vashist SK. Graphene-based immunoassay for human lipocalin-2. *Anal Biochem*. 2014;446:96-101.
406. Jang E, Lee S, Kim JH, Kim JH, Seo JW, Lee WH, et al. Secreted protein lipocalin-2 promotes microglial M1 polarization. *FASEB J*. 2013;27(3):1176-90.
407. Caramuta S, De Cecco L, Reid JF, Zannini L, Gariboldi M, Kjeldsen L, et al. Regulation of lipocalin-2 gene by the cancer chemopreventive retinoid 4-HPR. *International journal of cancer*. 2006;119(7):1599-606.

408. Sawant AP. Determining the role of p38alpha MAPK signaling pathway in regulating tumorigenesis upon plakophilin3 loss.: St. Xavier's college, Mumbai; 2014.
409. Braggs CJ. Upregulation of Lipocalin2 mediates neoplastic progression and radioresistance observed upon plakophilin3 loss: St. Xavier's college, Mumbai; 2014.
410. Wang L, Li H, Wang J, Gao W, Lin Y, Jin W, et al. C/EBP zeta targets to neutrophil gelatinase-associated lipocalin (NGAL) as a repressor for metastasis of MDA-MB-231 cells. *Biochim Biophys Acta*. 2011;1813(10):1803-13.
411. Cowland JB, Borregaard N. Molecular characterization and pattern of tissue expression of the gene for neutrophil gelatinase-associated lipocalin from humans. *Genomics*. 1997;45(1):17-23.
412. Leitao JM, Esteves da Silva JC. Firefly luciferase inhibition. *J Photochem Photobiol B*. 2010;101(1):1-8.
413. Marques SM, Esteves da Silva JC. Firefly bioluminescence: a mechanistic approach of luciferase catalyzed reactions. *IUBMB Life*. 2009;61(1):6-17.
414. Lorenz WW, McCann RO, Longiaru M, Cormier MJ. Isolation and expression of a cDNA encoding *Renilla reniformis* luciferase. *Proc Natl Acad Sci U S A*. 1991;88(10):4438-42.
415. Hart RC, Matthews JC, Hori K, Cormier MJ. *Renilla reniformis* bioluminescence: luciferase-catalyzed production of nonradiating excited states from luciferin analogues and elucidation of the excited state species involved in energy transfer to *Renilla* green fluorescent protein. *Biochemistry*. 1979;18(11):2204-10.
416. Greer LF, 3rd, Szalay AA. Imaging of light emission from the expression of luciferases in living cells and organisms: a review. *Luminescence*. 2002;17(1):43-74.

417. Wang LH, Chang GQ, Zhang HJ, Wang J, Lin YN, Jin WN, et al. Neutrophil gelatinase-associated lipocalin regulates intracellular accumulation of Rh123 in cancer cells. *Genes Cells*. 2012;17(3):205-17.
418. Yoo do Y, Ko SH, Jung J, Kim YJ, Kim JS, Kim JM. *Bacteroides fragilis* enterotoxin upregulates lipocalin-2 expression in intestinal epithelial cells. *Lab Invest*. 2013;93(4):384-96.
419. Gong X, Ming X, Deng P, Jiang Y. Mechanisms regulating the nuclear translocation of p38 MAP kinase. *J Cell Biochem*. 2010;110(6):1420-9.
420. Jiang Y, Chen C, Li Z, Guo W, Gegner JA, Lin S, et al. Characterization of the structure and function of a new mitogen-activated protein kinase (p38beta). *The Journal of biological chemistry*. 1996;271(30):17920-6.
421. Li Z, Jiang Y, Ulevitch RJ, Han J. The primary structure of p38 gamma: a new member of p38 group of MAP kinases. *Biochem Biophys Res Commun*. 1996;228(2):334-40.
422. Risco A, Cuenda A. New Insights into the p38gamma and p38delta MAPK Pathways. *J Signal Transduct*. 2012;2012:520289.
423. Gum RJ, McLaughlin MM, Kumar S, Wang Z, Bower MJ, Lee JC, et al. Acquisition of sensitivity of stress-activated protein kinases to the p38 inhibitor, SB 203580, by alteration of one or more amino acids within the ATP binding pocket. *The Journal of biological chemistry*. 1998;273(25):15605-10.
424. Kumar S, McDonnell PC, Gum RJ, Hand AT, Lee JC, Young PR. Novel homologues of CSBP/p38 MAP kinase: activation, substrate specificity and sensitivity to inhibition by pyridinyl imidazoles. *Biochem Biophys Res Commun*. 1997;235(3):533-8.
425. de Nadal E, Ammerer G, Posas F. Controlling gene expression in response to stress. *Nature reviews Genetics*. 2011;12(12):833-45.

426. Tanaka K, Oda N, Iwasaka C, Abe M, Sato Y. Induction of Ets-1 in endothelial cells during reendothelialization after denuding injury. *J Cell Physiol.* 1998;176(2):235-44.
427. Patel M, Predescu D, Tandon R, Bardita C, Pogoriler J, Bhorade S, et al. A novel p38 mitogen-activated protein kinase/Elk-1 transcription factor-dependent molecular mechanism underlying abnormal endothelial cell proliferation in plexogenic pulmonary arterial hypertension. *The Journal of biological chemistry.* 2013;288(36):25701-16.
428. Latinkic BV, Zeremski M, Lau LF. Elk-1 can recruit SRF to form a ternary complex upon the serum response element. *Nucleic Acids Res.* 1996;24(7):1345-51.
429. Wasyluk B, Hagman J, Gutierrez-Hartmann A. Ets transcription factors: nuclear effectors of the Ras-MAP-kinase signaling pathway. *Trends Biochem Sci.* 1998;23(6):213-6.
430. Ferreira I, Barragan M, Gubern A, Ballestar E, Joaquin M, Posas F. The p38 SAPK is recruited to chromatin via its interaction with transcription factors. *The Journal of biological chemistry.* 2010;285(41):31819-28.
431. Whitmarsh AJ, Yang SH, Su MS, Sharrocks AD, Davis RJ. Role of p38 and JNK mitogen-activated protein kinases in the activation of ternary complex factors. *Molecular and cellular biology.* 1997;17(5):2360-71.
432. Odrowaz Z, Sharrocks AD. ELK1 uses different DNA binding modes to regulate functionally distinct classes of target genes. *PLoS Genet.* 2012;8(5):e1002694.
433. Shin SY, Kim CG, Lim Y, Lee YH. The ETS family transcription factor ELK-1 regulates induction of the cell cycle-regulatory gene p21(Waf1/Cip1) and the BAX gene in sodium arsenite-exposed human keratinocyte HaCaT cells. *The Journal of biological chemistry.* 2011;286(30):26860-72.

434. Farre D, Roset R, Huerta M, Adsuara JE, Rosello L, Alba MM, et al. Identification of patterns in biological sequences at the ALGGEN server: PROMO and MALGEN. *Nucleic Acids Res.* 2003;31(13):3651-3.
435. Messeguer X, Escudero R, Farre D, Nunez O, Martinez J, Alba MM. PROMO: detection of known transcription regulatory elements using species-tailored searches. *Bioinformatics.* 2002;18(2):333-4.
436. Stormo GD. DNA binding sites: representation and discovery. *Bioinformatics.* 2000;16(1):16-23.
437. Wasserman WW, Sandelin A. Applied bioinformatics for the identification of regulatory elements. *Nature reviews Genetics.* 2004;5(4):276-87.
438. Pallai R, Bhaskar A, Sodi V, Rice LM. Ets1 and Elk1 transcription factors regulate cancerous inhibitor of protein phosphatase 2A expression in cervical and endometrial carcinoma cells. *Transcription.* 2012;3(6):323-35.
439. Nilsson M, Dahlman-Wright K, Karelmo C, Ebeling M, Gustafsson JA, Steffensen KR. Elk1 and SRF transcription factors convey basal transcription and mediate glucose response via their binding sites in the human LXRB gene promoter. *Nucleic Acids Res.* 2007;35(14):4858-68.
440. Koenig A, Linhart T, Schlengemann K, Reutlinger K, Wegele J, Adler G, et al. NFAT-induced histone acetylation relay switch promotes c-Myc-dependent growth in pancreatic cancer cells. *Gastroenterology.* 2010;138(3):1189-99 e1-2.
441. Sheikh RSAR. Identification of pathways regulated upon plakophilin3 loss.: University of Mumbai; 2015.
442. Patel SB, Cameron PM, O'Keefe SJ, Frantz-Wattley B, Thompson J, O'Neill EA, et al. The three-dimensional structure of MAP kinase p38beta: different features of the ATP-binding

- site in p38beta compared with p38alpha. *Acta Crystallogr D Biol Crystallogr*. 2009;65(Pt 8):777-85.
443. Beenstock J, Ben-Yehuda S, Melamed D, Admon A, Livnah O, Ahn NG, et al. The p38beta mitogen-activated protein kinase possesses an intrinsic autophosphorylation activity, generated by a short region composed of the alpha-G helix and MAPK insert. *The Journal of biological chemistry*. 2014;289(34):23546-56.
444. Polistena A, Cucina A, Dinicola S, Stene C, Cavallaro G, Ciardi A, et al. MMP7 expression in colorectal tumours of different stages. *In vivo*. 2014;28(1):105-10.
445. Jiang QH, Wang AX, Chen Y. Radixin Enhances Colon Cancer Cell Invasion by Increasing MMP-7 Production via Rac1-ERK Pathway. *TheScientificWorldJournal*. 2014;2014:340271.
446. Fingleton B, Powell WC, Crawford HC, Couchman JR, Matrisian LM. A rat monoclonal antibody that recognizes pro- and active MMP-7 indicates polarized expression in vivo. *Hybridoma*. 2007;26(1):22-7.
447. Lynch CC, Vargo-Gogola T, Matrisian LM, Fingleton B. Cleavage of E-Cadherin by Matrix Metalloproteinase-7 Promotes Cellular Proliferation in Nontransformed Cell Lines via Activation of RhoA. *Journal of oncology*. 2010;2010:530745.
448. Kim NG, Koh E, Chen X, Gumbiner BM. E-cadherin mediates contact inhibition of proliferation through Hippo signaling-pathway components. *Proc Natl Acad Sci U S A*. 2011;108(29):11930-5.
449. Gumbiner BM, Kim NG. The Hippo-YAP signaling pathway and contact inhibition of growth. *J Cell Sci*. 2014;127(Pt 4):709-17.

450. Chikte A. Matrix Metalloprotease-7 (MMP7) mediates neoplastic progression observed upon plakophilin3 loss: St. Xavier's College, Mumbai; 2014.
451. Basu S, Thorat R, Dalal SN. MMP7 Is Required to Mediate Cell Invasion and Tumor Formation upon Plakophilin3 Loss. *PLoS One*. 2015;10(4):e0123979.
452. Lee SK, Han YM, Yun J, Lee CW, Shin DS, Ha YR, et al. Phosphatase of regenerating liver-3 promotes migration and invasion by upregulating matrix metalloproteinases-7 in human colorectal cancer cells. *International journal of cancer*. 2012;131(3):E190-203.
453. Wang H, Quah SY, Dong JM, Manser E, Tang JP, Zeng Q. PRL-3 down-regulates PTEN expression and signals through PI3K to promote epithelial-mesenchymal transition. *Cancer Res*. 2007;67(7):2922-6.
454. Barresi V, Di Gregorio C, Reggiani-Bonetti L, Ieni A, Ponz-De Leon M, Barresi G. Neutrophil gelatinase-associated lipocalin: a new prognostic marker in stage I colorectal carcinoma? *Human pathology*. 2011;42(11):1720-6.
455. Barresi V, Reggiani-Bonetti L, Di Gregorio C, Vitarelli E, Ponz De Leon M, Barresi G. Neutrophil gelatinase-associated lipocalin (NGAL) and matrix metalloproteinase-9 (MMP-9) prognostic value in stage I colorectal carcinoma. *Pathol Res Pract*. 2011;207(8):479-86.
456. Marti J, Fuster J, Sola AM, Hotter G, Molina R, Pelegrina A, et al. Prognostic value of serum neutrophil gelatinase-associated lipocalin in metastatic and nonmetastatic colorectal cancer. *World J Surg*. 2013;37(5):1103-9.
457. Fernandez CA, Yan L, Louis G, Yang J, Kutok JL, Moses MA. The matrix metalloproteinase-9/neutrophil gelatinase-associated lipocalin complex plays a role in breast tumor growth and is present in the urine of breast cancer patients. *Clin Cancer Res*. 2005;11(15):5390-5.

458. Monier F, Surla A, Guillot M, Morel F. Gelatinase isoforms in urine from bladder cancer patients. *Clin Chim Acta*. 2000;299(1-2):11-23.
459. Yan L, Borregaard N, Kjeldsen L, Moses MA. The high molecular weight urinary matrix metalloproteinase (MMP) activity is a complex of gelatinase B/MMP-9 and neutrophil gelatinase-associated lipocalin (NGAL). Modulation of MMP-9 activity by NGAL. *The Journal of biological chemistry*. 2001;276(40):37258-65.
460. Hu L, Hittelman W, Lu T, Ji P, Arlinghaus R, Shmulevich I, et al. NGAL decreases E-cadherin-mediated cell-cell adhesion and increases cell motility and invasion through Rac1 in colon carcinoma cells. *Lab Invest*. 2009;89(5):531-48.
461. Hummerich L, Muller R, Hess J, Kokocinski F, Hahn M, Furstenberger G, et al. Identification of novel tumour-associated genes differentially expressed in the process of squamous cell cancer development. *Oncogene*. 2006;25(1):111-21.
462. Sorensen OE, Thapa DR, Roupe KM, Valore EV, Sjobring U, Roberts AA, et al. Injury-induced innate immune response in human skin mediated by transactivation of the epidermal growth factor receptor. *J Clin Invest*. 2006;116(7):1878-85.
463. Wakeman D, Schneider JE, Liu J, Wandu WS, Erwin CR, Guo J, et al. Deletion of p38-alpha mitogen-activated protein kinase within the intestinal epithelium promotes colon tumorigenesis. *Surgery*. 2012;152(2):286-93.
464. Gupta J, del Barco Barrantes I, Igea A, Sakellariou S, Pateras IS, Gorgoulis VG, et al. Dual function of p38alpha MAPK in colon cancer: suppression of colitis-associated tumor initiation but requirement for cancer cell survival. *Cancer Cell*. 2014;25(4):484-500.
465. Enslin H, Brancho DM, Davis RJ. Molecular determinants that mediate selective activation of p38 MAP kinase isoforms. *EMBO J*. 2000;19(6):1301-11.

466. Ho DT, Bardwell AJ, Abdollahi M, Bardwell L. A docking site in MKK4 mediates high affinity binding to JNK MAPKs and competes with similar docking sites in JNK substrates. *The Journal of biological chemistry*. 2003;278(35):32662-72.
467. Jacobs D, Glossip D, Xing H, Muslin AJ, Kornfeld K. Multiple docking sites on substrate proteins form a modular system that mediates recognition by ERK MAP kinase. *Genes Dev*. 1999;13(2):163-75.
468. Yang SH, Whitmarsh AJ, Davis RJ, Sharrocks AD. Differential targeting of MAP kinases to the ETS-domain transcription factor Elk-1. *EMBO J*. 1998;17(6):1740-9.
469. Mori M, Barnard GF, Mimori K, Ueo H, Akiyoshi T, Sugimachi K. Overexpression of matrix metalloproteinase-7 mRNA in human colon carcinomas. *Cancer*. 1995;75(6 Suppl):1516-9.
470. Maurel J, Nadal C, Garcia-Albeniz X, Gallego R, Carcereny E, Almendro V, et al. Serum matrix metalloproteinase 7 levels identifies poor prognosis advanced colorectal cancer patients. *International journal of cancer*. 2007;121(5):1066-71.
471. Lee HJ, Lee EK, Lee KJ, Hong SW, Yoon Y, Kim JS. Ectopic expression of neutrophil gelatinase-associated lipocalin suppresses the invasion and liver metastasis of colon cancer cells. *International journal of cancer*. 2006;118(10):2490-7.
472. Impola U, Jeskanen L, Ravanti L, Syrjanen S, Baldursson B, Kahari VM, et al. Expression of matrix metalloproteinase (MMP)-7 and MMP-13 and loss of MMP-19 and p16 are associated with malignant progression in chronic wounds. *Br J Dermatol*. 2005;152(4):720-6.
473. Mitsui H, Suarez-Farinas M, Gulati N, Shah KR, Cannizzaro MV, Coats I, et al. Gene expression profiling of the leading edge of cutaneous squamous cell carcinoma: IL-24-driven MMP-7. *J Invest Dermatol*. 2014;134(5):1418-27.

474. Rouleau C, Roy A, St Martin T, Dufault MR, Boutin P, Liu D, et al. Protein tyrosine phosphatase PRL-3 in malignant cells and endothelial cells: expression and function. *Molecular cancer therapeutics*. 2006;5(2):219-29.
475. Wang H, Vardy LA, Tan CP, Loo JM, Guo K, Li J, et al. PCBP1 suppresses the translation of metastasis-associated PRL-3 phosphatase. *Cancer Cell*. 2010;18(1):52-62.
476. Sklyarova T, van Hengel J, Van Wonterghem E, Libert C, van Roy F, Vandembroucke RE. Hematopoietic plakophilin-3 regulates acute tissue-specific and systemic inflammation in mice. *Eur J Immunol*. 2015.
477. Chen X, Bonne S, Hatzfeld M, van Roy F, Green KJ. Protein binding and functional characterization of plakophilin 2. Evidence for its diverse roles in desmosomes and beta -catenin signaling. *The Journal of biological chemistry*. 2002;277(12):10512-22.
478. Duan Y, Liao AP, Kuppireddi S, Ye Z, Ciancio MJ, Sun J. beta-Catenin activity negatively regulates bacteria-induced inflammation. *Lab Invest*. 2007;87(6):613-24.
479. Du Q, Zhang X, Cardinal J, Cao Z, Guo Z, Shao L, et al. Wnt/beta-catenin signaling regulates cytokine-induced human inducible nitric oxide synthase expression by inhibiting nuclear factor-kappaB activation in cancer cells. *Cancer Res*. 2009;69(9):3764-71.
480. Neumann J, Schaale K, Farhat K, Endermann T, Ulmer AJ, Ehlers S, et al. Frizzled1 is a marker of inflammatory macrophages, and its ligand Wnt3a is involved in reprogramming *Mycobacterium tuberculosis*-infected macrophages. *FASEB J*. 2010;24(11):4599-612.
481. Driessens G, Zheng Y, Locke F, Cannon JL, Gounari F, Gajewski TF. Beta-catenin inhibits T cell activation by selective interference with linker for activation of T cells-phospholipase C-gamma1 phosphorylation. *J Immunol*. 2011;186(2):784-90.

482. Sun J, Hobert ME, Duan Y, Rao AS, He TC, Chang EB, et al. Crosstalk between NF-kappaB and beta-catenin pathways in bacterial-colonized intestinal epithelial cells. *Am J Physiol Gastrointest Liver Physiol*. 2005;289(1):G129-37.
483. Kim C, Pasparakis M. Epidermal p65/NF-kappaB signalling is essential for skin carcinogenesis. *EMBO Mol Med*. 2014;6(7):970-83.
484. Chun KS, Keum YS, Han SS, Song YS, Kim SH, Surh YJ. Curcumin inhibits phorbol ester-induced expression of cyclooxygenase-2 in mouse skin through suppression of extracellular signal-regulated kinase activity and NF-kappaB activation. *Carcinogenesis*. 2003;24(9):1515-24.
485. Kundu JK, Shin YK, Kim SH, Surh YJ. Resveratrol inhibits phorbol ester-induced expression of COX-2 and activation of NF-kappaB in mouse skin by blocking IkappaB kinase activity. *Carcinogenesis*. 2006;27(7):1465-74.
486. Kundu S, Sengupta S, Bhattacharyya A. EGFR upregulates inflammatory and proliferative responses in human lung adenocarcinoma cell line (A549), induced by lower dose of cadmium chloride. *Inhal Toxicol*. 2011;23(6):339-48.
487. Hamilton LM, Torres-Lozano C, Puddicombe SM, Richter A, Kimber I, Dearman RJ, et al. The role of the epidermal growth factor receptor in sustaining neutrophil inflammation in severe asthma. *Clin Exp Allergy*. 2003;33(2):233-40.
488. Normanno N, De Luca A, Bianco C, Strizzi L, Mancino M, Maiello MR, et al. Epidermal growth factor receptor (EGFR) signaling in cancer. *Gene*. 2006;366(1):2-16.
489. Uribe P, Gonzalez S. Epidermal growth factor receptor (EGFR) and squamous cell carcinoma of the skin: molecular bases for EGFR-targeted therapy. *Pathol Res Pract*. 2011;207(6):337-42.

-
490. Getsios S, Simpson CL, Kojima S, Harmon R, Sheu LJ, Dusek RL, et al. Desmoglein 1-dependent suppression of EGFR signaling promotes epidermal differentiation and morphogenesis. *J Cell Biol.* 2009;185(7):1243-58.

7. Annexure I

List of genes altered upon PKP3 loss in FBM cells.

a. List of genes up-regulated more than two folds upon PKP3 loss in FBM cells.

CCL2	CBS	CENTG1	MARVELD3	SCARNA27	EXOSC5
SAA2	CSF2	TMC8	NRARP	REPS2	EHF
SAA1	CCNL1	EPPK1	TMPRSS3	RASIP1	HES2
WFDC2	LAPTM5	ARNT2	SCG5	CSTA	PTGIR
FRAS1	WNT7A	SCARF1	PPM1J	LCP1	OVOS2
WNT4	GALNT14	RASGRF1	LSR	IRF5	HAPLN3
MOBK2B	DAPP1	RAB17	SCARNA8	RGS16	SERPINA1
SAA4	AUTS2	MB	SIGLEC15	LIPE	TGM2
FEZ1	OVOL2	SNORA79	LAMC2	COBL	MICALCL
TUBB2B	JAK3	TNF	NLRP3	HRASLS	APOC1
LEMD1	SLAIN1	TLR2	HRK	H6PD	ZNF215
KRT7	ACAT1	SCARNA14	RAB11FIP4	SNORA12	CRISPLD1
GAL	ASGR1	LST1	JAG2	MMP15	CAMK1D
BSPRY	KLRC1	FA2H	CALB2	ANXA3	FBXO25
LCN2	HOOK1	KLRC2	SCARNA16	TMEM154	COLEC11
CXCL6	S100A8	CHRM2	PAPLN	SCARNA12	IL4I1
GJB3	IL7	CDH3	RLN2	TRIM6	ABCG1
KCNMB4	FUT1	MIRH1	CEACAM19	SCARNA11	PRICKLE1
IL32	HOXB9	FLI1	CNTNAP2	ADAMTSL3	KIF21B
MYO1D	BCL2A1	CADM1	CTSS	PTPRB	GPR160
SPTLC2	SH2D3A	KRT14	GPR162	NPL	CD163L1
BCL11A	CHRM3	UNC5B	ZNF285A	LTB	BMP6
CALCB	DYSF	MT1F	DENND2D	RRAGD	ZNF224
MMP9	LINCR	BIRC3	SYT17	ZNF513	PDCD2L
ICA1	ENPP6	C1QTNF6	BACH2	CD82	RUNDC2C
TMEM204	DMKN	SCARNA22	PDZK1IP1	KLHL3	OSCAR
NEURL	HSPC105	KRT17	F11R	GIMAP2	TNFRSF14
LAMP3	VNN1	BEX2	CG018	BMF	ZBTB20
SGPP2	CTSH	RGS9	GRB7	KREMEN2	PRSS16
HYAL1	HS6ST2	AATK	CYP2S1	MCTP2	MCAM
RAB37	KLRC3	TMEM92	ARHGEF16	DLL1	PTPRR
HSD11B1	B3GNT3	CRABP2	BIK	ARSI	ITM2C
ITGB2	IRF6	GJB2	KRT86	ANKRD6	PPL
AFAP1L2	CCDC113	ROBO4	IL23A	MAP6	ETV7
MIA	ST6GALNAC5	RIMS2	ARHGAP8	BBC3	WDR59
ADORA2A	PSTPIP1	CENTA2	IL1A	KRT16	ZNF345
GPR68	LMO2	MMP7	SORL1	FAM129A	MAP9
SPINT1	KLRC4	ARHGEF5	POTE2	TERT	LSS

LTBP4	ARG2	MT1L	HSD17B8	IKBKE	SRGAP1
NRXN2	DOCK4	C1QTNF1	ICAM1	CMTM4	BCKDHA
GPR172B	EVA1	GRB14	MT1X	VAMP5	ZNF284
NPAS1	HIC1	HOXB13	TRAF1	IGF2BP2	RGS14
NO145	AASS	NPAS2	FCGRT	NOXO1	WTIP
FBP1	FAM78A	TSPAN15	ATM	MT1B	EDG7
HSD11B2	HMGA2	RHBDF2	DENND2A	FXYD5	RAB4B
GUSBL2	GOLT1A	MARVELD2	MT1G	TERC	PRPF19
B4GALNT3	IFNAR2	KATNB1	SNAI3	INHBA	LRRK1
OCLN	SFRS16	SOX15	DEDD2	KRT5	
SIDT1	GRIN2A	TNFRSF9	SIPA1L3	RKHD1	
MTUS1	SBSN	RAPGEF5	ZNF790	RHPN2	
GJB5	BAIAP2L2	SALL4	TMEM16J	RPL10	
COL6A2	ZNF529	TRAPPC6A	KRT33A	COCH	
CENTD1	SNORA67	SIM2	GAS7	USP43	
RELB	SHROOM3	CYR61	CEBPA	TSEN54	
ZNF420	FGD6	FUT4	ZNF883	CAPN12	
S100A9	EPB41L5	SCD	IL24	DHRS12	
CTHRC1	TPM1	TRIB3	CDH1	TMEM25	
HSMPP8	SLFN5	GBP5	MT1H	PVR	
ALOX5AP	ERBB3	PCSK6	PRSS22	MMP14	
PDE11A	C1QL4	MTMR11	ATP8A1	CCL5	
STARD4	EFCAB4A	NLRP5	RLTPR	SNORA67	
NFE2L1	CAPS	SNORA84	FXYD2	NOTCH2NL	
NUPR1	SYTL1	COL16A1	ZNF226	SAMD4A	
ASNS	LRG1	GPR92	TMEM91	COL27A1	
RRAD	NT5E	GLS2	YAP1	PDXDC2	
KCNK5	ANKRD27	CYP27B1	CSNK2A2	ZDHHC13	
CEBPG	BATF2	PAIP2B	ZSCAN12	DNAJC7	
PLEKHF1	STX7	PAK6	ZNF342	GBP1	
ELF3	ALDH1L2	TTBK2	CSNK1G1	RASL10A	
SEMA7A	GPT2	P2RX4	UNC13D	FBXL20	
RNF125	PPM2C	KCNK6	SESN2	SHMT2	
STAT5A	FGD4	DDR1	ACBD4	DNAH5	
CNOT1	PLAC1	ZNF449	EMR2	KLHDC7B	
LAT2	TMEM71	AQP1	PVRL2	NEK3	
HCLS1	PARD6A	FMNL1	LONRF1	SC4MOL	
CSF3	CTAGE5	TMEM22	TFCP2L1	TMEM117	

b. List of genes down-regulated more than two folds upon PKP3 loss in FBM cells.

AKR1C1	CPZ	OASL	MLLT11	TCEAL4	GUCY1A2
UGT1A6	DKK1	PRR16	CDON	EPGN	LIPH
AKR1B10	SDC2	PGCP	IL7R	PDGFRB	SECTM1
NOV	WNT5A	STAC	BAMBI	SRPX	SPRY1
IGFBP1	F2RL2	FAM46A	ZNF488	SPTLC3	MMP16
SPOCD1	CCL26	GCNT1	TIMP4	TMEM37	IL20RB
IGFBP3	CFI	PLA2G4A	BDKRB1	CCDC80	PTPRS
PSG8	SLITRK6	ANGPT1	SLIT2	NEXN	TSPAN2
HS6ST3	PSG9	PAQR7	PRM3	CNRIP1	RASSF8
DHRS9	ABCG2	THBD	RP1L1	CYP4X1	GNAI1
UGT1A8	PRG4	SHC3	MAP2	TWIST2	ZNF469
NR2F1	AK5	PSG7	IFI27	REEP1	RCAN2
PSG6	PID1	SPOCK1	RNF43	PDE7B	TBX3
PTGS2	PGAP1	DSCR1L1	FOXF1	TMEM62	BNC2
ABI3BP	BMP4	AKR1C3	EREG	PTGFR	BHLHB9
VIT	SEMA3D	LYSMD4	KIRREL3	TTLL7	CA12
TLR4	GSG1	C3	ZNF365	NR0B1	GRM6
ANK3	SETBP1	LYPD6	WDR69	TRPC4	ZEB2
SOST	CPA4	FMN2	IGFBP4	TNIK	EPHX1
ANXA10	HTRA3	RGS4	ZNF521	PBX1	ZSWIM5
AR	DIO2	ERC2	ITGA11	BDKRB2	DPYSL5
COL8A1	PIR	ID2	PCDH9	PLP1	PPARG
TNFRSF11B	PFTK1	PCSK1	C1GALT1C1	SUSD5	SERPINE2
SH3BGR1	PPARGC1A	ANGPTL4	LMO1	PPAPDC1A	IFIT2
PTN	CACNA2D3	PDZRN3	NMNAT2	FAM70A	STC1
PSG4	FBN1	PEG10	CA5B	PREX1	LYPD1
EPHA4	ZNF323	CUL4B	SAMD11	DSEL	ACOX2
FN1	NPR3	RBP4	GAS1	IGFL2	RBP1
CLEC2B	HBG2	SNCA	ADAMTS15	PCDH7	DLX1
TMTC1	ARNTL	ST3GAL1	PKP3	GPR87	TFPI
KITLG	MAFB	MALL	NAV1	NEBL	OSGIN1
ZNF704	ATOH8	TSPAN12	PDE4DIP	SPINK5	POU3F4
METTL7A	HMOX1	SDK1	LAMA4	SMAD6	PHTF2
SCG2	P2RX6	CNTNAP3	IL22RA1	PELI2	EID3
TRPM4	PSCA	LGI2	S100A2	EPB41L1	HFE
PLCE1	GLP2R	GPC1	DSCR1	ANKRD25	CTSC
CD36	CA9	COL3A1	ERG	GLI2	SCNN1A
COL12A1	PTPRN2	ARID5B	ARHGAP28	IGFBP2	ITGA4

PIK3R3	ZFHX4	LEPREL1	ANG	RPL7L1	HOXC13
EFEMP1	PHF15	MMP19	GEM	STAT4	PIH1D2
SFRP1	ATP2B4	PPP1R3C	NBEA	FZD10	KRT8P30
ACSS1	DCLK2	ITGB8	S100P	RCBTB2	FAIM
EMP2	FAM59A	SCARA5	TMEM14A	EPS8	ANK1
MCTS1	SPOCK2	MYPN	TRIM16	WSB2	FTL
DIRC2	PDE4B	OLFML2A	ENPP2	BFSP1	TMPRSS5
RAMP1	ADAM12	AMOTL1	GPNMB	STRA6	DYRK3
RKHD3	SMOX	ATP10D	FAM81A	GNAZ	PANX2
SIX2	APOBEC4	SMPX	CYBRD1	TRIB2	IGFBP6
ODZ3	PITPNM3	GPRASP2	TLE6	MID1	ZNF618
CITED2	LRRC62	CAPSL	DLX2	MICAL3	
GULP1	VCX2	EBI2	GPR161	IL18	
OTUD1	TCF7L2	SRXN1	NRCAM	IFI44	
UGDH	DPYSL3	SGOL1	DPYD	CYP26B1	
MAPT	MLLT3	RGS22	PSD4	RAB9A	
ADAM21	MEIS2	LFNG	AP1S3	DUSP19	
SFRS1	RAB7B	BCL6	CBX2	CYB5R2	
SOLH	STK32A	ANKRD38	PRICKLE2	SYNGR1	
TBC1D8B	SGK	SYT15	FBXL17	KBTBD7	
PMP22	CBLB	PAQR9	IFIT1	FBLN2	
ZBTB33	CD24	PER3	ANKRD15	APOM	
CPA3	AHNAK2	LZTS1	MMP3	SULT1A1	
GNG11	ADORA1	TLE4	RRM2	KCNMB1	
TM4SF1	NAG	TNS4	SRGN	CLSPN	
PQLC3	PRDM11	HPSE	SGCB	CCKBR	
CLCF1	TAF13	MEGF6	VCX	TPM1	
SNX16	ZFYVE28	SEMA3A	SCARA3	FKBP7	
PAPSS2	HECW2	SULT1A2	CDKN2C	GCNT3	
HTATIP2	FGF2	TBC1D2	CDC42	SERPINE1	
ABCC2	AP1S2	SYNC1	WWTR1	PLEKHK1	
IL1R1	BRI3	CYP27C1	ID1	DRD2	
COL5A2	TMEM158	ITGBL1	HIST1H3D	RAB9P1	
CRIP1	LAMP2	IRS1	DNER	IFIT3	
CFD	IKZF2	GPR30	NOS1AP	AVPI1	
VAV3	PRR15	LHFP	OSTM1	PLCG2	
ZRANB3	GCLC	RGL1	HSPA2	NR2F2	
MSX2P	RASL11A	FAT4	SCAMP5	SYTL2	

8. Annexure II

List of genes altered upon PKP3 loss in HCT116 cells

a. List of genes up-regulated more than 1.5 folds upon PKP3 loss in HCT116 cells.

MAGED2	MALAT1	KRT23
DUSP26	FGF1	GIP
DAPL1	KBTBD10	SDCBP2
ATAD4	7A5	MMP7
TACSTD2	CLIC5	PIF1
OR13G1	C10orf81	CLDN12
IGFL2	PTPLB	C6orf25
SCGB2A2	DDI2	SECTM1
NGFRAP1L1	GBP5	PTPRR
GNA15	QTRT1	BCL11A
LIPG	FAM101A	OSTbeta
KRT7	GLULD1	SNORD110
MYH13	ANKRD22	SLPI
CA9	TMED9	SLAMF7
C1orf176	TMTC2	SDF2L1
GRHL3	TSPAN8	CNDP1
TMPRSS11E2	ME3	
SPRR1A	A2M	
LBA1	GPR110	
MYPN	PKIB	
BG542103	AQP7P2	
ELF5	PSCD3	
DAPP1	SNAR-G1	
ARHGAP9	NAV2	
TUBAL3	HRBL	
YAP1	NR4A3	
ERP27	CYP24A1	
ZNF365	GBP2	
PVRL4	CPA4	
RP5-821D11.2	TGFBI	
GON4L	PGM5P2	
GALNT5	EML2	
PTP4A1	ZFYVE9	
LBH	STK19	
GPR177	TMPRSS9	
PCDH19	ARPC4	
SCG3	CCDC48	
GPR87	SCARNA17	

b. List of genes down-regulated more than 1.5 folds

ZNF311	ZC3H7B
ODZ3	LARGE
HAPLN4	GH2
KALRN	LOXL4
AL096727	ZFP42
DNAH2	NLRP4
B3GAT1	
STXBP6	
ARL6IP5	
ALDH2	
FOXA2	
CD33	
TM9SF3	
MNS1	
TCF2	
UTS2D	
ABCA1	
BDNF	
ATG3	
MED6	
RPRM	
ZFP37	
L1CAM	
PKP3	
GAGE7	
HKDC1	
LSP1	
ZMAT1	
FAM128B	
CSTF2T	
SUSD2	
GCNT3	
GPR109B	
OPHN1	
DPPA2	
PPP3R1	
RGS2	
HOXB8	



RESEARCH ARTICLE

MMP7 Is Required to Mediate Cell Invasion and Tumor Formation upon Plakophilin3 Loss

Srikanta Basu, Rahul Thorat, Sorab N. Dalal*

Advanced Centre for Treatment Research and Education in Cancer (ACTREC), Tata Memorial Centre, Kharghar Node, Navi Mumbai, Maharashtra, India

* sdalal@actrec.gov.in



OPEN ACCESS

Citation: Basu S, Thorat R, Dalal SN (2015) MMP7 Is Required to Mediate Cell Invasion and Tumor Formation upon Plakophilin3 Loss. PLoS ONE 10(4): e0123979. doi:10.1371/journal.pone.0123979

Academic Editor: Jun Li, Sun Yat-sen University Medical School, CHINA

Received: October 10, 2014

Accepted: February 24, 2015

Published: April 13, 2015

Copyright: © 2015 Basu et al. This is an open access article distributed under the terms of the [Creative Commons Attribution License](https://creativecommons.org/licenses/by/4.0/), which permits unrestricted use, distribution, and reproduction in any medium, provided the original author and source are credited.

Data Availability Statement: All relevant data are within the paper and its Supporting Information files with the exception of the gene expression analysis which is available at NCBI GEO accession numbers GSE61512 and GSE64580.

Funding: This work was supported by a grant from the Department of Science and Technology (DST), Government of India to SND. The grant number is SR/SO/HS-011/2009. The work was also supported by intra-mural funds from ACTREC. SB was supported by a fellowship from the Council for Scientific and Industrial Research (CSIR) Govt. of India. The fellowship number is 09/513(0074)/2009-EMR-I. The funders had no role in study design, data

Abstract

Plakophilin3 (PKP3) loss results in increased transformation in multiple cell lines in vitro and increased tumor formation in vivo. A microarray analysis performed in the PKP3 knockdown clones, identified an inflammation associated gene signature in cell lines derived from stratified epithelia as opposed to cell lines derived from simple epithelia. However, in contrast to the inflammation associated gene signature, the expression of MMP7 was increased upon PKP3 knockdown in all the cell lines tested. Using vector driven RNA interference, it was demonstrated that MMP7 was required for in-vitro cell migration and invasion and tumor formation in vivo. The increase in MMP7 levels was due to the increase in levels of the Phosphatase of Regenerating Liver3 (PRL3), which is observed upon PKP3 loss. The results suggest that MMP7 over-expression may be one of the mechanisms by which PKP3 loss leads to increased cell invasion and tumor formation.

Introduction

Matrilysin (MMP7) is one of the smallest members of the MMP family and is a highly potent metallo-protease which can degrade casein, laminin, fibronectin, collagen III/IV/V/IX/X/XI, type I/II/IV/ V gelatins, elastin and proteoglycans [1, 2]. MMP-7 is secreted specifically by epithelial cells [3] and its over-expression has been observed in many tumor types such as colorectal cancer [4–7], epidermolysisbullosa associated skin cancer [8, 9], bladder cancer [10], gastric cancers [3, 11], pancreatic cancer [12] and esophageal cancer [13, 14]. An increase in the levels of MMP-7 mRNA was observed to correlate with increased dedifferentiation and metastasis in colon cancers [5, 15]. Loss of MMP7 either by antisense RNA mediated knockdown in colorectal cancer cell lines or by knockout in mice leads to decreased tumor incidence, while an increase in MMP7 expression causes increased tumor formation [16–18].

Desmosomes are cell-cell adhesion junctions present in both simple and stratified epithelial cells. Desmosomes anchor intermediate filaments in adjoining cells and thus play a central role in the formation of a tissue wide intermediate filament network, allowing cells to survive when they encounter mechanical stress during tissue repair [19, 20]. Three major protein families contribute to desmosome assembly, the desmosomal cadherins (desmogleins and

collection and analysis, decision to publish or preparation of the manuscript.

Competing Interests: The authors have declared that no competing interests exist.

desmocollins), the plakins family (desmosplakin) and the ARM repeat containing proteins (plakoglobin and plakophilins) (reviewed in [19, 20]).

Plakophilin3 (PKP3) is the most widely expressed plakophilin family member and is ubiquitously present in all the layers of the stratified epithelia and simple epithelia except in hepatocytes [21]. PKP3 forms a complex with a broad repertoire of desmosomal proteins like the desmosomal cadherins like desmoglein 1–3, desmocollins 1 and 3; keratin 18; desmoplakin and plakoglobin [22]. PKP3 plays a crucial role in the maintenance of the desmosomal structure and function by mediating recruitment of other desmosomal components to the cell border [23]. Previous results from our laboratory demonstrated that PKP3 loss leads to alterations in desmosome size, a decrease in cell-cell adhesion, increased cell migration and an increase in colony formation in soft agar and tumor formation and metastasis in immune-compromised mice [24]. PKP3 expression is known to decrease in high grade poorly differentiated oropharyngeal cancer [25], colon cancer [26], gastric cancer [27] and bladder cancers [28]. The epidermis of PKP3 knock-out mice (PKP3^{-/-}) show increase in epidermal proliferation, hair loss and are more prone to cutaneous inflammation. Under normal conditions, young PKP3^{-/-} mice, of the age of 3 weeks develop epidermal hyperplasia, severe skin inflammation and hair loss. In older mice, the inflammation persists and is accompanied by enlargement of regional lymph nodes [29].

Recent results from our lab have shown that PKP3 loss leads to an increase in PRL3 (Phosphatase of regenerating liver-3) protein levels leading to the dephosphorylation of keratin8 (K8), which results in increased neoplastic progression and metastasis [30]. To determine if alterations in the expression of other gene products were observed upon PKP3 knockdown, an expression analysis was performed comparing vector control cells to PKP3 knockdown cells. PKP3 knockdown clones generated from cell lines derived from the stratified epithelia (HaCaT and FBM) show an increase in expression of many inflammation associated genes and these changes were not observed in PKP3 knockdown clones derived from HCT116 cells. However, in contrast to other gene products, MMP7 mRNA and protein levels were increased upon PKP3 loss, in all cell lines tested. Our results suggest that in HCT116 cells, the increase in MMP7 levels is driven by PRL-3 over-expression in the PKP3 knockdown clones and that MMP7 is required for tumor formation in-vivo upon PKP3 loss.

Materials and Methods

Plasmids and constructs

The oligonucleotides used to generate the MMP7 shRNA constructs (S1 Table) were cloned downstream of the U6 promoter in pLKO.1-EGFPf-puro [31] digested with AgeI and EcoRI.

Cell culture and transfections

HCT116, HaCaT and FBM cells (Fetal buccal mucosal cell line) were cultured as described previously [23, 24, 30]. HCT116, HaCaT derived PKP3 knockdown clones and the respective vector control clones were maintained in selection media containing 5µg/ml of blasticidin, while the FBM derived PKP3 knockdown and the vector control clones were maintained in media containing 0.5µg/ml puromycin as described [24]. To generate HCT116 derived stable double knockdown clones for PKP3 and MMP7, the PKP3 knockdown clone, shpkp3-2 was transfected with MMP7 targeted shRNA encoding pLKO.EGFP-f plasmid using Lipofectamine LTX reagent (Life Technologies). The cells were maintained in media containing 5µg/ml blasticidin and 0.5µg/ml puromycin to obtain single cell clones. The PRL3 inhibitor-1 (Sigma) was added to cells in culture at a concentration of 10µM for either 24 or 48 hours.

Microarray analysis

RNA isolated from the FBM derived vector control and PKP3 knockdown cells and HCT116 derived vector control and PKP3 knockdown cells were Cy3 labeled and processed for the SurePrint G3 Human GE 8x60k microarray by single color hybridization. The results obtained from the microarray were analyzed using the Agilent Feature Extraction software. Using normalized signal intensities (g-processed signal) obtained from the microarray, the fold changes of genes altered in FBM derived PKP3 knockdown clone (shpkp3-2) has been compared to the vector control clone (vec). Similarly, the HCT116 derived derived PKP3 knockdown clone (shpkp3-2) has been compared to the vector control clone (vec). A functional classification of the differentially regulated genes was performed using GeneSpring GX 11.0 software and gene ontology browser. The significant pathway list for differentially regulated genes was obtained using the GeneSpring GX 11.0 and Biointerpreter software (Genotypic, Bangalore, India). The data for the FBM derived clones has been deposited in the NCBI GEO database (Accession number GSE61512), while the data for the HCT116 derived clones have been deposited in the NCBI GEO database (Accession number GSE64580). Functional classification of genes altered upon PKP3 loss was performed using the PANTHER Classification System software [32, 33].

Isolation of total RNA, real time PCR reactions and reverse transcriptase coupled PCR reactions

The forward and reverse oligonucleotides used in this study are shown in [S1 Table](#). Cells were collected in RLT buffer and total RNA isolated using the Qiagen RNeasy Kit, following the manufacturer's protocol and 2 μ g of RNA was reverse transcribed to cDNA using the ABI High Capacity Reverse Transcriptase Kit (Applied Biosystems, Life Technologies). The cDNA obtained was used for SyBr Green based Real time PCR using ABI SyBr Green PCR Master mix (Applied Biosystems, Life Technologies). Real Time PCR was performed using 10ng cDNA per reaction using the QuantStudio 12K Flex Real-Time PCR System (Life Technologies). The fold change in relative expression of each target gene compared to the loading control was calculated using the $2^{(-\Delta\Delta Ct)}$ method [34]. A change in expression of two-fold either way was considered significant. For reverse transcriptase coupled polymerase chain reactions, each reaction contained either 500ng or 1 μ g cDNA the fragments were amplified using Taq DNA polymerase (New England Biolabs).

Antibodies and Western blot analysis

For Western blots, the mouse monoclonal β actin antibody (clone AC74, catalogue number A5316, Sigma) was used at a dilution of 1:5000, the mouse monoclonal PKP3 antibody (clone 23E34, catalogue number 35-7600, Invitrogen) at a dilution of 1:2000, mouse monoclonal MMP7 antibody (clone JL07, sc-80205, Santa Cruz,) at a dilution of 1:100. Goat anti-mouse secondary antibody (Pierce) was used at a dilution of 1:2500. The blots were developed using Supersignal West Pico Chemiluminescent Substrate (Pierce) according to the manufacturer's instructions. Cells were lysed in 1X sample buffer as described [24] and protein concentration quantitated using Folin-Lowry's method. 75 μ g of the extract was resolved on 10% SDS-PAGE gels and transferred to nitrocellulose membranes (Mdi, Membrane Technologies) followed by Western blotting with the indicated antibodies. Western blots for MMP7 were performed as follows. Cells growing in serum containing media were replaced with fresh media and incubated for 24 hours or 48 hrs with or without the PRL3 inhibitor and the cell culture supernatants centrifuged for 10 mins at 7500xg to remove any cell debris. Three volumes of acetone were added to the supernatant and the reaction incubated at -20°C for 24 hours and then centrifuged

at 4500xg for 15 minutes at 4°C. The precipitate obtained was washed twice with acetone and the pellet air dried at RT for 16 hours. The precipitate was boiled in 1X SDS lysis buffer (2% SDS, 50mM Tris pH 6.8), then diluted ten-fold in 1X SDS lysis buffer and the protein concentration was measured using Folin-Lowry's method. 100µg of the lysate was resolved on 12% SDS-PAGE gels and transferred to nitrocellulose followed by Western blots with antibodies to MMP7. The blot was stained with Ponceau-S (Sigma) to demonstrate equal loading.

Scratch wound healing assays and matrigel invasion assays

Scratch wound healing assays were performed as described [30]. The plates were visualized under an Axiovert 200M Inverted microscope (Carl Zeiss) fitted with a cell incubator stage maintained at 37°C and 5% CO₂. Cells were observed by time lapse microscopy and images taken every 10 minutes for 20 hours using the AxioCamMRm Camera (Zeiss) with a 10X phase I objective. Axiovision software version 4.8 (Zeiss) was used to measure cell migration. Three independent experiments were performed in triplicates for each clone. Invasion assays were performed as described [35, 36]. Briefly, 2x10⁵ cells resuspended in 200µl of serum free media were added to the upper chambers and 400µl of serum containing media was added in the lower chamber. The inner side of the insert was pre-coated with 5µg of Matrigel (BD Biosciences). After 24 hours, cell culture inserts were then removed from the wells and the cells attached to the inner side of the insert were removed using cotton buds. The inserts with cells on the outer side of the membrane were fixed with 4% para-formaldehyde, stained with 1% crystal violet and mounted on slides using DPX mountant (Qualigens). Images were taken using Olympus SZ61 stereo microscope using a 10X objective lens. Three independent experiments were performed for each clone.

Soft agar assays

2500 cells of the HCT116 based plakophilin3 knockdown clones shpkp3-1 and shpkp3-2, the vector control clone (vec), the shpkp3-2 derived vector control and shpkp3-2 derived double knockdown clones were resuspended in 0.4% soft agarose as described [24]. The cells were maintained in media containing blasticidin (for vec, shpkp3-1 and shpkp3-2) and both puromycin and blasticidin for shpkp3-2 derived vector control and double knockdown clones. In three weeks, the total number of colonies formed on the soft agar plate was counted. Three independent experiments were performed in triplicates for each clone.

Tumor formation in nude mice

BALB/c Nude mice (CAnN.Cg-Foxn1nu/Crl) of 6–8 weeks old, provided by the ACTREC animal house facility, was used for the study. 1 x 10⁶ cells of the HCT116 based shpkp3-2 derived vector control and double knockdown clones were resuspended in 100µl of PBS and injected sub-cutaneously in the dorsal flank of mice. Six mice were injected for each clone. Tumor formation was monitored at intervals of 2 to 3 days and tumor size was calculated weekly for 5 weeks using the formula $(0.5 \times LV^2)$ where L is the largest dimension and V its perpendicular dimension [24]. The maximum tumor volume of 1045.421 mm³ was obtained 5th week post-injection for a mouse injected with shpkp3-2+vec. No surgical procedure was involved in the present study and therefore no anesthetic or analgesic was employed during these experiments. During injections, the animals were handled by trained, certified animal technicians and were injected by the in-house veterinarian with minimum distress to animals. Mice were sacrificed 5 weeks post injection. Animals were euthanized as per in-house Standard Operating Procedure (SOP) approved by the attending veterinarian (AV) of the ACTREC animal house facility. Carbon dioxide (CO₂), an inhalant euthanasia agent recommended by the Committee for the

Purpose of Control and Supervision of the Experiments on Animals (CPCSEA), Government of India, was used for euthanasia of mice. Euthanasia was performed under the supervision of the attending veterinarian and according to the American Veterinary Medical Association (AVMA) guidelines for the euthanasia of animals (2013 Edition). Briefly, a compressed CO₂ cylinder was used as a source for carbon dioxide to control the inflow of gas, which was connected to a euthanasia chamber. The mice were kept in the chamber and an optimal flow rate was maintained to fill 20% of the chamber volume. After keeping the mice in the chamber, the CO₂ cylinder supply valve was turned on to deliver the gas in the chamber so that animals were exposed to the gas slowly and steadily. After sufficient exposure like for 2 to 3 minutes, mice showed cessation of respiration and heart beats. The chamber was not prefilled with CO₂ and was vented out post sacrifice and before the next animal was introduced into the chamber. Thereafter, the mice were removed from the chamber and a cervical dislocation performed to ensure that the mice were dead.

Ethics statement

Animals were maintained in the ACTREC animal house facility following the national guidelines mentioned by the Committee for the Purpose of Control and Supervision of the Experiments on Animals (CPCSEA), Ministry of Environment and Forest, Government of India. A controlled environment was provided to the animals with a temperature of 22±2°C and relative humidity maintained at 40–70%. A 12 hours day night cycle was maintained (7:00 to 19:00 day and 19:00 to 7:00 night). The animals were given autoclaved balanced diet prepared in house and sterile water. Individually ventilated Cage system (IVC, M/S Citizen, India) was used to house mice used in the experiments. These IVCs were provided with autoclaved corn cob as bedding for the mice. Animal euthanasia was done under the guidelines of AVMA as mentioned above using CPCSEA recommended euthanizing agent, carbon dioxide. The Institutional Animal Ethics Committee (IAEC) of the Advanced Centre for Treatment Research and Education in Cancer (ACTREC) approved all the protocols used in this report. The project number for the study is 16/2008 and was approved in November 2008.

Results

PKP3 loss leads to alterations in the transcriptome of multiple cell types

Previous studies from our laboratory have demonstrated that loss of PKP3 in HCT116, HaCaT and FBM cells leads to an increase in transformation in vitro and increased tumor formation and metastasis in vivo [24]. To identify mechanisms downstream of PKP3 loss leading to tumor progression and metastasis, a gene expression analysis was performed to compare the transcriptome of the vector control (vec) and a PKP3 knockdown clone (shpkp3-2) derived from FBM cells. The mRNA purified from the FBM derived vector control (vec) PKP3 knockdown clones (shpkp3-2) was used to perform a single hybrid gene expression microarray using the 8x60K format. The data from these experiments has been uploaded to the NCBI GEO database (Accession no. GSE61512). The microarray was performed in duplicate and the analysis used the average values from the two sets of microarray data. The expression of 427 genes was up-regulated and 428 genes down-regulated in the PKP3 knockdown clone as compared to the vector control. An alteration in the expression of many of genes previously reported to be in pathways regulating inflammation were identified in the microarray (S1A Fig and S2 Table), which is consistent with an increase in inflammation being a hallmark of many tumors (reviewed in [37]). A microarray analysis was also to compare the transcriptome of the vector control (vec) and a PKP3 knockdown clone (shpkp3-2) derived from the HCT116 cells. The data from these experiments has been uploaded to the NCBI GEO database (Accession no.

GSE64580). The results from the microarray analysis along with the functional classification of the altered genes upon PKP3 loss are shown in [S1A Fig](#) and [S3 Table](#). As PKP3 knockdown leads to an increase in cellular transformation in three different cell lines (HaCaT, HCT116 and FBM), the data obtained from the microarray analysis was used as a reference to identify genes whose expression was altered upon loss of PKP3.

In confirmation of previously reported results [[24](#), [30](#)], a real time PCR analysis demonstrated that the mRNA levels of PKP3 was reduced in the PKP3 knockdown clones as compared to the vector controls ([Fig 1A](#)). The expression of genes which were found to be up-regulated or down-regulated more than two-fold in the FBM derived PKP3 knockdown clone was assessed using real time PCR to validate the results of the microarray and to analyze if the same genes were altered upon PKP3 knockdown in the HCT116 and HaCaT cell lines. A change in expression of two-fold either way was considered significant. A set of genes which included inflammation associated genes such as Interleukin 6 (IL6), Serum amyloid A1 (SAA1), Chemokine (C-C Motif) Ligand 2 (CCL2), S100A8, S100A9 and CBS, were up-regulated in HaCaT and FBM derived PKP3 knockdown clones ([Fig 1B](#)). None of these genes were expressed in HCT116 cells (data not shown). The expression of Epiplakin (EPPK1), Rho Guanine Nucleotide Exchange Factor (ARHGEF5), Matrix metalloprotease 9 (MMP9), MOB kinase activator 3B (MOBKL2b) and N terminal deleted isoform of TAp63 (Δ Np63) was found to be up-regulated while expression of Nuclear receptor subfamily-2 group-F member-1 (NR2F1) and Insulin like growth factor binding protein 3 (IGFBP3) was found to be down-regulated only in the FBM derived PKP3 knockdown clones while their expression was not altered in the HaCaT and HCT116 derived PKP3 knockdown clones ([S1B Fig](#)). The expressions of all the genes were normalized using the expression of GAPDH as a control as described in the Materials and Methods. These results suggested that PKP3 loss leads to varying alterations in the transcriptome in the three cell types studied and that PKP3 loss leads to the generation of an inflammation associated signature in cell lines derived from stratified epithelia, which is consistent with the observation that inflammation is observed in the epidermis of mice lacking PKP3 [[29](#)].

MMP7 is required for transformation upon loss of PKP3

The mRNA levels of the Matrix metalloprotease7 (MMP7) gene were found to be up-regulated upon PKP3 loss in all three cell types tested ([Fig 1C](#)). To determine whether the increase in MMP7 levels is required for tumor formation upon PKP3 loss, double knockdown clones were generated where MMP7 was knocked down in the PKP3 knockdown clone shpkp3-2 using vector driven RNA interference. Two double knockdown clones were obtained, shpkp3-2+shMMP7-1 and shpkp3-2+shMMP7-2. The vector control clone (shpkp3-2+vec) was generated by transfection of the empty vector in the shpkp3-2 clone. The expression of MMP7 in the vector control and the double knockdown clones was validated by real time PCR ([Fig 2a](#)). Since MMP7 is a secreted protein [[6](#), [38](#), [39](#)], cells were grown in the absence of serum and the supernatant collected for the indicated cell types. The proteins in the supernatant were precipitated using acetone as described in the Materials and Methods and a Western blot performed for MMP7. The cells were lysed and harvested for Western blots performed for PKP3 and actin as described [[30](#)]. PKP3 levels were reduced in both the single and double knockdown clones ([Fig 2B](#)). A Western blot for β actin served as a loading control. PKP3 knockdown led to an increase in the expression of MMP7 while knockdown of MMP7 causes a decrease in the expression of MMP7 as expected ([Fig 2B](#)). The blot was stained with ponceau-S to show equal protein loading for the cell supernatants.

PKP3 loss leads to an increase in cell migration as assayed by scratch wound healing assays [[24](#)]. To determine if MMP7 loss can reverse the increase in cell migration observed upon

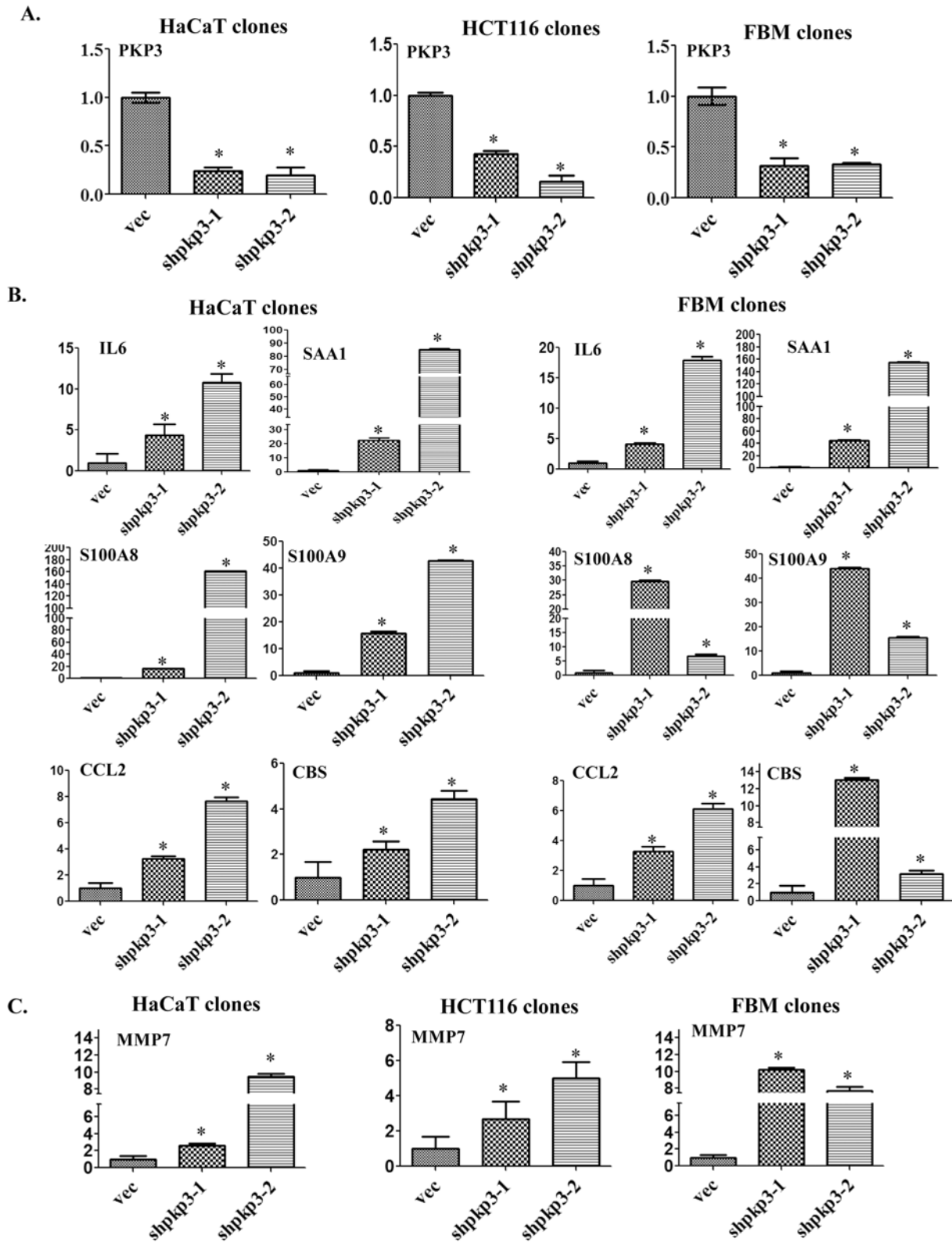


Fig 1. PKP3 loss leads to the generation of an inflammation associated signature in cell lines derived from stratified epithelia. The Y-axis in all panels reflects the fold change in transcription, which is calculated as described in the Materials and Methods. The X-axis indicates the clone name. mRNA was prepared from the vector controls (vec) or PKP3 knockdown clones (sh-pkp3-1 and shpkp3-2) derived from either HCT116, FBM or HaCaT cells as

indicated. **(A)** Real time PCR assays were performed using oligonucleotides specific to PKP3 and GAPDH. Relative expression of PKP3 in the HCT116, HaCaT and FBM derived PKP3 knockdown clones (shpkp3-1 and shpkp3-2) was compared to the respective vector control clones (vec). Expression of GAPDH has been used for normalization. **(B)** Real time PCRs were performed using oligonucleotides specific for IL6, SAA1, S100A8, S100A9, CCL2, CBS and GAPDH, in HaCaT and FBM derived PKP3 knockdown clones and the respective vector controls. Expression of GAPDH has been used for normalization. **(C)** Real time PCR was performed using oligonucleotides specific to MMP7 and GAPDH, with cDNA obtained from the vector control and PKP3 knockdown clones derived from the three cell types under study. Expression of GAPDH has been used for normalization. The standard errors are plotted and student's t test was performed (* indicates a p value <0.01).

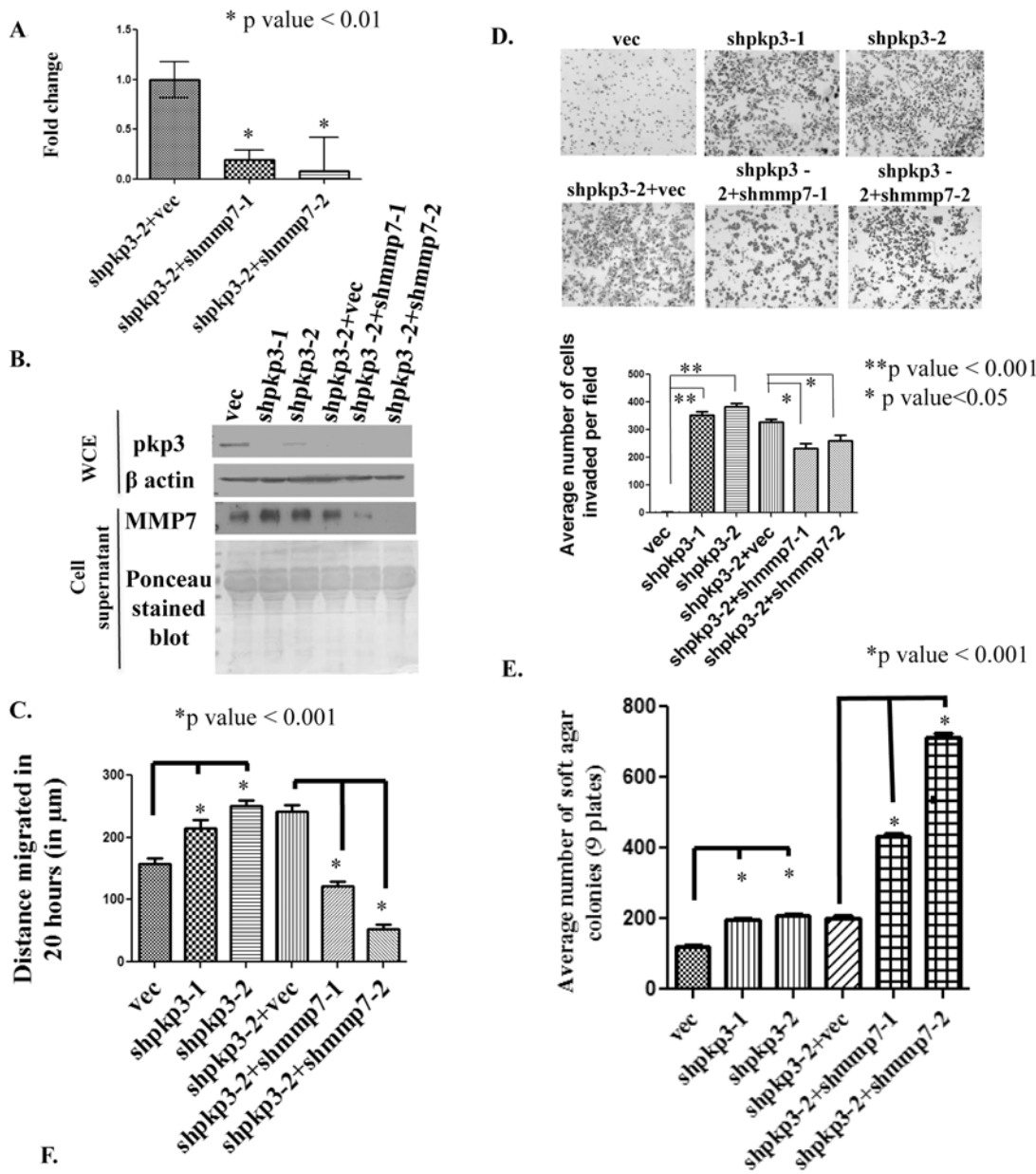
doi:10.1371/journal.pone.0123979.g001

PKP3 loss, scratch wound healing assays were performed. As reported earlier, pkp3 loss increased in-vitro cell migration of HCT116 cells, while MMP7 loss in the pkp3 knockdown clones decreased in-vitro cell migration in PKP3 knockdown cells (Fig 2C and S1C Fig). PKP3 loss leads to an increase in metastasis and this is often associated with an increase in cell invasion. To determine if PKP3 loss leads to increased invasion, matrigel invasion assays were performed as described [35, 36]. Loss of PKP3 leads to an increase in invasion as shown in Fig 2D. The increase in invasion observed upon PKP3 loss was reversed when MMP7 expression was inhibited (Fig 2D). These results suggested that MMP7 is required for the increased migration and invasion observed upon PKP3 knockdown in HCT116 cells.

PKP3 loss leads to an increase in anchorage independent growth and an increase in tumor formation and metastasis in vivo [24]. To determine the effect of MMP7 loss on anchorage independent growth soft agar assays were performed on the vector control and double knockdown clones. As reported earlier, pkp3 loss increased anchorage independent growth, but surprisingly, the double knockdown clones formed more colonies in soft-agar than the vector control clones (Fig 2E). Since this result was in contrast to the results obtained in the migration and invasion assays, we determined whether MMP7 loss leads to an alteration in tumor formation in vivo. It has been reported earlier that HCT116 derived pkp3 knockdown clones form larger tumors and show increased metastasis in vivo [24]. The vector control, shpkp3-2+vec and the double knockdown clones were injected subcutaneously in nude mice as previously described [24, 30]. The mice were observed for 5 weeks and tumor size measured at regular intervals. Five of the six mice injected with the vector control developed large tumors Fig 2F and S2A Fig). In contrast, only two out of six mice injected with shpkp3-2+shMMP7-1 and one of the six mice injected with shpkp3-2+shMMP7-2 were able to develop tumors at the site of injection and the tumors formed were much smaller in size than those formed in mice injected with the vector control clone (shpkp3-2+vec)(Fig 2F and S2A Fig). The average volume of the tumor formed in the mice was analyzed using the formula mentioned in Materials and Methods (data not shown).

PRL3 regulates MMP7 expression in the HCT116 derived PKP3 knockdown clones

Previous data from our laboratory has demonstrated that an elevation in the levels of Keratin 8 is observed in the HCT116 derived PKP3 knockdown clones and that this increase is due to an increase in the levels of the phosphatase of regenerating liver 3 (PRL-3) and inhibition of PRL-3 activity using a chemical inhibitor resulted in a decrease in cell migration [30]. An inhibition of PRL-3 activity using a chemical inhibitor of PRL-3 resulted in a decrease in cell migration in the HCT116 derived PKP3 knockdown clones [30]. A previous report demonstrated that PRL3 activity regulates MMP7 expression via the PI3K/AKT and ERK signaling pathway in the colon cancer derived cell line DLD1 [40]. Therefore, we hypothesized that the increase in MMP7 levels observed upon PKP3 knockdown was due to the increase in PRL-3 levels. To test this hypothesis the HCT116 derived vector control and PKP3 knockdown clones were treated with 5 or 10 μ M of the PRL-3 inhibitor for 24 hours. A real time PCR analysis demonstrated



Name of clone	No. of mice injected with cells	No. of mice developing tumor after 5 weeks
shpkp3-2+vec	6	5
shpkp3-2+shmpmp7-1	6	2
shpkp3-2+shmpmp7-2	6	1

Fig 2. Loss of MMP7 leads to a decrease in transformation in cells lacking PKP3. (A) mRNA prepared from HCT116 derived PKP3 knockdown cells transfected with the vector control (shpkp3-2 + vec) or the MMP7 knockdown construct (shpkp3-2 + shMMP7-1 and shpkp3-2 + MMP7-2) was used as a substrate for reverse transcriptase followed by real time PCR reactions using oligonucleotides specific for MMP7. All expression was normalized to the levels of GAPDH. The fold change is graphed on the Y-axis and the clone name is on the X-axis. Note that MMP7 levels are lowered in the double knockdown clones as compared to the vector control. The standard errors are plotted and student's t test was performed (* indicates a p value < 0.01). (B) 75 μ g of a whole cell extract (WCE) was resolved on 12% SDS PAGE gels followed by Western blotting with antibodies specific to PKP3. Note that PKP3 levels are lower in clones with a PKP3 knockdown. Western blots for β actin served as a loading control (upper panels). 100 μ g of acetone precipitated cell supernatants were resolved on 12% SDS PAGE gels followed by Western blotting with antibodies specific to MMP7. Note that MMP7 levels are higher in supernatants

prepared from the PKP3 knockdown cells as compared to the vector controls and the levels are lower in the double knockdown clones. The same blot was stained with Ponceau stain to demonstrate equal loading of proteins (lower panels). **(C)** Scratch wound healing assays were performed on the HCT116 derived vector control (vec), PKP3 knockdown clones (shpkp3-1 and shpkp3-2), shpkp3-2 derived vector control clone (shpkp3-2+vec) and shpkp3-2 derived MMP7 knockdown clones (shpkp3-2+shMMP7-1 and shpkp3-2+shMMP7-2) as described. **(D)** Matrigel invasion assays were performed in Boyden's chambers for HCT116 derived vector control cells, PKP3 knockdown clones and the double knockdown clones. The number of cells observed in ten random fields of the membrane for each clone was determined as described in Materials and Methods, representative images of for each clone are shown. The mean and standard deviation of three independent experiments are plotted. Note that loss of PKP3 leads to an increase in invasion as compared to the vector control and this phenotype is reversed in the double knockdown clones. **(E)** Soft agar colony formation assay was performed with the HCT116 derived vector control and pkp3 knockdown clones, the shpkp3-2 derived double knockdown clones and the shpkp3-2 derived vector control clone. The mean and standard deviation of three independent experiments is plotted. **(F)** 1×10^6 cells of the shpkp3-2 derived vector control or double knockdown clones were injected subcutaneously into nude mice and allowed to develop tumors. The table shows the number of mice injected with the respective clones and the number of mice among them which were able to develop tumors. Wherever indicated the p value was calculated using a student's t-test.

doi:10.1371/journal.pone.0123979.g002

that the levels of MMP7 mRNA in the PKP3 knockdown clones were decreased upon treatment with the PRL-3 inhibitor in a concentration dependent manner (Fig 3A). The mRNA levels of Lipocalin2 (LCN2) which is increased upon PKP3 knockdown in HCT116 cells, did not decrease upon treatment with the PRL-3 inhibitor (S2B Fig) suggesting that PRL3 activity does not regulate the expression of other gene products such as LCN2 in these cells. A Western blot analysis demonstrated that the levels of MMP7 protein were also decreased upon treatment with the inhibitor at 24 hours in HCT116 cells (Fig 3B), but not in the HaCaT derived PKP3 knockdown clones (S2C Fig). To determine whether PRL3 inhibitor treatment (which inhibits the activity of PRL3) resulted in a change in PRL-3 protein levels, a Western blot analysis was performed. It was observed that PRL-3 levels were higher in PKP3 knockdown clones as reported earlier [30], but no change in the levels of PRL-3 was observed upon treatment with the PRL-3 inhibitor (Fig 3C). A Western blot for actin served as a loading control. These results suggest that the increase in PRL-3 levels observed upon PKP3 loss is required for the increase in MMP7 mRNA and protein levels observed in HCT116 cells.

Discussion

The results in this report demonstrate that loss of PKP3 leads to an increase in the levels of MMP7 in three independently derived cell lines of different origins. The increase in MMP7 levels is required for cell migration and invasion in vitro and tumor formation in nude mice as loss of MMP7 in the PKP3 knockdown cells results in a reversal of these phenotypes. The increase in MMP7 mRNA is dependent on the expression of PRL-3, whose levels are elevated upon PKP3 loss [30]. Thus, the results in this paper suggest that the increased tumor formation observed upon PKP3 loss requires the expression of MMP7.

MMP7 mediates cell invasion and tumor formation upon PKP3 loss

MMP7 and membrane type-1 matrix metalloprotease (MT1-MMP) are metalloproteases which are exclusively produced by the epithelial cells of the colon while the rest of these matrix-metalloproteases such as MMP9, MMP11 (stromelysin 3) are produced by the stroma [3, 41–43]. MMP7 levels are increased in colon cancer tissues [4–6] and in the serum of colon cancer patients [7]. A study by Witty et.al., demonstrated that MMP7 knockdown clones derived from the colon cancer cell line SW620 do not form tumors as efficiently as the corresponding vector controls in orthotopic xenografts of colon cancer [18]. Further, studies by Wilson et. al., [16] and Guillen-Ahlers et.al. [17] demonstrated that loss of MMP7 in the intestine of Apc^{Min} mice leads to a decrease in tumor incidence. Our work has demonstrated that PKP3 loss leads to an increase in migration, invasion, tumor formation and metastasis and that these functions are dependent upon the increase in MMP7 expression upon PKP3 knockdown. To determine if a correlation exists between MMP7 and PKP3 levels across colon cancers at

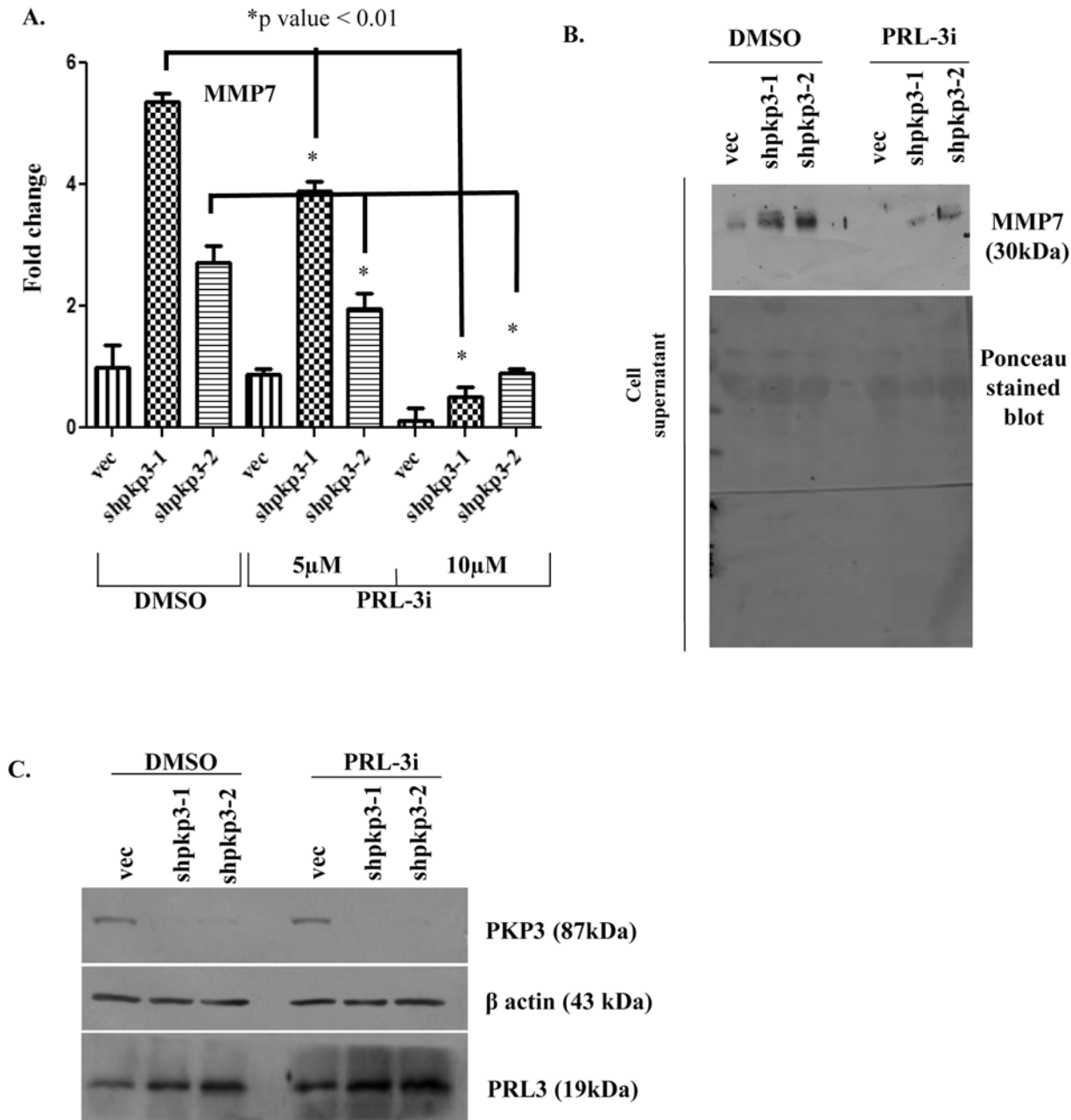


Fig 3. MMP7 expression decreases upon inhibition of PRL3 activity. (A) The HCT116 derived PKP3 knockdown clones (shpkp3-1 and shpkp3-2) or the vector control (vec) were treated with either the vehicle control (DMSO) or 5 or 10 μM PRL-3 inhibitor-1 (PRL-3i) for 24 hours. The mRNA prepared from the treated cells was used as a substrate for reverse transcriptase followed by real time PCR reactions using oligonucleotides specific for MMP7. All expression was normalized to the levels of GAPDH. The fold change is graphed on the Y-axis and the clone name is on the X-axis. The standard errors are plotted and student's t test was performed. Note that MMP7 levels are lowered upon treatment with PRL-3 inhibitor. (B) The HCT116 derived vector control (vec) and PKP3 knockdown clones (shpkp3-1 and shpkp3-2) were treated with either DMSO or 10 μM PRL3 inhibitor-1 (PRL3i) for 24 hours or 48 hours. The cell supernatants were collected and a 100 μg of acetone precipitated protein was resolved on 12% SDS PAGE gels followed by Western blotting with antibodies to MMP7. The same blot was stained with Ponceau stain to indicate equal loading. (C) The whole cell lysates of HCT116 derived vector control and plakophilin3 knockdown clones treated with DMSO or PRL3i for 24 hours were resolved on 12% poly-acrylamide gel. This was followed by Western blotting with antibodies to PKP3, β actin and PRL3. The molecular weights of these proteins are indicated in brackets.

doi:10.1371/journal.pone.0123979.g003

the transcript level, we analyzed the data sets in the Oncomine database (www.oncomine.org). When PKP3 levels in normal colon samples were compared with that in colon cancer, the levels were found to be unchanged, while MMP7 levels were higher in colon cancer samples. None of the databases present had actually validated the PKP3 levels using real time PCR or reverse transcriptase PCR. To determine if a correlation exists between MMP7 and PKP3 levels across colon cancers at the protein level, we examined the data deposited in the human protein atlas database (<http://www.proteinatlas.org/>). It was observed that a thorough immuno-histochemical analysis of PKP3 and MMP7 levels in a large dataset of colorectal cancer patients has not been performed to determine if any correlation exists between PKP3 and MMP7 levels. Surprisingly, MMP7 loss leads to an increase in colony formation in soft agar but a decrease in tumor formation in nude mice. These results suggest that the ability of MMP7 to induce the degradation of the extra-cellular matrix in vivo maybe essential for the ability of the PKP3 knockdown cells to form a tumor. Taken together these results suggest that the increase in MMP7 levels observed upon PKP3 loss is required for increased tumorigenesis in cells derived from the colon.

MMP7 over-expression upon PKP3 is regulated by PRL3

PRL-3 levels are increased in colorectal cancers [44] and PRL-3 expression leads to metastasis in tumors derived from the colon [45]. Lee et.al. [40] demonstrated that PRL3 increases cell migration and invasion by up-regulating expression of MMP7 in colorectal cancer cell line DLD-1, via the PI3K/AKT and ERK signaling pathway. Earlier reports from this laboratory have demonstrated that an increase in K8 levels upon PKP3 knockdown in HCT116 cells is dependent on increased levels of PRL-3 and that the inhibition of PRL-3 expression using shRNA constructs or the inhibition of PRL-3 activity using a specific inhibitor results in a reversal of the observed phenotype [30]. Similarly, the results in this paper demonstrate that inhibition of PRL-3 activity in the PKP3 knockdown clones results in a decrease in MMP7 levels. No increase in the levels of PRL-3 mRNA or stability was observed in HCT116 derived PKP3 knockdown cells [30] suggesting that the increase in PRL-3 protein levels occurred post-transcriptionally. One possible explanation for this observation is that PRL3 translation maybe increased upon PKP3 loss. Hofmann, et.al have demonstrated that PKP3 localizes to stress granules (sites of stalled mRNA-protein complexes) and forms a complex with RNA binding proteins like PolyA binding protein Cytoplasmic 1 (PABPC1), Fragile X Mental Retardation, Autosomal Homolog 1 (FXR1), and GTPase Activating Protein (SH3 Domain) Binding Protein 1 (G3BP) [46, 47]. Thus, PKP3 may regulate the translation of PRL-3 mRNA. Consistent with these observations, plakophilin1 has been reported to regulate translation initiation by directly binding to eIF4A (eukaryotic Initiation factor 4A) and promoting its activity [48].

PKP3 knockdown leads to differential alterations in transcriptome of three different cell types

PKP3 knockout mice show symptoms of severe itching, intercellular edema, neutrophil infiltration, epidermal hyperplasia, hair loss and muscle wasting [29]. Because of this dermatitis associated muscle wasting, the PKP3 null mice are smaller in size than the wild type mice and are very similar to the mouse model for atopic dermatitis, a severe form of skin inflammation. A previous gene expression analysis demonstrated that conditional deletion of the desmosomal protein Perp in stratified epithelia of mice led to up-regulation of inflammatory associated genes like S100A9 and the Chemokine (C-C motif) ligand 20 (CCL20)[49]. Another transcriptomic analysis performed by Jheon et.al.[50], demonstrated that Perp loss in the enamel of mice leads to alterations in gene expression. Consistent with these observations, in this study

we report that loss of PKP3 in cell lines derived from the HaCaT and FBM cell lines lead to the over-expression of multiple genes associated with inflammation (Fig 1B). These results provide a possible explanation for the skin inflammation phenotype obtained in PKP3 knockout mice [29] and maybe dependent on the loss of desmosome function observed upon PKP3 loss [23, 24]. To our surprise MMP7 levels did not decrease in the HaCaT cells upon treatment with the PRL-3 inhibitor suggesting that the increase in MMP7 in HaCaT cells occurs via mechanisms distinct from those observed in HCT116 cells and is consistent with our observations that PKP3 loss leads to cell type specific alterations in the transcriptome. The relevance of other alterations in gene expression that are specific to the FBM line is not clear. They may relate to the role of PKP3 in regulating desmosome formation in the oral cavity or these changes might have a role to play in the increased migration and cellular transformation observed in these cells upon PKP3 loss [24]. Thus, PKP3 loss can lead to both cell type dependent and cell type independent alterations in gene expression.

The results reported here lead to the generation of the following model. PKP3 loss leads to an increase in PRL-3 translation leading to an increase in K8 levels [30] or an increase in MMP7 mRNA levels (this report). Both K8 and MMP7 are independently required for the increase in migration and transformation observed upon PKP3 loss suggesting that either one can serve as a potential drug target in metastatic colon cancer. The role of PKP3 in regulating the increase in PRL-3 protein levels remains to be determined and should be a focus for future investigation.

Supporting Information

S1 Table. List of oligonucleotides used in the study.

(DOCX)

S2 Table. Alterations in gene expression upon PKP3 knockdown in FBM cells and functional classification of the altered genes. Compiled data with complete dataset, differentially expressed genes and functional classification of altered genes observed upon PKP3 knockdown in FBM cell line.

(XLSX)

S3 Table. Alterations in gene expression upon PKP3 knockdown in HCT116 cells and functional classification of the altered genes. Compiled data with complete dataset, differentially expressed genes and functional classification of altered genes observed upon PKP3 knockdown in HCT116 cell line.

(XLSX)

S1 Fig. S1A Fig, Functional classification of genes whose expression is altered ≥ 2 folds in FBM derived clones and ≥ 1.5 folds in HCT116 derived clones upon PKP3 knockdown. The mRNA expression profile of the FBM derived vector control (vec) was compared with that of the PKP3 knockdown clone (shpkp3-2). Similarly, mRNA expression profile of the HCT116 derived vector control (vec) was compared with that of the PKP3 knockdown clone (shpkp3-2). Differentially expressed genes which show more than two fold (for FBM) and more than 1.5 folds up-regulation or down-regulation in the PKP3 knockdown clones compared to the vector control clone were selected. The pie charts show functional classification of genes obtained from the microarray data analysis using the PANTHER Classification tool (<http://www.pantherdb.org/about.jsp>). S1B Fig, Cell type specific alterations in FBM derived PKP3 knockdown clones. Reverse transcriptase PCRs were performed using oligonucleotides specific for SAA4, EPPK1, MOBKL2b, MMP9, NR2F1, Δ Np63, IGFBP3, ARHGEF5 and GAPDH, in HaCaT, HCT116 and FBM derived PKP3 knockdown clones and the respective vector

controls. Expression of GAPDH has been used for normalization. The PCR product size has been indicated in base pairs. S1C Fig, MMP7 loss leads to a decrease in migration. Phase contrast images of wound healing at 0 hours (start) and 20 hours (end of experiment) have been shown.

(TIF)

S2 Fig. S2A Fig, Tumor formation is inhibited in the PKP3 knockdown cells upon MMP7 knockdown. 10^6 cells of the vector control or the double knockdown clones were injected subcutaneously into nude mice and allowed to develop tumors. Representative images of mice have been shown. S2B Fig, LCN2 expression is not altered upon inhibition of PRL-3. The HCT116 derived PKP3 knockdown clones (shpkp3-1 and shpkp3-2) or the vector control (vec) were treated with either the vehicle control (DMSO) or 10 μ M PRL-3 inhibitor-1 (PRL-3i) for 24 hours. The mRNA prepared from the treated cells was used as a substrate for reverse transcriptase followed by real time PCR reactions using oligonucleotides specific for LCN2. All expression was normalized to the levels of GAPDH. The fold change is graphed on the Y-axis and the clone name is on the X-axis. The standard errors are plotted and student's t test was performed (* indicates a p value <0.01). Note that LCN2 levels are increased upon treatment with PRL-3 inhibitor. S2C Fig, MMP7 expression does not change upon inhibition of PRL3 activity in HaCaT derived clones. The HaCaT derived PKP3 knockdown clones (shpkp3-1 and shpkp3-2) or the vector control (vec) were treated with either the vehicle control (DMSO) or 10 μ M PRL-3 inhibitor-1 (PRL-3i) for 24 hours. The cell supernatants were collected and a 100 μ g of acetone precipitated protein was resolved on 12% SDS PAGE gels followed by Western blotting with antibodies to MMP7. The same blot was stained with Ponceau to indicate equal loading.

(TIF)

Acknowledgments

We thank the ACTREC microscopy facility for help with acquisition of images used in this report.

Author Contributions

Conceived and designed the experiments: SB SND. Performed the experiments: SB RT. Analyzed the data: SB SND. Contributed reagents/materials/analysis tools: SB. Wrote the paper: SB SND.

References

1. Woessner JF Jr, Taplin CJ. Purification and properties of a small latent matrix metalloproteinase of the rat uterus. *J Biol Chem.* 1988; 263(32):16918–25. PMID: [3182822](#)
2. Miyazaki K, Hattori Y, Umenishi F, Yasumitsu H, Umeda M. Purification and characterization of extracellular matrix-degrading metalloproteinase, matrin (pump-1), secreted from human rectal carcinoma cell line. *Cancer Res.* 1990; 50(24):7758–64. PMID: [2253219](#)
3. McDonnell S, Navre M, Coffey RJ Jr, Matrisian LM. Expression and localization of the matrix metalloproteinase pump-1 (MMP-7) in human gastric and colon carcinomas. *Mol Carcinog.* 1991; 4(6):527–33. PMID: [1793490](#)
4. Zeng ZS, Shu WP, Cohen AM, Guillem JG. Matrix metalloproteinase-7 expression in colorectal cancer liver metastases: evidence for involvement of MMP-7 activation in human cancer metastases. *Clin Cancer Res.* 2002; 8(1):144–8. PMID: [11801551](#)
5. Mori M, Barnard GF, Mimori K, Ueo H, Akiyoshi T, Sugimachi K. Overexpression of matrix metalloproteinase-7 mRNA in human colon carcinomas. *Cancer.* 1995; 75(6 Suppl):1516–9.

6. Polistena A, Cucina A, Dinicola S, Stene C, Cavallaro G, Ciardi A, et al. MMP7 expression in colorectal tumours of different stages. *In vivo*. 2014; 28(1):105–10. PMID: [24425843](#)
7. Maurel J, Nadal C, Garcia-Albeniz X, Gallego R, Carcereny E, Almendro V, et al. Serum matrix metalloproteinase 7 levels identifies poor prognosis advanced colorectal cancer patients. *International journal of cancer*. 2007; 121(5):1066–71. PMID: [17487834](#)
8. Kivisaari AK, Kallajoki M, Ala-aho R, McGrath JA, Bauer JW, Konigova R, et al. Matrix metalloproteinase-7 activates heparin-binding epidermal growth factor-like growth factor in cutaneous squamous cell carcinoma. *Br J Dermatol*. 2010; 163(4):726–35. doi: [10.1111/j.1365-2133.2010.09924.x](#) PMID: [20586780](#)
9. Kivisaari AK, Kallajoki M, Mirtti T, McGrath JA, Bauer JW, Weber F, et al. Transformation-specific matrix metalloproteinases (MMP)-7 and MMP-13 are expressed by tumour cells in epidermolysis bullosa-associated squamous cell carcinomas. *Br J Dermatol*. 2008; 158(4):778–85. doi: [10.1111/j.1365-2133.2008.08466.x](#) PMID: [18284387](#)
10. Szarvas T, Becker M, vom Dorp F, Gethmann C, Totsch M, Bankfalvi A, et al. Matrix metalloproteinase-7 as a marker of metastasis and predictor of poor survival in bladder cancer. *Cancer science*. 2010; 101(5):1300–8. doi: [10.1111/j.1349-7006.2010.01506.x](#) PMID: [20180812](#)
11. Yamashita K, Azumano I, Mai M, Okada Y. Expression and tissue localization of matrix metalloproteinase 7 (matrilysin) in human gastric carcinomas. Implications for vessel invasion and metastasis. *International journal of cancer*. 1998; 79(2):187–94. PMID: [9583735](#)
12. Yamamoto H, Itoh F, Iku S, Adachi Y, Fukushima H, Sasaki S, et al. Expression of matrix metalloproteinases and tissue inhibitors of metalloproteinases in human pancreatic adenocarcinomas: clinicopathologic and prognostic significance of matrilysin expression. *J Clin Oncol*. 2001; 19(4):1118–27. PMID: [11181677](#)
13. Yamashita K, Mori M, Shiraishi T, Shibuta K, Sugimachi K. Clinical significance of matrix metalloproteinase-7 expression in esophageal carcinoma. *Clin Cancer Res*. 2000; 6(3):1169–74. PMID: [10741748](#)
14. Ohashi K, Nemoto T, Nakamura K, Nemori R. Increased expression of matrix metalloproteinase 7 and 9 and membrane type 1-matrix metalloproteinase in esophageal squamous cell carcinomas. *Cancer*. 2000; 88(10):2201–9. PMID: [10820340](#)
15. Yoshimoto M, Itoh F, Yamamoto H, Hinoda Y, Imai K, Yachi A. Expression of MMP-7(PUMP-1) mRNA in human colorectal cancers. *International journal of cancer*. 1993; 54(4):614–8. PMID: [8514452](#)
16. Wilson CL, Heppner KJ, Labosky PA, Hogan BL, Matrisian LM. Intestinal tumorigenesis is suppressed in mice lacking the metalloproteinase matrilysin. *Proc Natl Acad Sci U S A*. 1997; 94(4):1402–7. PMID: [9037065](#)
17. Guillen-Ahlers H, Buechler SA, Suckow MA, Castellino FJ, Ploplis VA. Sulindac treatment alters collagen and matrilysin expression in adenomas of ApcMin/+ mice. *Carcinogenesis*. 2008; 29(7):1421–7. doi: [10.1093/carcin/bgn123](#) PMID: [18499699](#)
18. Witty JP, McDonnell S, Newell KJ, Cannon P, Navre M, Tressler RJ, et al. Modulation of matrilysin levels in colon carcinoma cell lines affects tumorigenicity in vivo. *Cancer Res*. 1994; 54(17):4805–12. PMID: [8062282](#)
19. Desai BV, Harmon RM, Green KJ. Desmosomes at a glance. *J Cell Sci*. 2009; 122(Pt 24):4401–7. doi: [10.1242/jcs.037457](#) PMID: [19955337](#)
20. Garrod DR, Merritt AJ, Nie Z. Desmosomal adhesion: structural basis, molecular mechanism and regulation (Review). *Mol Membr Biol*. 2002; 19(2):81–94. PMID: [12126234](#)
21. Schmidt A, Langbein L, Pratzel S, Rode M, Rackwitz HR, Franke WW. Plakophilin 3—a novel cell-type-specific desmosomal plaque protein. *Differentiation; research in biological diversity*. 1999; 64(5):291–306. PMID: [10374265](#)
22. Bonne S, Gilbert B, Hatzfeld M, Chen X, Green KJ, Van Roy F. Defining desmosomal plakophilin-3 interactions. *J Cell Biol*. 2003; 161(2):403–16. PMID: [12707304](#)
23. Gosavi P, Kundu ST, Khapare N, Sehgal L, Karkhanis MS, Dalal SN. E-cadherin and plakoglobin recruit plakophilin3 to the cell border to initiate desmosome assembly. *Cell Mol Life Sci*. 2011; 68(8):1439–54. doi: [10.1007/s00018-010-0531-3](#) PMID: [20859650](#)
24. Kundu ST, Gosavi P, Khapare N, Patel R, Hosing AS, Maru GB, et al. Plakophilin3 downregulation leads to a decrease in cell adhesion and promotes metastasis. *Int J Cancer*. 2008; 123(10):2303–14. doi: [10.1002/ijc.23797](#) PMID: [18729189](#)
25. Papagerakis S, Shabana AH, Depondt J, Gehanno P, Forest N. Immunohistochemical localization of plakophilins (PKP1, PKP2, PKP3, and p0071) in primary oropharyngeal tumors: correlation with clinical parameters. *Hum Pathol*. 2003; 34(6):565–72. PMID: [12827610](#)

26. Aigner K, Descovich L, Mikula M, Sultan A, Dampier B, Bonne S, et al. The transcription factor ZEB1 (deltaEF1) represses Plakophilin 3 during human cancer progression. *FEBS letters*. 2007; 581(8): 1617–24. PMID: [17391671](#)
27. Demirag GG, Sullu Y, Gurgenyatagi D, Okumus NO, Yucel I. Expression of plakophilins (PKP1, PKP2, and PKP3) in gastric cancers. *Diagn Pathol*. 2011; 6:1. doi: [10.1186/1746-1596-6-1](#) PMID: [21194493](#)
28. Takahashi H, Nakatsuji H, Takahashi M, Avirmed S, Fukawa T, Takemura M, et al. Up-regulation of plakophilin-2 and Down-regulation of plakophilin-3 are correlated with invasiveness in bladder cancer. *Urology*. 2012; 79(1):240 e1–8.
29. Sklyarova T, Bonne S, D'Hooge P, Denecker G, Goossens S, De Rycke R, et al. Plakophilin-3-deficient mice develop hair coat abnormalities and are prone to cutaneous inflammation. *J Invest Dermatol*. 2008; 128(6):1375–85. PMID: [18079750](#)
30. Khapare N, Kundu ST, Sehgal L, Sawant M, Priya R, Gosavi P, et al. Plakophilin3 Loss Leads to an Increase in PRL3 Levels Promoting K8 Dephosphorylation, Which Is Required for Transformation and Metastasis. *PLoS One*. 2012; 7(6):e38561. doi: [10.1371/journal.pone.0038561](#) PMID: [22701666](#)
31. Sehgal L, Thorat R, Khapare N, Mukhopadhaya A, Sawant M, Dalal SN. Lentiviral mediated transgenesis by in vivo manipulation of spermatogonial stem cells. *PLoS One*. 2011; 6(7):e21975. doi: [10.1371/journal.pone.0021975](#) PMID: [21760937](#)
32. Mi H, Muruganujan A, Casagrande JT, Thomas PD. Large-scale gene function analysis with the PANTHER classification system. *Nat Protoc*. 2013; 8(8):1551–66. doi: [10.1038/nprot.2013.092](#) PMID: [23868073](#)
33. Mi H, Muruganujan A, Thomas PD. PANTHER in 2013: modeling the evolution of gene function, and other gene attributes, in the context of phylogenetic trees. *Nucleic Acids Res*. 2013; 41(Database issue):D377–86. doi: [10.1093/nar/gks1118](#) PMID: [23193289](#)
34. Schmittgen TD, Livak KJ. Analyzing real-time PCR data by the comparative C(T) method. *Nat Protoc*. 2008; 3(6):1101–8. PMID: [18546601](#)
35. Kleinman HK, Jacob K. Invasion assays. *Current protocols in cell biology / editorial board, Juan S Bonifacio [et al]*. 2001; Chapter 12:Unit 12.2.
36. Albin A, Iwamoto Y, Kleinman HK, Martin GR, Aaronson SA, Kozlowski JM, et al. A rapid in vitro assay for quantitating the invasive potential of tumor cells. *Cancer Res*. 1987; 47(12):3239–45. PMID: [2438036](#)
37. Hanahan D, Weinberg RA. Hallmarks of cancer: the next generation. *Cell*. 2011; 144(5):646–74. doi: [10.1016/j.cell.2011.02.013](#) PMID: [21376230](#)
38. Jiang QH, Wang AX, Chen Y. Radixin Enhances Colon Cancer Cell Invasion by Increasing MMP-7 Production via Rac1-ERK Pathway. *ScientificWorldJournal*. 2014; 2014:340271. doi: [10.1155/2014/340271](#) PMID: [25136657](#)
39. Fingleton B, Powell WC, Crawford HC, Couchman JR, Matrisian LM. A rat monoclonal antibody that recognizes pro- and active MMP-7 indicates polarized expression in vivo. *Hybridoma*. 2007; 26(1): 22–7. PMID: [17316082](#)
40. Lee SK, Han YM, Yun J, Lee CW, Shin DS, Ha YR, et al. Phosphatase of regenerating liver-3 promotes migration and invasion by upregulating matrix metalloproteinases-7 in human colorectal cancer cells. *International journal of cancer*. 2012; 131(3):E190–203. doi: [10.1002/ijc.27381](#) PMID: [22131018](#)
41. Porte H, Chastre E, Prevot S, Nordlinger B, Empereur S, Basset P, et al. Neoplastic progression of human colorectal cancer is associated with overexpression of the stromelysin-3 and BM-40/SPARC genes. *International journal of cancer*. 1995; 64(1):70–5. PMID: [7665251](#)
42. Zeng ZS, Guillem JG. Distinct pattern of matrix metalloproteinase 9 and tissue inhibitor of metalloproteinase 1 mRNA expression in human colorectal cancer and liver metastases. *Br J Cancer*. 1995; 72(3): 575–82. PMID: [7669564](#)
43. Okada A, Bellocq JP, Rouyer N, Chenard MP, Rio MC, Chambon P, et al. Membrane-type matrix metalloproteinase (MT-MMP) gene is expressed in stromal cells of human colon, breast, and head and neck carcinomas. *Proc Natl Acad Sci U S A*. 1995; 92(7):2730–4. PMID: [7708715](#)
44. Rouleau C, Roy A, St Martin T, Dufault MR, Boutin P, Liu D, et al. Protein tyrosine phosphatase PRL-3 in malignant cells and endothelial cells: expression and function. *Mol Cancer Ther*. 2006; 5(2):219–29. PMID: [16505094](#)
45. Saha S, Bardelli A, Buckhaults P, Velculescu VE, Rago C, St Croix B, et al. A phosphatase associated with metastasis of colorectal cancer. *Science*. 2001; 294(5545):1343–6. PMID: [11598267](#)
46. Hofmann I, Casella M, Schnolzer M, Schlechter T, Spring H, Franke WW. Identification of the junctional plaque protein plakophilin 3 in cytoplasmic particles containing RNA-binding proteins and the recruitment of plakophilins 1 and 3 to stress granules. *Mol Biol Cell*. 2006; 17(3):1388–98. PMID: [16407409](#)

47. Fischer-Keso R, Breuninger S, Hofmann S, Henn M, Rohrig T, Strobel P, et al. Plakophilins 1 and 3 bind to FXR1 and thereby influence the mRNA stability of desmosomal proteins. *Mol Cell Biol*. 2014.
48. Wolf A, Krause-Gruszczynska M, Birkenmeier O, Ostareck-Lederer A, Huttelmaier S, Hatzfeld M. Plakophilin 1 stimulates translation by promoting eIF4A1 activity. *J Cell Biol*. 2010; 188(4):463–71. doi: [10.1083/jcb.200908135](https://doi.org/10.1083/jcb.200908135) PMID: [20156963](https://pubmed.ncbi.nlm.nih.gov/20156963/)
49. Beaudry VG, Jiang D, Dusek RL, Park EJ, Knezevich S, Ridd K, et al. Loss of the p53/p63 regulated desmosomal protein Perp promotes tumorigenesis. *PLoS genetics*. 2010; 6(10):e1001168. doi: [10.1371/journal.pgen.1001168](https://doi.org/10.1371/journal.pgen.1001168) PMID: [20975948](https://pubmed.ncbi.nlm.nih.gov/20975948/)
50. Jheon AH, Mostowfi P, Snead ML, Ihrie RA, Sone E, Pramparo T, et al. PERP regulates enamel formation via effects on cell-cell adhesion and gene expression. *J Cell Sci*. 2011; 124(Pt 5):745–54. doi: [10.1242/jcs.078071](https://doi.org/10.1242/jcs.078071) PMID: [21285247](https://pubmed.ncbi.nlm.nih.gov/21285247/)